MALAYSIAN JOURNAL OF SCIENCE

Vol. 42 ● No 1 ● February 2023

JURNAL SAINS MALAYSIA

MJS

ISSN 1394 - 3065

The Malaysian Journal of Science is indexed or cited in the following Scientific Databases: Elsevier Bibliographic Databases (ACI, Scopus, EMBASE, Compendex, GEOBASE, EMBiology, Elsevier BIOBASE, FLUIDEX and World Textiles); CAB Abstracts and Chemical Abstracts Service Database

http://www.myjurnal.my/public/browse-journal-view.php?id=194
www.mjs.um.edu.my

MALAYSIAN JOURNAL OF SCIENCE
MJS
ISSN 1394-3065

Regular Issue

Malaysian Journal of Science 42 (1): 1-6 (February 2023) https://mjs.um.edu.my

EFFECTS OF VARIOUS LIGHT INTENSITIES ON PHYCOCYANIN COMPOSITION OF CYANOBACTERIUM *LIMNOSPIRA FUSIFORMIS* (VORONICHIN) NOWICKA-KRAWCZYK, MÜHLSTEINOVÁ & HAUER

Haider A. Kareem[1a], Haider A. Alghanmi[2a]*

Abstract: Phycocyanin denotes a photosynthetic pigment discovered in Rhodophyta and cyanobacteria, which has been used in medical, industrial, and agricultural applications. In general, phycocyanin production by cyanobacteria depends on many environmental conditions, mainly light during the cultivation period. The goal of this research was to see how various light intensities of 47, 52, as well as 60 µmol m-2 s-1, affected the Phycocyanin production of cyanobacterium Limnospira fusiformis cultured in Zarrouk medium with a maximum temperature of 28°C. The outcomes revealed that with mild light intensity (52 µmol m-2 s-1), increased phycocyanin production of 11.94 ng/mg took place. With regard to greater light intensity (60 µmol m-2 s-1), the lesser phycocyanin production of 0.57 ng/mg took place. These results give a good impression that moderate lighting increases phycocyanin production, but high light intensity inhibits it. The statistical analysis results also showed that there are significant differences between the light intensities used in the study at a level of $p<0.05$. Therefore, this study concluded that phycocyanin was affected by light intensity. Light regime optimization gives a good yield of this pigment. In this study, high phycocyanin production by cyanobacterium Limnospira fusiformis occurred in mild light intensity (52 µmol m-2 s-1).

Keywords: *Limnospira fusiformis, cyanobacteria, light intensity, photosynthetic pigment, phycocyanin*

1. Introduction

Algae that grow in high solar radiation habitats have auxiliary pigments that shelter them from oxidation as well as radiation damage, owing to the double conjugate bonds in the chromophore. The combination of the attachment pigments and their arrangement gives the algae various colors, for instance, red, brown, green, and golden algae (Barsanti & Gualtieri, 2014; Lee, 2018). Carotenoids, chlorophyll, and phycobiliproteins are among the colorful components discovered in algae and cyanobacteria. Moreover, phycoerythrin, allophycocyanin, and phycocyanin are the most common phycobiliproteins, and they are built up of distinct α and β polypeptides subunits (Ferreira & Gouveia, 2020).

Some microalgae such as *Limnospira* (Nowicka-Krawczyk et al., 2019) showed an excellent application in commercial, medical, and pharmacological because it has excellent nutritional properties as well as a wide variety of active compounds. They include several natural pigments and compounds with functional qualities and high protein content. Allophycocyanin (AP) and phycoerythrin (PE) are minor amounts of phycobiliproteins derived from *Spirulina*, while phycocyanin is plentiful. Phycocyanin is a bright blue pigment that, depending on its purity, has a variety of vital uses (Barsanti & Gualtieri, 2014; Becker & Venkataraman, 1984; Berg, 2002; Silva, 2008).

Authors information:
[a]Biology Department, College of Education, University of Al-Qadisiyah, Al Diwaniyah, IRAQ. Email: haider.ammar@qu.edu.iq[1]; haider.alghanmi@qu.edu.iq[2]
*Corresponding Author: haider.alghanmi@qu.edu.iq

Phycocyanin is an algae-derived light-harvesting pigment-binding protein. It is a common coloring additive in nutritional and dairy items, for instance, cosmetics, beverages, candies, gums, and jellies in China and Japan. Phycocyanin is heat and light-sensitive. In comparison to gardenia or indigo, it has a pure blue colorant. Phycocyanin can be utilized to treat a number of malignancies, such as squamous cell carcinoma. Also, phycocyanin isolated from *Spirulina platensis* showed anticancer efficacy (Tripathi et al., 2021). The antioxidant compounds present in Spirulina microalga, for instance, phycocyanin, phenolic compounds, as well as polyunsaturated fatty acids, may explain its ability to reduce blood lipid levels and boost HDL cholesterol (Colla et al., 2007; Colla et al., 2008).

Nutrients like nitrogen, phosphorus, calcium, magnesium, iron, manganese and light affect the pigment biosynthesis (Norena-Caro et al., 2021). Light is one of the most critical components that affect microalgae and cyanobacteria pigments production because it allows them to gather energy and carry out photosynthesis (Atta et al., 2013). However, the majority of cultivations rely on sunlight as a source of energy. Artificial light is more often utilized in cultivations for high added value bioproducts like phycocyanin, with effective and standardized photosynthetic regulation photon flux density, leading to high productivities of these pigments (Blanken et al., 2013). The light intensity impact as well as the quality of the phycocyanin amount in *Synechococcus* sp. NKBG042902 cells were studied by Takano

Received: January 23, 2022
Accepted: July 14, 2022
Published: February 28, 2022

DOI:https//doi.org/10.22452/mjs.vol42no1.1
Malaysian Journal of Science 42(1): 1-6 (February 2023)

et al. (1995), which indicated that the phycocyanin concentration was maximum as the cyanobacterium was cultivated under 25 µmol m^{-2} s^{-1} illumination utilizing a cool-white fluorescent light, as well as the phycocyanin and biomass productivities were 21-100 $mg1^{-1}$ day^{-1}, accordingly. The light spectrum and nutritional content affect *Spirulina platensis* production. According to Wicaksono et al. (2019), when the red and nutritional spectrums were mixed, the optimal production of phycocyanin, as well as dry weight of Spirulina, were achieved, producing 0.6677/0.5 g L^{-1} and 5.1078 mg g^{-1}, accordingly.

The purpose of this research was to see how varying light intensities affected the growth and production of phycocyanin in the cyanobacterium *Limnospira fusiformis*.

2. Methods and Material

2.1 Cyanobacterial strain

The axenic culture of a *Limnospira fusiformis* isolated from wastewater (Photo 1) was obtained from the Biology department laboratory, College of Education, the University of Al-Qadisiyah/Iraq. It was identified morphologically and genetically, according to Alghanmi (2020). The strain was maintained in Zarrouk medium described in Vonshak (1997) and cultivated in a 100 ml flask containing Zarrouk medium with pH 9.6 in a growth chamber having a controlled temperature of 28°C, 25 µmol m^{-2} s^{-1} of light intensity, as well as photoperiod 16 hours, light/8 dark.

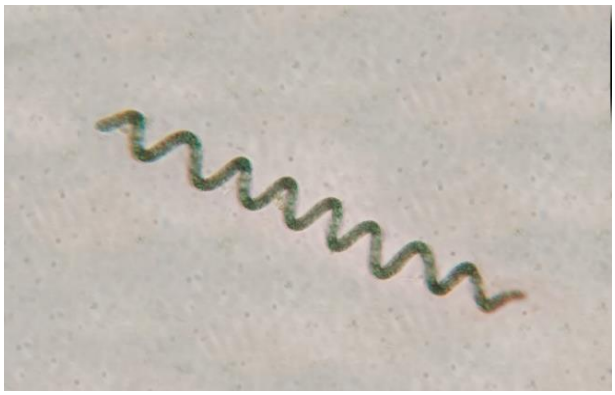

Photo 1. Cyanobacterial strain identified as *Limnospira fusiformis* under light microscope (magnification at 40x).

2.2 Effect of light intensity on phycocyanin production

The influence of various light intensities, 47, 52, and 60 µmol m^{-2} s^{-1}, on the growth rate, including phycocyanin production of cyanobacterium *L. fusiformis* cultured in Zarrouk medium (pH 9.6) with an ideal temperature of 28°C and a photoperiod of 16 light:8.

2.3 Growth curve estimation

The growth curve of *L. fusiformis* was estimated depending on the chlorophyll-a pigment determination in accordance with the Zavrel et al. (2015) method. The samples were gathered every day for 30 days from the culture of *L. fusiformis*, then treated with 90% acetone for extracted chlorophyll-a later determined using a spectrophotometer at wavelength 665 and A720 nm. The chlorophyll was estimated by the equation below:

Chl a [µg/L] = 12.9447 (A665 − A720).

2.4 Pigment extraction and analysis

L. fusiformis dried powder was suspended in a 1:15 w/v ratio in (0.1 M) sodium phosphate buffer with pH 7. First, the suspension was homogenized for 10 min utilizing sonication. Next, three RFT freezing and thawing cycles were performed, then the suspension was centrifuged at 4000 *g* for 30 mins, the crude extract with a blue color comprising C-phycocyanin was recovered. Following that, the samples were then filtered utilizing Millipore 0.45 µm filter paper, which was dried in an oven at 40°C for 8 hrs. Note that the dried paper was weighed and placed in a tube, to which 5 ml of 0.1 M phosphate buffer (pH 7) was administered. Next, the mixture was homogenized for 10 minutes before being frozen at -20°C for an hour and subsequently thawed at room temperature for another hour. This procedure was carried out three times. Lastly, the sample was centrifuged at 8,000 *g* for 10 minutes and filtrated using 0.45 µm Millipore filter paper and then was used for the measurement by the HPLC device (Moraes et al., 2011).

2.5 High-performance liquid chromatography (HPLC)

A Shimadzu HPLC system (Kyoto, Japan) was employed for executing chromatographic analysis. The HPLC system included a SIL-9A autosampler injector (Shimadzu), as well as an LC-9ADvp pump (Shimadzu). The chromatographic separations were accomplished employing an Orbit 100 C4, 5 µm, 250 × 4.0 mm. Note that the mobile phase was made up of water having 0.1% v/v TFA (solvent A) as well as CH_3CN with 0.1% v/v TFA (solvent B). Moreover, at a constant flow rate of 0.8 mL min^{-1}, the subsequent gradient program was utilized from 0 to 10 min, and the components were raised from 45% - 100% in B. The injection had a volume of 100 µL. The photodiode array detector set at 620 nm was utilized to observe the column effluent. The detection of c-phycocyanin was analyzed by matching the retention time and absorbance spectrum of the standard (Figure 1). The standard of phycocyanin was purchased from Sigma Aldrich with CAS-Number P2172-10MG. The concentration of phycocyanin extracted from *L. fusiformis* was calculated by serial concentrations of standard external materials to build a calibration curve between concentration and its equivalent peak area (Moraes et al., 2011).

DOI:https//doi.org/10.22452/mjs.vol42no1.1
Malaysian Journal of Science 42(1): 1-6 (February 2023)

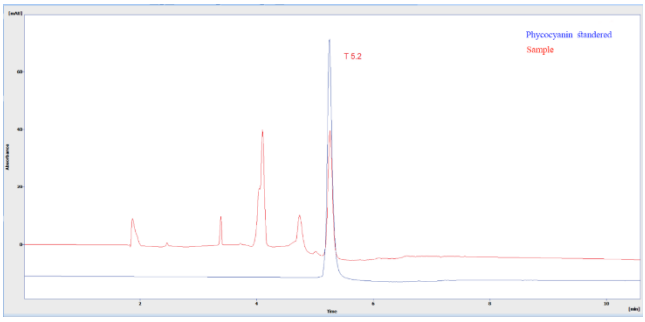

Figure 1. Phycocyanin of *Limnospira fusiformis* with red color matching the standard phycocyanin in blue color at retention time 5.2 min.

2.6 Statistical Analysis

Every experiment was analyzed in triplicate to ensure that the findings were reproducible. The data was evaluated utilizing a one-way analysis of variance (ANOVA), which was then subsequently followed by the least significant differences (LSD). All analyses were carried out with SPSS 26 at $p < 0.05$.

3. Findings and Discussion

Algal pigments like C-phycocyanin (C-PC), among the key primary pigments of the cyanobacterium *Spirulina*, a microalga utilized as a dietary supplement in various countries, include a wide spectrum of pigments, which include phycobiliproteins, aside from their health advantages, algal pigments possess tremendous commercial potential in the pharmaceutical industry as natural colorants, cosmetics, as well as nutraceutical industries (Kuddus et al., 2013). Moreover, light is one of the optimum conditions affecting pigment production in cyanobacteria. Here, microalgae provide an effective technique for turning solar energy into biomass since phototrophic cell factories are driven by sunlight to produce bioproducts, antioxidants, bioactive compounds, vitamins, proteins, dyes, fats, and sugars (Brennan & Owende, 2010).

The growth curve estimated by chlorophyll concentration (Figure 2) showed good growth of *L. fusiformis* under three light intensities 47, 52, and 60 µmol m^{-2} s^{-1}, with the highest growth registered at 52 µmol m^{-2} s^{-1}. The results of phycocyanin production by *L. fusiformis* in table 1 and Figure 3 show higher production of phycocyanin of 11.94 ng/mg occurred in the mild light intensity 52 µmol m^{-2} s^{-1}. At a greater light intensity of 60 µmol m^{-2} s^{-1}, however, a lesser phycocyanin content (0.57 ng/mg) was found. These findings are consistent with those of Ma et al. (2015). When incubating cyanobacterium *Nostoc sphaeroides* at different light intensities 10, 30, 60, 90, as well as 120 µmol m^{-2} s^{-1}, they discovered that the cyanobacterium colonies were soft and pale when exposed to low (10,30 µmol m^{-2} s^{-1}) as well as high (120 µmol m^{-2} s^{-1}) light intensity. Furthermore, towards the conclusion, the spherical aggregation was disrupted. Under the strong light intensity, this was much more severe. White light at 90 µmol m^{-2} s^{-1}, on the other hand, provided the best light conditions for phycobiliprotein accumulation and growth in *N. sphaeroides*. Moreover, Schipper et al. (2020) investigated the phycocyanin production by the desert cyanobacteria *Leptolyngbya* sp. QUCCCM56 under various light intensities. Their findings revealed that the maximum light intensity for phycocyanin production was observed at minimal light intensity (80 µmol m^{-2} s^{-1}) and rising light intensities of 300 and 1800 µmol m^{-2} s^{-1} resulted in substantial decreases in phycocyanin content of 53.0% and 78.7%, accordingly.

The elevation in phycocyanin content at 52 µmol $m^{-2}s^{-1}$ might be linked to an adjustment necessary to protect the chlorophyll molecules from light, as clarified by Grossman (2003) that cyanobacteria modify their phycobiliprotein ratios to maximize photosynthetic efficiency in response to changes in light quality.

Cyanobacteria may evolve to change their light absorption qualities in response to light availability in various environments like freshwater, wastewater and soil, allowing them to regulate photosynthesis. As a result, the pigment concentration involved in light absorption, such as phycocyanin, may fluctuate based on the particular climatic conditions of light intensity (Khandual et al., 2021). Moreover, Szwarc and Zieliński (2018) reported that the light spectrum influenced both the phycocyanin content as well as the biomass of *Limnospira platensis* biomass. High light intensity alters the features of every photosynthetic system. However, as per Eriksen (2008), extremely intense light can cause photoinhibition. Subsequently, the pigment that absorbs particular light wavelengths is prioritized (Boisen & Eggum, 1991).

DOI:https//doi.org/10.22452/mjs.vol42no1.1
Malaysian Journal of Science 42(1): 1-6 (February 2023)

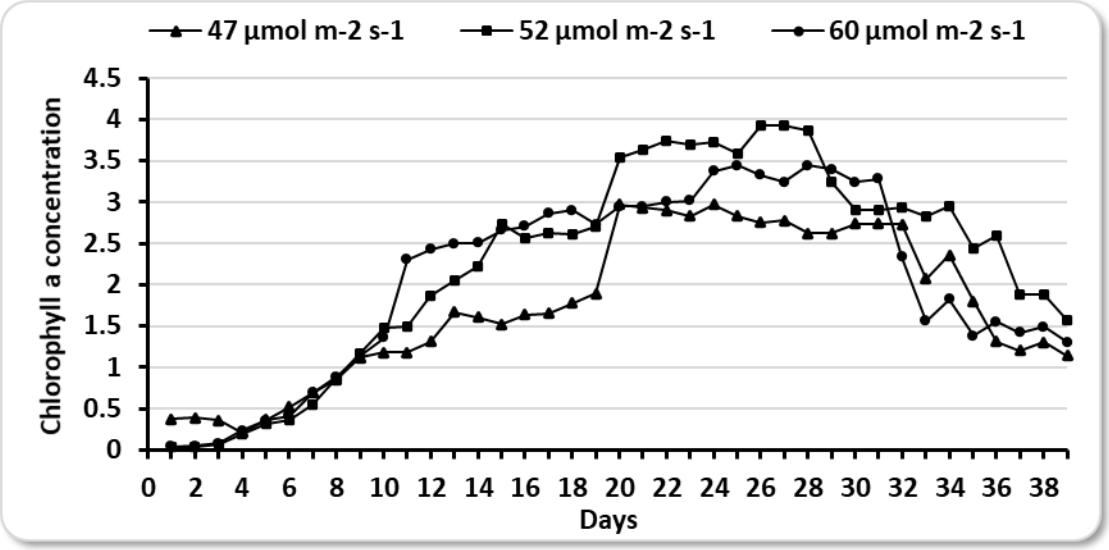

Figure 2. Growth curve estimated by chlorophyll production of *Limnospira fusiformis*

Table 1. Different light intensity effects on phycocyanin production by *Limnospira fusiformis*

Ligh intensity µmol m-2 s-1 / *Limnospira fusiformis*	47 Mean±SE	52 Mean±SE	60 Mean±SE	LSD
Phycocyanin ng/mg	1.76±0.058 b	11.94.0205 a	0.57±0.0001 c	0.05

**lowercase letters indicate the differences between the light intensities*

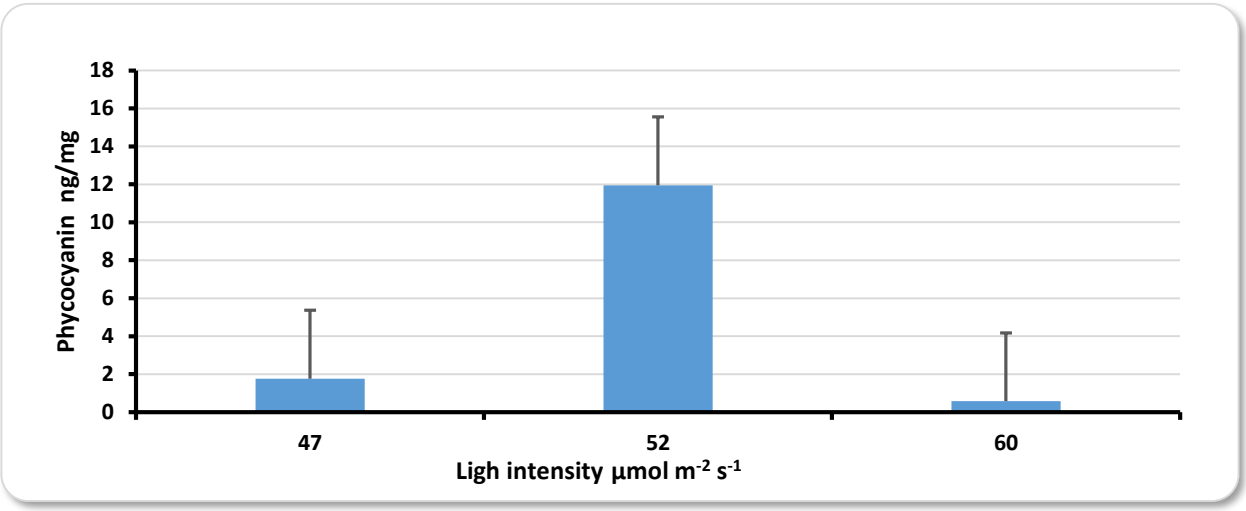

Figure 3. Different light intensities effects on phycocyanin production by Limnospira fusiformis

DOI:https//doi.org/10.22452/mjs.vol42no1.1
Malaysian Journal of Science 42(1): 1-6 (February 2023)

4. Conclusion

Phycocyanin is an important pigment that poses pharmacological, medical. Moreover, economic values, the production of this pigment is affected by light intensity. Hence, the current study suggested that light stress may influence the production of phycocyanin where they noticed that high phycocyanin production by cyanobacterium Limnospira fusiformis occurred at light intensity (52 µmol m-2 s-1). In contrast, the low production of phycocyanin occurred at low and high light intensities.

5. Acknowledgement

We appreciate the assistance of Assist Prof. Ahmed J. Hassan (University of Al-Qadisiyah) with the statistical analysis.

6. References

Alghanmi, H. A. (2020). Evaluating the effect of different doses of gamma radiation on carbohydrates, proteins, and lipids content of arthrospira fusiformis. EurAsian Journal of BioSciences, 14(1).

Atta, M., Idris, A., Bukhari, A., & Wahidin, S. (2013). Intensity of blue LED light: a potential stimulus for biomass and lipid content in fresh water microalgae Chlorella vulgaris. Bioresource technology, 148, 373-378.

Barsanti, L., & Gualtieri, P. (2014). Algae: anatomy, biochemistry, and biotechnology. CRC press.

Becker, E. W., & Venkataraman, L. V. (1984). Production and utilization of the blue-green alga Spirulina in India. Biomass, 4(2), 105-125. https://doi.org/https://doi.org/10.1016/0144-4565(84)90060-X

Berg, J. (2002). DNA replication, recombination and repairBerg JM, Tymoczko JL and Stryer L: Biochemistry. In: New York: WH Freeman & Co.

Blanken, W., Cuaresma, M., Wijffels, R. H., & Janssen, M. (2013). Cultivation of microalgae on artificial light comes at a cost. Algal Research, 2(4), 333-340.

Boisen, S., & Eggum, B. O. (1991). Critical evaluation of in vitro methods for estimating digestibility in simple-stomach animals. Nutr Res Rev, 4(1), 141-162. https://doi.org/10.1079/nrr19910012

Brennan, L., & Owende, P. (2010). Biofuels from microalgae—a review of technologies for production, processing, and extractions of biofuels and co-products. Renewable sustainable energy reviews, 14(2), 557-577.

Colla, L. M., Furlong, E. B., & Costa, J. A. V. (2007). Antioxidant properties of Spirulina (Arthospira) platensis cultivated under different temperatures and nitrogen regimes. Brazilian archives of biology technology, 50(1), 161-167.

Colla, L. M., Muccillo-Baisch, A. L., & Costa, J. A. V. (2008). Spirulina platensis effects on the levels of total cholesterol, HDL and triacylglycerols in rabbits fed with a hypercholesterolemic diet. Brazilian archives of biology technology, 51(2), 405-411.

Eriksen, N. T. (2008). Production of phycocyanin--a pigment with applications in biology, biotechnology, foods and medicine. Appl Microbiol Biotechnol, 80(1), 1-14. https://doi.org/10.1007/s00253-008-1542-y

Ferreira, A., & Gouveia, L. (2020). Chapter 28 - Microalgal biorefineries. In E. Jacob-Lopes, M. M. Maroneze, M. I. Queiroz, & L. Q. Zepka (Eds.), Handbook of Microalgae-Based Processes and Products (pp. 771-798). Academic Press. https://doi.org/https://doi.org/10.1016/B978-0-12-818536-0.00028-2

Grossman, A. R. (2003). A molecular understanding of complementary chromatic adaptation. Photosynth Res, 76(1-3), 207-215. https://doi.org/10.1023/a:1024907330878

Khandual, S., Sanchez, E. O. L., Andrews, H. E., & de la Rosa, J. D. P. (2021). Phycocyanin content and nutritional profile of Arthrospira platensis from Mexico: efficient extraction process and stability evaluation of phycocyanin. BMC Chemistry, 15(1), 24. https://doi.org/10.1186/s13065-021-00746-1

Kuddus, M., Singh, P., Thomas, G., & Al-Hazimi, A. (2013). Recent developments in production and biotechnological applications of C-phycocyanin. BioMed research international, 2013.

Lee, R. E. (2018). Phycology. Cambridge university press.

Ma, R., Lu, F., Bi, Y., & Hu, Z. (2015). Effects of light intensity and quality on phycobiliprotein accumulation in the cyanobacterium Nostoc sphaeroides Kützing. Biotechnol Lett, 37(8), 1663-1669. https://doi.org/10.1007/s10529-015-1831-3

Moraes, C. C., Sala, L., Cerveira, G. P., & Kalil, S. J. (2011). C-phycocyanin extraction from Spirulina platensis wet biomass. Brazilian Journal of Chemical Engineering, 28(1), 45-49.

Norena-Caro, D. A., Malone, T. M., & Benton, M. G. (2021). Nitrogen Sources and Iron Availability Affect Pigment Biosynthesis and Nutrient Consumption in Anabaena sp. UTEX 2576. Microorganisms, 9(2), 431. https://doi.org/10.3390/microorganisms9020431

DOI:https//doi.org/10.22452/mjs.vol42no1.1
Malaysian Journal of Science 42(1): 1-6 (February 2023)

Nowicka-Krawczyk, P., Mühlsteinová, R., & Hauer, T. (2019). Detailed characterization of the Arthrospira type species separating commercially grown taxa into the new genus Limnospira (Cyanobacteria). Scientific Reports, 9(1), 694. https://doi.org/10.1038/s41598-018-36831-0

Schipper, K., Fortunati, F., Oostlander, P. C., Al Muraikhi, M., Al Jabri, H. M. S. J., Wijffels, R. H., & Barbosa, M. J. (2020). Production of phycocyanin by Leptolyngbya sp. in desert environments. Algal Research, 47, 101875. https://doi.org/https://doi.org/10.1016/j.algal.2020.101875

Silva, L. A. (2008). Estudo do processo biotecnológico de produção, extração e recuperação do pigmento ficocianina da Spirulina platensis.

Szwarc, D., & Zieliński, M. (2018). Effect of Lighting on the Intensification of Phycocyanin Production in a Culture of Arthrospira platensis. Proceedings 2(20), 1305. https://www.mdpi.com/2504-3900/2/20/1305

Takano, H., Arai, T., Hirano, M., & Matsunaga, T. (1995). Effects of intensity and quality of light on phycocyanin production by a marine cyanobacterium Synechococcus sp. NKBG 042902. Appl Microbiol Biotechnol, 43(6), 1014-1018. https://doi.org/10.1007/BF00166918

Tripathi, R., Shalini, R., & Singh, R. K. (2021). Prophyletic origin of algae as potential repository of anticancer compounds. In Evolutionary Diversity as a Source for Anticancer Molecules (pp. 155-189). Elsevier.

Vonshak, A. (1997). Spirulina platensis arthrospira: physiology, cell-biology and biotechnology. CRC press.

Wicaksono, H., Satyantini, W., & Masithah, E. (2019). The spectrum of light and nutrients required to increase the production of phycocyanin Spirulina platensis. IOP Conference Series: Earth and Environmental Science,

Zavrel, T., Sinetova, M. A., & Červený, J. (2015). Measurement of Chlorophyll a and Carotenoids Concentration in Cyanobacteria. Bio-protocol, 5(9), e1467. https://doi.org/10.21769/BioProtoc.1467

DOI:https//doi.org/10.22452/mjs.vol42no1.1
Malaysian Journal of Science 42(1): 1-6 (February 2023)

MALAYSIAN JOURNAL OF SCIENCE
MJS
ISSN 1394-3065

Regular Issue

Malaysian Journal of Science 42 (1): 7-16 (February 2023) https://mjs.um.edu.my

LARVICIDAL ACTIVITY OF THE SYNTHESISED LIGNANS, NEOLIGNANS, AND COUMARIN AGAINST *Crocidolimia binotalis* 2ND INSTAR LARVAE

Siti Fadilah Juhan[1a], Siti Mariam Mohd Nor[2a]*, Mohd Shukri Mat Ali[3b] and Siti Zulaika Md Nor[4a]

Abstract: Five compounds comprising of 8-O-4'-neolignan (7), two arylnaphthalene lignans (5, 8), aryldihydrobenzofuran neolignan (4), and lignan (6) were synthesised by enzymatic coupling reaction using horseradish peroxidase (HRP) between vanillin (1) with methyl ferulate (2) or methyl sinapate (3). All of these compounds, as well as previously synthesised palladium-catalysed coupling products of neolignan (9), 8-O-4'-neolignan (10), arylcoumarin (11), and lignan (12), were examined for larvicidal activity against *Crocidolomia binotalis* (*C. binotalis*) 2nd instar larvae. It was revealed that seven out of nine synthesised compounds had a mortality rate of more than 90% after 24 hours of exposure. Neolignan (10) and lignan (6) demonstrated strongest larvicidal activity with LD_{50} = 2.218 mg/L and LD_{50} = 1.678 mg/L, respectively compared to the standard azadirachtin (LD_{50} =2.818 mg/L). The results showed that the synthesised compounds have a high potential for use in the control of *C. binotalis* larvae and could be used in the development of new and more effective compounds as larvicides.

Keywords: *Lignan, neolignan, coumarin, horseradish peroxidase, larvicidal*

1. Introduction

Insects pose a significant threat to crops because they can consume plant leaves, roots, and stems hence rendering them to be unfit for consumption, other uses, and potentially damaging the plants. Insecticides are chemicals that are used in crop plantations to control insect and disease infestations. Insecticides are widely available on the market and can be classified in a variety of ways depending on the (i) chemical structure (natural, synthetic, organic, inorganic), (ii) toxicity (extreme, high, moderate, less), (iii) stages in the life cycle (larvicides, pupicides, ovicides, adulticides), (iv) mode of entry (systemic, contact, stomach, fumigant, repellent), and (iv) mode of action (AChE inhibitors, GABA chloride channel blockers, ecdysone receptor agonists, sodium channel modulators, juvenile hormone mimics, inhibitors of chitin biosynthesis, ryanodine receptor modulators, and others) (IRAC Website; CFR Website; Akashe et al., 2018; Yadav & Devi, 2017). Crop protection with insecticides has been extremely beneficial to agriculture, particularly in terms of increasing yield production. However, the development of resistance of plant pathogens to conventional insecticides, as well as toxic effects and environmental concerns, piqued researchers' interest in developing synthetic or natural in the origin of new insecticides.

Novel insecticides are abundant in higher plants and have been used worldwide (Isman, 2006). Many plant species, particularly those native to the tropics, have the potential to be used as bioinsecticides (Lewis et al., 2016). As they are frequently biodegradable and active against a limited range of species, these insecticides may lead to the development of new classes of safer insect control agents. They can also be suitable materials for use in integrated pest management (Hikal et al., 2017; Hubbard et al., 2014).

Lignans, neolignans, and coumarins are among the plant insecticides that have been widely reported. Lignans and phenolic compounds originating from C_6C_3 precursors function as insect-feeding regulators or insect growth and development regulators. These compounds interact with the insect's endocrine system, which is involved in insect development (Harmatha & Dinan, 2003). Examples of lignans activities include an insecticidal activity of podophyllotoxin against 5th instar larvae of *Pieris rapae* L. (Di et al., 2007) and the 3rd instar larvae of *Mythimna separata* (Xu & Xiao, 2009); antifeedant activity of gomisin J against *Tribolium castaneum* adults (Guo et al., 2020); repellent and feeding deterrent activities of (-)-sesamin against *T. castaneum* adults (Wang et al., 2020); insecticidal activity of haedoxan A

Authors information:
[a]Department of Chemistry, Faculty of Science, Universiti Putra Malaysia, 43400 Serdang, Selangor, MALAYSIA. E-mail: dila8904@gmail.com[1]; smariam@upm.edu.my[2]; ikaamdnor@yahoo.com[4]
[b]Genebank and Seed Centre, Malaysian Agricultural Research and Development Institute (MARDI), 43400 Serdang, Selangor, MALAYSIA. E-mail: mshukri@mardi.gov.my[3]
*Corresponding Author: smariam@upm.edu.my

Received: August 25, 2022
Accepted: October 7, 2022
Published: February 28, 2023

DOI:https//doi.org/10.22452/mjs.vol42no1.2
Malaysian Journal of Science 42(1): 7-16 (February 2023)

against 3rd instar larvae of *M. separata (*Li et al., 2019), and insecticidal activity of phrymarolin B against 4th instar larvae of *M. separata* (Xiao et al., 2013). Examples for neolignans include the growth inhibition activity of licarin A against neonate larvae of *Spodoptera litura* (González-Coloma et al., 1994) and insecticidal activity of honokiol against the 3rd instar larvae of *M. separata* (Yang et al., 2015). Whereas, the example for coumarins activities include acaricidal and growth inhibition activities of osthole ester against *M. separata* and *Tetranychus cinnabarinus* (Shan et al., 2022), insecticidal activity of psoralen against neonate larvae of *Spodoptera frugiperda* (Ayil-Gutiérrez et al., 2015), and insecticidal activity of surangin B against the 3rd instar larvae of *Plutella xylostella* (Issakul et al., 2011).

This study investigated the insecticidal activity of new potential lignans, neolignans, and coumarins against *C. binotalis* larvae. *C. binotalis* was chosen as the target pest because it is a common pest in Malaysia for vegetable crops replacing *P. xylostella*, *S. litura*, and *Hellula undalis* (Lim et al., 1996; Ooi & Kelderman, 1979). Another reason for using *C. binotalis* in this study is because of their ease of rearing and availability. There is a lack of reports on the effect of synthetic compounds on this pest in Malaysia (Hashim & Ibrahim, 2003; Hashim et al., 2002; Ng et al., 2003), as well as in neighbouring countries such as Indonesia (Sastrosiswojo & Setiawati, 1992; Shepard & Schellhorn, 1994) and India (Kannan et al., 2011; Srinivasan & Veeresh, 1986).

Previously, we investigated the palladium-catalysed Heck coupling reaction between a series of methyl cinnamate derivatives and an activated C-I bond of iodovanillin or a non-activated C-H bond of vanillin (Juhan et al., 2018). Furthermore, the aim of this research is to employ an enzymatic method to perform the coupling reaction of vanillin (**1**) and methyl ferulate (**2**) or methyl sinapate (**3**) and to investigate the larvicidal activity of all coupling products obtained from both chemical and enzymatic coupling methods. In the modified enzymatic coupling reaction, HRP as a catalyst in the presence of hydrogen peroxide (H_2O_2) and phosphate buffer (pH7.2) was used to synthesise lignan and neolignan derivatives (Wakimoto et al., 2009).

It was discovered that the structures of the compound play an important role in enhancing insecticidal activities such as introducing methoxy group, which is essential for maintaining the activities, at a specific position (Di et al., 2007). The formation of ester derivatives (Xu & Xiao, 2009), the number of methylenedioxy, and the position of hydroxyl groups also demonstrated promising activities (Guo et al., 2020; Kirst, 2010). The presence of different functional groups in their structures such as hydroxyl, methoxy, and ester led to the selection of vanillin, iodovanillin, and all methyl cinnamate derivatives for our study. These three functional groups were found in the structures of commercially available insecticides such as azadirachtin (Lin et al., 2021), organophosphates (Rathnayake & Northrup, 2016; Roger et al., 1969), and carbamates (Metcalf, 1971) that contributed to their activities. Based on these considerations, it was hypothesised that the products of these coupling reactions would have comparable or better insecticidal activity.

2. Experimental

2.1 General

All commercially available solvents and chemicals were directly used without further purification. Precoated aluminium backed plates of thin layer chromatography (TLC) (Silica gel 60 F245, Merck KGaA) were used to monitor all reactions. TLC plates were visualised using UV Lamp UVGL-58 and stained with basic $KMnO_4$ solution. Silica gel 60 (100-150 mesh) was used for purification using column chromatography. The organic layers were dried over sodium sulphate and concentrated using a Buchi Switzerland rotavapor R-215. IR spectra were recorded using the Perkin-Elmer FT-IR Model Spectrum 100 series. The NMR spectra were recorded at 500 MHz on a JEOL JNM-ECX500 using $CDCl_3$ as the solvent. Chemical shifts were measured in ppm in relation to the TMS signal. Melting points were measured three times for each compound using a digital Electrothermal IA9000 Series. EIMS spectra were recorded using a Shimadzu QP5050A and HRMS spectra were obtained using an AGILENT 6550 iFunnel Q-TOF.

2.2 Coupling Reactions

2.2.1 General Procedure

Vanillin (**1**) (1.0 mmol) and methyl ferulate (**2**) or methyl sinapate (**3**) (1.0 mmol) were added into phosphate buffer (pH 7.2, 23 mL) and stirred for 10 minutes. The reaction mixture was further treated with HRP (0.4 mg). 1 M of H_2O_2 (1.8 mL) was added slowly into the mixture within 30 minutes and the mixture was continuously stirred for 3 days at room temperature. The reaction was terminated with ethyl acetate (AcOEt) (10 mL) and subsequently washed with 1 M of HCl (3×10 mL) and saturated brine solution (3×30 mL) before being dried, evaporated, and purified (Wakimoto et al., 2009).

Methyl 5-((*E*)-2-(methoxycarbonyl)vinyl)-2,3-dihydro-2-(4-hydroxy-3-methoxyphenyl)-7-methoxybenzofuran-3-carboxylate (**4**): R_f 0.25 (hexane:AcOEt, 3:2); white solid; yield, 20%; mp 143-144°C (lit, 151-152°C) (Isman, 1993); ν_{max} (UATR, cm^{-1}) 3381, 2953, 1725, 1631, 1604, 1436, 1158, 1137; δ_H (500 MHz, $CDCl_3$, ppm) 7.63 (d, 1H, *J* 16.0 Hz, C*H*=C), 7.17 (s, 1H, *H*-Ar), 7.01 (s, 1H, *H*-Ar), 6.90 (d, *J* 8.0 Hz, 1H, *H*-

DOI:https//doi.org/10.22452/mjs.vol42no1.2
Malaysian Journal of Science 42(1): 7-16 (February 2023)

Ar), 6.89 (s, 1H, *H*-Ar), 6.88 (d, *J* 8.0 Hz, 1H, *H*-Ar), 6.30 (d, *J* 16.0 Hz, 1H, C*H*=C), 6.09 (d, *J* 8.0 Hz, 1H, C*H*-C), 5.70 (br. s, 1H, O*H*), 4.33 (d, *J* 8.0 Hz, 1H, C*H-C*), 3.90 (s, 3H, CH_3), 3.86 (s, 3H, CH_3), 3.82 (s, 3H, CH_3), 3.79 (s, 3H, CH_3); δ_C (125 MHz, $CDCl_3$, ppm) 170.7, 167.6, 150.0, 146.7, 146.1, 145.5, 144.7, 131.4, 128.6, 125.7, 119.4, 117.9, 115.6, 114.5, 112.2, 108.7, 87.5, 56.1, 56.0, 55.5, 52.8, 51.6; *m/z* (HRMS) 414.1321 $[M]^+$ (Calcd for $C_{22}H_{22}O_8$: 414.1315), 437.1215 $[M+Na]^+$ (Calcd for $C_{22}H_{22}O_8Na$: 437.1212).

Dimethyl-1,2-dihydro-6-hydroxy-1-(4-hydroxy-3-methoxyphenyl)-7-methoxynaphthalene-2,3-dicarboxylate (**5**): R_f 0.30 (hexane:AcOEt, 3:2); brown solid; yield, 3%; mp 136-138°C; ν_{max} (UATR, cm^{-1}) 3405, 2944, 1703, 1509, 1215; δ_H (500 MHz, $CDCl_3$, ppm) 7.64 (s, 1H, C*H*=C), 6.82 (s, 1H, H-Ar), 6.70 (d, *J* 8.0 Hz, 1H, *H*-Ar), 6.68 (s, 1H, *H*-Ar), 6.60 (d, *J* 2.3 Hz, 1H, *H*-Ar), 6.39 (dd, *J* 2.3, 8.0 Hz, 1H, *H*-Ar), 4.53 (d, *J* 2.3 Hz, 1H, C*H*-C), 3.96 (d, *J* 3.4 Hz, 1H, C*H*-C), 3.89 (s, 3H, CH_3), 3.77 (s, 3H, CH_3), 3.73 (s, 3H, CH_3), 3.61 (s, 3H, CH_3); δ_C (125 MHz, $CDCl_3$, ppm) 172.9, 167.1, 147.7, 146.4, 145.8, 144.4, 137.7, 134.3, 131.2, 123.9, 122.4, 120.4, 115.6, 114.2, 112.2, 110.1, 56.0, 55.8, 52.4, 51.9, 47.2, 45.6; *m/z* (HRMS) 414.1315 $[M]^+$ (Calcd for $C_{22}H_{22}O_8$: 414.1315), 437.1208 $[M+Na]^+$ (Calcd for $C_{22}H_{22}O_8Na$: 437.1212).

(2*E*,3*E*)-Dimethyl 2,3-bis(4-hydroxy-3,5-dimethoxybenzylidene)succinate (**6**): R_f 0.28 (petroleum ether:AcOEt, 2:3); yellow solid; yield, 14%; mp 129-130°C; ν_{max} (UATR, cm^{-1}) 3413, 2944, 1705, 1598, 1510, 1234; δ_H (500 MHz, $CDCl_3$, ppm) 7.81 (s, 2H, 2×C*H*=C), 6.80 (s, 4H, 4×*H*-Ar), 5.77 (br. s, 2H, 2×O*H*), 3.76 (s, 12H, 4×CH_3), 3.66 (s, 6H, 2×CH_3); δ_C (125 MHz, $CDCl_3$, ppm) 167.7, 146.9, 142.5, 136.7, 125.9, 124.7, 107.1, 56.1, 52.4; *m/z* (EIMS) 474 (M^+, $C_{24}H_{26}O_{10}$ requires 474).

(*Z*)-Methyl 2-(4-formyl-2-methoxyphenoxy)-3-(4-hydroxy-3,5-dimethoxyphenyl) acrylate (**7**): R_f 0.43 (hexane:AcOEt, 3:2); white solid; yield, 29%; mp 69-70°C; ν_{max} (UATR, cm^{-1}) 3404, 2928, 1702, 1512, 1260; δ_H (500 MHz, $CDCl_3$, ppm) 9.82 (s, 1H, C*H*O), 7.49 (s, 1H, *H*-Ar), 7.38 (s, 1H, C*H*=C), 7.32 (d, *J* 8.0 Hz, 1H, *H*-Ar), 6.97 (s, 2H, 2×*H*-Ar), 6.85 (d, *J* 8.0 Hz, 1H, *H*-Ar), 5.77 (br. s, 1H, O*H*), 3.98 (s, 3H, CH_3), 3.77 (s, 3H, CH_3), 3.76 (s, 6H, 2×CH_3); δ_C (125 MHz, $CDCl_3$, ppm) 190.7, 163.6, 150.9, 149.4, 146.9, 137.1, 136.9, 131.7, 128.9, 126.3, 123.1, 113.1, 110.2, 107.6, 56.1, 56.0, 52.6; *m/z* (HRMS) 388.1120 $[M]^+$ (Calcd for $C_{20}H_{20}O_8$: 388.1158), 411.0996 $[M+Na]^+$ (Calcd for $C_{20}H_{20}O_8Na$: 411.1056).

Dimethyl-1,2-dihydro-7-hydroxy-1-(4-hydroxy-3,5-dimethoxyphenyl)-6,8-dimethoxynaphthalene-2,3-dicarboxylate (**8**): R_f 0.22 (hexane:AcOEt, 2:3); yellow solid; yield, 14%; mp 181-183°C; ν_{max} (UATR, cm^{-1}) 3437, 2949, 1701, 1600, 1447, 1189, 1096; δ_H (500 MHz, $CDCl_3$, ppm) 7.62 (s, 1H, C*H*=C), 6.68 (s, 1H, *H*-Ar), 6.25 (s, 2H, 2×*H*-Ar), 5.81 (br. s, 1H, O*H*), 5.36 (br. s, 1H, O*H*), 4.97 (s, 1H, C*H*-C), 3.99 (s, 1H, C*H*-C), 3.90 (s, 3H, CH_3), 3.73 (s, 9H, 3×CH_3), 3.62 (s, 6H, 2×CH_3); δ_C (125 MHz, $CDCl_3$, ppm) 172.4, 167.0, 146.8, 144.9, 140.9, 137.6, 133.5, 123.8, 123.4, 122.8, 107.3, 104.3, 60.6, 56.3, 52.5, 51.9, 46.5, 39.4; *m/z* (HRMS) 474.1548 $[M]^+$ (Calcd for $C_{24}H_{26}O_{10}$: 474.1526), 497.1442 $[M+Na]^+$ (Calcd for $C_{24}H_{26}O_{10}Na$: 497.1424).

2.3 Bioassay

C. binotalis larvae (cabbage head caterpillar) that are used in this research were collected from a laboratory colony reared on cabbage plants or using an artificial diet from the Genebank and Seed Centre, Malaysian Agricultural Research and Development Institute (MARDI), Serdang.

The larvicidal activity of the synthesised compounds was assessed with a slight modification using a conventional leaf disc method (Wu et al., 2016). Leaf discs (150 mm in diameter) were trimmed with a cork borer from clean organic cabbage leaves and kept in a moist chamber. The solution of the synthesised compounds and azadirachtin in acetone was prepared at 100 ppm for screening. The leaf discs were immersed in acetone alone or in an acetone solution containing the compounds for 5 seconds before being air dried at room temperature. Ten 2nd instar larvae of *C. binotalis* of the same size (2-3 hours pre-starved) and five treated leaf discs were positioned into the test container and covered with a moistened towel. One container was considered a single replicate and the experiment was conducted with three replicates of each compound (29-32 larvae). The untreated leaves were used as a negative control and the leave treated with azadirachtin was used as the positive control. The number of larvae that died at 24 hours was recorded and the values of corrected mortality (CM) were determined as follows: CM rate (%) = (T – C) × 100/(100% – C), where C is the mortality rate of the negative control and T is the mortality rate of the treated *C. binotalis* (Ren et al., 2020). When larvae did not react to the stimulation or did not move after being touched, they were considered dead. All the screened compounds with less than a 50% of mortality rate are considered not active and will not be further subjected to LD_{50} (lethal dose causes 50% mortality) determination.

The toxicity of the active compounds was tested in acetone at up to five different concentrations ranging from 0 to 15 ppm. The LD_{50}, 95% confidence limits (CLs), the slope of the concentration-mortality curve, and the standard error of the slope were calculated using Polo Plus software by probit analysis. The differences between LD_{50} values were considered significant if 95% of the CLs did not overlap.

DOI:https//doi.org/10.22452/mjs.vol42no1.2
Malaysian Journal of Science 42(1): 7-16 (February 2023)

3. Results and Discussion

3.1 Enzymatic Coupling Reaction

The reaction applied for the vanillin (**1**) and methyl cinnamate derivatives (**2**) and (**3**) was adapted from Wakimoto et al. (2009). First, both compounds (**2**) and (**3**) were prepared from their respective acids via common Fischer esterification (Juhan et al., 2018). The reaction of vanillin (**1**) and methyl ferulate (**2**) with HRP yielded compounds (**4**) and (**5**), whereas the reaction with methyl sinapate (**3**) produced compounds (**6**-**8**). All compounds were obtained through the homocoupling of methyl ferulate (**2**) or methyl sinapate (**3**) except for compound (**7**) whereby this compound was obtained through heterocoupling of vanillin (**1**) and methyl sinapate (**3**) (Scheme 1). This finding demonstrated that the enzymatic reaction preferred the formation of dihydrobenzofuran neolignan (**4**) and arylnaphthalene type of lignans (**5**, **8**). However, these reactions contributed to a low yield (3-29%) with a high recovery of starting material even though the reaction time was increased up to three days. Spectroscopic data of lignan (**6**) and 8-O-4' neolignan (**7**) were reported in our previous study (Juhan et al., 2018) while the others were discussed in this paper and compared with data from the literature.

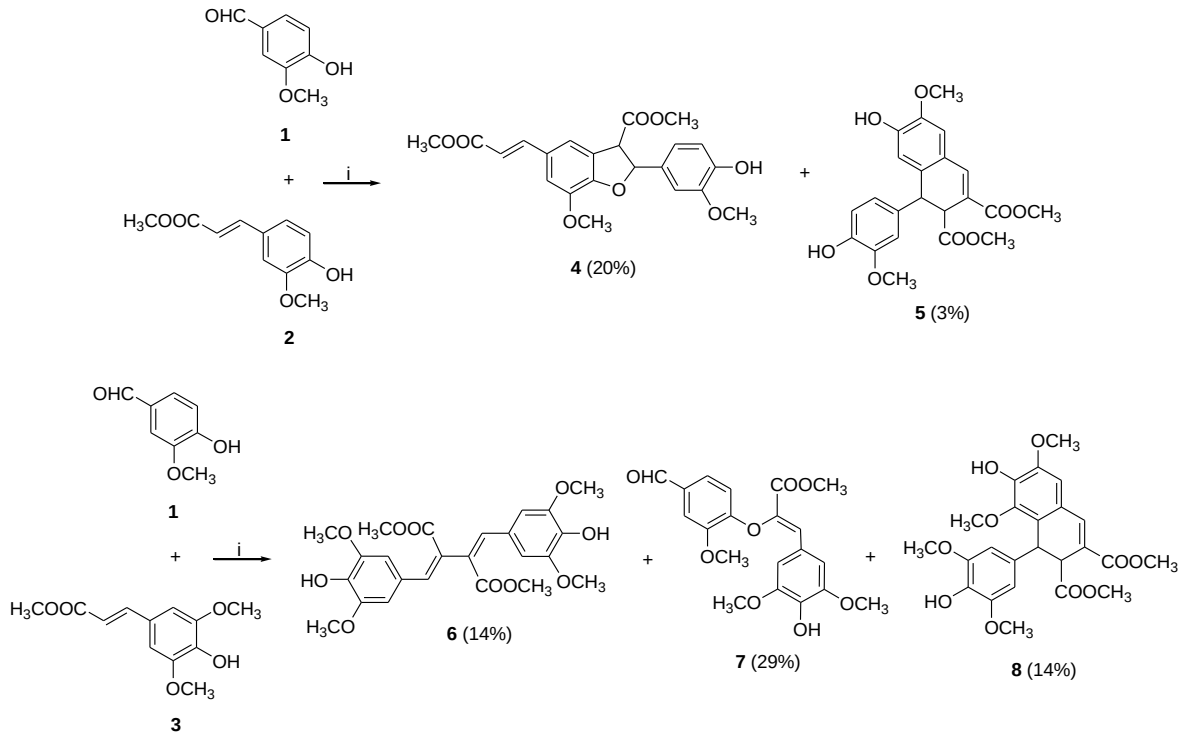

Scheme 1. The enzymatic coupling reaction between vanillin (**1**) with methyl ferulate (**2**) or methyl sinapate (**3**). Reagents and conditions: i) HRP, 1 M of H_2O_2, phosphate buffer pH7.2, RT, 3d. All of the synthesised compounds were separated using column chromatography. The same lignan (**6**) and neolignan (**7**) were also produced in the previous coupling reaction with a palladium catalyst (Figure 1).

All synthesised compounds in this work (**4**-**8**) and all compounds synthesised earlier (**9**-**12**) using palladium-catalysed coupling reaction (Juhan et al., 2018) (Figure 1) were further studied for their larvicidal activity. To the best of our knowledge, no research on the larvicidal activity of these synthesised compounds **(4-12)** against *C. binotalis* has been reported.

Neolignan (**4**) and lignan (**5**) were obtained both as white and brown solids with a melting point of 145-144°C and 136-138°C, respectively. The IR spectrum for both compounds showed the presence of hydroxyl groups with a broad band at 3381 cm^{-1} and 3405 cm^{-1}, whereas the band for carbonyl of esters appeared at 1725 cm^{-1} and 1703 cm^{-1}, respectively. Both neolignan (**4**) and lignan (**5**) shared the same molecular formula of $C_{22}H_{22}O_8$, which their HRMS analyses gave *m/z* 414.1324 $[M]^+$ and *m/z* 414.1315 $[M]^+$ (Calculated for $C_{22}H_{22}O_8$ requires 414.1315).

DOI:https//doi.org/10.22452/mjs.vol42no1.2
Malaysian Journal of Science 42(1): 7-16 (February 2023)

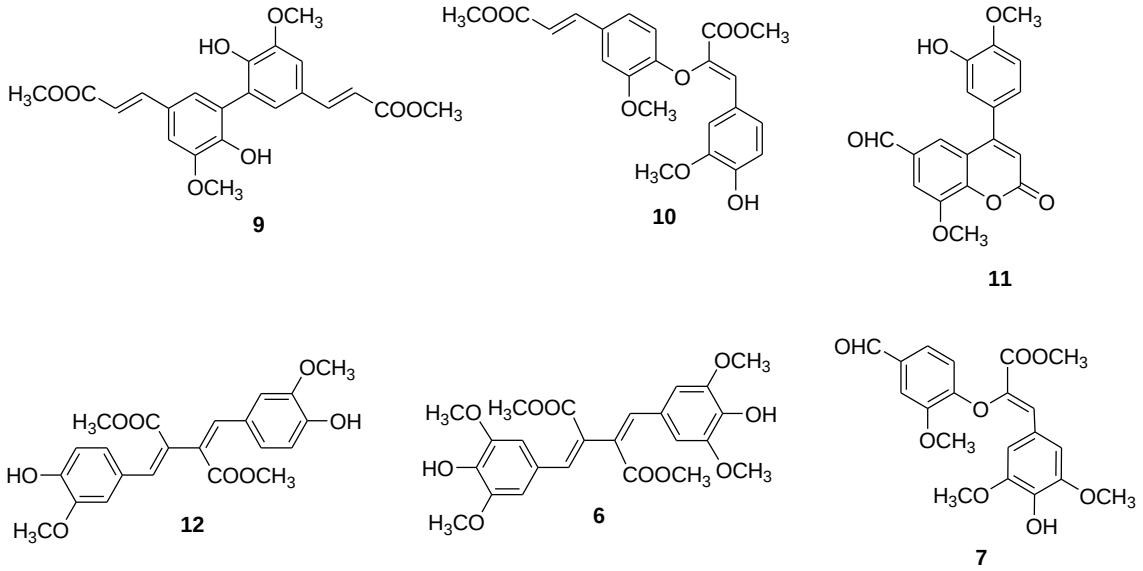

Figure 1. Neolignans (**7**, **9**-**10**), coumarin (**11**), and lignans (**6**, **12**) were synthesised via a palladium-catalysed coupling reaction of vanillin (**1**) with methyl ferulate (**2**) or methyl sinapate (**3**) (Juhan et al., 2018).

In both ^{1}H NMR spectra, two singlets of methoxy protons and two singlets of methyl protons of ester appeared at δ 3.90, 3.86, 3.82, and 3.79 ppm for compound (**4**), whereas at δ 3.89, 3.77, 3.73, and 3.61 ppm for compound (**5**). Two sets of a doublet in (**4**) appeared at δ 4.33 ppm and 6.09 ppm corresponding to H3 and H2, and another two sets (J=16 Hz) were presented at δ 6.30 ppm and 7.63 ppm referring to the two *trans* protons of H2'' and H1''. Two doublets of H1 and H2 in (**5**) were observed at δ 4.53 ppm and 3.96 ppm. It was confirmed that compound (**5**) was bonded and cyclised through the alkene functional group by the signal of only one proton observed at δ 7.64 ppm (s) representing H4. Besides that, compound (**5**) showed two broad peaks at δ 5.51 ppm and 5.84 ppm representing hydroxyl groups attached to a benzene ring at C7 and C4' while only one OH peak appeared at δ 5.70 ppm for compound (**4**).

The ^{13}C NMR supports the structure of the compounds by showing two carbons in the downfield region at δ 170.7 ppm and 167.6 ppm for neolignan (**4**) and δ 172.9 ppm and 167.1 ppm for lignan (**5**) referring to the two carbonyl esters in each compound. The formation of dyhdrobenzofuran ring was established by the presence of signals at δ 87.5 ppm and 56.0 ppm for C2 and C3, respectively. In contrast, the naphthalene type of lignan (**5**) was represented by the peaks observed at δ 137.7 ppm (C4), 47.2 ppm (C2), and 45.6 ppm (C1). All NMR data of compound (**4**) agree with the data from Moussouni et al. (2011).

The HMBC analysis of compound (**4**) also supports the proposed structure by showing correlations between H2 with C3, C1', C2', and C6'. On the other hand, there were also correlations between H3 with C2, C3a, and C1'. The HMBC analysis of compound **5** showed correlations between H1 with C2, 2-$COOCH_3$, C3, C4a, C8, C1', and C6'. Other correlations between H2 with C1, 2-$COOCH_3$, C3, 3-$COOCH_3$, C4a, and C1' were also observed (Figure 2).

Lignan (**8**) with a melting point of 181-183°C was obtained as a yellow solid formed by the free radical coupling mechanism. This compound was isolated previously from the ethanol extract of rapeseed (*Brassica napus L.*) and is known as dimethyl (±)-thomasidioate by Fang et al. (2012). The IR analysis for compound (**8**) revealed a broad band at 3437 cm^{-1} referring to a hydroxyl group while the presence of a carbonyl aldehyde absorption was observed at 1701 cm^{-1}. Compound (**8**) has a molecular formula of $C_{24}H_{26}O_{10}$ as indicated by analysis of its HRMS with *m/z* 474.1548 $[M]^+$ (calculated for $C_{24}H_{26}O_{10}$ requires 474.1526). Therefore, compound (**8**) is thus confirmed to be a combination of two methyl sinapate (**3**) units.

The integration of the ^{1}HNMR spectrum presented one proton at δ 6.68 ppm belonging to H5 for the first unit of methyl sinapate (**3**). Two protons appeared as singlets (δ 6.25 ppm) attributed to the symmetrical H2' and H6' in the second unit of methyl sinapate (**3**) suggesting bonds between C8a and C1. An olefinic proton (H4) was observed at δ 7.62 ppm while another two protons assigned to H2 and H1 appeared at δ 3.99 ppm and 4.97 ppm, respectively. In support of the assignments, ^{13}C NMR analysis depicted two carbon signals at δ 39.4 ppm and 46.5 ppm corresponding to C1 and C2, respectively. Two carbonyl esters are seen at δ 172.4 ppm and 167.0 ppm. NMR data of this compound agreed with the previously reported data (Fang et al., 2012).

DOI:https//doi.org/10.22452/mjs.vol42no1.2
Malaysian Journal of Science 42(1): 7-16 (February 2023)

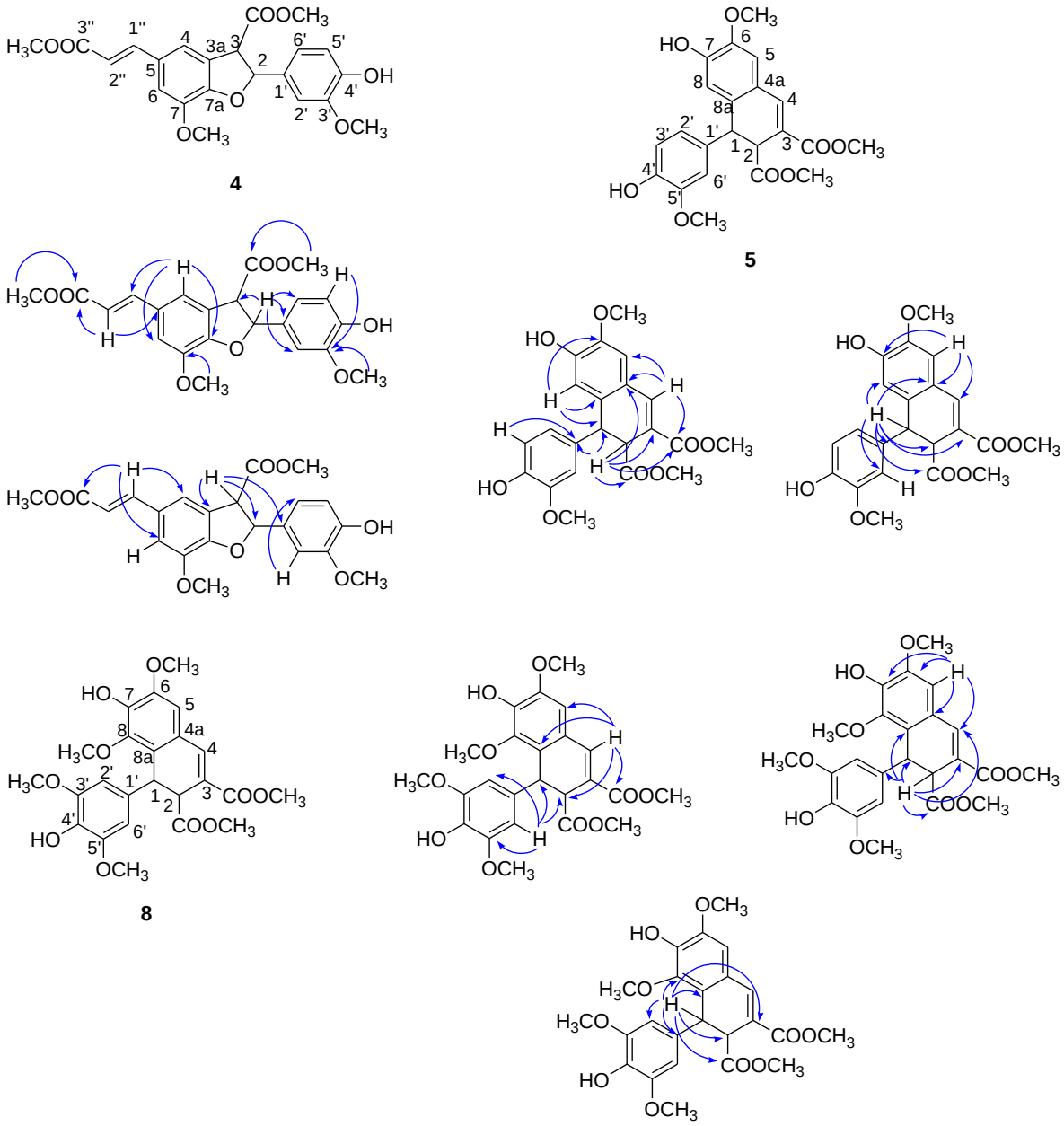

Figure 2. HMBC correlations of compounds **4-5** and **8**.

The HMBC measurement of (**8**) exhibited correlations between H1 with C2, 2-$COOCH_3$, C3, C8, C8a, C1', C2', and C6' thus rationalised the position of C1 to the ring. The correlations between H2 with C1, C1', 2-$COOCH_3$, C3, C4, and C8a, and H4 with C2, 3-$COOCH_3$, C5, and C8a supported the proposed structure. Besides that, the benzene protons of H2' and H6' showed a correlation with C3', C5', C1, and C2 meanwhile the benzene proton of H5 was correlated with C4, C4a, C6, and C7 (Figure 2). With all these findings, it can be deduced that the bond between the two units of methyl sinapate (**3**) forms a naphthalene type of lignan.

3.2 Larvicidal Activity

At a concentration of 100 ppm, 5,5-neolignan (**9**), 8-O-4'-neolignan (**10**), coumarin (**11**), lignans (**6**, **12**), and dihydrobenzofuran neolignan (**4**) demonstrated strong activity with a mortality rate of more than 90% (Table 1). It is worth noting that the presence of two ester groups in the structures is important for larvicidal activity. This hypothesis was supported by comparisons with commercial insecticides azadirachtin and toosendanin, both of which have three and two ester groups, respectively. Among the larva species

DOI:https//doi.org/10.22452/mjs.vol42no1.2
Malaysian Journal of Science 42(1): 7-16 (February 2023)

tested with these two standards are *Actebia fennica*, *Mamestra configurata*, *Malanchra picta*, *S. litura* (Isman, 1993), and *S. frugiperda* (Céspedes et al., 2015). Other commercial insecticides with ester groups, such as organophosphates (malathion and diazinon) and carbamates (methomyl), are used to control the fall armyworm, *S. frugiperda* (Yu, 1992) and the addition of an ester group to podophyllotoxin against the oriental armyworm, *M. separata* (Xu & Xiao, 2009) also proved this finding.

Table 1. Larvicidal screening results of synthesised compounds (4-12) and against the 2nd instar larvae of *C. binotalis* at a concentration of 100 ppm for 24 hours of exposure.

Compound	Corrected Mortality Rate (%)[a]
Acetone[b]	0.00
Azadirachtin[c]	100.00 ± 0.00
9	96.66 ± 5.77
10	93.10 ± 0.00
11	100.00 ± 0.52
12	90.30 ± 5.53
4	93.33 ± 5.77
5	0.00
6	96.77 ± 5.25
7	50.06 ± 3.23
8	51.72 ± 5.77

[a] Data are expressed as means ± SE from experiments with three replicates. Corrected as Xu et al., 2020 (Ren et al., 2020). [b] Negative control. [c] Positive control.

Compound (**10**) was observed to have good activity compared to moderate activity seen in compound (**7**) with mortality rates of 93.10% and 50.06%, respectively. The structural differences between these two neolignans demonstrated that the presence of extra ester groups in compound (**10**) made it more active in terms of larvicidal activity. Other findings revealed that uncyclized lignans (**6**, **12**) were more active with mortality rates of 90.3% and 96.77%, respectively compared to the cyclised lignans (**5**, **8**) with mortality rates of 0.00% and 51.72% (Table 1). It was thought that the presence of more double bonds in the uncyclised lignans (**6**, **12**) resulted in increased larval mortality.

When similar structures of lignans as seen in compounds (**5**) and (**8**) were compared, it was discovered that compound (**8**) has higher larvicidal activity than compound **(5**) due to the extra methoxy groups (Table 1). The presence of a methoxy group has been reported to increase podophyllotoxin's insecticidal activity against *P. rapae* L. 5th instar larvae (Di et al., 2007). It was also discovered that the presence of two methoxy groups in methyleugenol increased its activity against *S. litura* (Bhardwaj et al., 2010). Coumarin (**11**), like azadirachtin, demonstrated the highest activity with 100% larvae mortality. This finding indicated that the presence of a hydroxyl group in the structure could increase bioactivity. Previous research found that coumarin derivatives with hydroxyl groups had the most potent insecticidal activity against *Musca domestica* adults and *Aedes albpictus* 4th instar larvae (Wang et al., 2011).

Table 2. Toxicity of compounds (**4**), (**6**), and (**9**-**12**) against the 2nd instar larvae of *C. binotalis*.

Compound	Total insect used	Slope ± SE	LD_{50} (mg/L) (95% CL)[a]	TR[b]
Azadirachtin	197	1.728 ±0.460	2.818 (1.213-4.086)	1.7
9	182	3.288 ± 0.584	3.537 (2.823-4.193)	2.1
10	181	2.080 ± 0.542	2.218 (1.088-2.988)	1.3
11	182	5.326 ± 0.906	4.269 (2.488-5.515)	2.5
12	182	3.097 ± 0.766	4.673 (3.786-6.166)	2.8
4	152	4.499 ± 1.559	9.849 (8.297-15.144)	5.9
6	150	2.107 ± 0.520	1.678 (0.968-2.335)	1

[a] Where 95% of CLs do not overlap, LC_{50} values differ significantly. [b] Toxicity ratio (TR) = LD_{50} of a compound / LD_{50} of compound (**6**).

All compounds with high mortality rates were subjected to LD_{50} determination (Table 2). The results showed that all compounds were toxic to *C. binotalis* larvae. The most active compounds were 8-O-4'-neolignan (**10**) and lignan (**6**) with LD_{50} values of 2.218 mg/L and 1.678 mg/L, respectively. These values are lower than the commercial standard azadirachtin (LD_{50} = 2.818 mg/L). Compound (**6**) outperformed azadirachtin in terms of larvicidal activity by 1.6 times. In comparison, compound (**10**) has one double bond and one oxygen atom, whereas compound (**6**) has two double bonds between two phenyl groups to form a continuous long-conjugated double bond. These distinct properties, combined with the presence of methoxy (Di et al., 2007), ester (Che et al., 2013), and hydroxyl (Gua et al., 2022) groups in the structures enhanced their larvicidal activity.

DOI:https//doi.org/10.22452/mjs.vol42no1.2
Malaysian Journal of Science 42(1): 7-16 (February 2023)

When compared to the standard, compounds (**9**), (**11**), and (**12**) showed significant toxic effects with LD_{50} values of 3.537 mg/L, 4.269 mg/L and 4.673 mg/L, respectively (Table 2). Compound (**4**) was found to be the least toxic among the studied compounds due to the separated conjugated system by the formation of the dihydrofuran ring. The presence of a methyl cinnamate fragment attached to a dihydrofuran ring likely contributed to its low toxicity as reported for methyl 4-methoxycinnamate against *S. litura* (Bhardwaj et al., 2010).

4. Conclusion

Five coupling products, 8-O-4'-neolignan (**7**), two arylnaphthalene lignans (**5, 8**), aryldihydrobenzofuran neolignan (**4**), and lignan (**6**) were synthesised via enzymatic coupling reactions. In comparison, all synthesised compounds and four chemical-catalysed coupling products (**9-12**) were screened against *C. binotalis* larvae in which seven compounds were active and proceeded with LD_{50} identification. 8-O-4'-Neolignan (**10**) and lignan (**6**) showed the strongest larvicidal activities with LD_{50} lower than the standard azadirachtin. Both compounds may be effective to conventional synthetic insecticides in the pest control of *C. binotalis*.

5. Acknowledgement

We are grateful for the research facilities provided by the Department of Chemistry, Faculty of Science, Universiti Putra Malaysia, and the Malaysian Agricultural Research and Development Institute (MARDI). The authors also sincerely thank the FRGS (Vote No. 5524651) and the Geran Putra (Vote No. 9666700) for the research funding.

6. References

Akashe, M. M., Pawade, U. V., & Nikam, A. V. (2018). Classification of pesticides: A review. *Int. J. Res. Ayurveda Pharm.*, *9*(4), 144-150.

Ayil-Gutiérrez, B. A., Villegas-Mendoza, J. M., Santes-Hernández, Z., Paz-González, A. D., Mireles-Martínez, M., Rosas-García, N. M., & Rivera, G. (2015). Ruta graveolens extracts and metabolites against *Spodoptera frugiperda*. *Nat. Prod. Comm.*, 10, 1955-1958.

Bhardwaj, A., Tewary, D. K., Kumar, R., Kumar, V., Sinha, A. K., & Shanker, A. (2010). Larvicidal and structure-activity studies of natural phenylpropanoids and their semisynthetic derivatives against the tobacco armyworm *Spodoptera litura* (F_{AB}.) (Lepidoptera: Noctuidae). *Chemistry & Biodiversity*, *7*(1), 168-177.

Céspedes, C. L., Martinez-vázquez, M., Calderón, J. S., Salazar, J. R., & Eduardo, A. (2015). Insect growth regulatory activity of some extracts and compounds from *Parthenium argentatum* on fall armyworm *Spodoptera frugiperda*. *A Journal of Biosciences*, *56*, 95-105.CFR (Code of Federal Regulations). Title 40 CFR Part 156 - Labeling Requirements for Pesticides and Devices. Retrieved from https://www.ecfr.gov/current/title-40/chapter-I/subchapter-E/part-156. Accessed 14 July 2022.

Che, Z., Yu, X., Zhi, X., Fan, L., Yao, X., & Xu, H. (2013). Synthesis of novel 4α-(acyloxy)-2'(2',6')-(di)halogenopodophyllotoxin derivatives as insecticidal agents. *Journal of Agricultural and Food Chemistry*, *61*(34), 8148-8155.

Di, X., Liu, Y., Liu, Y., Yu, X., Xiao, H., Tian, X., & Gao. R. (2007). Synthesis and insecticidal activities of pyridine ring derivatives of podophyllotoxin. *Pesticide Biochemistry and Physiology*, *89*, 81-87.

Fang, J., Reichelt, M., Kai, M., & Schneider, B. (2012). Metabolic profiling of lignans and other secondary metabolites from rapeseed (*Brassica napus* L.). *J. Agric. Food Chem.*, *60*, 10523–10529.

González-Coloma, A., Escoubas, P., Mizutani, J., & Lajide, L. (1994). Insect growth inhibitors from *Machilus japonica*. *Phytochemistry*, *35*(3), 607-610.

Guo, S-S., Pang, X., Wang, Y., Geng, Z-F., Cao, J-Q., Liang, J-Y., Deng, Z-W., & Du, S-S. (2020). Chemical constituents isolated from stems of *Schisandra chinensis* and their antifeedant activity against *Tribolium castaneum*. *Natural Product Research*, *34*(18), 2595-2601.

Harmatha, J., & Dinan, L. (2003). Biological activities of lignans and stilbenoids associated with plant-insect chemical interaction. *Phytochemistry Reviews 2*, 321-330.

Hashim, N., & Ibrahim, Y. B. (2003). Efficacy of entomopathogenic fungi, *Paecilomyces fumosoroseus*, *Beauveria bassiana* and *Metarhizium anisopliae* var. majus against *Crocidolomia binotalis* (Lepidoptera; Pyralidae). *Pertanika J. Trop. Agric. Sci.*, *26*, 103-108.

Hashim, N., Ibrahim, Y. B., & Tan, Y. H. (2002). Electron microscopy of entomopathogenic fungal invasion on the cabbage-heart caterpillar *Crocidolomia binotalis* Zeller (Lepidoptera: Pyralidae). *Asean J Sci Technol Dev*, *19*, 111-125.

Hikal, W. M., Baeshen, R. S., & Said-Al Ahl, H. A. H. (2017). Botanical insecticide as simple extractives for pest control. *Cogent Biology*, *3*(1), 1-16.

DOI:https//doi.org/10.22452/mjs.vol42no1.2
Malaysian Journal of Science 42(1): 7-16 (February 2023)

Hubbard, M., Hynes, R. K., Erlandson, M., & Bailey, K. L. (2014). The biochemistry behind biopesticide efficacy. *Sustain. Chem. Process*, *2*(18), 1-8.

IRAC (Insecticide Resistance Action Committee). The IRAC Mode of Action Classification. Retrieved from https://irac-online.org/mode-of-action. Accessed 14 July 2022.

Isman, M. B. (1993). Growth inhibitory and antifeedant effects of azadirachtin on six noctuids of regional economic importance. *J. Pestic. Sci.*, *38*, 57-63.

Isman, M. B. (2006). Botanical insecticides, deterrents and repellents in modern agriculture and an increasing regulated world. *Annual Review of Entomology*, *51*(1), 45-66.

Issakul, K., Jatisatienr, A., Pawelzik, E., & Jatisatienr, C. (2011). Potential of *Mammea siamensis* as a botanical insecticide: Its efficiency on diamondback moth and side effects on non-target organisms. *J. Med. Plant. Res.*, *5*, 2149-2156.

Juhan, S. F., Mohd Nor, S. M., Kassim, N. K., Mohd Faudzi, S. M., & Mat Ali, M. S. (2018). One-step synthesis of new derivatives of 4-arylcoumarins and neolignans. *Chemistry Research Journal*, *3*(4), 85-97.

Kannan, M., Vijayaraghavan, C., Jayaprakash, S. A., & Uthamsamy, S. (2011). Studies on the biology and toxicity of newer insecticide molecules on cabbagehead caterpillar, *Crocidolomia binotalis* (Zeller) (Lepidoptera: Pyralidae) in India. *The 6th International Workshop on Management of the Diamondback Moth and Other Crucifer Insect Pests*, 31-37.

Kilani, M. S., Morakchi, G. H., & Sifi, K. (2021). Azadirachtin-based insecticide: Overview, risk assessments, and future directions. *Front. Agron.*, *3*(32), 1-13.

Kirst, H. (2010). The spinosyn family of insecticides: realizing the potential of natural products research. *J Antibiot*, *63*, 101–111.

Lewis, S. E., Silburn, D. M., Kookana, R. S., & Shaw, M. (2016). Pesticide behavior, fate, and effects in the Tropics: An overview of the current state of knowledge. *Journal of Agricultural and Food Chemistry, 64*(20), 3917-3924.

Li, Y., Wei, J., Fang, J., Lv, W., Ji, Y., Aioub, A. A., Zhang, J., & Hu, Z. (2019). Insecticidal activity of four lignans isolated from *Phryma leptostachya*. *Molecules, 24*, 1976.

Lim, G. S., Sivapragasam, A., & Loke, W. H. (1996). Crucifer insect pest problems: trends, issues and management strategies. Proceedings: *The Management of Diamondback Moth and Other Crucifer Pests*, 3-16.

Lin, M., Yang, S., Huang, J., & Zhou, L. (2021). Insecticidal triterpenes in Meliaceae: Plant species, molecules and activities: Part Ⅰ (*Aphanamixis-Chukrasia*). *Int J Mol Sci.*, *22*(24), 1-33.

Metcalf, R. L. (1971). Structure-activity relationships for insecticidal carbamates. *Bull World Health Organ.*, *44*(1-3), 43-78.

Moussouni, S., Saru, M. L., Ioannou, E., Mansour, M., Detsi, A., Roussis, V., & Kefalas, P. (2011). Crude peroxidase from onion solid waste as a tool for organic synthesis. Part II: Oxidative dimerization-cyclization of methyl *p*-coumarate, methyl caffeate and methyl ferulate. *Tetrahedron Lett.*, *52*, 1165-1168.

Ng, L. T., Yuen, P. M., Loke, W. H., & Azizol, A. K. (2003). Effects of *Azadirachta excelsa* on feeding behavoiur, body weight and mortality of *Crocidolomia binotalis* (Zeller) (Lepidoptera: Pyralidae). *J Sci Food Agric*, *83*, 1327-1330.

Ooi, P. A. C., & Kelderman, W. (1979). The biology of three common pests of cabbages in Cameron Highland, Malaysia. *Malaysian Journal of Agriculture*, *52*, 85-101.

Rathnayake, L. K., & Northrup, S. H. (2016). Structure and mode of action of organophosphate pesticides: A computational study. *Computational and Theoretical Chemistry*, *1088*, 9-23.

Ren, Z., Lv, M., Li, T., Hao, M., Li, S., & Xu, H. (2020). Construction of oxime ester derivatives of osthole from *Cnidium monnieri*, and evaluation of their agricultural activities and control efficiency. *Pest Manag. Sci.*, *76*, 3560-3567.

Roger, J. C., Upshall, D. G., & Casida, J. E. (1969). Structure-activity and metabolism studies on organophosphate teratogens and their alleviating agents in developing hen eggs with special emphasis on bidrin. *Biochemical Pharmacology*, *18*(2), 373-392.

Sastrosiswojo, S., & Setiawati, W. (1992). Biology and control of *Crocidolomia binotalis* in Indonesia. *Asian Vegetable Research and Development Center, Taipei*, 81-87.

Shan, X., Lv, M., Wang, J., Qin, Y., & Xu, H. (2022). Acaricidal and insecticidal efficacy of new esters derivatives of a natural coumarin osthole. *Industrial Crops and Products*, *182*, 114855.

DOI:https//doi.org/10.22452/mjs.vol42no1.2
Malaysian Journal of Science 42(1): 7-16 (February 2023)

Shepard, B. M., & Schellhorn, N. A. (1994). A *Plutella/Crocidolomia* management program for cabbage in Indonesia. Proceedings: *The Management of Diamondback Moth and Other Crucifer Pests*, 262-266.

Srinivasan, K., & Veeresh, G. K. (1986). The development and comparison of visual damage thresholds for the chemical control of *Plutella xylostella* and *Crocidolomia binotalis* on cabbage in India. *International Journal of Tropical Insect Science*, *7*, 547-557.

Wakimoto, T., Nitta, M., Kasahara, K., Chiba, T., Ye, Y., Tsuji, K., Kan. T., Nukaya, H., Ishiguro. M., Koike, M., Yokoo, Y., & Suwa, Y. (2009). Structure-activity relationship study on α_1-adrenergic receptor antagonists from beer. *Bioorganic and Medicinal Chemistry Letters*, *19*, 5905-5908.

Wang, X., Wei, X., Huang, X., Shen, L., Tian, Y., & Xu, H. (2011). Insecticidal constructure and bioactivities of compounds from *Ficus sarmentosa* var. henryi. *Agricultural Sciences in China*, *10*(9), 1402–1409.

Wang, Y., Zhang, L-T., Zhang, D., Guo, S-S., Xi, C., & Du, S-S. (2020). Repellent and feeding deterrent activities of butanolides and lignans isolated from *Cinnamomum camphora* against *Tribolium castaneum*. *Journal of Chemistry*, 1-7.

Wu, H., Wu, H., Wang, W., Liu, T., Qi, M., Feng, J., Li, X., & Liu, Y. (2016). Insecticidal activity of sesquiterpene lactones and monoterpenoid from the fruits of *Carpesium abrotanoides. Industrial Crops and Products*, *92*, 77-83.

Xiao, X. M., Ji, Z. Q., Zhang, J. W., Shi, B. J., Wei, S. P., & Wu, W. J. (2013). A new lignan from *Phryma leptostachya*. *Chem. Nat. Cmpd*., *49*, 21-23.

Xu, H., & Xiao. X. (2009). Natural products-based insecticidal agents 4. Semisynthesis and insecticidal activity of novel esters of 2-chloropodophyllotoxin against *Mythimna separata* Walker in vivo. *Bioorganic and Medicinal Chemistry Letters*, *21*, 5177-5180.

Yadav, I. C., & Devi, N. L. (2017). Pesticides classification and its impact on human and environment. *Environment Science & Engineering: Vol. 6 Toxicology* (pp.140-158). Studium Press LLC, USA.

Yang, C., Zhi, X., & Xu, H. (2015). Synthesis of benzoxazole derivatives of honokiol as insecticidal agents against *Mythimna separata* Walker. *Bioorganic and Medicinal Chemistry Letters*, *25*, 2217-2219.

Yu. S. J. (1992). Detection and biochemical characterization of insecticide resistance in fall armyworm (Lepidoptera: Noctuidae). *Entomological Society of America*, *85*(3), 675-682.

DOI:https//doi.org/10.22452/mjs.vol42no1.2
Malaysian Journal of Science 42(1): 7-16 (February 2023)

MALAYSIAN JOURNAL OF SCIENCE
MJS
ISSN 1394-3065

Regular Issue

Malaysian Journal of Science 42 (1): 17-31 (February 2023) https://mjs.um.edu.my

A TWO-WAREHOUSE INVENTORY MODEL WITH REWORK PROCESS AND TIME-VARYING DEMAND

Nurnadiah Binti Nurhasril[1a], Dr. Siti Suzlin Binti Supadi[2b] and Prof. Dr. Mohd Bin Omar[3b]

Abstract: A two-warehouse inventory model with deteriorating items and rework process with time-varying demand rate is presented. The last-in-first-out (LIFO) and first-in-first-out (FIFO) policies are considered with the assumption that the holding cost is higher in the rented warehouse (RW) compared to the owned warehouse (OW). The aim of the proposed model is to ascertain the optimum values of time in a production cycle that will minimise the total relevant cost, TRC*. We have utilised Microsoft Excel Solver as a solution tool, in which the generalised reduced gradient (GRG Nonlinear) method has been chosen as the solving method. The result is further verified using the built-in function in the Mathematica software. We observed that given same changes made to the parameters in both the LIFO and FIFO systems, a lower TRC* is obtained in the former. This shall mean that the LIFO system is less expensive than the FIFO system, provided that the holding cost in RW is higher than that in OW. The flow of inventory in the LIFO system suggests that items stored last in the OW will be dispatched first. This is an important factor for manufacturers for ensuring that items are distributed at optimal freshness.

Keywords: *Two-warehouse model, LIFO policy, FIFO policy, rework process, deterioration*

1. Introduction

In the classical inventory model, a single-warehouse system is generally considered where the capacity of the warehouse is known and limited. A single warehouse is more suitable for small businesses in which it is able to accommodate sufficient stock for their operation. However, for large businesses, a supplementary storage facility with a large space capacity is essential to hold excess inventories due to several factors such as temporary discounts and launching of new products. In order to manage the volatility in demand, companies often use rented warehouses (RWs) along with owned warehouses (OWs) to stock inventories sufficiently over time to absorb any fluctuations in demand (Kumar et al., 2018). Therefore, it is essential to focus on the inventory problem with more than just one warehouse, which will make the inventory system hold greater validity and relevance in real-life situations.

Over the years, numerous researchers have considered the two-warehouse system in their inventory models. The two-warehouse inventory model was first introduced by Hartley (1976) with the assumption that the holding cost in RW is greater than that in OW. Sarma (1983) proposed the inventory model with two-level storage and optimum release rule. Goswami et al. (1992) proposed an economic quantity model with two warehouses under time-varying linearly increasing demand. They assumed that transportation costs from RW to OW are proportional to the quantity transported and that items are delivered in an irregular pattern from RW to OW. Panda et al. (2010) also considered two-warehouse inventory models and focused on multiple retailers with price- and stock-dependent demand.

Another common and unrealistic assumption in the classical inventory model is that the received items are of perfect quality. However, in real-life situations, this assumption may not always be true. Realistically, items such as food, cosmetics, medicine, among others deteriorate over time. The existence of deterioration was first considered by Ghare et al. (1963). Rafaat (1991) also conducted a survey on the literature relating to inventory models with deteriorating items. Singh et al. (2013) had further incorporated an imperfect production process where the demand rate is assumed to be time dependent, while the production rate is dependent on the demand rate. Agrawal et al. (2013) considered the presence of deteriorating items in their model and provided the option to choose between a single- or two-warehouse system. They concluded that the cost acquired at OW due to high deterioration rate could be balanced out by purchasing more items to be stored in RW, hence reducing the shortage cost.

Authors information:
[a]Universiti Malaya, 50603, Kuala Lumpur, Faculty of Science, Institute of Mathematical Sciences, Kuala Lumpur, MALAYSIA. E-mail: nadiahhasril@gmail.com[1]
[b]Universiti Malaya, Kuala Lumpur, MALAYSIA. E-mail: suzlin@um.edu.my[2]; mohd@um.edu.my[3]
*Corresponding Author: nadiahhasril@gmail.com; suzlin@um.edu.my

Received: July 3, 2021
Accepted: June 18, 2022
Published: February 28, 2023

DOI:https//doi.org/10.22452/mjs.vol42no1.3
Malaysian Journal of Science 42(1): 17-31 (February 2023)

Throughout the years, several other researchers such as Pakkala et al. (1991), Bankherouf (1997), Lee et al. (2000), Wee et al. (2005), Rong et al. (2008), Lee et al. (2009), Panda et al. (2012), Yadav et al. (2013), Bhunia et al. (2014), Kaliraman et al. (2017), Chakrabarty et al. (2018), Shaikh et al. (2019), Indrajitsingha et al. (2019), Aastha et al. (2020), and Gupta et al. (2020) have considered two-warehouse inventory models for deteriorating items with different types of demand.

It is generally assumed that the RW offers better preserving facilities than the OW; therefore, it charges a higher holding cost (Lee, 2006). The two-warehouse inventory models discussed above naturally adopt the LIFO (last-in-first-out) inventory policy. However, their studies do not focus or highlight the aforementioned point. The inventory policy needs to be further investigated, especially in the handling of deteriorating items.

Motivated from this significant point, Lee (2006) considered the two-warehouse inventory problem for deteriorating items and modified the LIFO model by Pakkala et al. (1992). Items stored later in RW will be utilised prior to those stored in OW in this model. Lee (2006) further proposed a model with a policy that is the opposite of the LIFO phenomenon, known as the FIFO (first-in-first-out) policy. In this model, items that are stored in OW first will be the first to be exhausted. It was concluded that the key in choosing between the two mentioned models are the deterioration rates and holding costs.

Similarly, Xu et al. (2017) considered a constant demand rate with deteriorating items over a finite time horizon in their two-warehouse inventory problem. They compared their model with the LIFO, modified LIFO, and FIFO inventory models and derived the critical conditions of the production cycle number, inventory holding and deterioration costs in the two warehouses.

Unlike other studies on LIFO and FIFO policies, Alamri et al. (2008) proposed a new policy named allocation-in-fraction-out (AIFO). The policy implies that inventory in both warehouses experience simultaneous consumption fractions, which indicate that the items are depleted by the end of the same cycle.

Introducing a rework process in an inventory model would allow the reduction of the costs involved in a production process. Wee et al. (2012) developed an economic production quantity model for deteriorating items with rework and stochastic preventive maintenance time. LIFO policy and lost sales were also considered in their study. Wee et al. (2013) then developed a production model using the FIFO rule for deteriorating items with stochastic preventive maintenance time and rework process. They assumed that the deterioration rates for both serviceable and recoverable items are the same.

Chung et al. (2009) suggested an inventory model that incorporates a two-warehouse system and the existence of defectives due to an imperfect quality production process. The defectives are assumed to be sold as a single batch at a discounted price. Yu (2009) developed an inventory model with deteriorating loss, shortage backordering, and trade credit with the aim to optimise the two-echelon system. A supplier and a distributor are considered in the two-warehouse environment system where the rental cost of the rented warehouse decreases over time. The study implied that coordination among distributors and suppliers is necessary to reduce total costs.

Ghiami et al. (2020) adopted the conventional logic of the OW and RW method into their study. They modelled a two-warehouse supply chain for a deteriorating product involving a retailer and a wholesaler. The retailer's main store or shelf is considered to be the OW, while the back-room for keeping extra stock is the RW. A continuous resupply FIFO policy is applied between the two-warehouses.

Considering the gaps within the study area where the aforementioned factors are considered simultaneously, the aim of this study is to develop a two-warehouse model by incorporating the LIFO and FIFO policies while considering a rework process. Our first approach is to consider an increasing demand rate instead of the commonly used constant demand rate. This approach would allow inventory operators to plan their production accordingly when launching new items into the market. Following the current trend, we could see that a newly launched product will experience a linearly increasing demand rate at the beginning of the launching period to a certain extent. A different approach on the purpose of RW has been incorporated in this paper, where the space is utilised to store finished products from a rework process with special requirements.

The second dilemma we have encountered is that some of the existing studies done have only considered a perfect production process. In other words, the presence of defective items is overlooked. Therefore, we have included a more realistic condition by introducing an imperfect production process, hence producing defective items. Aiming to lower the total relevant cost of the inventory model, a rework process is introduced in this study. In addition, we have proposed to separate perfect items from the defectives and assumed that the items are being repaired or will undergo the rework process only in the RW, once the production period has ended. This would be convenient and beneficial to manufacturers who have limited resources such as machines or operators, as they are

DOI:https//doi.org/10.22452/mjs.vol42no1.3
Malaysian Journal of Science 42(1): 17-31 (February 2023)

able to focus on the production process first and the rework process later.

The final motivating factor would be the commonly used assumption that a storage facility or warehouse has an unlimited capacity. This is unrealistic as a storage space would be quickly filled up during an ongoing production process. Hence, we have included an approach where the OW would have limited capacity. Once the OW has reached its maximum capacity, excess items may be stored in a second warehouse, known as the rented warehouse.

In summary, we have proposed a two-warehouse inventory model with deteriorating items and a rework process for time-varying demand rate problem. The LIFO and FIFO policies are also incorporated in our model.

2. Mathematical Formulations

2.1 Notations

Listed below are the notations used in the models discussed in this paper.

$\boldsymbol{f(t)}$	linearly increasing demand rate $\boldsymbol{f(t) = a + bt}$, where $\boldsymbol{a}$ is the initial inventory level and $\boldsymbol{b}$ is the gradient for the demand function
$\boldsymbol{P}$	constant production rate, units per unit time where $\boldsymbol{P > f(t)}$ for all $\boldsymbol{t}$
$\boldsymbol{R}$	rework process rate, units per unit time where $\boldsymbol{R > f(t)}$ for all $\boldsymbol{t}$
$\boldsymbol{x}$	product defect rate, units per unit time
$\boldsymbol{\alpha}$	deteriorating rate in OW and RW, units per unit time where $\boldsymbol{0 \leq \alpha \leq 1}$
$\boldsymbol{S}$	production setup cost, $ per setup
$\boldsymbol{c_P}$	production processing cost per unit item, $
$\boldsymbol{c_R}$	rework processing cost per unit item, $
$\boldsymbol{c_D}$	deterioration cost per unit item, $
$\boldsymbol{t_i}$	time for each stage
$\boldsymbol{T}$	batch cycle time period
$\boldsymbol{I_i(t)}$	inventory level at time $\boldsymbol{t_i}$ where $\boldsymbol{0 \leq i \leq 5}$ for LIFO policy and $\boldsymbol{0 \leq i \leq 6}$ for FIFO policy
$\boldsymbol{h_1, h_2}$	holding costs per unit item, $ in OW and RW, respectively
$\boldsymbol{W}$	maximum inventory of OW, items
$\boldsymbol{Q}$	maximum inventory of RW, items
$\boldsymbol{TRC}$	total relevant costs per unit time, $

2.2 Assumptions

The following are the assumptions adopted in this study:

(i) Lead time is zero, while the replenishment rate is finite.
(ii) RW has an unlimited capacity.
(iii) The perfect items from the production process are stored in OW, while the imperfect items from the rework process are sent to RW. The inventories in both warehouses decrease due to deterioration of items and fulfilment of demand.
(iv) The rework process is assumed to be perfect since special care is given to the process. Hence, all items that have been reworked are assumed to be perfect. The total number of reworked items is equal to the total defective items from the normal production process.
(v) The production rate, $\boldsymbol{P}$, and rework rate, $\boldsymbol{R}$, are assumed to be different.

DOI:https//doi.org/10.22452/mjs.vol42no1.3
Malaysian Journal of Science 42(1): 17-31 (February 2023)

2.3 LIFO Policy

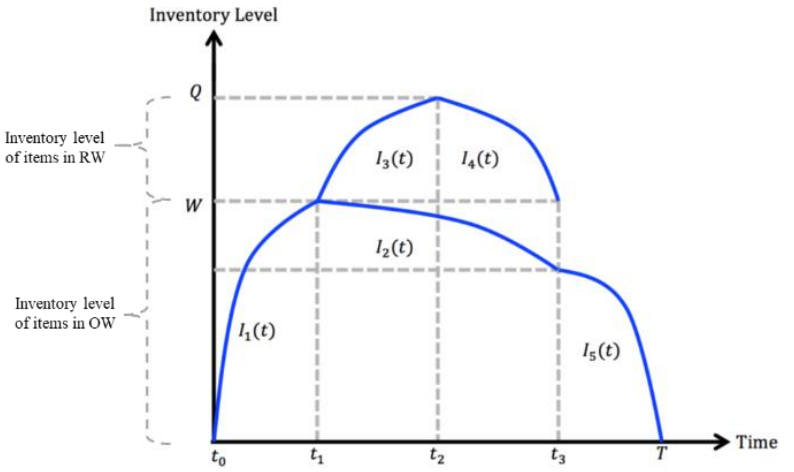

Figure 1. Inventory level with LIFO policy

Figure 1 illustrates the production system of a two-warehouse model with LIFO policy. The inventory stage can be divided into four intervals separated by $\boldsymbol{t_1}$, $\boldsymbol{t_2}$, $\boldsymbol{t_3}$, and $\boldsymbol{T}$.

The production cycle begins at $\boldsymbol{t_0}$, where fulfilment of demand and deterioration occurs simultaneously in the first interval. Since the production process is assumed to be imperfect, defective items are produced in this interval. The defectives are separated and kept aside to be sent to RW at $\boldsymbol{t_1}$. The differential equation representing the change of inventory level in OW during the interval $\boldsymbol{t_0 \leq t \leq t_1}$ is represented by:

$$\frac{dI_1(t)}{dt} = P - x - f(t) - \alpha I_1(t) \qquad ; t_0 \leq t \leq t_1 \qquad (1)$$

By solving differential equation (1) with the initial condition, $\boldsymbol{I_1(t_0) = 0}$, the inventory level in this interval is given as:

$$I_1(t) = \left[\frac{(P - x - a)}{\alpha} + \frac{b}{\alpha^2}\right](1 - e^{-\alpha t}) - \frac{bt}{\alpha} \qquad (2)$$

While defective items were sent to RW to undergo rework process, items in OW are kept idle or on standby during the interval $\boldsymbol{t_1 \leq t \leq t_3}$. However, due to deterioration, items will deplete at the rate $\boldsymbol{\alpha}$ in which the change of inventory level is represented by:

$$\frac{dI_2(t)}{dt} = -\alpha I_2(\mathrm{t}) \qquad ; t_1 \leq t \leq t_3 \qquad (3)$$

Considering the boundary condition $\boldsymbol{I_2(t_1) = W}$, where $\boldsymbol{W}$ represents the maximum capacity of OW, we have the following inventory level:

$$I_2(t) = We^{\alpha(t_1 - t)} \qquad (4)$$

The rework process in RW begins in the interval $\boldsymbol{t_1 \leq t \leq t_2}$, where items are depleted due to deterioration and fulfilment of demand. Hence, the differential equation representing the change of inventory level during this interval is denoted by:

$$\frac{dI_3(t)}{dt} = R - f(t) - \alpha I_3(\mathrm{t}) \qquad ; t_1 \leq t \leq t_2 \qquad (5)$$

Considering the boundary condition $\boldsymbol{I_3(t_1) = 0}$, the inventory level in this interval is denoted by:

$$I_3(t) = \frac{1}{\alpha}(R - a - bt) + \frac{b}{\alpha^2} - \left[\frac{1}{\alpha}(R - a - bt_1) + \frac{b}{\alpha^2}\right] e^{\alpha(t_1 - t)} \qquad (6)$$

DOI:https//doi.org/10.22452/mjs.vol42no1.3
Malaysian Journal of Science 42(1): 17-31 (February 2023)

The rework process in RW ends at $\boldsymbol{t_2}$, in which the reworked items are assumed to be as good as new. The items will now deplete in the interval $\boldsymbol{t_2 \leq t \leq t_3}$ due to deterioration and fulfilment of demand and eventually utilised completely at $\boldsymbol{t_3}$. The change of inventory level is represented by:

$$\frac{dI_4(t)}{dt} = -f(t) - \alpha I_4(\mathrm{t}) \qquad ; \; t_2 \leq t \leq t_3 \tag{7}$$

Considering the boundary condition $\boldsymbol{I_4(t_3) = 0}$, the inventory level in this interval is denoted by:

$$I_4(t) = \left[\frac{1}{\alpha}(a + bt_3) - \frac{b}{\alpha^2}\right] e^{\alpha(t_3 - t)} - \frac{(a + bt)}{\alpha} + \frac{b}{\alpha^2} \tag{8}$$

Once the items in RW are completely depleted at $\boldsymbol{t_3}$, fulfilment of demand and deterioration will be covered by the remaining inventory in OW during the last interval $\boldsymbol{t_3 \leq t \leq T}$. The production cycle ends at $\boldsymbol{T}$, in which the inventory level in OW reaches zero and is completely utilised. The change in inventory level in this interval is denoted by:

$$\frac{dI_5(t)}{dt} = -f(t) - \alpha I_5(\mathrm{t}) \qquad ; \; t_3 \leq t \leq T \tag{9}$$

Considering the boundary condition $\boldsymbol{I_5(T) = 0}$, the inventory level in this interval is denoted by:

$$I_5(t) = \left[\frac{(a + bT)}{\alpha} - \frac{b}{\alpha^2}\right] e^{\alpha(T - t)} - \frac{(a + bt)}{\alpha} + \frac{b}{\alpha^2} \tag{10}$$

Note that items in RW that entered the production cycle last are the items to be utilised first, hence the name 'last-in-first-out' policy.

The maximum inventory of OW, $\boldsymbol{W}$, is governed by equation $\boldsymbol{W = I_1(t_1)}$; hence, we have the following equation:

$$W = \left[\frac{(P - x - a)}{\alpha} + \frac{b}{\alpha^2}\right](1 - e^{-\alpha t_1}) - \frac{bt_1}{\alpha} \tag{11}$$

Next, let $\boldsymbol{A_i}$ denote the time-weighted inventory for each interval, where $\boldsymbol{i = 1, 2, \ldots, 5}$, and it represents the amount of inventory under the curve $\boldsymbol{I_i(t)}$. The following are the respective equations for $\boldsymbol{A_i}$ in the corresponding intervals:

In the interval $\boldsymbol{t_0 \leq t \leq t_1}$,

$$\begin{aligned} A_1 &= \int_0^{t_1} I_1(t)\, dt \\ &= \frac{(P - x)t_1}{\alpha} - \frac{1}{\alpha}\left(at_1 + \frac{b}{2}{t_1}^2\right) + \frac{bt_1}{\alpha^2} + \left(\frac{P - x - a}{\alpha^2} + \frac{b}{\alpha^3}\right)(e^{-\alpha t_1} - 1) \end{aligned} \tag{12}$$

In the interval $\boldsymbol{t_1 \leq t \leq t_3}$,

$$A_2 = \int_{t_1}^{t_3} I_2(t)dt = \frac{W}{\alpha}\left[1 - e^{\alpha(t_1 - t_3)}\right] \tag{13}$$

In the interval $\boldsymbol{t_1 \leq t \leq t_2}$,

$$\begin{aligned} A_3 &= \int_{t_1}^{t_2} I_3(t)dt \\ &= \frac{R}{\alpha}(t_2 - t_1) - \frac{1}{\alpha}\left(at_2 + \frac{b}{2}{t_2}^2\right) + \frac{1}{\alpha}\left(at_1 + \frac{b}{2}{t_1}^2\right) + \frac{b}{\alpha^2}(t_2 - t_1) \\ &\quad + \left[\frac{1}{\alpha^2}(R - a - bt_1) + \frac{b}{\alpha^3}\right]\left[e^{\alpha(t_1 - t_2)} - 1\right] \end{aligned} \tag{14}$$

DOI:https//doi.org/10.22452/mjs.vol42no1.3
Malaysian Journal of Science 42(1): 17-31 (February 2023)

In the interval $\boldsymbol{t_2 \le t \le t_3}$,

$$A_4 = \int_{t_2}^{t_3} I_4(t)dt$$
$$= \frac{1}{\alpha}\left(at_2 + \frac{b}{2}{t_2}^2\right) - \frac{1}{\alpha}\left(at_3 + \frac{b}{2}{t_3}^2\right) + \frac{b}{\alpha^2}(t_3 - t_2)$$
$$+ \left[\frac{1}{\alpha^2}(a + bt_3) - \frac{b}{\alpha^3}\right]\left[e^{\alpha(t_3 - t_2)} - 1\right] \quad (15)$$

In the interval $\boldsymbol{t_3 \le t \le T}$,

$$A_5 = \int_{t_3}^{T} I_5(t)dt$$
$$= \frac{1}{\alpha}\left(at_3 + \frac{b}{2}{t_3}^2\right) - \frac{1}{\alpha}\left(aT + \frac{b}{2}T^2\right) + \frac{b}{\alpha^2}(T - t_3)$$
$$+ \left[\frac{1}{\alpha^2}(a + bT) - \frac{b}{\alpha^3}\right]\left[e^{\alpha(T - t_3)} - 1\right] \quad (16)$$

Assuming that the rework process is perfect, all defective items that have undergone rework will turn into perfect items. Hence, we have the following equation:

$$xt_1 = R(t_2 - t_1)$$
$$t_2 = \frac{(R + x)t_1}{R} \quad (17)$$

The total inventory holding cost is the sum of the holding costs in both OW and RW, which is given as:

$$HC = \frac{h_1}{T}(A_1 + A_2 + A_5) + \frac{h_2}{T}(A_3 + A_4)$$
$$= \frac{h_1}{T}\left\{\frac{1}{\alpha}\left[(P - x)t_1 - \left(at_1 + \frac{b}{2}{t_1}^2\right) + \left(at_3 + \frac{b}{2}{t_3}^2\right) - \left(aT + \frac{b}{2}T^2\right) - \frac{1}{\alpha^2}(a + bt_3) + \frac{b}{\alpha^3}\right.\right.$$
$$\left.\left. - \frac{W}{\alpha}e^{\alpha(t_1 - t_3)} + \left[\frac{1}{\alpha^2}(a + bT) - \frac{b}{\alpha^3}\right]e^{\alpha(T - t_3)}\right]\right\}$$
$$+ \frac{h_2}{T}\left\{\frac{1}{\alpha}\left[R(t_2 - t_1) + \left(at_1 + \frac{b}{2}{t_1}^2\right) - \left(at_3 + \frac{b}{2}{t_3}^2\right)\right] - \frac{R}{\alpha^2}\right.$$
$$\left. + \left[\frac{1}{\alpha^2}(R - a - bt_1) + \frac{b}{\alpha^3}\right]e^{\alpha(t_1 - t_2)} + \left[\frac{1}{\alpha^2}(a + bt_3) - \frac{b}{\alpha^3}\right]e^{\alpha(t_3 - t_2)}\right\} \quad (18)$$

The total number of deteriorated items is:

$$G = \alpha(A_1 + A_2 + A_3 + A_4 + A_5)$$
$$= \left[(P - x)t_1 + R(t_2 - t_1) + W\left[1 - e^{\alpha(t_1 - t_3)}\right] - \left(aT + \frac{b}{2}T^2\right)\right]$$
$$- \frac{1}{\alpha}[P + R - x - b(t_1 - t_3)] + \left(\frac{P - x - a}{\alpha} + \frac{b}{\alpha^2}\right)e^{-\alpha t_1}$$
$$+ \left[\frac{1}{\alpha}(R - a - bt_1) + \frac{b}{\alpha^2}\right]e^{\alpha(t_1 - t_2)} + \left[\frac{1}{\alpha}(a + bt_3) - \frac{b}{\alpha^2}\right]e^{\alpha(t_3 - t_2)} + \left[\frac{1}{\alpha}(a + bT) - \frac{b}{\alpha^2}\right]e^{\alpha(T - t_3)} \quad (19)$$

DOI:https//doi.org/10.22452/mjs.vol42no1.3
Malaysian Journal of Science 42(1): 17-31 (February 2023)

Hence, the total deteriorating cost is given by:

$$
\begin{aligned}
DC &= \frac{c_D G}{T} \\
&= \frac{c_D}{T}\Big\{\Big[(P-x)t_1 + R(t_2-t_1) + W\big[1-e^{\alpha(t_1-t_3)}\big] - \Big(aT + \frac{b}{2}T^2\Big)\Big] \\
&- \frac{1}{\alpha}[P+R-x-b(t_1-t_3)] + \Big(\frac{P-x-a}{\alpha} + \frac{b}{\alpha^2}\Big)e^{-\alpha t_1} \\
&+ \Big[\frac{1}{\alpha}(R-a-bt_1) + \frac{b}{\alpha^2}\Big]e^{\alpha(t_1-t_2)} + \Big[\frac{1}{\alpha}(a+bt_3) - \frac{b}{\alpha^2}\Big]e^{\alpha(t_3-t_2)} \\
&+ \Big[\frac{1}{\alpha}(a+bT) - \frac{b}{\alpha^2}\Big]e^{\alpha(T-t_3)}\Big\}
\end{aligned} \tag{20}
$$

Finally, the total relevant cost per unit time, i.e., $\boldsymbol{TRC}^*$, for the model with LIFO policy is:

$$
\begin{aligned}
TRC(t_1,t_3,T) &= \frac{S}{T} + \frac{c_P P t_1}{T} + \frac{c_R x t_1}{T} \\
&+ \frac{h_1}{T}\Big\{\frac{1}{\alpha}\Big[(P-x)t_1 - \Big(at_1 + \frac{b}{2}{t_1}^2\Big) + \Big(at_3 + \frac{b}{2}{t_3}^2\Big) - \Big(aT + \frac{b}{2}T^2\Big)\Big] - \frac{1}{\alpha^2}(a+bt_3) + \frac{b}{\alpha^3} - \frac{W}{\alpha}e^{\alpha(t_1-t_3)} \\
&\quad + \Big[\frac{1}{\alpha^2}(a+bT) - \frac{b}{\alpha^3}\Big]e^{\alpha(T-t_3)}\Big\} \\
&+ \frac{h_2}{T}\Big\{\frac{1}{\alpha}\Big[R(t_2-t_1) + \Big(at_1 + \frac{b}{2}{t_1}^2\Big) - \Big(at_3 + \frac{b}{2}{t_3}^2\Big)\Big] - \frac{R}{\alpha^2} + \Big[\frac{1}{\alpha^2}(R-a-bt_1) + \frac{b}{\alpha^3}\Big]e^{\alpha(t_1-t_2)} \\
&\quad + \Big[\frac{1}{\alpha^2}(a+bt_3) - \frac{b}{\alpha^3}\Big]e^{\alpha(t_3-t_2)}\Big\} \\
&+ \frac{c_D}{T}\Big\{\Big[(P-x)t_1 + R(t_2-t_1) + W\big[1-e^{\alpha(t_1-t_3)}\big] - \Big(aT + \frac{b}{2}T^2\Big)\Big] - \frac{1}{\alpha}[P+R-x-b(t_1-t_3)] \\
&\quad + \Big(\frac{P-x-a}{\alpha} + \frac{b}{\alpha^2}\Big)e^{-\alpha t_1} + \Big[\frac{1}{\alpha}(R-a-bt_1) + \frac{b}{\alpha^2}\Big]e^{\alpha(t_1-t_2)} + \Big[\frac{1}{\alpha}(a+bt_3) - \frac{b}{\alpha^2}\Big]e^{\alpha(t_3-t_2)} \\
&\quad + \Big[\frac{1}{\alpha}(a+bT) - \frac{b}{\alpha^2}\Big]e^{\alpha(T-t_3)}\Big\}
\end{aligned} \tag{21}
$$

Referring to equation (21), we note that finding the optimal values of $\boldsymbol{t_1}$, $\boldsymbol{t_3}$, and $\boldsymbol{T}$ analytically is extremely tedious. Hence, we have explored alternative methods and obtained the best solution for $\boldsymbol{TRC}$ numerically, which will be discussed in Section 2.5.

2.4 FIFO Policy

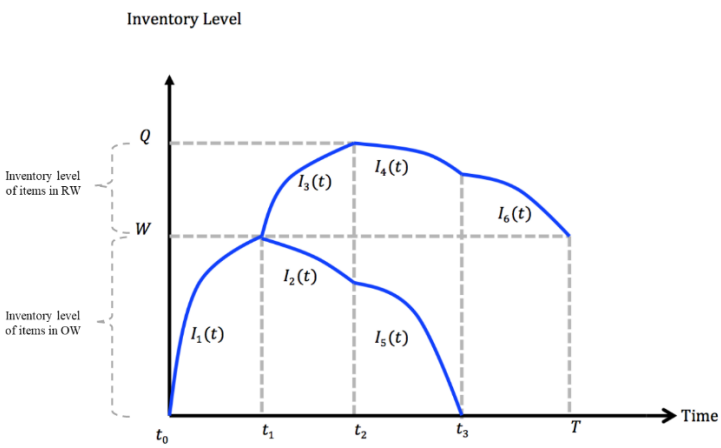

Figure 2. Inventory level with FIFO policy

The FIFO policy is a phenomenon opposite to the LIFO policy. In this system, items in OW which are stored first will be completely utilised first. Figure 2 illustrates the production system of the two-warehouse model with FIFO policy.

Similarly, the production cycle begins at $\boldsymbol{t_0}$ where deterioration and fulfilment of demand occurs simultaneously in the first interval. Since the production process is assumed to be imperfect, defective items are produced in this interval. The defectives are

DOI:https//doi.org/10.22452/mjs.vol42no1.3
Malaysian Journal of Science 42(1): 17-31 (February 2023)

separated and kept aside to be sent to RW at $\boldsymbol{t_1}$. The differential equation representing the change of inventory level in OW during the interval $\boldsymbol{t_0 \leq t \leq t_1}$ is denoted by:

$$\frac{dI_1(t)}{dt} = P - x - f(t) - \alpha I_1(t) \qquad ; \quad t_0 \leq t \leq t_1 \tag{22}$$

By solving differential equation (22) with the initial condition, $\boldsymbol{I_1(t_0) = 0}$, the inventory level in this interval is given as:

$$I_1(t) = \left[\frac{(P - x - a)}{\alpha} + \frac{b}{\alpha^2}\right](1 - e^{-\alpha t}) - \frac{bt}{\alpha} \tag{23}$$

While defective items were sent to RW to undergo rework process, items in OW are kept idle or on standby during the interval $\boldsymbol{t_1 \leq t \leq t_2}$. However, due to deterioration, items will deplete at the rate $\boldsymbol{\alpha}$ in which the change of inventory level is represented by:

$$\frac{dI_2(t)}{dt} = -\alpha I_2(\mathrm{t}) \qquad ; \quad t_1 \leq t \leq t_2 \tag{24}$$

Considering the boundary condition $\boldsymbol{I_2(t_1) = W}$, where $\boldsymbol{W}$ represents the maximum capacity of OW, we have the following inventory level:

$$I_2(t) = We^{\alpha(t_1 - t)} \tag{25}$$

The rework process in RW begins in the interval $\boldsymbol{t_1 \leq t \leq t_2}$, in which items are depleted due to deterioration and fulfilment of demand. The change of inventory level during this interval is represented by:

$$\frac{dI_3(t)}{dt} = R - f(t) - \alpha I_3(\mathrm{t}) \qquad ; \quad t_1 \leq t \leq t_2 \tag{26}$$

Considering the boundary condition $\boldsymbol{I_3(t_1) = 0}$, the inventory level in this interval is denoted by:

$$I_3(t) = \frac{1}{\alpha}(R - a - bt) + \frac{b}{\alpha^2} - \left[\frac{1}{\alpha}(R - a - bt_1) + \frac{b}{\alpha^2}\right]e^{\alpha(t_1 - t)} \tag{27}$$

The rework process in RW ends at $\boldsymbol{t_2}$ where these items will be on standby while demands are fulfilled by items in OW during the interval $\boldsymbol{t_2 \leq t \leq t_3}$. However, items in RW will continue to deplete due to deterioration only. The change of inventory level during this interval is denoted by:

$$\frac{dI_4(t)}{dt} = -\alpha I_4(\mathrm{t}) \qquad ; \quad t_2 \leq t \leq t_3 \tag{28}$$

Considering the boundary condition $\boldsymbol{I_4(t_2) = Q}$, the inventory level in this interval is denoted by:

$$I_4(t) = Qe^{\alpha(t_2 - t)} \tag{29}$$

Simultaneously, items stored in OW will begin depleting to fulfil demand in the interval $\boldsymbol{t_2 \leq t \leq t_3}$ until they are fully depleted at $\boldsymbol{t_3}$. The change of inventory level in this interval is represented by:

$$\frac{dI_5(t)}{dt} = -f(t) - \alpha I_5(\mathrm{t}) \qquad ; \quad t_2 \leq t \leq t_3 \tag{30}$$

Considering the boundary condition $\boldsymbol{I_5(t_3) = 0}$, the inventory level in this interval is denoted by:

$$I_5(t) = \left[\frac{1}{\alpha}(a + bt_3) - \frac{b}{\alpha^2}\right]e^{\alpha(t_3 - t)} - \frac{(a + bt)}{\alpha} + \frac{b}{\alpha^2} \tag{31}$$

DOI:https//doi.org/10.22452/mjs.vol42no1.3
Malaysian Journal of Science 42(1): 17-31 (February 2023)

Once all items in OW are fully depleted at $\boldsymbol{t_3}$, demand will be fulfilled by the remaining inventory in RW during the last interval, while deterioration occurs simultaneously. The production cycle ends at $\boldsymbol{T}$, in which the inventory will be fully depleted. The change in the inventory level is denoted by:

$$\frac{dI_6(t)}{dt} = -f(t) - \alpha I_6(\mathrm{t}) \qquad ; \quad t_3 \le t \le T \tag{32}$$

Considering the boundary condition $\boldsymbol{I_6(T) = 0}$, the inventory level in this interval is denoted by:

$$I_6(t) = \left[\frac{(a+bT)}{\alpha} - \frac{b}{\alpha^2}\right] e^{\alpha(T-t)} - \frac{(a+bt)}{\alpha} + \frac{b}{\alpha^2} \tag{33}$$

The maximum inventory of OW, $\boldsymbol{W}$, is governed by equation $\boldsymbol{W = I_1(t_1)}$. Hence, we have:

$$W = \left[\frac{(P-x-a)}{\alpha} + \frac{b}{\alpha^2}\right](1 - e^{-\alpha t_1}) - \frac{bt_1}{\alpha} \tag{34}$$

and the maximum inventory of RW, $\boldsymbol{Q}$, is governed by equation $\boldsymbol{Q = I_3(t_2)}$, where:

$$Q = \frac{1}{\alpha}(R - a - bt_2) + \frac{b}{\alpha^2} - \left[\frac{1}{\alpha}(R - a - bt_1) + \frac{b}{\alpha^2}\right] e^{\alpha(t_1 - t_2)} \tag{35}$$

Next, let $\boldsymbol{A_i}$ denote the time-weighted inventory for each interval, where $\boldsymbol{i = 1, 2, \ldots, 6}$, and it represents the amount of inventory under the curve $\boldsymbol{I_i(t)}$. The following are the respective equations for $\boldsymbol{A_i}$ in the corresponding intervals:

In the interval $\boldsymbol{t_0 \le t \le t_1}$,

$$\begin{aligned} A_1 &= \int_0^{t_1} I_1(t)\, dt \\ &= \left[\frac{(P-x)}{\alpha} + \frac{b}{\alpha^2}\right] t_1 - \frac{1}{\alpha}\left(at_1 + \frac{b}{2}{t_1}^2\right) + \left(\frac{P-x-a}{\alpha^2} + \frac{b}{\alpha^3}\right)(e^{-\alpha t_1} - 1) \end{aligned} \tag{36}$$

In the interval $\boldsymbol{t_1 \le t \le t_2}$, for OW and RW, respectively

$$A_2 = \int_{t_1}^{t_3} I_2(t)dt = \frac{W}{\alpha}\left[1 - e^{\alpha(t_1 - t_2)}\right] \tag{37}$$

$$\begin{aligned} A_3 &= \int_{t_1}^{t_2} I_3(t)dt \\ &= \left[\frac{R}{\alpha} + \frac{b}{\alpha^2}\right](t_2 - t_1) + \frac{1}{\alpha}\left[\left(at_1 + \frac{b}{2}{t_1}^2\right) - \left(at_2 + \frac{b}{2}{t_2}^2\right)\right] \\ &+ \left[\frac{1}{\alpha^2}(R - a - bt_1) + \frac{b}{\alpha^3}\right]\left[e^{\alpha(t_1 - t_2)} - 1\right] \end{aligned} \tag{38}$$

In the interval $\boldsymbol{t_2 \le t \le t_3}$, for OW and RW, respectively

$$A_4 = \int_{t_2}^{t_3} I_4(t)dt = \frac{Q}{\alpha}\left[1 - e^{\alpha(t_2 - t_3)}\right] \tag{39}$$

$$\begin{aligned} A_5 &= \int_{t_2}^{t_3} I_5(t)dt \\ &= \frac{b}{\alpha^2}(t_3 - t_2) + \frac{1}{\alpha}\left[\left(at_2 + \frac{b}{2}{t_2}^2\right) - \left(at_3 + \frac{b}{2}{t_3}^2\right)\right] \\ &+ \left[\frac{1}{\alpha^2}(a + bt_3) - \frac{b}{\alpha^3}\right]\left[e^{\alpha(t_3 - t_2)} - 1\right] \end{aligned} \tag{40}$$

In the interval $\boldsymbol{t_3 \le t \le T}$,

DOI:https//doi.org/10.22452/mjs.vol42no1.3
Malaysian Journal of Science 42(1): 17-31 (February 2023)

$$A_6 = \int_{t_3}^{T} I_6(t)dt$$
$$= \frac{b}{\alpha^2}(T - t_3) + \frac{1}{\alpha}\left[\left(at_3 + \frac{b}{2}{t_3}^2\right) - \left(aT + \frac{b}{2}T^2\right)\right]$$
$$+ \left[\frac{1}{\alpha^2}(a + bT) - \frac{b}{\alpha^3}\right]\left[e^{\alpha(T-t_3)} - 1\right] \tag{41}$$

Similar to LIFO policy, we have:

$$xt_1 = R(t_2 - t_1)$$
$$t_2 = \frac{(R + x)t_1}{R} \tag{42}$$

The total inventory holding cost is the sum of the holding costs in both OW and RW, which is given as:

$$HC = \frac{h_1}{T}(A_1 + A_2 + A_5) + \frac{h_2}{T}(A_3 + A_4 + A_6)$$
$$= \frac{h_1}{T}\left\{\frac{1}{\alpha}\left[(P - x)t_1 - \left(at_1 + \frac{b}{2}{t_1}^2\right) - \left(at_3 + \frac{b}{2}{t_3}^2\right) + \left(at_2 + \frac{b}{2}{t_2}^2\right) - \frac{1}{\alpha^2}(a + bt_2)\right.\right.$$
$$\left.\left. + \frac{b}{\alpha^3} - \frac{W}{\alpha}e^{\alpha(t_1-t_2)} + \left[\frac{1}{\alpha^2}(a + bt_3) - \frac{b}{\alpha^3}\right]e^{\alpha(t_3-t_2)}\right]\right\}$$
$$+ \frac{h_2}{T}\left\{\frac{1}{\alpha}\left[R(t_2 - t_1) + \left(at_1 + \frac{b}{2}{t_1}^2\right) - \left(at_2 + \frac{b}{2}{t_2}^2\right) + \left(at_3 + \frac{b}{2}{t_3}^2\right) - \left(aT + \frac{b}{2}T^2\right)\right]\right.$$
$$\left. - \frac{1}{\alpha^2}(a + bt_3) + \frac{b}{\alpha^3} - \frac{Q}{\alpha}e^{\alpha(t_2-t_3)} + \left[\frac{1}{\alpha^2}(a + bT) - \frac{b}{\alpha^3}\right]e^{\alpha(T-t_3)}\right\} \tag{43}$$

The deteriorating cost per unit time is given by:

$$DC = \frac{c_D\alpha}{T}(A_1 + A_2 + A_3 + A_4 + A_5 + A_6)$$
$$= \frac{c_D}{T}\left\{Pt_1 - \left(aT + \frac{b}{2}T^2\right) - \frac{1}{\alpha}(\alpha + bt_2) - \frac{1}{\alpha}(a + bt_3) + \frac{2b}{\alpha^2} - We^{\alpha(t_1-t_2)} - Qe^{\alpha(t_2-t_3)}\right.$$
$$\left. + \left[\frac{1}{\alpha}(a + bt_3) - \frac{b}{\alpha^2}\right]e^{\alpha(t_3-t_2)} + \left[\frac{1}{\alpha}(a + bT) - \frac{b}{\alpha^2}\right]e^{\alpha(T-t_3)}\right\} \tag{44}$$

Finally, $\boldsymbol{TRC}^*$ for FIFO policy is:

$$TRC(t_1, t_3, T) = \frac{S}{T} + \frac{c_P P t_1}{T} + \frac{c_R x t_1}{T} + \frac{h_1}{T}\left\{\frac{1}{\alpha}\left[(P - x)t_1 - \left(at_1 + \frac{b}{2}{t_1}^2\right) + \left(at_2 + \frac{b}{2}{t_2}^2\right) - \left(at_3 + \frac{b}{2}{t_3}^2\right)\right]\right.$$
$$\left. - \frac{1}{\alpha^2}(a + bt_2) + \frac{b}{\alpha^3} - \frac{W}{\alpha}e^{\alpha(t_1-t_2)} + \left[\frac{1}{\alpha^2}(a + bt_3) - \frac{b}{\alpha^3}\right]e^{\alpha(t_3-t_2)}\right\}$$
$$+ \frac{h_2}{T}\left\{\frac{1}{\alpha}\left[R(t_2 - t_1) + \left(at_1 + \frac{b}{2}{t_1}^2\right) - \left(at_2 + \frac{b}{2}{t_2}^2\right) + \left(at_3 + \frac{b}{2}{t_3}^2\right)\right.\right.$$
$$\left.\left. - \left(aT + \frac{b}{2}T^2\right)\right] - \frac{1}{\alpha^2}(a + bt_3) + \frac{b}{\alpha^3} - \frac{Q}{\alpha}e^{\alpha(t_2-t_3)} + \left[\frac{1}{\alpha^2}(a + bT) - \frac{b}{\alpha^3}\right]e^{\alpha(T-t_3)}\right\}$$
$$+ \frac{c_D}{T}\left\{Pt_1 - \left(aT + \frac{b}{2}T^2\right) - \frac{1}{\alpha}(a + bt_2) - \frac{1}{\alpha}(a + bt_3) + \frac{2b}{\alpha^2} - We^{\alpha(t_1-t_2)}\right.$$
$$\left. - Qe^{\alpha(t_2-t_3)} + \left[\frac{1}{\alpha}(a + bt_3) - \frac{b}{\alpha^2}\right]e^{\alpha(t_3-t_2)} + \left[\frac{1}{\alpha}(a + bT) - \frac{b}{\alpha^2}\right]e^{\alpha(T-t_3)}\right\} \tag{45}$$

We have utilised the same approach as in Section 2.3 in which the optimal solution of $\boldsymbol{TRC(t_1, t_3, T)}$ is obtained numerically as discussed in the next section.

DOI:https//doi.org/10.22452/mjs.vol42no1.3
Malaysian Journal of Science 42(1): 17-31 (February 2023)

2.5 Solution Procedure

Numerical algorithms for constrained nonlinear optimisation can be widely categorised into gradient-based methods and direct search methods. The first derivatives (gradients) or second derivatives (Hessians) information is used in the gradient search methods, while derivative information is not used in direct search method (Wolfram, 2020).

$\boldsymbol{TRC}^*$ is a non-polynomial equation, where its second derivative with respect to $\boldsymbol{t_1}$, $\boldsymbol{t_3}$, and $\boldsymbol{T}$ is hard to differentiate. Hence, a closed-form solution could not be derived and an optimal solution cannot be guaranteed. In this study, generalised reduced gradient (GRG) has been chosen as the solving method. Hence, the Microsoft Excel Solver is used as a solution tool. GRG converts the constrained problem into an unconstrained one. The extended reduced gradient method, known as the GRG method, accommodates nonlinear inequality constraints. Using this method, a search direction is found in which the current active constraints remain precisely active for any small move.

The following algorithm is used:

1. Set $\boldsymbol{t_0} = \mathbf{0}$.
2. Determine the values of $\boldsymbol{t_1}$, $\boldsymbol{t_3}$, and $\boldsymbol{T}$, which satisfy the following constraints:
   For LIFO,
   $\boldsymbol{I_1(t_0) = 0, I_1(t_1) = I_2(t_1), I_3(t_1) = 0, I_4(t_3) = 0, I_2(t_3) = I_5(t_3)}$ and $\boldsymbol{I_5(T) = 0}$

   For FIFO,
   $\boldsymbol{I_1(t_0) = 0, I_1(t_1) = I_2(t_1), I_3(t_1) = 0, I_4(t_3) = I_6(t_3), I_2(t_2) = I_5(t_2), I_5(t_3) = 0}$ and $\boldsymbol{I_6(T) = 0}$
3. Compute $\boldsymbol{t_2} = \frac{(\boldsymbol{R}+\boldsymbol{x})\boldsymbol{t_1}}{\boldsymbol{R}}$.
4. Compute $\boldsymbol{TRC}^*$ using equations (21) and (45) for LIFO and FIFO respectively.

Aside from the GRG method, we have utilised the Wolfram Language function, which solves for numeric local constrained optimisation, which is known as the FindMinimum function. This function uses the interior point methods to find the solution to problems with constraints (Wolfram, 2020). We have utilised the built-in function to verify our results and we note that both the Microsoft Excel Solver and Mathematica software, provide the same results.

2.6 Numerical Example and Sensitivity Analysis

The following numerical example has been considered to provide an illustration of the proposed policies in this study. The parameters used in the model are $\boldsymbol{P = 3000}$, $\boldsymbol{R = 1000}$, $\boldsymbol{x = 500}$, $\boldsymbol{\alpha = 0.04}$, $\boldsymbol{a = 550}$, and $\boldsymbol{b = 200}$. The costs involved in this model are given as follows, $\boldsymbol{S = \$1000}$, $\boldsymbol{c_P = \$2.00}$, $\boldsymbol{c_R = \$3.00}$, $\boldsymbol{d = \$2.50}$, $\boldsymbol{h_1 = \$1.50}$, and $\boldsymbol{h_2 = \$2.50}$.

Based on the parameters considered, the optimal solution of $\boldsymbol{TRC}^*$ for the LIFO policy is \$3047.39, and it is achieved at $\boldsymbol{t_1^* = 0.2556}$, $\boldsymbol{t_3^* = 0.4609}$, and $\boldsymbol{T^* = 1.1354}$ (correct to four decimal places).

On the other hand, using the same parameters as LIFO policy, the optimal solution of $\boldsymbol{TRC}^*$ for the FIFO policy is \$3076.34, which is achieved at $\boldsymbol{t_1^* = 0.2516}$, $\boldsymbol{t_3^* = 1.0588}$, and $\boldsymbol{T^* = 1.1203}$ (correct to four decimal places).

Table 1 shows the changes in $\boldsymbol{TRC}^*$ as the parameters are reduced and increased by 25% in both the LIFO and FIFO systems. The changes in the total number of items produced, defective items, demand, and deteriorated items are presented in Table 2.

We note that the results obtained are similar in both systems in which the value of $\boldsymbol{TRC}^*$ increases as the parameters increased. This behaviour is true for all parameters except when the value of $\boldsymbol{P}$ is increased. Since the increment in $\boldsymbol{P}$ shall mean that the items are produced at a faster rate in a shorter period, we note that fewer items are being produced. In return, fewer number of defective items are produced in the system. The decrement of the processing, rework processing, and holding costs in RW result in the decrement of $\boldsymbol{TRC}^*$.

Table 1. Comparison of the difference in the TRC^* under varying parameters.

Parameters	−25%, Optimal, +25%	LIFO				FIFO			
		$\boldsymbol{TRC}^*$	$\boldsymbol{t_1^*}$	$\boldsymbol{t_3^*}$	$\boldsymbol{T^*}$	$\boldsymbol{TRC}^*$	$\boldsymbol{t_1^*}$	$\boldsymbol{t_3^*}$	$\boldsymbol{T^*}$
	2250	3083.67	0.36	0.63	1.19	3113.57	0.35	1.09	1.17
$\boldsymbol{P}$	3000	3047.39	0.26	0.46	1.14	3076.34	0.25	1.06	1.12
	3750	3020.29	0.20	0.36	1.11	3046.72	0.20	1.05	1.10
	750	3040.90	0.26	0.46	1.14	3054.10	0.26	1.11	1.14
$\boldsymbol{R}$	1000	3047.39	0.26	0.46	1.14	3076.34	0.25	1.06	1.12
	1250	3051.26	0.25	0.46	1.13	3089.49	0.25	1.03	1.11
	375	2972.45	0.26	0.41	1.14	2995.95	0.25	1.08	1.12
$\boldsymbol{x}$	500	3047.39	0.26	0.46	1.14	3076.34	0.25	1.06	1.12
	625	3121.25	0.26	0.51	1.14	3154.57	0.25	1.04	1.12
$\boldsymbol{\alpha}$	0.03	3031.63	0.26	0.46	1.15	3060.93	0.25	1.07	1.13
	0.04	3047.39	0.26	0.46	1.14	3076.34	0.25	1.06	1.12

DOI:https//doi.org/10.22452/mjs.vol42no1.3
Malaysian Journal of Science 42(1): 17-31 (February 2023)

	0.05	3063.01	0.25	0.46	1.12	3091.63	0.25	1.05	1.11
	412.5	2637.03	0.21	0.43	1.17	2672.17	0.21	1.06	1.15
a	550.0	3047.39	0.26	0.46	1.14	3076.34	0.25	1.06	1.12
	687.5	3440.62	0.30	0.50	1.11	3460.15	0.30	1.07	1.11
	150	2951.18	0.26	0.48	1.21	2982.44	0.26	1.12	1.19
b	200	3047.39	0.26	0.46	1.14	3076.34	0.25	1.06	1.12
	250	3136.46	0.25	0.45	1.08	3163.42	0.25	1.01	1.06

Table 2. Analysis of change in various parameters on the total inventory items.

		LIFO				FIFO			
Parameters	−25%, Optimal, +25%	Total Items Produced	Total Defectives	Total Demand	Total Deteriorated Items	Total Items Produced	Total Defectives	Total Demand	Total Deteriorated Items
	2250	807.82	179.51	795.24	12.57	795.75	176.83	783.51	12.24
P	3000	766.82	127.80	753.37	13.45	754.71	125.78	741.65	13.06
	3750	747.80	99.71	733.92	13.88	736.22	98.16	722.73	13.49
	750	771.66	128.61	758.16	13.49	768.02	128.00	754.64	13.38
R	1000	766.82	127.80	753.37	13.45	754.71	125.78	741.65	13.06
	1250	764.38	127.40	750.95	13.43	747.10	124.52	734.23	12.88
	375	768.19	96.02	754.40	13.79	758.15	94.77	744.70	13.46
x	500	766.82	127.80	753.37	13.45	754.71	125.78	741.65	13.06
	625	766.22	159.63	753.13	13.09	752.52	156.78	739.85	12.67
	0.03	772.56	128.76	762.27	10.29	760.10	126.68	750.11	9.99
α	0.04	766.82	127.80	753.37	13.45	754.71	125.78	741.65	13.06
	0.05	760.73	126.79	744.27	16.46	749.47	124.91	733.46	16.02
	412.5	629.74	104.96	617.34	12.40	615.37	102.56	603.48	11.89
a	550.0	766.82	127.80	753.37	13.45	754.71	125.78	741.65	13.06
	687.5	904.79	150.80	890.55	14.24	897.59	149.60	883.56	14.03
	150	788.97	131.50	774.26	14.71	774.37	129.06	760.16	14.21
b	200	766.82	127.80	753.37	13.45	754.71	125.78	741.65	13.06
	250	748.97	124.83	736.52	12.45	739.00	123.17	726.86	12.15

2.7 Comparison between LIFO and FIFO policies

In general, the TRC^* of the LIFO system is lower than the TRC^* of the FIFO system, where $TRC^*_{LIFO} = \$3047.39 < TRC^*_{FIFO} = \$3076.34$. Based on the sensitivity analysis of both policies, the following are the features that we have identified.

We observed that changes in the value of t_1 affect the number of total produced items and defective items, while changes in the value of T affect the total demand in the system. Note that in FIFO policy, items that are stored in OW will be utilised or distributed first, followed by items in RW. Hence, items are stored longer in RW, which in turn results in a higher holding cost.

Referring to the optimal solution presented, we can see that TRC^* for the FIFO policy is higher than the TRC^* in the LIFO policy. Hence, we can conclude that given the same value of parameters, the LIFO system has a lower TRC^*.

3. Conclusion

3.1 Conclusion and Further Research

The total relevant cost, TRC^*, for both policies is a nonlinear equation, where its second derivative with respect to t_1, t_3, and T is complicated. Hence, we have utilised the optimisation tools in Microsoft Excel Solver and Mathematica to obtain an optimal solution for the proposed

DOI:https//doi.org/10.22452/mjs.vol42no1.3
Malaysian Journal of Science 42(1): 17-31 (February 2023)

model. According to the results obtained, we observed that the equation for TRC^* is convex at the optimal values of t_1, t_3, and T. In other words, the optimal solution of TRC^* is minimum at the aforementioned optimal times. A sensitivity analysis was conducted for both policies to provide illustration on the derived results. In addition, we also note that several studies such as Sett et al. (2012) and Lee (2006) to name a few, derived similar results as obtained in this paper.

Several limitations were identified while conducting the study. First, the assumption that deterioration rate is constant is unrealistic. Deterioration rates may be affected by environmental factors and workmanship of the items produced. The type of deterioration rates may be further explored as different storage space may have different facilities, which may result in the difference in the deterioration rate. Next, shortages and backlog are also commonly present in the market when demand is higher than supply. Hence, exploring this factor further would be beneficial in planning the right number of items to be produced to ensure fulfilment of demand.

3.2 Managerial Insights

The proposed model in this paper may provide managerial insights to aid manufacturers in optimising the total cost of their production system when managing two storage facilities involving deteriorating items.

Our approach in incorporating a linearly increasing demand rate would allow inventory operators to plan their production accordingly when launching new items into the market. We observe that a newly launched product such as cosmetics, fashion items, and mobile phones experience a linearly increasing demand rate for a certain period of time upon being introduced into the market.

Furthermore, introducing an imperfect production process in the manufacturing system is a more realistic condition. In some instances, rework process is a more cost-efficient approach rather than producing scrap and disposing defective items. Besides, we have assumed that the rework process is only carried out in RW. This would be beneficial to manufacturers with limited number of machines as they are able to focus solely on production process first, prior to repairing the defectives.

4. Acknowledgements

We would like to express our gratitude towards the University of Malaya Research Grants (RF016B-2018) for providing the financial support for this study. We highly appreciate and would like to thank the reviewers for their valuable suggestions, which led to substantial improvement of this paper.

5. References

Aastha, Pareek, S., Cárdenas-Barrón, L. P., Mittal, M. (2020). Impact of Imperfect Quality Items on Inventory Management for Two Warehouses with Shortages. International Journal of Mathematical, Engineering and Management Sciences, 5:869–885.

Agrawal, S., Banerjee, S., Papchristos, S. (2013). Inventory model with deteriorating items, ramp-type demand and partially backlogged shortages for a two warehouse system. Applied Mathematical Modelling, 37:8912–8929.

Alamri, A. A., Syntetos, A. A. (2018). Beyond LIFO and FIFO: Exploring an allocation-in-fraction-out (AIFO) policy in a two-warehouse inventory model. International Journal of Production Economics, 206:33–45.

Benkherouf, L. (1997). A deterministic order level inventory model for deteriorating items with two storage facilities. Int. J. Production Economics, 48:167–175.

Bhunia, A. K., Jaggi, C. K., Sharma, A., Sharma, R. (2014). A two-warehouse inventory model for deteriorating items under permissible delay in payment with partial backlogging. Applied Mathematics and Computation, 232:1125–1137.

Bhunia, A. K., Maiti, M. (1998). A two warehouse inventory model for deteriorating items with a linear trend in demand and shortages. The Journal of Operational Research Society, 49(3):287–292.

Chakrabarty, R., Roy, T., Chaudhuri, K. S. (2018). A two-warehouse inventory model for deteriorating items with capacity constraints and back-ordering under financial considerations. International Journal of Applied and Computational Mathematics 4(2):1–16.

Chung, K. J., Her, C. C., Lin, S. D. (2009). A two-warehouse inventory model with imperfect quality production processes. Computers & Industrial Engineering, 56:193–197.

Ghare, P.M., Schrader, S.F. (1963). A model for exponentially decaying inventory. Journal of Industrial Engineering, 14(5):238–243.

DOI:https//doi.org/10.22452/mjs.vol42no1.3
Malaysian Journal of Science 42(1): 17-31 (February 2023)

Ghiami, Y., Beullens, P. (2020). The continuous resupply policy for deteriorating items with stock-dependent observable demand in a two-warehouse and two-echelon supply chain. Applied Mathematical Modelling, 82:271–292.

Goswami, A., Chaudhuri, K. S. (1992). An economic order quantity model for items with two levels of storage for a linear trend in demand. The Journal of The Operational Research Society, 43:157–167.

Gupta, M., Tiwari, S., & Jaggi, C. K. (2020). Retailer's ordering policies for time-varying deteriorating items with partial backlogging and permissible delay in payments in a two-warehouse environment. Annals of Operations Research, 295:139–161.

Hartley, V. R. (1976). Operations Research: A Managerial Emphasis. Goodyear, Santa Monica, CA, 12:315–317.

Indrajitsingha, S. K., Samanta, P. N., Misra, U. K. (2019). A fuzzy two-warehouse inventory model for single deteriorating item with selling-price-dependent demand and shortage under partial-backlogged condition. Applications and Applied Mathematics: An International Journal (AAM), 14(1):511–536.

Kaliraman, N. K., Raj, R., Chandra, S., Chaudhary, H. (2017). Two warehouse inventory model for deteriorating items with exponential demand rate and permissible delay in payment. Yugoslav Journal of Operations Research, 27(1):109–124.

Kumar, A., Chanda, U. (2018). Two-warehouse inventory model for deteriorating items with demand influenced by innovation criterion in growing technology market. Journal of Management Analytics, 5(11):1–15.

Lee, C. C. (2006). Two-warehouse inventory model with deterioration under FIFO dispatching policy. European Journal of Optimal Research, 174:861–873.

Lee, C. C., Hsu, S. L. (2009). A two-warehouse production model for deteriorating inventory items with time-dependent demands. European Journal of Operational Research, 194:700–710.

Lee, C. C., Ma, C. Y. (2000). Optimal inventory policy for deteriorating items with two-warehouse and time-dependent demands. Production Planning & Control: The Management of Operations, 11(7):689–696.

Pakkala, T. P. M., Achary, K. K. (1991). A two-warehouse probabilistic order-level inventory model for deteriorating items. The Journal of The Operational Research Society, 42(12):1117–1122.

Pakkala, T. P. M., Achary, K. K. (1992). A deterministic inventory model for deteriorating items with two warehouses and finite replenishment rate. European Journal of Operational Research, 57:71–76.

Panda, D., Maiti, M. K., Maiti, M. (2010). Two warehouse inventory models for single vendor multiple retailers with price and stock dependent demand. Applied Mathematical Modelling, 34:3571–3585.

Panda, G. C., Sahu, S., Meher, M. K. (2012). A two warehouse inventory model for deteriorating items with an exponential demand and shortage. American Journal of Operational Research, 2(6):93–97.

Rafaat, F. (1991). Survey of literature on continuously deteriorating inventory models. Journal of Operations Research Society, 42:27–37.

Rong, M., Mahapatra, N. K., Maiti, M. (2008). A two warehouse inventory model for a deteriorating item with partially/fully backlogged shortage and fuzzy lead time. European Journal of Operational Research, 189:59–75.

Sarma, K. V. S. (1983). A deterministic inventory model two levels of storage and an optimum release rule. Opsearch, 20:175–180.

Sett, B.K., Sarkar, B., Goswami, A. (2012). Two-warehouse inventory model with increasing demand and time varying deterioration. Scientia Iranica E, 19(6):1969–1977.

Shaikh, A. A., Cardenas-Barron, L. E., Tiwair, S. (2019). A two-warehouse inventory model for non-instantaneous deteriorating items with interval-valued inventory costs and stock-dependent demand under inflationary conditions. Neural Computing & Applications, 31:1931–1948.

Singh, S. R., Jain, S., Pareek, S. (2013). An imperfect quality items with learning and inflation under two limited storage capacity. International Journal of Industrial Engineering Computations, 4:479–490.

Wee, H. M., Widyadana, G. A. (2012). Economic production quantity models for deteriorating items with rework and stochastic preventive maintenance time. International Journal of Production Research, 50(11):2940–2952.

Wee, H. M., Widyadana, G. A. (2013). A production model for deteriorating items with stochastic preventive maintenance time and rework process with FIFO rule. Omega, 41:941–954.

DOI:https//doi.org/10.22452/mjs.vol42no1.3
Malaysian Journal of Science 42(1): 17-31 (February 2023)

Wee, H. M., Yu, J. C. P., Law, S. T. (2005). Two-warehouse inventory model with partial backordering and Weibull distribution deterioration under inflation. Journal of the Chinese Institute of Industrial Engineers, 22(6):451–462.

Xu, X., Bai, Q., Chen, M. (2017). A comparison of different dispatching policies in two-warehouse inventory systems for deteriorating items over a finite time horizon. Applied Mathematical Modelling, 41:359–374.

Yadav, A. S., Swami, A. (2013). A two-warehouse inventory model for decaying items with exponential demand and variable holding cost. International Journal of Inventive Engineering and Sciences (IJIES), 1(5):18–22.

Yu, J. C. P. (2019). Optimizing a two-warehouse system under shortage backordering, trade credit, and decreasing rental conditions. International Journal of Production Economics, 209:147–155.

Numerical Nonlinear Global Optimization. https://reference.wolfram.com/language/tutorial/ConstrainedOptimizationGlobalNumerical.html

Some Notes on Internal Implementation. https://reference.wolfram.com/language/tutorial/SomeNotesOnInternalImplementation.html

DOI:https//doi.org/10.22452/mjs.vol42no1.3
Malaysian Journal of Science 42(1): 17-31 (February 2023)

MALAYSIAN JOURNAL OF SCIENCE
MJS
ISSN 1394-3065

Regular Issue

Malaysian Journal of Science 42 (1): 32-41 (February 2023) https://mjs.um.edu.my

TWO-SAMPLE TEST FOR RANDOMLY CENSORED DATA

Ayushee[1a], Narinder Kumar[2a]* and Manish Goyal[3b]

Abstract: In this study, a nonparametric test was proposed for the two-sample scale problem, when sample observations are randomly right censored. The proposed test was based on the extremes of observations as an extension of the widely used Gehan's test for the two-sample problem. Critical values were obtained through simulations of various lifetime distributions at various sample sizes. Power performance for the proposed test was investigated considering various distributions. Upon comparing with the Gehan's test, it was found that the proposed test has more statistical power and efficiency for some special cases. An empirical experiment with a real-life data set was also presented.

Keywords: *Nonparametric test, two-sample scale, right censored, critical values*

1. Introduction

In statistical analysis, nonparametric approaches do not require any assumptions regarding the distribution of a population. Two-sample nonparametric tests are employed to compare the distribution of two samples. Two-sample scale problems arise when the analyzer is interested in determining whether the populations follow the same distribution, or when there is a difference in their scale parameters. This issue has numerous applications in the field of Agriculture, Engineering, Business, Trade, Industries, and Medicine. For the two-sample scale problem, nonparametric tests have been proposed by Mood (1954), Sukhatme (1957), Kössler (1994), Kössler & Kumar (2010), and Goyal & Kumar (2020).

In real life, there are certain situations, where we do not have the complete information about the data, there involves the role of censoring, these cases are of much practical use. We say that an observation is censored when we do not observe it completely. Censored observations can be statistically-treated in various forms, ranging from parametric to nonparametric approaches. Several nonparametric tests are also available for censored data. Kaplan & Meier's (1958) method is marked as a great finding in the field of survival analysis, especially from the perspective of nonparametric approaches. This impelled the advancement of existing nonparametric approaches in the presence of censored data. Some two-sample nonparametric tests with censored data are discussed hereafter.

Authors information:
[a]Department of Statistics, Panjab University, Sector 14, Chandigarh, INDIA. Email: ayusheechoudhary98@gmail.com[1]; nkumar@pu.ac.in[2]
[b]Department of Statistics, Post Graduate Government College, Sector 11, Chandigarh, INDIA. Email: manishgoyal33@gmail.com[3]
*Corresponding Author: nkumar@pu.ac.in

In the context of industrial life-testing, Halperin (1960) considered a special case of that by Wilcoxon (1945), which involved statistics for comparing two samples in the presence of type-I censoring. A rank order theory for the two-sample problem was developed by Rao, Savage & Sobel (1960) when the data were censored. To arrive at an early decision, a sequential modification to Wilcoxon's test was proposed by Alling (1963). Furthermore, for comparing two samples in the presence of random censoring, Gehan (1965) proposed a generalized form of Wilcoxon's test, conditioned on the observational pattern. Efron (1967) proposed a two-sample problem with censored data as an extension of Gehan's method. Mantel (1967) proposed an approach to simplify both the method of computation and determination of the permutation distribution of Gehan's statistic. Lee, Desu & Gehan (1975) presented a Monte-Carlo study on a series of two-sample tests with or without censoring. For an in-depth literature review, one can refer to the monographs: Survival analysis by Miller (2011) and Lifetime Data: Statistical Models and Methods by Deshpande & Purohit (2015).

The statistical problem we have considered in this study mostly arises in the field of medicine, wherein we compare two treatments for their effects on patients' health and life, where the observations under study are the lifetimes of patients. A common problem in clinical trials arises when the data is not observed completely, or we have partial information about it; we consider such an observation to be censored. We considered random censoring, as it is mostly used in clinical trials due to the failure to follow-up or termination of the study.

Received: December 23, 2021
Accepted: February 15, 2022
Published: February 28, 2023

DOI:https//doi.org/10.22452/mjs.vol42no1.4
Malaysian Journal of Science 42(1): 32-41 (February 2023)

The proposed distribution-free two-sample test is based on the extension of Gehan's test statistics, whereby for each individual, the observation is either time to censoring or time to failure. From the point when the study was initiated, an observation was noted as time to failure if the patient was found to be dead or relapsed before a pre-fixed time T. Moreover, it was noted as time to censored if the patient was alive until time T, or in remission at time T. In other words, for two different treatments if n_1 (n_2) is the total patients that participated in the study, out of which r_1 (r_2) are censored at time T, then n_1-r_1 (n_2-r_2) individuals have failed. Two-sample scale problem involves comparing the survival of these n_1 and n_2 patients. The objective of the study is to propose a new test that has more efficiency and power with respect to Gehan's test for the two-sample scale problem.

The remainder of this paper is structured as follows. Section 2 defines a newly proposed test statistic. The mean and variance of the test statistic are evaluated in Section 3. Critical points of the test statistic at various sample sizes and percentage censoring are given in Section 4, along with a comparison of critical points of Gehan's test statistic. The asymptotic relative efficiency of the test statistic is derived in Section 5, and a real-life data example for the statistic is illustrated in Section 6. The statistical power of the proposed test is given in comparison to the statistical power of Gehan's test at various sample sizes and percentage censoring in Section 7.

2. The Proposed Test Statistic

Let us suppose that we have two samples, X and Y, with n_1, n_2 individuals, randomly allocated to two treatments, A and B, respectively. Suppose that an experiment was conducted for a fixed time T, and all the individuals were followed up. If x_i, y_j represents the time to failure and x_i', y_j' represents the time to censoring for all ($i = 1, 2, \dots, n_1$ and $j = 1, 2, \dots, n_2$), we have the following observations:

$$\left.\begin{array}{ll} x_1', x_2', \dots, x_{r_1}', & r_1 \text{ censored} \\ x_{r_1+1}, x_{r_1+2}, \dots, x_{n_1}, & n_1 - r_1 \text{ failures} \end{array}\right\} \text{ treatment } A,$$

$$\left.\begin{array}{ll} y_1', y_2', \dots, y_{r_2}', & r_2 \textit{ censored} \\ y_{r_2+1}, y_{r_2+2}, \dots, y_{n_2}, & n_2 - r_2 \text{ failures} \end{array}\right\} \text{ treatment } B.$$

Furthermore, the cumulative distribution functions of time to failure x_i, y_j are $F_1(x), F_2(y)$ and that of the time to censoring x_i', y_j' are $G_1(x), G_2(y)$.

The null hypothesis is:

$H_0: F_1(t) = F_2(t), \quad (t \le T)$ (Treatments A and B are equally effective),

against the alternative

$H_1: F_1(t) = F_2(\theta t), \quad (t \le T \ \ \& \ \ \theta \ne 1)$

(Treatments A and B are significantly different.)

In the proposed test, we have taken a sub-sample of size two from each sample, and compared their extremes to derive more information from the samples. Let (x_1, x_2) and (y_1, y_2) be the uncensored sub-samples chosen from samples X and Y respectively. If the maximum of the sub-sample (x_1, x_2) from the random sample X treated with A is greater than the maximum of the subsample (y_1, y_2) from the random sample Y treated with B, then we assign 1 to the kernel U_{ij}. Otherwise, we assign -1 to the kernel U_{ij}.

If in the subsample from sample X, one observation is censored and the other is uncensored, with the censored value greater than the uncensored value, and observations in the subsample from sample Y are uncensored. Here, if the maximum of the subsample of two observations (x_1', x_2) from sample X is greater than the maximum of the subsample of any two observations (y_1, y_2) from sample Y, we assign 1 to the kernel U_{ij}. A similar procedure is done for the opposite case, i.e., when one censored and one uncensored observation comes in the sub-sample from sample Y, and both uncensored come in the subsample from sample X, we assign -1 to the kernel U_{ij}. For remainder of the cases, we assign zero to the kernel U_{ij}. In mathematical terms, the kernel for the proposed test is:

DOI:https//doi.org/10.22452/mjs.vol42no1.4
Malaysian Journal of Science 42(1): 32-41 (February 2023)

$$U_{ij} = \begin{cases} 1, & \text{if } Max(x_{i_1}, x_{i_2}) > Max(y_{j_1}, y_{j_2}) \text{ or } Max(x'_{i_1}, x_{i_2}) \geq Max(y_{j_1}, y_{j_2}) \\ -1, & \text{if } Max(x_{i_1}, x_{i_2}) < Max(y_{j_1}, y_{j_2}) \text{ or } Max(x_{i_1}, x_{i_2}) \leq Max(y'_{j_1}, y_{j_2}) \\ 0, & \text{elsewhere,} \end{cases} \quad (1)$$

where $i_1 \neq i_2$ in $(1, 2, \ldots, n_1)$ and $j_1 \neq j_2$ in $(1, 2, \ldots, n_2)$ Define the statistic $V = \sum_{i,j} U_{ij}$, where the sum is extended over all n_1, n_2 combinations. There will be a contribution to statistic V for all possible comparisons where both the patients have failed and, in all comparisons, where a patient who is censored has more survival than one who has failed earlier.

3. The Mean and Variance of Test Statistic

We have considered the same observational pattern described by Gehan (1965), i.e., if we have n_1, n_2 observations that can be settled in the following observational pattern:

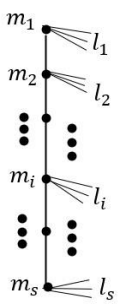

when we rank the data, then m_i's are the total uncensored observations at the ith rank with dissimilar values, and l_i's are the total randomly right censored observations with values larger than the observational value at the ith rank, but should be smaller than the observational value at the $(i+1)^{th}$ rank.

The dots at the upright line represent the ordered ranks of the dissimilar values of time to failure observations, and these fall at s dissimilar failure dots. Any observation that has either censored or failed can be characterized in the manner of the above pattern. Prior to the first failure, any censored observation will be counted as l_1 with $m_1 = 0$. Generally, these observations do not yield any difference between A and B treatments. Therefore, we omit these observations. As our calculation is restricted to the defined observational pattern, the omission of these observations does not have any consequence on mean and variance.

For example, if we have the following sample of survival times of patients (in months): $6, 8, 10+, 11, 11+, 13, 14+, 15+$ (the $+$ sign represents a censored observation at that particular point), the observational pattern will be:

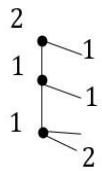

Suppose, H_0 is true, i.e., the survival of patients in both the treated groups is same. We consider the conditional mean denoted by $E(V|P, H_0)$ and variance by $var(V|P, H_0)$ of V under H_0, where P is the observational pattern. The expectation was considered over the possible number of samples $\binom{n_1 + n_2}{n_1}$ that are equally likely and follow same defined observational pattern. Due to symmetry, we can easily observe:

$$E(V|P, H_0) = E\left(\sum_{i,j} U_{ij} \,|P, H_0\right) = 0. \quad (2)$$

The variance of V under H_0 is restricted to the defined pattern P, and can be defined as:

$$var(V|P, H_0) = E\left(\sum_{i,j} U_{ij} - E\left(\sum_{i,j} U_{ij}\right)\middle| P, H_0\right)^2. \quad (3)$$

From eq. (2), we know that $E\left(\sum_{i,j} U_{ij} \,|P, H_0\right) = 0$. Thus, eq. (3) becomes:

$$var(V|P, H_0) = E\left(\sum_{i=1}^{n_1}\sum_{j=1}^{n_2} U_{ij}^2 + \sum_{i \neq i'=1}^{n_1}\sum_{j=1}^{n_2} U_{ij}U_{i'j} + \sum_{i=1}^{n_1}\sum_{j \neq j'=1}^{n_2} U_{ij}U_{ij'} + \sum_{i \neq i'=1}^{n_1}\sum_{j \neq j'=1}^{n_2} U_{ij}U_{i'j'}\middle| P, H_0\right). \quad (4)$$

DOI:https//doi.org/10.22452/mjs.vol42no1.4
Malaysian Journal of Science 42(1): 32-41 (February 2023)

After evaluating each term of eq. (4), we obtain:

$$var(V|P,H_0) = \frac{24\binom{n_1+n_2-4}{n_1-2}}{\binom{n_1+n_2}{n_1}}K_1 + \left\{\frac{\binom{n_1+n_2-6}{n_1-4}}{\binom{n_1+n_2}{n_1}} + \frac{\binom{n_1+n_2-6}{n_2-4}}{\binom{n_1+n_2}{n_1}}\right\}K_2. \quad (5)$$

In eq. (5), the coefficient of K_1 is the proportion of times a specific pair of observations (i,j) turns up in samples X and Y. Similarly, the coefficient of K_2 is the proportion of times a specific pair $(i,i'$and $i \neq i')$ turns up in any one of the samples with observation j from the other sample. Here

$$K_1 = \sum_{i=1}^{s}\left[\binom{m_i}{1}\binom{M_{i-1}}{3} + \binom{m_i}{1}\binom{n_1+n_2-M_i-L_{i-1}}{3} + \binom{l_i}{1}\binom{M_i}{3} + \binom{m_i}{1}\binom{M_{i-1}}{1}\binom{n_1+n_2-M_i-L_{i-1}}{2} + \binom{m_i}{1}\binom{M_{i-1}}{2}\binom{n_1+n_2-M_i-L_{i-1}}{1}\right], \quad (6)$$

where the first and second terms in eq. (6) represent the total number of ways of pairing any failed observation at i^{th} rank with any three observations at a lesser rank and any three observations of a rank greater than i respectively. The third term represents the total number of ways of pairing a censored observation immediately after the ith rank, with any three that have failed earlier. The fourth term shows the total number of ways of pairing any failed observation with one of rank lesser than i and two other observations with a rank greater than i. The last term represents the total number of ways of pairing any failed observation with any two observations of a rank lesser than i and one other observation with a rank greater than i. Similarly,

$$K_2 = \sum_{i=1}^{s}\left[120\binom{m_i}{1}\binom{M_{i-1}}{5} + 56\binom{m_i}{1}\binom{n_1+n_2-M_i-L_{i-1}}{5} + 120\binom{l_i}{1}\binom{M_i}{5} + 56\binom{m_i}{1}\binom{M_{i-1}}{1}\binom{n_1+n_2-M_i-L_{i-1}}{4} - 72\binom{m_i}{1}\binom{M_{i-1}}{4}\binom{n_1+n_2-M_i-L_{i-1}}{1} + 56\binom{m_i}{1}\binom{M_{i-1}}{2}\binom{n_1+n_2-M_i-L_{i-1}}{3} + 24\binom{m_i}{1}\binom{M_{i-1}}{3}\binom{n_1+n_2-M_i-L_{i-1}}{2}\right] \quad (7)$$

The first and second terms within square brackets in eq. (7), represent the total number of ways of pairing any failed observation at the ith rank with any five observations of a lesser rank and any five of a rank greater than i respectively. The third term shows the total number of ways of pairing any censored observation immediately after the ith rank with any five that have failed earlier. The Fourth term shows the total number of ways of pairing any failed observation with a rank lesser than i and four other observations with a rank greater than i. The fifth term shows the total number of ways of pairing any failed observation with any four observations of a rank lesser than i and one other observation with a rank greater than i. The sixth term shows the total number of ways of pairing any failed observation with any two observations of a rank lesser than i and three other observations with a rank greater than i. The last term represents the total number of ways of pairing any failed observation with any three observations of a rank lesser than i and two other observations with a rank greater than i, and

$$M_j = \sum_{i=1}^{j} m_i, \qquad M_0 = 0,$$

$$L_j = \sum_{i=1}^{j} l_i\ , \qquad L_0 = 0.$$

m_i and l_i are in their original meanings, as defined initially in this Section.

4. Critical Points

In hypothesis testing, we determine whether sufficient evidence exists from the sample to accept or reject H_0. Critical points are essentially the cut-off values such that if the calculated test statistic value comes out to be greater than the cut-off value, we reject H_0; otherwise, we do not reject H_0. These values are specific for a test statistic that depends on the type of test and the level of significance α. Using this concept, critical points are found using a

DOI:https//doi.org/10.22452/mjs.vol42no1.4
Malaysian Journal of Science 42(1): 32-41 (February 2023)

simulation study for both the tests V (proposed) and G (by Gehan 1965). We consider three different lifetime distributions (Lindley, Exponential and Weibull) for generating time to failure observations and Exponential distribution for generating time to censored observations. Two samples, each of size n, are generated from these distributions, and the standardized test statistic value can be found using the following formula:

$$Z = \frac{V - E(V|P, H_0)}{\sqrt{var(V|P, H_0)}} \tag{8}$$

where $E(V|P, H_0)$ and $var(V|P, H_0)$ are given in eqs. (2) and (5). We then find Z_α such that $P(Z > Z_\alpha) = 0.025$. This process is simulated 10,000 times, and the critical points are found as the average of Z_α-values. Critical points are given in Tables $1 - 3$ for various censoring percentages $(pcens)$ and sample sizes $(n_1 = n_2 = n)$ for each distribution.

Table 1. Critical points of the proposed test, when the time to failure distribution is Lindley and time to censoring distribution is Exponential

Test	V	G	V	G	V	G	V	G
n \ $pcens$	0.2	0.2	0.3	0.3	0.4	0.4	0.5	0.5
10	2.91112	3.35186	1.97061	3.31972	1.47104	3.24155	1.21353	3.07304
15	2.89617	3.80541	1.96009	3.91377	1.55739	3.86303	1.38231	3.72432
20	2.84070	4.27193	2.04971	4.46372	1.67048	4.40178	1.51094	4.23448
25	2.92921	4.74102	2.12339	4.92879	1.76357	4.88847	1.63321	4.73802
30	3.01728	5.10966	2.24109	5.39651	1.89059	5.35712	1.77043	5.16320

Table 2. Critical points of the proposed test, when both time to failure and time to censoring distributions are Exponential

Test	V	G	V	G	V	G	V	G
n \ $pcens$	0.2	0.2	0.3	0.3	0.4	0.4	0.5	0.5
10	2.92186	3.38056	1.91547	3.32851	1.43057	3.24729	1.21353	3.06260
15	2.90303	3.91751	1.95929	3.93480	1.53092	3.88975	1.33974	3.70345
20	2.88096	4.40868	2.04536	4.52102	1.64325	4.41977	1.46696	4.22876
25	2.93422	4.96588	2.14505	5.00451	1.75391	4.87901	1.60609	4.70970
30	3.02035	5.34874	2.25501	5.50358	1.86846	5.35288	1.73120	5.11489

Table 3. Critical points of the proposed test, when the time to failure distribution is Weibull and time to censoring distribution is Exponential

Test	V	G	V	G	V	G	V	G
n \ $pcens$	0.2	0.2	0.3	0.3	0.4	0.4	0.5	0.5
10	2.93616	3.44826	1.91492	3.33473	1.38603	3.15828	1.13679	2.90428
15	2.94675	4.09885	1.98431	4.013749	1.50179	3.81971	1.27410	3.52024
20	2.98755	4.72489	2.07529	4.69799	1.63558	4.44922	1.43581	4.07413
25	3.03894	5.30250	2.21491	5.23519	1.76892	4.95976	1.55849	4.51801
30	3.16017	5.86804	2.31089	5.76923	1.90151	5.42111	1.68737	4.98331

5. Asymptotic Relative Efficiency

Herein, we find the asymptotic relative efficiency (ARE) of the proposed test statistic V relative to the usual $F-$test, assuming Exponential lifetime distribution. Let us suppose that the time to failure probability density function of a patient who is receiving treatment A is given as

$$f_1(x) = \phi \exp(-\phi x),$$

and that for a patient who is receiving treatment B is given as

DOI:https//doi.org/10.22452/mjs.vol42no1.4
Malaysian Journal of Science 42(1): 32-41 (February 2023)

$$f_2(y) = \theta\phi \exp(-\theta\phi y).$$

Our interest is to test the hypothesis:

$$H: F_1(t) = F_2(\theta t) \qquad (t \leq T).$$

Thus, our null hypothesis would be, $H_0: \theta = 1$. This type of test would be relevant in situations when we are interested in determining whether there is any constant proportion (θ) of failure times of the patients who are receiving treatment B to that of who are receiving treatment A.

Another competent test for the above hypothesis is to consider $\bar{t}_1/\bar{t}_2$, following F- distribution with degrees of freedom $(2(n_1 - r_1), 2(n_2 - r_2))$, where

$$\bar{t}_1 = \frac{\left(\sum_{i=1}^{r_1} x_i' + \sum_{i=r_1+1}^{n_1} x_i\right)}{(n_1 - r_1)}, \quad \bar{t}_2 = \frac{\left(\sum_{i=1}^{r_2} y_i' + \sum_{i=r_2+1}^{n_2} y_i\right)}{(n_2 - r_2)}.$$

We aim to find the ARE of the proposed test relative to F test in the situation, when all the individuals enter study at time zero and the experiment is stopped at time T. The ARE of the proposed V test relative to F test is given by,

$$ARE_{VF} = \lim_{n\to\infty} \frac{\left(\left.\frac{\partial E(n^{-2}V)}{\partial\theta}\right|_{\theta=1}\right)^2}{\left(nvar(n^{-2}V|H_0)\right)} \times \frac{\left(nvar(z|H_0)\right)}{\left(\left.\frac{\partial E(z)}{\partial\theta}\right|_{\theta=1}\right)^2}. \tag{9}$$

For F test, it is appropriate to transform the F statistic to $z = \frac{1}{2}\log(F)$, where z is following the Normal distribution asymptotically with $var \cong \frac{1}{2}\left(\frac{1}{2(n_1 - r_1)} + \frac{1}{2(n_2 - r_2)}\right)$ and

$$E(z) = E_s E(z|s),$$

$$var(z|H_0) = E_s var(z|H_0, s) + var_s E(z|H_0, s).$$

Herein, the observational pattern is defined by the total sample size $(2n)$ and total failure observations preceding time T. The expectations and variances of z are calculated under the conditional pattern, where $s = 2n - r_1 - r_2$ is fixed, and then allow variation in s. The calculations are asymptotic as $n, s \to \infty$. Under H_0, s follows a Binomial distribution with mean $2n(1 - e^{-\phi T})$. Thus,

$$E(z) \cong \frac{1}{2}\log\theta \quad \text{and} \quad \left.\frac{\partial E(z)}{\partial\theta}\right|_{\theta=1} = \frac{1}{2}, \tag{10}$$

$$var(z|H_0) \cong \frac{1}{2n(1 - e^{-\phi T})}. \tag{11}$$

For the proposed test, we have $V = \sum_{i,j} U_{ij}$, as defined earlier, thus:

$$E(V) = n^2\left\{\Pr\left(Max(X_{i_1}, X_{i_2}) > Max(Y_{j_1}, Y_{j_2})\right) + \Pr\left(Max(X_{i_1}', X_{i_2}) \geq Max(Y_{j_1}, Y_{j_2})\right)\right.$$
$$\left. - \Pr\left(Max(X_{i_1}, X_{i_2}) < Max(Y_{j_1}, Y_{j_2})\right) - \Pr\left(Max(X_{i_1}, X_{i_2}) \leq Max(Y_{j_1}', Y_{j_2})\right)\right\} \tag{12}$$

where random variables X and X' denote the time to failure and time to censoring of the patients who are receiving treatment A, and determined by the probability density function $f_1(x)$. Similarly, random variables Y and Y' denote the time to failure and time to censoring of the patients who are receiving treatment B, and determined by probability density function $f_2(y)$. Herein, $X' \equiv Y' \equiv T$ and according to the assumed lifetime distribution, for a patient receiving treatment A and B, the probability of being censored at T is $e^{-T\phi}$ and $e^{-T\theta\phi}$ respectively. We now obtain these probabilities as follows:

$$\Pr\left(Max(X_{i_1}, X_{i_2}) > Max(Y_{j_1}, Y_{j_2})\right) + \Pr\left(Max(X_{i_1}', X_{i_2}) \geq Max(Y_{j_1}, Y_{j_2})\right)$$

DOI:https//doi.org/10.22452/mjs.vol42no1.4
Malaysian Journal of Science 42(1): 32-41 (February 2023)

$$= 2\theta\phi \int_0^T \left(1-\left(1-e^{-\phi u}\right)^2\right)\left(1-e^{-\theta\phi u}\right)e^{-\theta\phi u}du$$

$$= \theta\left\{\frac{4}{(1+\theta)}\left(1-e^{-(1+\theta)\phi T}\right)-\frac{4}{(1+2\theta)}\left(1-e^{-(1+2\theta)\phi T}\right)-\frac{2}{(2+\theta)}\left(1-e^{-(2+\theta)\phi T}\right)\right.$$
$$\left.-\frac{1}{(1+\theta)}\left(1-e^{-2(1+\theta)\phi T}\right)\right\}, \qquad (13)$$

and

$$\Pr\left(Max\left(X_{i_1},X_{i_2}\right)<Max\left(Y_{j_1},Y_{j_2}\right)\right)+\Pr\left(Max\left(X_{i_1},X_{i_2}\right)\le Max\left(Y'_{j_1},Y_{j_2}\right)\right)$$

$$= 2\theta\phi \int_0^T \left(1-e^{-\phi u}\right)^2\left(1-e^{-\theta\phi u}\right)e^{-\theta\phi u}du$$

$$= \theta\left\{\frac{2}{\theta}\left(1-e^{-\theta\phi T}\right)-\frac{1}{\theta}\left(1-e^{-2\theta\phi T}\right)+\frac{2}{(2+\theta)}\left(1-e^{-(2+\theta)\phi T}\right)-\frac{1}{(1+\theta)}\left(1-e^{-2(1+\theta)\phi T}\right)\right.$$
$$\left.-\frac{4}{(1+\theta)}\left(1-e^{-(1+\theta)\phi T}\right)+\frac{4}{(1+2\theta)}\left(1-e^{-(1+2\theta)\phi T}\right)\right\}. \qquad (14)$$

Substituting eqs. (13) and (14) in eq. (12), we arrive at

$$E(n^{-2}V) = \theta\left\{\frac{8}{(1+\theta)}\left(1-e^{-(1+\theta)\phi T}\right)-\frac{8}{(1+2\theta)}\left(1-e^{-(1+2\theta)\phi T}\right)-\frac{1}{\theta}\left(1-e^{-2\theta\phi T}\right)\right.$$
$$\left.-\frac{4}{(2+\theta)}\left(1-e^{-(2+\theta)\phi T}\right)+\frac{2}{(1+\theta)}\left(1-e^{-2(1+\theta)\phi T}\right)-\frac{2}{\theta}\left(1-e^{-\theta\phi T}\right)\right\}.$$

Thus,

$$\left.\frac{\partial E(n^{-2}V)}{\partial\theta}\right|_{\theta=1} = \left\{\frac{8}{9}-2\phi Te^{-\phi T}+6\phi Te^{-2\phi T}-\frac{8}{9}e^{-3\phi T}-\frac{20}{3}\phi Te^{-3\phi T}+\frac{4}{3}\phi Te^{-4\phi T}\right\}. \quad (15)$$

Now,

$$var(n^{-2}V|H_0) = n^{-4}E\left\{\left(\sum_{i=1}^{n_1}\sum_{j=1}^{n_2}U_{ij}-E\left(\sum_{i=1}^{n_1}\sum_{j=1}^{n_2}U_{ij}\right)\middle|H_0\right)\right\}^2$$

$$\Rightarrow \qquad var(n^{-2}V|H_0) = n^{-4}E\left\{\left(\sum_{i=1}^{n_1}\sum_{j=1}^{n_2}U_{ij}\middle|H_0\right)\right\}^2. \qquad (16)$$

Since, $E\left(\sum_{i=1}^{n_1}\sum_{j=1}^{n_2}U_{ij}\right)=0$ and $E\left(\sum_{i\neq i'=1}^{n_1}\sum_{j}^{n_2}U_{ij}U_{i'j}\right)=E\left(\sum_{i=1}^{n_1}\sum_{j\neq j'=1}^{n_2}U_{ij}U_{ij'}\right)$. Also, $E\left(\sum_{i\neq i'=1}^{n_1}\sum_{j\neq j'=1}^{n_2}U_{ij}U_{i'j'}\right)=0$, since U_{ij} *and* $U_{i'j'}$ are independent of each other and have expectation zero. Further evaluating each term of eq. (16), we get

$$var(n^{-2}V|H_0) = n^{-1}\left\{\frac{2}{3}\left(1-e^{-\phi T}\right)^3+2e^{-\phi T}\left(1-e^{-\phi T}\right)\right\}. \qquad (17)$$

Substituting eqs. (10), (11), (15) and (17) in eq. (9), we get the ARE of V to F as,

$$ARE_{VF} = \frac{\left(\frac{8}{9}-2\phi Te^{-\phi T}+6\phi Te^{-2\phi T}-\frac{8}{9}e^{-3\phi T}-\frac{20}{3}\phi Te^{-3\phi T}+\frac{4}{3}\phi Te^{-4\phi T}\right)^2}{\frac{1}{3}(1-e^{-\phi T})^4+e^{-\phi T}(1-e^{-\phi T})^2}. \quad (18)$$

Similarly, we can determine the ARE of the proposed V test to G (Gehan's test) as,

$$ARE_{VG} = \frac{\left(\frac{8}{9}-2\phi Te^{-\phi T}+6\phi Te^{-2\phi T}-\frac{8}{9}e^{-3\phi T}-\frac{20}{3}\phi Te^{-3\phi T}+\frac{4}{3}\phi Te^{-4\phi T}\right)^2\left(\frac{4}{3}\left(1-e^{-\phi T}\right)+4e^{-\phi T}\right)}{(1-e^{-2\phi T})^2\left(\frac{1}{3}(1-e^{-\phi T})^2+e^{-\phi T}\right)}, \qquad (19)$$

DOI:https//doi.org/10.22452/mjs.vol42no1.4
Malaysian Journal of Science 42(1): 32-41 (February 2023)

where

$$\phi T = \frac{total\ study\ time}{average\ failure\ time\ on\ treatment\ A}.$$

Using eqs. (18) and (19), the $AREs$ of the proposed test V with respect to (w.r.t.) F test and Gehan's test G for various values of ϕT are shown in Table 4.

Table 4. ARE of the V test w.r.t. F and G (Gehan) tests for various values of ϕT

ϕT	$\to 0$	1	2	3	4	5	$\to \infty$
ARE_{VF}	1.778	1.879	0.988	1.262	1.720	2.045	2.370
ARE_{VG}	1.778	2.013	1.179	1.607	2.253	2.709	3.160

When the value of ϕT is greater than two, the ARE for our test with respect to both F test and Gehan's test increases with ϕT. The value of ARE with respect to Gehan's test is always greater than 1, i.e., our test performs better than Gehan's test for all ϕT considered here. Moreover, the proposed test performs better than F test for all considered values, except at $\phi T = 2$.

6. Real-Life Example

We worked on a real-life example derived from Stablein & Koutrouvelis (1985), which is based on a trial of patients who suffered from locally unrestricted gastric cancer and were treated with chemotherapy and chemotherapy with radiotherapy. This data offers the survival time (in days) for the 45 patients on each treatment.

To check the distribution of data, we applied a Kolmogorov-Smirnov test and found that this data set follows Exponential distribution. Our aim is to determine if there is a significant difference in the survival times of the patients treated with chemotherapy and chemotherapy with radiotherapy. The critical value of the proposed test statistic for sample size $(45, 45)$ in the case of Exponential distribution is found to be $= 4.9453$ using the procedure described in Section 4. The standardized test statistic (z) for this data is $= 8.4554$. Since the calculated test statistic value turns out to be greater than its critical value, the null hypothesis of no significant difference is rejected. It is concluded that there is a significant difference in the survival time of the patients treated with chemotherapy and chemotherapy with radiotherapy.

7. Power Comparison of The Proposed Test

The statistical power of a test is defined as the probability that the test rejects the null hypothesis when it is true. Using the critical values shown in Section 4, the statistical power of the proposed test and Gehan's test was computed through a Monte-Carlo simulation. Data were simulated from three lifetime distributions viz., Lindley, Exponential and Weibull 10,000 times, with a scale parameter of the second sample as $\theta = 2, 3,$ and 4. The statistical power of the proposed test V and Gehan's test G is shown in the Tables 5-7 with same sample sizes and censoring percentages that we have considered for computing the critical points.

Table 5. Statistical power of the V and G tests, when the time to failure distribution is Lindley and time to censoring distribution is Exponential

	Test	V	G	V	G	V	G	V	G
					$pcens$				
n	θ	0.2	0.2	0.3	0.3	0.4	0.4	0.5	0.5
	2	0.395	0.298	0.255	0.290	0.203	0.254	0.141	0.207
10	3	0.611	0.569	0.404	0.483	0.301	0.441	0.204	0.362
	4	0.693	0.717	0.474	0.639	0.372	0.549	0.263	0.509
	2	0.414	0.379	0.396	0.375	0.360	0.314	0.235	0.277
15	3	0.698	0.642	0.595	0.620	0.494	0.588	0.382	0.526
	4	0.767	0.849	0.730	0.782	0.603	0.738	0.424	0.632
	2	0.570	0.442	0.498	0.434	0.406	0.404	0.307	0.374
20	3	0.843	0.772	0.771	0.745	0.671	0.698	0.451	0.622
	4	0.926	0.911	0.879	0.878	0.750	0.818	0.571	0.793
	2	0.681	0.511	0.638	0.509	0.493	0.501	0.374	0.424
25	3	0.935	0.832	0.909	0.822	0.776	0.812	0.599	0.736
	4	0.980	0.934	0.963	0.928	0.875	0.934	0.665	0.857
	2	0.807	0.579	0.727	0.559	0.605	0.555	0.405	0.504
30	3	0.982	0.888	0.965	0.863	0.878	0.844	0.651	0.794
	4	0.995	0.970	0.988	0.952	0.944	0.934	0.792	0.916

DOI:https//doi.org/10.22452/mjs.vol42no1.4
Malaysian Journal of Science 42(1): 32-41 (February 2023)

Table 6. Statistical power of the V and G tests, when both time to failure and time to censoring distributions are Exponential

n	Test / θ	V	G	V	G	V	G	V	G
					$pcens$				
		0.2	0.2	0.3	0.3	0.4	0.4	0.5	0.5
	2	0.203	0.214	0.180	0.179	0.143	0.158	0.129	0.156
10	3	0.313	0.372	0.281	0.341	0.211	0.290	0.190	0.263
	4	0.409	0.554	0.350	0.471	0.283	0.434	0.227	0.397
	2	0.302	0.235	0.255	0.218	0.202	0.211	0.163	0.208
15	3	0.503	0.472	0.450	0.431	0.391	0.425	0.215	0.379
	4	0.630	0.615	0.581	0.575	0.461	0.554	0.333	0.490
	2	0.381	0.304	0.338	0.279	0.274	0.286	0.214	0.224
20	3	0.716	0.575	0.603	0.498	0.493	0.489	0.346	0.465
	4	0.830	0.764	0.777	0.697	0.634	0.654	0.416	0.599
	2	0.501	0.357	0.453	0.329	0.336	0.285	0.229	0.272
25	3	0.825	0.641	0.740	0.637	0.643	0.592	0.426	0.530
	4	0.921	0.826	0.883	0.806	0.766	0.757	0.552	0.678
	2	0.613	0.388	0.509	0.372	0.434	0.367	0.274	0.316
30	3	0.904	0.749	0.834	0.672	0.709	0.648	0.496	0.620
	4	0.981	0.878	0.952	0.835	0.835	0.827	0.646	0.752

Table 7. Statistical power of the V and G tests, when the time to failure distribution is Weibull and time to censoring distribution is Exponential

n	Test / θ	V	G	V	G	V	G	V	G
					$pcens$				
		0.2	0.2	0.3	0.3	0.4	0.4	0.5	0.5
	2	0.325	0.360	0.278	0.295	0.238	0.251	0.168	0.233
10	3	0.477	0.613	0.421	0.576	0.371	0.484	0.263	0.416
	4	0.538	0.798	0.499	0.681	0.427	0.617	0.319	0.550
	2	0.478	0.455	0.436	0.428	0.393	0.363	0.267	0.330
15	3	0.723	0.769	0.685	0.725	0.582	0.665	0.439	0.567
	4	0.807	0.916	0.769	0.879	0.674	0.808	0.506	0.734
	2	0.645	0.514	0.599	0.506	0.499	0.498	0.351	0.430
20	3	0.897	0.859	0.862	0.836	0.752	0.801	0.572	0.723
	4	0.957	0.954	0.929	0.920	0.839	0.906	0.665	0.849
	2	0.786	0.625	0.717	0.614	0.612	0.598	0.447	0.532
25	3	0.975	0.917	0.942	0.910	0.875	0.869	0.707	0.816
	4	0.995	0.977	0.979	0.972	0.953	0.945	0.801	0.921
	2	0.864	0.701	0.816	0.695	0.699	0.667	0.537	0.601
30	3	0.992	0.942	0.980	0.938	0.932	0.910	0.803	0.873
	4	0.999	0.986	0.995	0.983	0.971	0.970	0.882	0.955

According to the Tables 5-7, we observe the following about the statistical power of the tests:

a. The power of both tests increases with an increase in the sample size (n) and scale parameter (θ). However, the power decreases with an increase in the censoring percentage $(pcens)$.
b. In the case of Lindley and Weibull distribution, from Tables 5 and 7, we observe that for the smaller censoring percentage, the proposed test performs better than Gehan's test for all scale parameters considered here when the sample size is ≥ 20.
c. In the case of Exponential distribution, from Table 6, we observe that for the smaller censoring percentage, the proposed test performs better than Gehan's test for all scale parameters considered here when the sample size is ≥ 15.

6. References

Alling D. (1963). Early decision in the Wilcoxon two-sample test. Journal of the American Statistical Association 58: 713-720.

Deshpande JV. & Purohit SG. (2015). Lifetime Data: Statistical Models and Methods (2nd edition), Singapore: World Scientific Publishing Co. Pvt. Ltd.

Efron B. (1967). The two-sample problem with censored data. Berkeley Symposium on Mathematical Statistics and Probability 5.4: 831-853.

DOI:https//doi.org/10.22452/mjs.vol42no1.4
Malaysian Journal of Science 42(1): 32-41 (February 2023)

Gehan EA. (1965). A generalized Wilcoxon test for comparing arbitrarily singly-censored samples. Biometrika 52: 202-223.

Goyal M. & Kumar N. (2020). Two new classes of nonparametric tests for scale parameters. Journal of Statistical Computation and Simulation 90: 3093-3105.

Halperin M. (1960). Extension of the Wilcoxon-Mann-Whitney test to samples censored at the same fixed point. Journal of the American Statistical Association 55: 125-138.

Kaplan EL. & Meier P. (1958). Non-Parametric estimation from incomplete observations. Journal of the American Statistical Association 53: 457-481.

Kössler W. (1994). Restrictive adaptive tests for the treatment of the two-sample scale problem. Computational Statistics & Data Analysis 18: 513–524.

Kössler W. & Kumar N. (2010). An adaptive test for the two-sample scale problem based on U-statistics. Communications in Statistics - Simulation and Computation 39: 1785-1802.

Lee ET., Desu MM. & Gehan EA. (1975). A Monte Carlo study of the power of some two-sample tests. Biometrika 62: 425-432.

Mantel N. (1967). Ranking procedures for arbitrarily restricted observation. Biometrics 23: 65-78.

Miller RG. (2011). Survival Analysis (2nd edition), New York, USA: John Wiley & Sons.

Mood AM. (1954). On the asymptotic efficiency of certain nonparametric two-sample tests. Annals of Mathematical Statistics 25: 514–522.

Rao UVR., Savage IR. & Sobel M. (1960). Contributions to the theory of rank order statistics: the two-sample censored case. Annals of Mathematical Statistics 31: 415-426.

Stablein DM. & Koutrouvelis IA. (1985). A two-sample test sensitive to crossing hazards in uncensored and singly censored data. Biometrics 41: 643-652.

Sukhatme BV. (1957). On certain two-sample nonparametric tests for variances. Annals of Mathematical Statistics 28: 188–194.

Wilcoxon F. (1945). Individual comparisons by ranking methods. Biometrics 1: 80-83.

DOI:https//doi.org/10.22452/mjs.vol42no1.4
Malaysian Journal of Science 42(1): 32-41 (February 2023)

MALAYSIAN JOURNAL OF SCIENCE
MJS
ISSN 1394-3065

Regular Issue

Malaysian Journal of Science 42 (1): 42-61 (February 2023) https://mjs.um.edu.my

MODELLING THE MULTITEAM PREY–PREDATOR DYNAMICS USING THE DELAY DIFFERENTIAL EQUATION

Pankaj Kumar[1a], Shiv Raj[2a]*

Abstract: In nature, many species form teams and move in herds from one place to another. This helps them in reducing the risk of predation. Time delay caused by the age structure, maturation period, and feeding time is a major factor in real-time prey–predator dynamics that result in periodic solutions and the bifurcation phenomenon. This study analysed the behaviour of teamed-up prey populations against predation by using a mathematical model. The following variables were considered: the prey population Pr1, the prey population Pr2, and the predator population Pr3. The interior equilibrium point was calculated. A local satiability analysis was performed to ensure a feasible interior equilibrium. The effect of the delay parameter on the dynamics was examined. A Hopf bifurcation was noted when the delay parameter crossed the critical value. Direction analysis was performed using the centre manifold theorem. The graphs of analytical results were plotted using MATLAB.

Keywords: *Prey population, predator population, equilibrium point, delay parameter, direction analysis, hopf bifurcation*

1. Introduction

Numerous applied mathematicians and ecologists have increasingly focused on the predator–prey relationship because of its generality and significance. Several complicated models for two or more interacting species systems have been developed considering the effects of crowding, age structure, time delay, functional response, switching, and other factors (Kesh et al., 2000; Vayenas et al., 2005; Song et al., 2006; Kundu et al., 2018; Kumar et al., 2022).

In the natural world, all species live in the wild. Some live alone, whereas others live in flocks, hives, packs, or herds. For some animals, living with or near other creatures facilitates their survival and ensures that the demands of each individual member are fulfilled through teamwork. Furthermore, building a team and interacting with others is a fundamental tool through which a team member can consistently achieve positive outcomes and readily meet their needs. This study focused on a system in which herds of prey coexist and are attacked by the same type of predator. The problem of multiteam games is relatively new. For certain animals, forming a team more considerably improves their efficiency of food search as a group compared with when this activity is performed alone and reduces the danger of predation.

The interaction of two prey with one predator is often unstable. The probability of the coexistence of all the three species in a given environment is substantially less. Practically, the predator always wins (Poole, 1974). Determining the types of interactions in a multiteam environment can enable researchers to understand the importance of prey teamwork. The finding of such a study would be similar to those reported by Poole on Leslie–Gower computations (Vance, 1978). Examination of the relationship between the prey population and attack rate cannot be beneficial for determining the type of behavioural characteristics exhibited by animals to identify predators (Abrams et al. 1993). By performing an initial assessment of the model's normalised form, a study demonstrated the presence of dynamics in practical predator–prey systems that can be closely represented by fundamental situations (Klebanoff et al., 1994).

A study identified the necessary criteria for all species to survive indefinitely and determined the condition when species becomes extinct in the system (Kesh et al. 2000). By utilising a stochastic logistic differential equation that calculates ecosystem function, a study examined the long-term unexpected behaviour of the at-risk group (Grasman et al., 2001). Another study reported that strong diffusions or interspecific competitions or slower prey intrinsic growth rates and faster predator intrinsic reduction rates are required to obtain a nonconstant solution (Pedersen et al. 2001). To maintain a stable food web, the predator spends its time between preys with different relative densities (Green, 2004). A predator's behaviour towards a certain prey species is affected by the amount of readily digested food.

Authors information:
[a]Department of Mathematics, Lovely Professional University, Phagwara, Punjab 14441, INDIA. E-mail: pankaj.kumar1@lpu.co.in; shivrajswami86@gmail.com
*Corresponding Author: shivrajswami86@gmail.com

Received: April 23, 2022
Accepted: July 3, 2022
Published: February 28, 2023

DOI:https//doi.org/10.22452/mjs.vol42no1.5
Malaysian Journal of Science 42(1): 42-61 (February 2023)

These genes and therefore the predator population's lifestyle are regulated by a biosynthetic repression approach (Vayenas et al., 2005). Protection evolution in prey species is improved by survival and decreased density fluctuations based on parameters. The inclusion of a predator's optimal meal choice into the model enhanced cohabitation and reduced overall density variations (Yamauchi et al., 2005). If the impulsive duration surpasses a threshold value, the structure remains typically stable (Song et al., 2006).

Many types of animals prefer to be together in a herd. Because different groups share the same habitat, they may cooperate, compete, or form a predator–prey relationship. New paradigm for predator–prey teams were reported in a previous study (Elettreby, 2009). By applying nonlinear feedback control inputs, three prey–predator populations could be stabilised over time asymptotically. The functional parameter limit is set under which variables converge to limit cycles (El-Gohary et al. 2007).

The system exhibits a stationary distribution that is ergodic under certain conditions. The system's solution remains globally asymptotically stable under certain conditions (Liu et al., 2013). Two preys and one predator comprise a dynamic system modelling multiple teams. During an attack, the individuals of both prey groups would support one another and the pace of predation for both groups would differ (Tripathi et al., 2014). A study proposed and tested a mathematical model of hunting for two competing prey species. The pace of growth and functional responses might be nonlinear functions that are general in nature. The findings suggest the presence of a crucial characteristic governing the system's dynamics that is termed as an intraspecific interference factor (Deka et al., 2016). The criteria for local asymptotic stability were achieved in the lack of climate fluctuation. The authors defined the probabilistic approach by including Gaussian white noise notions into all regular equations (Kundu et al., 2018). The authors evaluated the predator–prey relationship in three species in three dimensions by using an ordinary differential equation. For the calculation, the subjective population sizes of two prey species and one predator creature that share their habitats were considered (Aybar et al. 2018). Prey cooperation benefits both prey populations in many ecosystems. If one prey is harmful and the other is weak for a predator, the predator may continue to follow the weak prey (Mishra et al., 2019). In the presence of only one predator in the system, a fourth-order nonlinear differential equation can be used to represent the system (Zhang et al., 2020). A study used a three-species prey–predator system considering that a predator is layman by nature because it survives on two prey animals (Manna et al., 2020). In this study, we considered two prey populations and two predator populations. When two prey species live in two types of habitats and can defend themselves in groups, only one of the two predators can move between the two types of habitats (Frahan, 2020). Trends of a group and the effectiveness of herbicide are both affected by a predator (Emery et al., 2020).

A one-predator model with temporal delays and a weak Allee effect in the prey's growth function is utilised when two prey populations are engaged in direct competition. Despite its simplicity, the system exhibits a wide range of dynamic behaviour, such as the equilibrium point's biostability (Rihan et al., 2020). A high degree of fear of a prey animal and a higher quality of living for second prey may improve the chances of living of that species (Sahoo et al. 2021). One prey is hazardous, whereas the other is harmless to the predator. The predation processes of both prey teams are independently followed by Monod–Haldane and Holling type II functional responses (Alsakaji et al., 2021). Using stochastic Lyapunov functionals, a study proposed some necessary conditions for extinction and persistence in the mean of the three species (Rihan et al. 2022). To examine delay models in population dynamics, we used the model adopted by Rihan (2021). Few studies have investigated the effect of prey maturation on a predator–prey model through mathematical modelling. Predation of mature prey can be evaluated using delay differential equations (Kumar et al., 2021). Time lag is a crucial factor that should be included in the mathematical model to examine the dynamic behaviour of these types of biological systems (Kumar et al., 2022).

No study has used the delay model for studying the dynamics of prey–predator systems. Thus, this study examined the dynamics of multiteam prey–predator systems by using delay differential equations.

2. Mathematical Model

This study examined the dynamics of a two-prey one-predator delay differential model where both preys support each other to prevent predation. The predator is expected to take time τ during the gestation phase in this scenario. Thus, the model can be represented as follows:

DOI:https//doi.org/10.22452/mjs.vol42no1.5
Malaysian Journal of Science 42(1): 42-61 (February 2023)

This study examined the dynamics of a two-prey one-predator delay differential model where both preys support each other to prevent predation. The predator is expected to take time τ during the gestation phase in this scenario. Thus, the model can be represented as follows:

$$\frac{dP_{r1}(t)}{dt} = a_1P_{r1}(t)\big(1 - P_{r1}(t)\big) - P_{r1}(t)P_{r3}(t) + P_{r3}(t)P_{r2}(t)P_{r1}(t) \quad (1)$$

$$\frac{dP_{r2}(t)}{dt} = b_1P_{r2}(t)\big(1 - P_{r2}(t)\big) - P_{r2}(t)P_{r3}(t) + P_{r3}(t)P_{r2}(t)P_{r1}(t) \quad (2)$$

$$\frac{dP_{r3}(t)}{dt} = -c_1 P_{r3}^2(t) + d_1P_{r1}(t-\tau)P_{r3}(t) + e_1P_{r2}(t-\tau)P_{r3}(t) \quad (3)$$

where τ > 0 is the lag time necessary for the predator's gestation period; P_{r1} (t) and P_{r2} (t) are the populations of the two teams of preys, respectively; and P_{r3} (t) is the population of predators. All the parameters have positive values, that is, the values of a_1, b_1, c_1, d_1, and e_1 are more than zero. The system (Poole, 1974; Vance, 1978; Abrams et al., 1993) is related to the following starting functions:

$$(P_{r1}(\theta), P_{r2}(\theta), P_{r3}(\theta)) \in C_+ = C\Big((-\tau, 0), R_+^3\Big), P_{r3}(0),\ P_{r2}(0), P_{r1}(0) > 0$$

The variables and parameters considered in the model by Poole (1974) and Abrams et al. (1993) are listed in Table 1.

Table 1. Description of variables and parameters

Variables/Parameters	Description
P_{r1}	First prey population
P_{r2}	Second prey population
P_{r3}	Predator population
a_1	Natural growth rate of P_{r1}
b_1	Natural growth rate of P_{r2}
c_1	Death rate of the predator population due to mutual competition.
d_1	Rate of predation of P_{r1}
e_1	Rate of predation of P_{r2}
τ	Delay parameter

2.1 Equilibrium Point

The systems (Poole, 1974; Vance, 1978; Abrams et al., 1993) have eight equilibria with specific nonnegativity requirements. In this part, we focus only on the stability and local Hopf bifurcation of the inner equilibrium because the other seven equilibria do not exhibit any effect of delay on the stability of results. To calculate the equilibrium point, equate equation [1] to zero

$$\frac{dP_{r1}}{dt} = 0$$

$$a_1P_{r1} - a_1 P_{r1}^2 - P_{r1}P_{r3} + P_{r1}P_{r2}P_{r3} = 0$$

$$P_{r1}(a_1 - a_1 P_{r1} - P_{r3} + P_{r2}P_{r3}) = 0$$

$$\text{Either } P_{r1} = 0 \ or\ a_1 - a_1 P_{r1} - P_{r3} + P_{r2}P_{r3} = 0$$

$$\frac{dP_{r2}}{dt} = 0$$

$$b_1P_{r2} - b_1 P_{r2}^2 - P_{r2}P_{r3} + P_{r1}P_{r2}P_{r3} = 0$$

$$P_{r2}(b_1 - b_1 P_{r2} - P_{r3} + P_{r1}P_{r3} = 0$$

DOI:https//doi.org/10.22452/mjs.vol42no1.5
Malaysian Journal of Science 42(1): 42-61 (February 2023)

$$\frac{dP_{r3}}{dt} = 0$$
$$-c_1 P_{r3}^2 + d_1 P_{r1} P_{r3} + e_1 P_{r2} P_{r3} = 0$$
$$P_{r3}(-c_1 P_{r3} + d_1 P_{r1} + e_1 P_{r2}) = 0$$

As $P_{r1} \neq 0, P_{r2} \neq 0, P_{r3} \neq 0$ so we have three equations in P_{r1}, P_{r2}, P_{r3}

$$a_1 - a_1 P_{r1} - P_{r3} + P_{r2} P_{r3} = 0$$
$$a_1(1 - P_{r1}) + (-1 + P_{r2}) P_{r3} = 0 \quad (4)$$
$$b_1 - b_1 P_{r2} - P_{r3} + P_{r1} P_{r3} = 0$$
$$b_1(1 - P_{r2}) + (-1 + P_{r1}) P_{r3} = 0 \quad (5)$$
$$-c_1 P_{r3} + d_1 P_{r1} + e_1 P_{r2} = 0 \quad (6)$$

Multiply (4) by $-(-1 + P_{r1})$ and (5) by $(-1 + P_{r1})$ then add

$$a_1(1 - P_{r1})(-)(-1 + P_{r1}) - (-1 + P_{r1})(-1 + P_{r2}) P_{r3} = 0$$
$$b_1(1 - P_{r1})(-1 + P_{r2}) + (-1 + P_{r1})(-1 + P_{r2}) P_{r3} = 0$$

Add these equations

$$a_1(1 - P_{r1})(1 - P_{r1}) + b_1(1 - P_{r1})(-1 + P_{r2}) = 0$$
$$a_1(1 - P_{r1})^2 - b_1(1 - P_{r2})^2 = 0$$
$$a_1(1 - P_{r1})^2 = b_1(1 - P_{r2})^2$$
$$\frac{a_1}{b_1}(1 - P_{r1})^2 = b_1(1 - P_{r2})^2$$

Taking square root

$$\sqrt{\frac{a_1}{b_1}}(1 - P_{r1}) = (1 - P_{r2})$$

$$P_{r2} = 1 - \sqrt{\frac{a_1}{b_1}}(1 - P_{r1})$$

Put this value in (5)

$$\left[1 - \left\{1 - \sqrt{\frac{a_1}{b_1}}(1 - P_{r1})\right\}\right] b_1 + (-1 + P_{r1}) P_{r3} = 0$$
$$\left[1 - 1 + \sqrt{\frac{a_1}{b_1}}(1 - P_{r1})\right] b_1 + (-1 + P_{r1}) P_{r3} = 0$$
$$b_1\left[\sqrt{\frac{a_1}{b_1}}(1 - P_{r1})\right] + (-1 + P_{r1}) P_{r3} = 0$$
$$\sqrt{a_1 b_1}(1 - P_{r1}) + (-1 + P_{r1}) P_{r3} = 0$$
$$(-1 + P_{r1}) P_{r3} = -\sqrt{a_1 b_1}(1 - P_{r1})$$
$$(-1 + P_{r1}) P_{r3} = \sqrt{a_1 b_1}(-1 + P_{r1})$$
$$P_{r3} = \sqrt{a_1 b_1}$$

DOI:https//doi.org/10.22452/mjs.vol42no1.5
Malaysian Journal of Science 42(1): 42-61 (February 2023)

Let $E^*(P_{r1}^*,\ P_{r2}^*,\ P_{r3}^*)$ denote the interior equilibrium

where

$$P_{r3}^* = \sqrt{a_1 b_1}, \qquad P_{r2}^* = \frac{c_1\sqrt{a_1 b_1} - d_1\left(1-\sqrt{b_1/a_1}\right)}{e_1 + d_1\sqrt{b_1 a_1}}, P_{r1}^* = \frac{b_1 c_1 + e_1\left(1-\sqrt{\frac{b_1}{a_1}}\right)}{e_1 + d_1\sqrt{\frac{b_1}{a_1}}}$$

$$c_1\sqrt{a_1 b_1} \le d_1 + e, \qquad c_1 a_1 + d_1 > d_1\sqrt{b_1/a_1}, \qquad c_1 b_1 + e_1 > e_1\sqrt{a_1/b_1}$$

2.2 Stability

Now, we calculate stability of the aforementioned system of equation

$$\frac{dP_{r1}}{dt} = a_1 P_{r1} - a_1 P_{r1}^2 - P_{r1}P_{r3} + P_{r1}P_{r2}P_{r3}$$

$$\frac{dP_{r2}}{dt} = b_1 P_{r2} - b_1 P_{r2}^2 - P_{r2}P_{r3} + P_{r1}P_{r2}P_{r3}$$

$$\frac{dP_{r3}}{dt} = -c_1 P_{r3}^2 + d_1 P_{r1}(t-\tau)P_{r3} + e_1 P_{r2}(t-\tau)P_{r3}$$

Differentiation w.r.t. P_{r1}

$$m_1 = a_1 - 2a_1 P_{r1} - P_{r3} + P_{r2}P_{r3}, \qquad m_2 = P_{r2}P_{r3}, \qquad m_3 = d_1 P_{r3} e^{-\lambda\tau}$$

Differentiation w.r.t. P_{r2}

$$m_4 = P_{r1}P_{r3}, \qquad m_5 = b_1 - 2b_1 P_{r2} - P_{r3} + P_{r1}P_{r3}, \qquad m_6 = e_1 P_{r3} e^{-\lambda\tau}$$

Differentiation w.r.t. P_{r3}

$$m_7 = -P_{r1} + P_{r1}P_{r2}, \qquad m_8 = -P_{r2} + P_{r1}P_{r2}, \qquad m_9 = -2c_1 P_{r3}$$

Let $v_1 = P_{r1} - P_{r1}^*, v_2 = P_{r2}P_{r2}^*$ and $v_3 = P_{r3}P_{r3}^*$then equations [1], [2] and [3] can be expressed in this form

$$\frac{dv_1}{dt} = -a_1 P_{r1}^* - P_{r1}^* v_3 + P_{r1}^* P_{r2}^* v_3 + P_{r1}^* P_{r3}^* v_2 - a_1 v_1^2 - (1 - P_{r2}^*)v_1 v_3 + P_{r1}^* v_2 v_3 + P_{r3}^* v_1 v_2 + v_1 v_2 v_3 \tag{7}$$

$$\frac{dv_2}{dt} = -b_1 P_{r2}^* v_2 - P_{r2}^* v_3 + P_{r1}^* P_{r2}^* v_3 + P_{r2}^* P_{r3}^* v_1 - b_1 v_2^2 - (1 - P_{r1}^*)v_2 v_3 + P_{r2}^* v_1 v_2 + P_{r3}^* v_1 v_2 + v_1 v_2 v_3 \tag{8}$$

$$\frac{dv_3}{dt} = -c_1 P_{r3}^* v_3 - d_1 P_{r3}^* v_1(t-\tau) + e_1 P_{r3}^* v_2(t-\tau) - c_1 v_3^2 - d_1 v_1(t-\tau)v_3 + e_1 v_2(t-\tau)v_3 \tag{9}$$

The stability of the equilibrium $E^*(P_{r1}^*,\ P_{r2}^*,\ P_{r3}^*)$ can be examined by investigating the stability of the origin for equations [7], [8], and [9]. Now, we compute the linearised system's characteristics equations [7], [8], and [9] at (0, 0, 0)

$$\begin{vmatrix} \lambda - m_1 & -m_2 & -m_3 \\ -m_4 & \lambda - m_5 & -m_6 \\ -m_7 & -m_8 & \lambda - m_9 \end{vmatrix} = 0$$

$$\begin{vmatrix} \lambda - (a_1 - 2a_1 P_{r1} - P_{r3} + P_{r2}P_{r3}) & -P_{r2}P_{r3} & -d_1 P_{r3} e^{-\lambda\tau} \\ -P_{r1}P_{r3} & \lambda - (b_1 - 2b_1 P_{r2} - P_{r3} + P_{r1}P_{r3}) & -e_1 P_{r3} e^{-\lambda\tau} \\ P_{r1} - P_{r1}P_{r2} & P_{r2} - P_{r1}P_{r2} & \lambda + 2c_1 P_{r3} \end{vmatrix} = 0$$

After simplification, we obtain the characteristic equation

$$\lambda^3 + X\lambda^2 + Y_1\lambda + e^{-\lambda\tau}(Y_2\lambda + Z_2) = 0 \tag{10}$$

When τ = 0, equation [10] becomes

$$\lambda^3 + X\lambda^2 + (Y_1 + Y_2)\lambda + Z_2 = 0 \tag{11}$$

The Routh–Hurwitz criteria implies that with τ = 0, the equilibrium point E^* is locally asymptotically stable if

$$(\boldsymbol{H_1})X > 0, \qquad (Y_1 + Y_2) > 0, \qquad Z_2 > 0, \qquad X(Y_1 + Y_2) > Z_2 \ hold$$

DOI:https//doi.org/10.22452/mjs.vol42no1.5
Malaysian Journal of Science 42(1): 42-61 (February 2023)

Let us suppose that the condition in $(\boldsymbol{H_1})$ is satisfied. Then, equation [11] with $\tau = \tau_j (j = 0, 1, \dots \dots)$ has a simple pair of conjugate purely imaginary roots $\pm i\omega_0$

$$\tau_j = \frac{1}{\omega_0}\left[arccos\frac{\omega_0^2(\omega_0^2 Y_2 + Z_2 X - Y_1 Y_2)}{Y_2^2\omega_0^2 + Z_2^2} + 2j\pi\right]$$

We have the following conditions:

1. If $\tau \epsilon [0, \tau_0)$, all the roots of equation [11] have negative real parts.
2. If $\tau = \tau_0$, the equation [11] has a pair of conjugate purely imaginary roots $\pm i\omega_0$ and real part is negative for all other solutions.

Proof If $\lambda = 0$ is a solution of (11) if Z_2 = 0. This condition contradicts the third requirement stated in $(\boldsymbol{H_1})$, implying that $\lambda = 0$ is not a solution of [11]. Assume that for some $\tau \geq 0, i\omega$ with $\omega > 0$ is a solution of [11].

$$-i\,\omega^3 - X\omega^2 + iY_1\omega + e^{-\omega\tau}(iY_2\omega + Z_2) = 0$$
$$-i\,\omega^3 - X\omega^2 + iY_1\omega + (cos\,\omega\tau - isin\,\omega\tau)\,(iY_2\omega + Z_2) = 0$$
$$i\,(-\omega^3 + Y_1\omega + Y_2\omega cos\,\omega\tau - Z_2 sin\,\omega\tau) + (-X\omega^2 + Z_2 cos\,\omega\tau + Y_2\omega sin\,\omega\tau) = 0$$

Separating real and imaginary parts

$$-\omega^3 + Y_1\omega + Y_2\omega cos\,\omega\tau - Z_2 sin\,\omega\tau = 0 \quad (12)$$
$$-X\omega^2 + Z_2 cos\,\omega\tau + Y_2\omega sin\,\omega\tau = 0 \quad (13)$$

which gives $$\omega^6 + \alpha\omega^4 + \beta\omega^2 + \gamma = 0 \quad (14)$$

where $\alpha = X^2 - 2Y_1, \beta = Y_1^2 - Y_2^2, \gamma = -Z_2^2$

Let $l = \omega^2$, then equation [14] becomes

$$l^3 + \alpha l^2 + \beta l + \gamma = 0 \quad (15)$$

Supposed $l_1, l_2\ and\ l_3$ are the roots of equation [15] and connected by

Sum of the roots $$l_3 + l_2 + l_1 = -\alpha \quad (16)$$

Product of the roots $$l_3\, l_2\, l_1 = -\gamma \quad (17)$$

Thus, equation [17] has either one or three positive real roots.

Depending on the determinant $\Delta_1$of the equation [15]

where $\Delta_1 = \left(\frac{S}{2}\right)^2 + \left(\frac{T}{3}\right)^3$ and $T = \beta - \frac{1}{3}\alpha^2,\ S = \frac{2}{27}\alpha^3 - \frac{1}{3}\alpha\beta + \gamma$

Three situations are possible for the solution of [15]:

a) If $\Delta_1 > 0$, then one real root and a pair of imaginary roots can be obtained for equation [15]. When the real root is positive, it can be written as follows:

$$l_1 = \sqrt[3]{\frac{-S}{2} + \sqrt{\Delta_1}} + \sqrt[3]{\frac{-S}{2} - \sqrt{\Delta_1}} - \frac{1}{3}\alpha$$

b) If $\Delta_1 = 0$, all three real roots and two repeated roots are obtained for equation [15]. If $\alpha > 0$, we obtain only one positive root, $l_1 = 2\sqrt[3]{\frac{-S}{2}} - \frac{1}{3}\alpha. If\ \alpha < 0$, we obtain only one positive root, $l_1 = 2\sqrt[3]{\frac{-S}{2}} - \frac{1}{3}\alpha$ for , $\sqrt[3]{\frac{-S}{2}} > -\frac{1}{3}\alpha$ and three positive real roots for $\frac{\alpha}{6} < \sqrt[3]{\frac{-S}{2}} < -\frac{1}{3}\alpha$, $l_1 = 2\sqrt[3]{\frac{-S}{2}} - \frac{1}{3}\alpha,\ l_2 = l_3 = -\sqrt[3]{\frac{-S}{2}} - \frac{1}{3}\alpha$

c) If $\Delta_1 < 0$, we obtain all the three roots are real and distinct, $l_1 = 2\sqrt{\frac{|T|}{3}}\cos\left(\frac{\xi}{3}\right) - \frac{\alpha}{3}$

$$l_2 = \sqrt{\frac{|T|}{3}}cos\left(\frac{\xi}{3} + \frac{2\pi}{3}\right) - \frac{\alpha}{3}, \qquad l_3 = 2\sqrt{\frac{|T|}{3}}\cos\left(\frac{\xi}{3} + \frac{4\pi}{3}\right) - \frac{\alpha}{3}$$

Where $\cos\xi = \left(-\frac{S}{2\sqrt{\left(\frac{|T|}{3}\right)^3}}\right)$, $0 < \xi < \pi$. Moreover, if $\alpha > 0$, only one positive root exists. Otherwise, if $\alpha < 0$, we obtain all three real positive roots or only one positive real root. It is equivalent to max (l_1, l_2, l_3) only when we obtain one positive real root. The number of positive real roots depends on the sign of α. Equation [15] has only one positive real root when $\alpha \geq 0$ is present. Otherwise, we obtained three positive real roots. When $\alpha = X^2 - 2Y_1 > 0$, one positive real root is obtained for [15]. Let the obtained positive real root be denoted by symbol l_0. Then, equation [14] would have only one positive real root $\omega_0 = \sqrt{l_0}$. From equation [13], we have

DOI:https//doi.org/10.22452/mjs.vol42no1.5
Malaysian Journal of Science 42(1): 42-61 (February 2023)

$$cos\omega_0\tau = \frac{\omega_0^2(\omega_0^2 Y_2 + Z_2 X - Y_1 Y_2)}{Y_2^2\omega_0^2 + Z_2^2}$$

Express

$$\tau_j = \frac{1}{\omega_0}\left[arccos\frac{\omega_0^2(\omega_0^2 Y_2 + Z_2 X - Y_1 Y_2)}{Y_2^2\omega_0^2 + Z_2^2} + 2j\pi\right] \quad (18)$$

where $j = 0, 1, 2, 3, 4, 5, \ldots.. \pm i\omega_0$ obtained a root of equation [10] when $\tau = \tau_j$.
Furthermore, if (H_1) standards are fulfilled, all the roots of equation [10] with τ = 0 have negative real values. We determine the outcomes of lemma1 by summarising the preceding discussion and using the lemma provided. The proof is completed with the following outcomes from theorem lemma 1.

Theorem 2 Assume the condition in (H1) is fulfilled. If $\tau \epsilon [0, \tau_0)$, then the zero solution of equations [7], [8], and [9] is asymptotically stable. Using the classic Hopf bifurcation theorem for retarded functional differential equations, we can obtain the following factors:

Lemma 3. Let $n(l_0) = (3l_0^2 + 2\alpha l_0 + \beta) \neq 0$ and condition in (H_1) are satisfied. For $(j = 0, 1, \ldots)$, $\lambda(\tau) = \delta(\tau) + i\omega(\tau)$ is denoted as the solution of equation [10] that fulfils the condition $\delta(\tau_j) = 0, \omega(\tau_j) = \omega_0$ were

$$\tau_j = \frac{1}{\omega_0}\left[arccos\frac{\omega_0^2(\omega_0^2 Y_2 + Z_2 X - Y_1 Y_2)}{Y_2^2\omega_0^2 + Z_2^2} + 2j\pi\right]$$

Then, $\pm i\omega_0$ are pair of simple roots. If the transversality condition (H_1) $\delta'(\tau_J) = \left.\frac{Re\,\lambda(\tau)}{d\tau}\right|_{\lambda=i\omega_0} \neq 0$ holds good, we obtain a Hopf bifurcation for [7], (8) and (9) at $v = 0$ and $\tau = \tau_j$.
Proof. Assume $\lambda = \lambda(\tau)$ is a solution of equation [10]. Put $\lambda(\tau)$ in [10] and differentiating with respect to τ on both sides, we get

$$\left[(3\lambda^2 + 2X\lambda + Y_1) + \left((\lambda Y_2 + Z_2)(-\tau) + Y_2\right)e^{-\lambda\tau}\right]\frac{d\lambda}{d\tau} = \lambda(\lambda Y_2 + Z_2)e^{-\lambda\tau}$$

Thus

$$\left(\frac{d\lambda}{d\tau}\right)^{-1} = \frac{(3\lambda^2 + 2X\lambda + Y_1)e^{\lambda\tau}}{\lambda(\lambda Y_2 + Z_2)} + \frac{Y_2}{\lambda(\lambda Y_2 + Z_2)} - \frac{\tau}{\lambda}$$

From [12]–[15], we have

$$-\alpha'(\tau_J) = Re\left[\frac{(3\lambda^2 + 2X\lambda + Y_1)e^{\lambda\tau}}{\lambda(\lambda Y_2 + Z_2)}\right] + Re\left[\frac{Y_2}{\lambda(\lambda Y_2 + Z_2)}\right]$$

$$= \frac{1}{\Omega}[3\omega_0^6 + 2(X^2 - 2Y_1)\omega_0^4 + (Y_1^2 - 2XZ_2 - Y_2^2)\omega_0^2]$$

$$= \frac{1}{\Omega}(3\omega_0^6 + 2\alpha\omega_0^4 + \beta\omega_0^2)$$

$$= \frac{\omega_0^2}{\Omega}(3\omega_0^4 + 2\alpha\omega_0^2 + \beta)$$

$$= \frac{\omega_0^2}{\Omega}(3l_0^2 + 2\alpha l_0 + \beta)$$

$$= \frac{\omega_0^2}{\Omega}n(l_0)$$

where $\Omega = Y_2^2\omega_0^2 + Z_2^2$

$n(l_0) = 3l_0^2 + 2\alpha l_0 + \beta$. Observed, when $\Omega > 0$ and $\omega_0 > 0$

We find that

Sign $[\delta'(\tau_J)] = sign[n(l_0)]$ proves the theorem.

DOI:https//doi.org/10.22452/mjs.vol42no1.5
Malaysian Journal of Science 42(1): 42-61 (February 2023)

3. Direction Analysis and Stability of the Hopf Bifurcation Solution

In the previous section, we observed that a set of solutions can be obtained as bifurcates from the favourable steady state E* at a crucial level of τ. The direction, stability, and period of these bifurcating periodic solutions should be determined. We build precise equations defining the properties of the Hopf bifurcation at the critical value by using normal form theory and the centre manifold theorem at the critical point τ_j in this section.

Normalizing delay value τ by the time scaling $t \longrightarrow \frac{t}{\tau}$ system [7], [8], and [9] is transformed into

$$\frac{dv_1}{dt} = -a_1P_{r1}^*v_1 - P_{r1}^*v_3 + P_{r1}^*P_{r2}^*v_3 + P_{r1}^*P_{r3}^*v_2 - av_1^2 - (1-P_{r2}^*)v_1v_3 + P_{r1}^*v_2v_3 + P_{r3}^*v_1v_2 + v_1v_2v_3 \quad (19)$$

$$\frac{dv_2}{dt} = -b_1P_{r2}^*v_2 - P_{r2}^*v_3 + P_{r1}^*P_{r2}^*v_3 + P_{r2}^*P_{r3}^*v_1 - bv_2^2 - (1-P_{r1}^*)v_2v_3 + P_{r2}^*v_1v_3 + P_{r3}^*v_1v_2 + v_1v_2v_3 \quad (20)$$

$$\frac{dv_3}{dt} = -c_1P_{r3}^*v_3 + d_1P_{r3}^*v_1(t-1) + e_1P_{r3}^*v_2(t-1) - c_1v_3^2 + d_1v_1(t-1)v_3 + e_1v_2(t-1)v_3 \quad (21)$$

Take phase plane $C = C((-1,0), R_+^3)$. WLOG, denote the critical value τ_j by τ_0. If $\tau = \tau_0 + \sigma$, then $\sigma = 0$ is a value for Hopf bifurcation for equations [19]–[21]. For the simplicity of notations, we rewrite [19]–[21] in this form

$$v'(t) = L_\sigma(v_t) + G(\sigma, v_t) \quad (22)$$

where $v(t) = v_1(t), v_2(t), v_3(t) \epsilon R^3, v_t(\theta) = v(t+\theta)$ and

$$L_\sigma\varphi = (\tau_0+\sigma)\begin{bmatrix} -a_1P_{r1}^* & P_{r1}^*P_{r3}^* & -P_{r1}^* + P_{r1}^*P_{r2}^* \\ P_{r2}^*P_{r3}^* & -b_1P_{r2}^* & -P_{r2}^* + P_{r1}^*P_{r2}^* \\ 0 & 0 & -c_1P_{r3}^* \end{bmatrix}\begin{bmatrix} \varphi_1(0) \\ \varphi_2(0) \\ \varphi_3(0) \end{bmatrix} + (\tau_0+\sigma)\begin{bmatrix} 0 & 0 & 0 \\ 0 & 0 & 0 \\ d_1P_{r3}^* & e_1P_{r3}^* & 0 \end{bmatrix}\begin{bmatrix} \varphi_1(-1) \\ \varphi_2(-1) \\ \varphi_3(-1) \end{bmatrix}$$ and

$$G(\sigma,\varphi) = (\tau_0+\sigma)\begin{bmatrix} G_1 \\ G_2 \\ G_3 \end{bmatrix}$$ respectively, were

$$G_1 = -a_1\varphi_1^2(0) - (1-P_{r2}^*)\varphi_1(0)\varphi_3(0) + P_{r1}^*\varphi_2(0)\varphi_3(0) + P_{r3}^*\varphi_2(0)\varphi_1(0) + \varphi_3(0)\varphi_2(0)\varphi_1(0),$$

$$G_2 = -b_1\varphi_1^2(0) - (1-P_{r1}^*)\varphi_3(0)\varphi_2(0) + P_{r2}^*\varphi_3(0)\varphi_1(0) + P_{r3}^*\varphi_2(0)\varphi_1(0) + \varphi_3(0)\varphi_2(0)\varphi_1(0),$$

$$G_3 = -c_1\varphi_3^2(0) + d_1\varphi_1(-1)\varphi_3(0) + c_1\varphi_2(-1)\varphi_3(0),$$

$$\varphi(0) = (\varphi_1(\theta), \varphi_2(\theta), \varphi_3(\theta))^T \epsilon\, C(C-1,0), R).$$

Using the Riesz representation theorem, we can find a function $\measuredangle(\theta,\sigma)$ of bounced variation for $\theta \epsilon [-1,0)$ as

$$L_\sigma\varphi = \int_{-1}^{0} d\measuredangle(\theta,0)\,\varphi(0) for\ \varphi \epsilon C.$$

We choose

$$\measuredangle(\theta,\sigma) = (\tau_0+\sigma)\begin{bmatrix} -a_1P_{r1}^* & P_{r1}^*P_{r3}^* & -P_{r1}^* + P_{r2}^*P_{r1}^* \\ P_{r2}^*P_{r3}^* & -b_1P_{r2}^* & -P_{r2}^* + P_{r2}^*P_{r1}^* \\ 0 & 0 & -c_1P_{r3}^* \end{bmatrix}\chi(\theta) + (\tau_0+\sigma)\begin{bmatrix} 0 & 0 & 0 \\ 0 & 0 & 0 \\ d_1P_{r3}^* & e_1P_{r3}^* & 0 \end{bmatrix}\chi(\theta+1)$$

where χ is the Delta Dirac function for $\varphi \epsilon C([-1,0], R_+^3)$,

Let us define a function

$$A(\sigma)\varphi = \begin{cases} d\varphi(0) & \theta \epsilon [-1,0) \\ \int_{-1}^{0} d \measuredangle (\theta,\varphi) & \theta = 0 \end{cases}$$

DOI:https//doi.org/10.22452/mjs.vol42no1.5
Malaysian Journal of Science 42(1): 42-61 (February 2023)

$$H(\sigma)\,\varphi = \begin{cases} 0 & \theta \in [-1,0) \\ G(\sigma,\varphi) & \theta = 0 \end{cases}$$

Then, the system (22) is equivalent to

$$v_t' = X(\sigma)v_t + H(\sigma)v_t \tag{23}$$

For $\varepsilon \in C'([-1,0], R_+^3)$, define

$$X^*\epsilon(s) = \begin{cases} \dfrac{-d\epsilon(s)}{d\theta} & s \in [-1,0, \\ \displaystyle\int_{-1}^{0} d \nprec^T (-1,0)\varepsilon(-t) & s = 0 \end{cases}$$

The bilinear inner product is as follows:

$$< \varepsilon(s), \varphi(\theta) > = \in (0)\,\varphi(0) - \int_{-1}^{0}\int_{v=0}^{0} \epsilon(v-\theta)d \nprec (\theta)\varphi(v)dv \tag{24}$$

X^* *and* $X(0)$are adjoint operators; thus, $i\omega_0$ are the eigen values of $X(0)$. They are the eigen values of X^*. Suppose that $\beta(\theta) = \beta(0)e^{i\omega_{0\theta}}$is an eigen vector of $X(0)$ corresponding to the eigenvalue $i\omega_0$. Then, $X(0) = i\omega_0\beta(\theta)$. When $\theta = 0$, we obtain

$$\left[i\omega_0 I - \int_{-1}^{0} d \nprec (\theta)e^{i\omega_0\theta}\right]\beta(0) = 0$$

which yields $\beta(0) - (1, x_1 y_1)^T$,
where

$$x_1 = \frac{(P_{r1}^* - P_{r2}^*P_{r1}^*)P_{r3}^*P_{r2}^* + (P_{r2}^* - P_{r2}^*P_{r1}^*)(i\omega_0 + a_1P_{r1}^*)}{P_{r1}^*P_{r3}^*(P_{r2}^* - P_{r2}^*P_{r1}^*) - (P_{r1}^* - P_{r2}^*P_{r1}^*)(i\omega_0 + P_{r2}^*b_1)}$$

$$y_1 = \frac{P_{r2}^*P_{r3}^{*2}P_{r1}^* - (i\omega_0 + a_1P_{r1}^*)(i\omega_0 + b_1P_{r2}^*)}{P_{r1}^*P_{r3}^*(P_{r2}^* - P_{r2}^*P_{r1}^*) - (P_{r1}^* - P_{r2}^*P_{r1}^*)(i\omega_0 + P_{r2}^*b_1)}$$

Similarly, it can be verified that $\beta^*(s) = D(1, x_2 y_2)e^{i\omega_0\tau_0 s}$is the eigen vector of X^*corresponding to $-i\omega_0$,
where

$$x_2 = \frac{P_{r2}^*P_{r3}^*(P_{r1}^* - P_{r2}^*P_{r1}^*) + (P_{r2}^* - P_{r2}^*P_{r1}^*)(a_1P_{r1}^* - i\omega_0)}{P_{r1}^*P_{r3}^*(P_{r2}^* - P_{r1}^*P_{r2}^*) - (P_{r1}^* - P_{r1}^*P_{r2}^*)(b_1P_{r2}^* - i\omega_0)}$$

$$y_2 = \frac{P_{r1}^*P_{r2}^*P_{r3}^{*2} - (a_1P_{r1}^* - i\omega_0)(b_1P_{r2}^* - i\omega_0)}{P_{r1}^*P_{r3}^*(P_{r2}^* - P_{r2}^*P_{r1}^*) - (P_{r1}^* - P_{r2}^*P_{r1}^*)(b_1P_{r2}^* - i\omega_0)}$$

To assume $< \beta^*(s), \beta(\theta) \geq 1$, we have to calculate the value of D. From [24], we obtain $< \beta^*(s), \beta(\theta) >$

$$= \bar{D}(1, \bar{x}_2, \bar{y}_2)(1, x_1, y_1)^T - \int_{-1}^{0}\int_{v=0}^{\theta} \bar{D}(1, \bar{x}_2, \bar{y}_2)\, e^{-i\omega_0\tau_0(v-\theta)} d \nprec (\theta)(1, x_1, y_1)^T e^{-\omega_0\tau_0}dv$$

$$= \bar{D}\{1 + x_1\bar{x}_2 + y_1\bar{y}_2 - \int_{-1}^{0} (1, \bar{x}_2, \bar{y}_2)\, \theta e^{i\omega_0\tau_0\theta} d \nprec (\theta)(1, x_1, y_1)^T\}$$

$$= \bar{D}\{1 + x_1\bar{x}_2 + y_1\bar{y}_2 - \tau_0\, \bar{y}_2P_{r3}^*(d_1x_1 + e_1y_2)e^{i\omega_0\tau_0}\}$$

Hence, we can choose

$$\bar{D} = \frac{1}{1 + x_1\bar{x}_2 + y_1\bar{y}_2 + \tau_0\bar{y}_2P_{r3}^*(d_1\sigma_{1+}e_1y)e^{i\omega_0\tau_0}}$$

Such that

$$< \beta^*(s), \beta(\theta) \geq 1, < \beta^*(s), \beta(\theta) = 0$$

Continue the coordinates defining the vector by following the algorithm and using the same notations as their manifold c_0 at $\sigma = 0$. Let v_t be a solution of equation [23] with $\sigma = 0$. Define

$$m(t) = < \beta^*(s), v_t(\theta) > \tag{25}$$

$$V(t,\theta) = v_t(\theta) - 2Re\, m(t)\beta(\theta) \tag{26}$$

According to manifold, we obtain centre C_0. Accordingly,

$$V(t,\theta) = V(m(t)\,\bar{m}(t), \theta),$$

DOI:https//doi.org/10.22452/mjs.vol42no1.5
Malaysian Journal of Science 42(1): 42-61 (February 2023)

where

$$V(m,\bar{m},\theta) = V_{20}(\theta)\frac{m^2}{2} + V_{11}(\theta)m\bar{m} + V_{02}(\theta)\frac{\bar{m}^2}{2} + \cdots$$

m and $\bar{m}$ are local values for the manifold centre C_0 in the direction of β^* and $\bar{\beta}^*$. When V is real, v_t is real. We assume only the real solution. For solution $v_t \in C_0$ of [23], since $\sigma = 0$,

$$\begin{aligned} m'(t) &= i\omega_0\tau_0 m + < \bar{\beta}^*(\theta), G(0, V(m,\bar{m},\theta) + 2Re\{m(t)\beta(\theta)\}) > \\ &= i\omega_0\tau_0 m + \bar{\beta}^*(0)G(0, V(m,\bar{m},0) + 2Re\{m(t)\beta(\theta)\}) \\ &= i\omega_0\tau_0 m + \bar{\beta}^*(0)\, G_0(m,\bar{m}) \end{aligned} \tag{27}$$

where $s(m,\bar{m}) = \bar{\beta}^*(0)\ G_0(m,\bar{m})$

$$= s_{20}(\theta)\frac{m^2}{2} + s_{11}(\theta)m\bar{m} + s_{02}(\theta)\frac{\bar{m}^2}{2} + s_{21}\frac{m^2\bar{m}}{2} + \cdots \tag{28}$$

Noticing

$$v_t(\theta) = (v_{it}, v_{2t}, v_{3t}) = V(t,\theta) + m\beta(\theta) + \bar{m}\bar{\beta}(\theta)$$

and $\beta(0) = (1, x_1, y_1)^T e^{i\omega_0\tau_0\theta}$, we have

$$v_{1t}(0) = m + \bar{m} + V_{20}^{(1)}\frac{m^2}{2} + V_{11}^{(1)}(0)m\bar{m} + V_{02}^{(1)}(0)\frac{\bar{m}^2}{2} + \cdots,$$

$$v_{2t}(0) = x_1 m + \bar{x}_1\bar{m} + V_{20}^{(2)}\frac{m^2}{2} + V_{11}^{(2)}(0)m\bar{m} + V_{02}^{(2)}(0)\frac{\bar{m}^2}{2} + \cdots,$$

$$v_{3t}(0) = y_1 m + \bar{y}_1\bar{m} + V_{20}^{(3)}(0)\frac{m^2}{2} + V_{11}^{(3)}(0)m\bar{m} + V_{02}^{(3)}(0)\frac{\bar{m}^2}{2} + \cdots,$$

$$v_{1t}(-1) = me^{-i\omega_0\tau_0} + \bar{m}e^{i\omega_0\tau_0} + V_{20}^{(1)}(-1)\frac{m^2}{2} + V_{11}^{(1)}(-1)m\bar{m} + V_{02}^{(1)}(-1)\frac{\bar{m}^2}{2} + \cdots,$$

$$v_{2t}(-1) = x_1 e^{-i\omega_0\tau_0} + \bar{x}e^{i\omega_0\tau_0}\bar{m} + V_{20}^{(2)}(-1)\frac{m^2}{2} + V_{11}^{(2)}(-1)m\bar{m} + V_{02}^{(2)}(-1)\frac{\bar{m}^2}{2} + \cdots,$$

Comparing coefficients with (28), we have

$s_{20} = -2\tau_0\bar{D}[a_1 + (1 - P_{r2}^*)y_1 - x_1(P_{r1}^* y_1 + P_{r3}^*) + \bar{x}_2(b_1 x_1^2 + (1 - P_{r1}^*)x_1 y_1) - x_1 P_{r3}^* - y_1 P_{r2}^* + \bar{y}_2 y_1\big(c_1 y_1 - d_1 e^{-i\omega_0\tau_0} - e_1 x_1 e^{-i\omega_0\tau_0}\big)],$

$s_{11} = -2\tau_0\bar{D}[a_1 + (1 - P_{r2}^*)Re\{y_1\} - P_{r1}^* Re\{\bar{y}_1 x_1\} - P_{r3}^* Re\{x_1\} + \bar{x}_2(x_1\bar{x}_1 b_1 + (1 - P_{r1}^*)Re\{x_1\bar{y}_1\} - P_{r2}^* Re\{\bar{y}_1\} - P_{r3}^*\{x_1\} + \bar{y}_2(c_1 y_1\bar{y}_1 - d_1 Re\{y_1 e^{i\omega_0\tau_0}\} - e_1 Re\{y_1\bar{x}_1 e^{i\omega_0\tau_0}\})],$

$s_{02} = -2\tau_0\bar{D}\big[a_1 + (1 - P_{r2}^*)\bar{y}_1 - \bar{x}_1(P_{r1}^*\bar{y}_1 + P_{r3}^*) + \bar{x}_2(b_1\bar{x}_1^2 + (1 - P_{r1}^*)\bar{x}_1\bar{y}_1) - \bar{x}_1 P_{r3}^* - \bar{y}_1 P_{r2}^* + \bar{y}_2\bar{y}_1\big(c_1\bar{y}_1 - d_1 e^{-i\omega_0\tau_0}\big)\big]$

$s_{21} = -2\tau_0\bar{D}[a_1\left(V_{20}^{(1)}(0) + 2V_{11}^{(1)}(0)\right) + (1 - P_{r2}^*)(\frac{1}{2}V_{20}^{(1)}(0)\bar{y}_1 + V_{11}^{(1)}(0)y_1 + \frac{1}{2}V_{20}^{(3)}(0) + V_{11}^{(3)}(0) - (2Re\{x_1\bar{y}_1\} + x_1 y_1) - P_{r1}^*\left(\frac{1}{2}W_{20}^{(2)}(0)\bar{y}_1 + \frac{1}{2}V_{20}^{(3)}(0)\bar{x}_1 + V_{11}^{(2)}(0)y_1 + V_{11}^{(3)}(0)x_1\right) - P_{r3}^*\left(\frac{1}{2}V_{20}^{(2)}(0) + \frac{1}{2}V_{20}^{(1)}(0)\bar{x}_1 + V_{11}^{(2)}(0) + V_{11}^{(1)}(0)x_1\right) + \bar{x}_2\left(b_1 V_{20}^{(2)}(0)\bar{x}_1 + 2V_{11}^{(2)}(0)x_1\right) + (1 - P_{r1}^*)(\frac{1}{2}V_{20}^{(2)}(0)\bar{y}_1 + V_{11}^{(3)}(0)x_1 - (2Re\{x_1\bar{y}_1\} + x_1 y_1) - P_{r2}^*\left(\frac{1}{2}V_{20}^{(1)}(0)\bar{y}_1 + \frac{1}{2}V_{20}^{(3)}(0) + V_{11}^{(1)}(0)y_1 + V_{11}^{(1)}(0)y_1 + V_{11}^{(3)}(0) - P_{r3}^*\left(\frac{1}{2}V_{20}^2(0) + \frac{1}{2}V_{20}^{(1)}(0)\bar{x}_1 + V_{11}^{(2)}(0) + V_{11}^{(1)}(0)x_1\right)\right) + \bar{y}_2(c_1\left(V_{20}^{(3)}(0)\bar{y}_1 + 2V_{11}^{(3)}(0)y_1\right) - d_1\left(\frac{1}{2}V_{20}^{(1)}(-1)\bar{y}_1 + V_{11}^{(1)}(-1)y_1 + \frac{1}{2}V_{20}^{(3)}(0)e^{i\omega_0\tau_0} + V_{11}^{(3)}(0)e^{-i\omega_0\tau_0}\right) - e_1(\frac{1}{2}V_{20}^{(1)}(-1)\bar{y}_1 + V_{11}^{(2)}(-1)y_1 + \frac{1}{2}V_{20}^{(3)}(0)\bar{x}_1 e^{i\omega_0\tau_0} + V_{11}^{(3)}x_1 e^{-i\omega_0\tau_0}))]$

Because of the presence of $V_{20}(\theta)$ and $V_{11}(\theta)$ in s_{21}, we need to further compute them. From (23) and (26), we have

$$\begin{aligned} V' &= v_t' - m'\beta - \bar{m}'\beta \\ &= \begin{cases} XV - 2Re\{\bar{\beta}^*(0)G_0\beta(\theta)\}, & \theta \in [-1,0), \\ XV - 2Re\{\bar{\beta}^*(0)G_0\beta(0)\} + G_0 & \theta = 0 \end{cases} \\ &\triangleq XV + N(m,\bar{m},\theta), \end{aligned} \tag{29}$$

DOI:https//doi.org/10.22452/mjs.vol42no1.5
Malaysian Journal of Science 42(1): 42-61 (February 2023)

where

$$N(m,\overline{m},\theta) = N_{20}(\theta)\frac{m^2}{2} + N_{11}(\theta)m\overline{m} + N_{02}(\theta)\frac{\overline{m}^2}{2} + N_{21}\frac{m^2\overline{m}}{2} + \ldots, \quad (29)$$

On the other hand, on C_0near the origin

$$V' = V_m m' + V_{\overline{m}}\overline{m}'$$

Expanding the aforementioned series and comparing the coefficient, we obtain

$$[X - 2i\omega_0 I]V_{20}(\theta) = -N_{20}(\theta) \quad (30)$$

$$XV_{11}(\theta) = -N_{11}(\theta) \quad (31)$$

From (27), we know that for $\theta \epsilon [-1,0)$,

$$N(m,\overline{m},\theta) = -\beta^{\bar{y}}(0)\bar{G}_0\beta(\theta) - \beta^*(0)\bar{G}_0\bar{\beta}(\theta) = -s\beta(\theta) - \bar{s}\bar{\beta}(\theta).$$

Comparing the coefficient with (30), we obtain $\theta \epsilon [-1,0]$ that

$$N_{20}(\theta) = -s_{20}\beta(\theta) - \bar{s}_{02}\bar{\beta}(\theta)$$

$$N_{11}(\theta) = -s_{11}\beta(\theta) - \bar{s}_{11}\bar{\beta}(\theta)$$

From (29), (30), and (31) and the definition of X, we obtain

$$V_{20}(\theta) = 2i\omega_0\tau_0 V_{20}(\theta) + s_{20}\beta(\theta) + \bar{s}_{02}\bar{\beta}(\theta)$$

Solving for $V_{20}(\theta)$, we obtain

$$V_{20}(\theta) = \frac{is_{20}}{\omega_0\tau_0}\beta(0)e^{i\omega_0\tau_{0\theta}} + \frac{i\bar{s}_{02}\bar{\beta}(0)}{3\omega_0\tau_0}e^{-i\omega_0\tau_0\theta} + P_1 e^{2i\omega_0\tau_0\theta}$$

Similarly,

$$V_{11}(\theta) = \frac{-is_{11}}{\omega_0\tau_0}\beta(0)e^{i\omega_0\tau_{0\theta}} + \frac{i\bar{s}_{11}\bar{\beta}(0)}{\omega_0\tau_0}e^{-i\omega_0\tau_0\theta} + P_2$$

where $P_1$and P_z are both three-dimensional vectors and can be calculated by setting $\theta = 0$ in N. Accordingly, we obtain

$$N(m,\overline{m},\theta) = -2Re\{\bar{\beta}^*(0)G_0\beta(0)\} + G_0$$

when

$$N_{20}(\theta) = -s_{20}\beta(\theta) - \bar{s}_{02}\bar{\beta}(\theta) + G_{m^2}$$

$$N_{11}(\theta) = -s_{11}\beta(\theta) - \bar{s}_{11}\bar{\beta}(\theta) + F_{m\overline{m}}$$

where

$$G_0 = G_{m^2}\frac{m^2}{2} + G_{m\overline{m}}m\overline{m} + G_{\overline{m}^2}\frac{\overline{m}^2}{2} + \cdots$$

Combining the definition of X, we obtain

$$\int_{-1}^{0} d \nless (\theta)V_{20}(\theta) = 2i\omega_0\tau_0 V_{20}(0) + s_{20}\beta(0) + \bar{s}_{02}\bar{\beta}(0) - G_{m^2}$$

and

$$\int_{-1}^{0} d \nless (\theta)V_{11}(\theta) = s_{11}\beta(0) - \bar{s}_{11}\bar{\beta}(0) - G_{m\overline{m}}$$

Notice that

$$(i\omega_0\tau_0 I - \int_{-1}^{0} e^{i\omega_0\tau_0\theta} d \nless (\theta))\beta(0) = 0$$

and

$$-i\omega_0\tau_0 I - \int_{-1}^{0} e^{-i\omega_0\tau_0\theta}\ d \nless (\theta))\bar{\beta}(0) = 0$$

We have

DOI:https//doi.org/10.22452/mjs.vol42no1.5
Malaysian Journal of Science 42(1): 42-61 (February 2023)

$$(2i\omega_0\tau_0 I - \int_{-1}^{0} e^{2i\omega_0\tau_0\theta} d \prec (\theta))P_1 = G_{m^2}$$

Similarly, we have

$$-\left(\int_{-1}^{0} d \prec (\theta)\right) P_2 = G_{m\bar{m}}$$

Hence, we obtain

$$\begin{bmatrix} 2i\omega_0 + a_1 P_{r1}^* & -P_{r1}^* P_{r3}^* & P_{r1}^* - P_{r2}^* P_{r1}^* \\ -P_{r3} P_{r2}^* & 2i\omega_0 + b_1 P_{r2}^* & P_{r2}^* - P_{r2}^* P_{r1}^* \\ -d_1 P_{r3}^* e^{-2i\omega_0\tau_0} & -e_1 P_{r3}^* e^{-2i\omega_0\tau_0} & 2i\omega_0 + c_1 P_{r3}^* \end{bmatrix} P_1 =$$

$$-2\begin{bmatrix} a_1 + (1 - P_{r2}^*)y_1 - x_1(P_{r1}^* y_1 + P_{r3}^*) \\ b_1 x_1^2 + (1 - P_{r1}^*)x_1 y_1) - x_1 P_{r3}^* - y_1 P_{r2}^* \\ y_1(c_1 y_1 - d_1 e^{-i\omega_0\tau_0} - e_1 x_1 e^{-i\omega_0\tau_0}) \end{bmatrix}$$

and

$$\begin{bmatrix} a_1 P_{r1}^* & -P_{r1}^* P_{r3}^* & -P_{r2}^* P_{r1}^* + P_{r1}^* \\ -P_{r2}^* P_{r3} & b_1 P_{r2}^* & -P_{r2}^* P_{r1}^* + P_{r2}^* \\ -d_1 P_{r3}^* & -e_1 P_{r3}^* & c_1 P_{r3}^* \end{bmatrix} P_2$$

$$= -2\begin{bmatrix} a_1 + (1 - P_{r2}^*)Re\{y_1\} - P_{r1}^* Re\{\bar{y}_1 x_1\} - P_{r3}^* Re\{x_1\} \\ x_1 \bar{x}_1 b_1 + (1 - P_{r1}^*)Re\{x_1 \bar{y}_1\} - P_{r2}^* Re\{\bar{y}_1\} - P_{r3}^* Re\{x_1\}) \\ c_1 y_1 \bar{y}_1 - d_1 Re\{y_1\} - e_1 Re\{y_1 \bar{x}_1\} e^{i\omega_0\tau_0}) \end{bmatrix}$$

Then, s_{21}can be denoted by the variables.
We determined that s_{ij}can be calculated using the variables. Thus, we computed these quantities as follows:

$$Z_2(0) = \frac{i}{2\omega_0\tau_0}\left(s_{11}s_{20} - 2|s_{11}|^2 - \frac{|s_{02}|^2}{3}\right) + \frac{s_{21}}{2} \tag{32}$$

$$\sigma_2 = -\frac{Re\{Z_2(0)\}}{Re\{\lambda'(\tau_0)\}} \tag{33}$$

$$\beta_2 = 2Re\{Z_2(0)\}$$

$$T_2 = -\frac{I_m\{Z_2(0)\} + \sigma_2 I_m\{\lambda'(Z_0)\}}{\tau_0\omega_0} \tag{34}$$

Theorem. σ_2 calculates the direction of the Hopf bifurcation: if σ_2 <0($\sigma_2 > 0$), we obtain the supercritical Hopf bifurcation. When $\tau > \tau_0$ ($\tau < \tau_0$), we observed the bifurcating period solutions. P_2 indicates that the bifurcating periodic solution is stable. If $\beta_2 < 0$ ($\beta_2 > 0$), we observe that bifurcating periodic solutions are arbitrary and asymptotically stable (unstable). The bifurcating periodic solution is determined by T_2. When T_2> 0 (T_2 < 0), the period increases (decreases), respectively.

DOI:https//doi.org/10.22452/mjs.vol42no1.5
Malaysian Journal of Science 42(1): 42-61 (February 2023)

4. Numerical Example

In this part, we used MATLAB to perform a numerical simulation of the system (Poole, 1974; Abrams et al., 1993). We use these parametric values:

Set 1

$(a_1 = 1.2; b_1 = 1.4; c_1 = 1; d_1 = 1; e_1 = 2)$

We can observe the positive interior equilibrium point when the initial value is 0.2, 0.4, or 0.6.

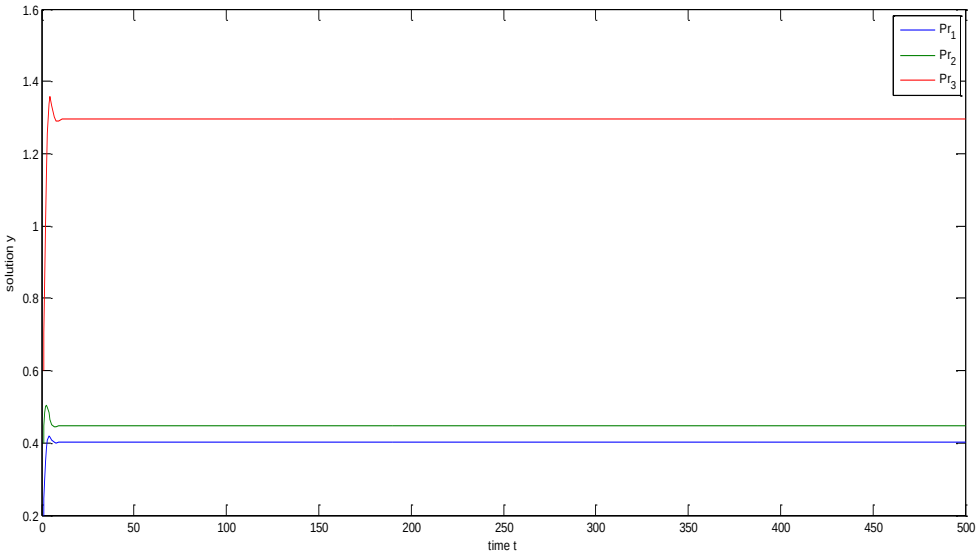

Figure 1. In the absence of delay, the system is stable

DOI:https//doi.org/10.22452/mjs.vol42no1.5
Malaysian Journal of Science 42(1): 42-61 (February 2023)

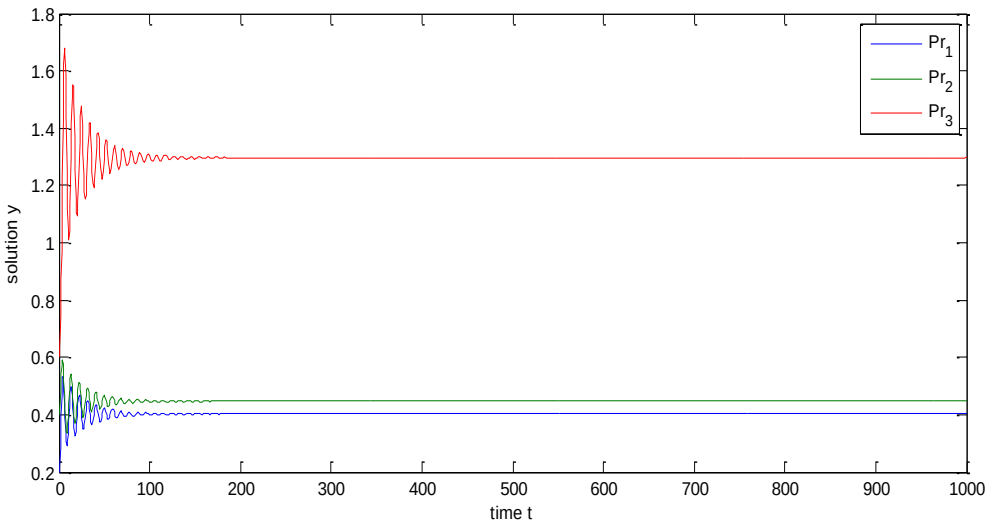

Figure 2. Asymptotically stable when $\tau = 1.5 < \tau_0 = 1.7387$

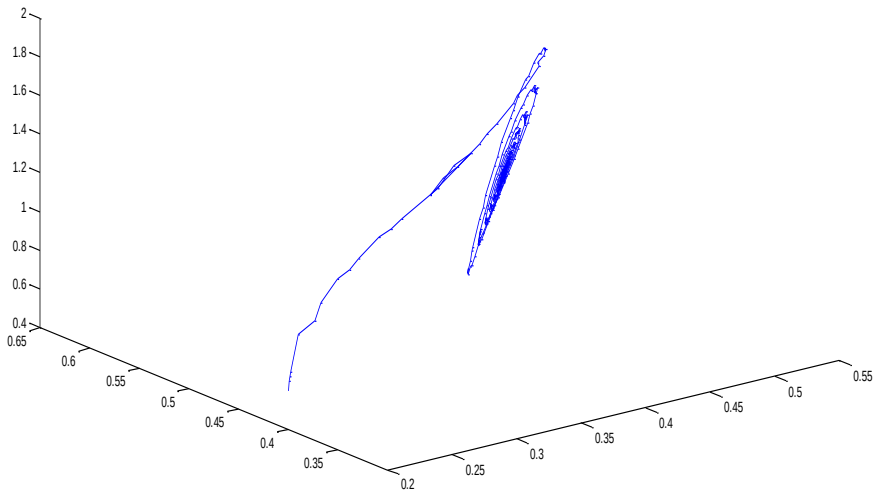

Figure 2.1 Phase plane graph for asymptotically stable when $\tau = 1.5 < \tau_0 = 1.7387$

DOI:https//doi.org/10.22452/mjs.vol42no1.5
Malaysian Journal of Science 42(1): 42-61 (February 2023)

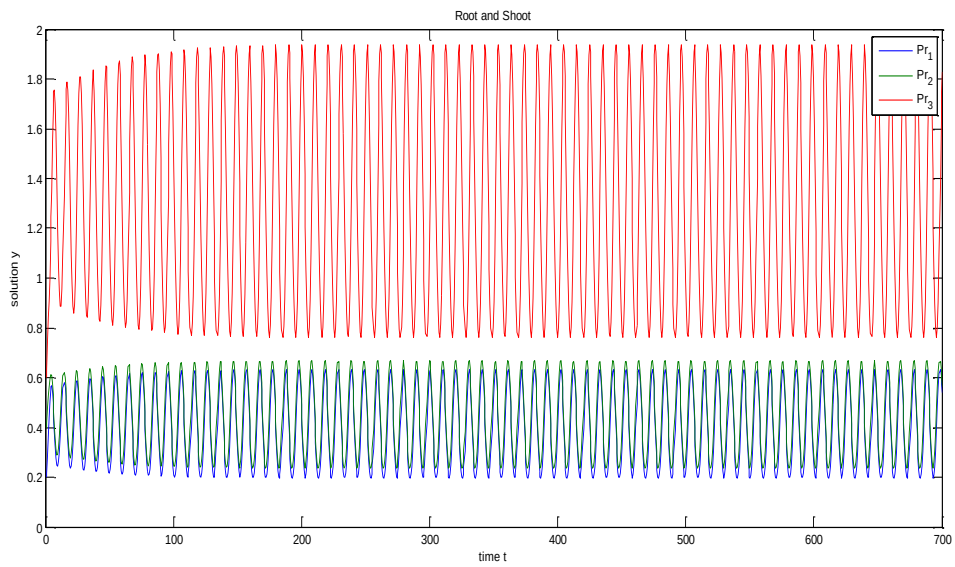

Figure 3. Hopf Bifurcation when $\tau = 1.85 > \tau_0 = 1.7387$

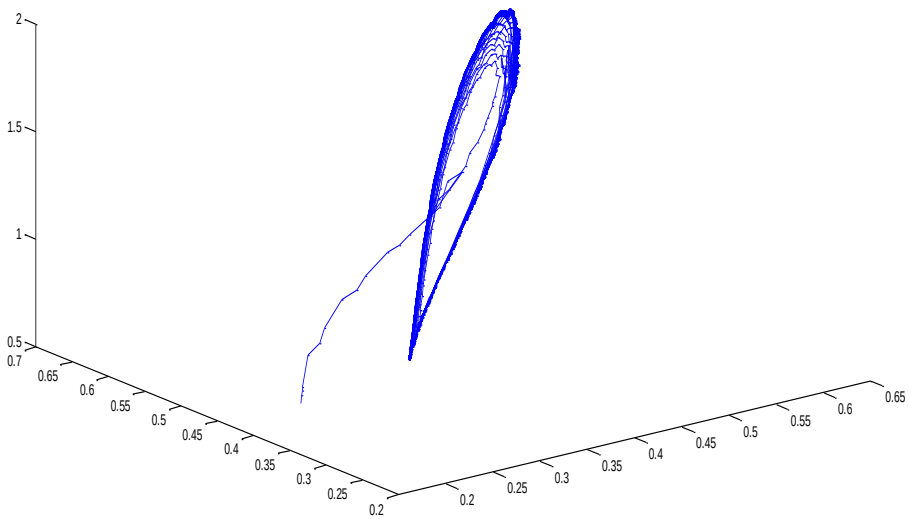

Figure 3.1 Phase plane graph for Hopf Bifurcation when $\tau = 1.85 > \tau_0 = 1.7387$

DOI:https//doi.org/10.22452/mjs.vol42no1.5
Malaysian Journal of Science 42(1): 42-61 (February 2023)

Set 2 (a_1 = 1; b_1 = 1.44; c_1 = 1; d_1= 1; e_1 =1.2)
The positive interior equilibrium point is obtained when the initial value is 0.2, 0.4, and 0.6.

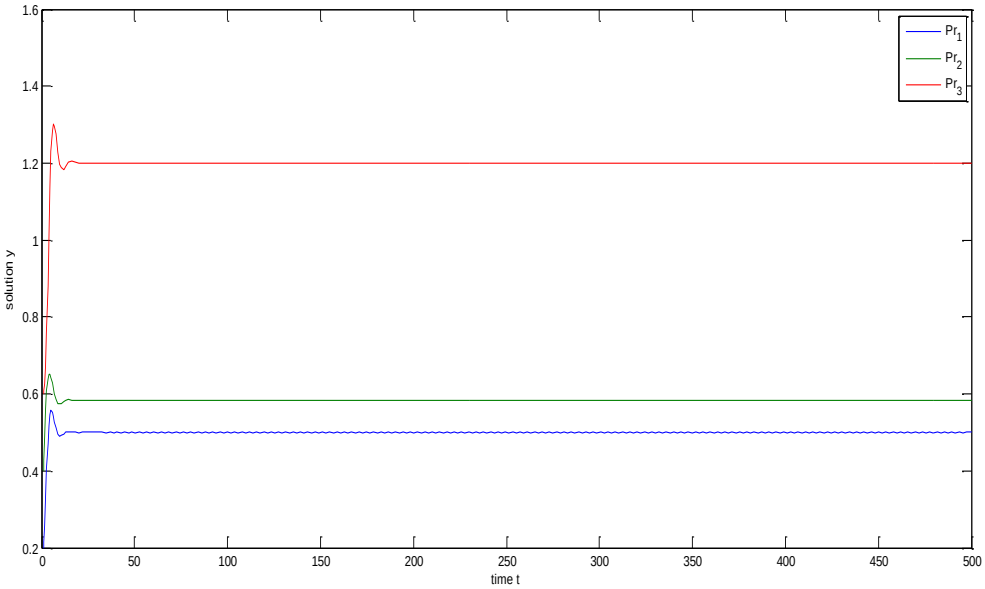

Figure 4. In the absence of delay, the system is stable

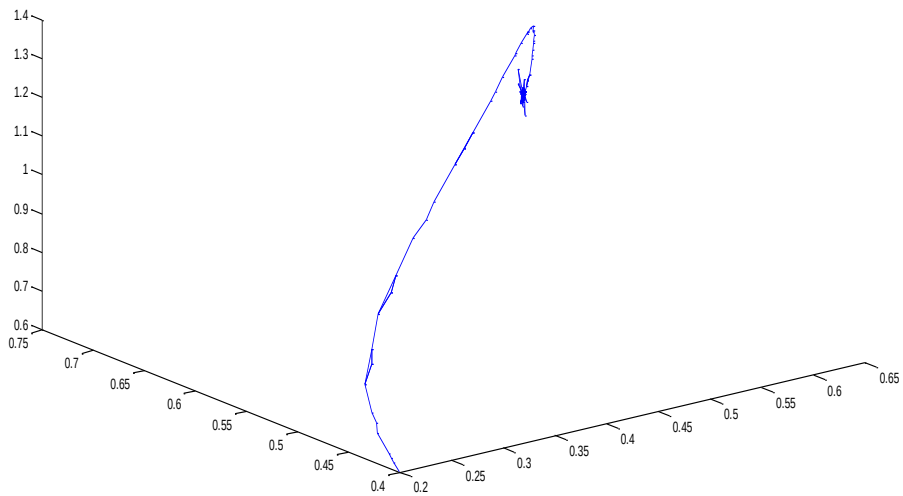

Figure 4.1 Phase plane graph in the absence of delay in the system

DOI:https//doi.org/10.22452/mjs.vol42no1.5
Malaysian Journal of Science 42(1): 42-61 (February 2023)

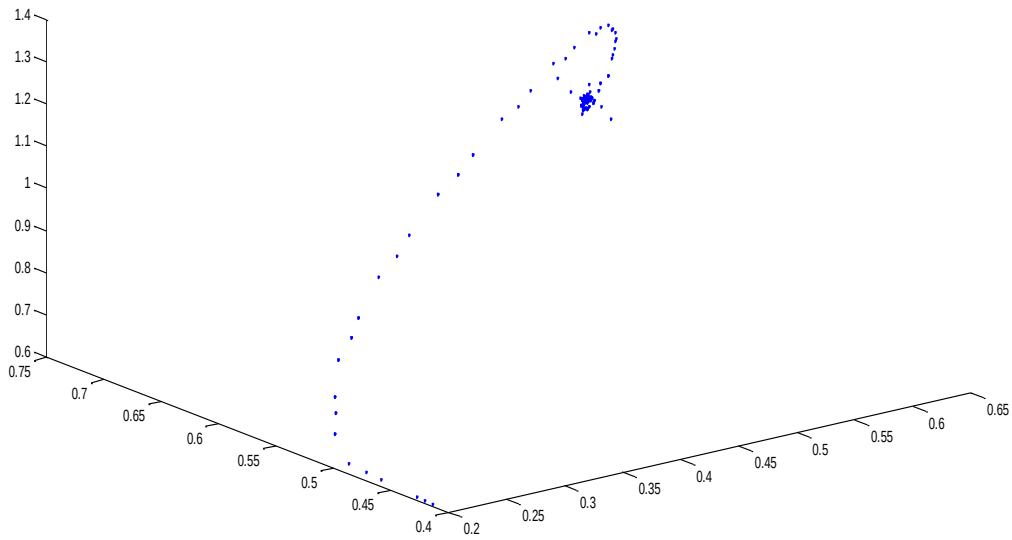

Figure 4.2 Phase plane graph in the absence of delay in the system

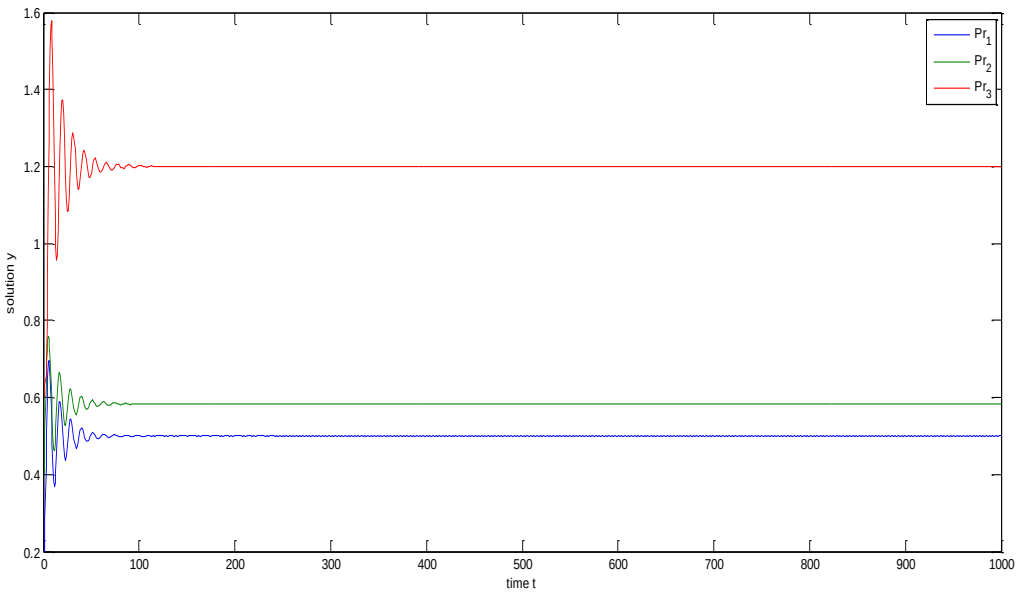

Figure 5. Asymptotically stable when $\tau < \tau_0 = 1.7387$

DOI:https//doi.org/10.22452/mjs.vol42no1.5
Malaysian Journal of Science 42(1): 42-61 (February 2023)

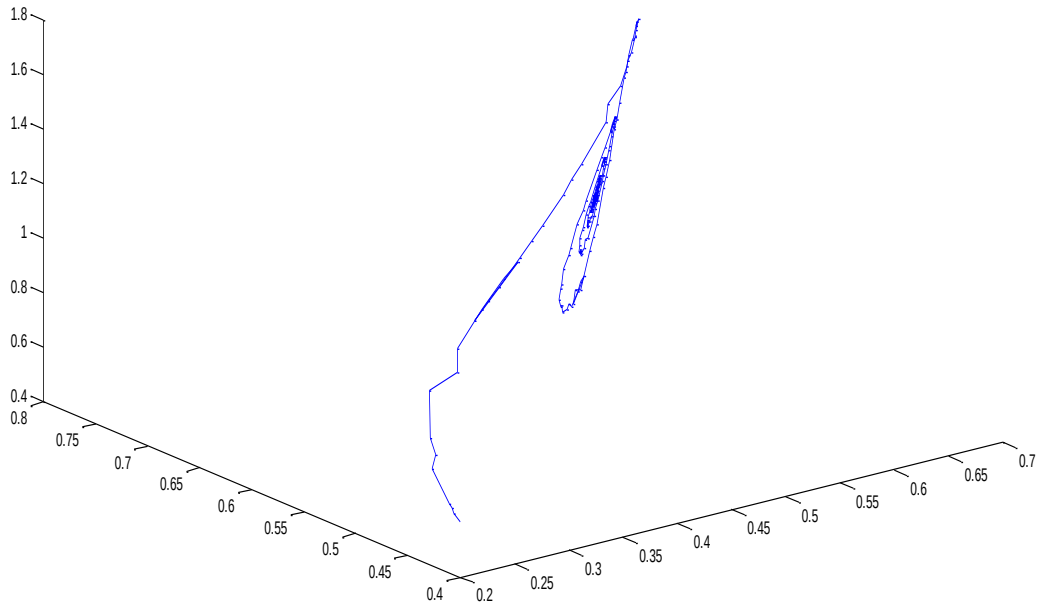

Figure 5.1 Phase plane graph for asymptotically stable when $\tau < \tau_0 = 1.7387$

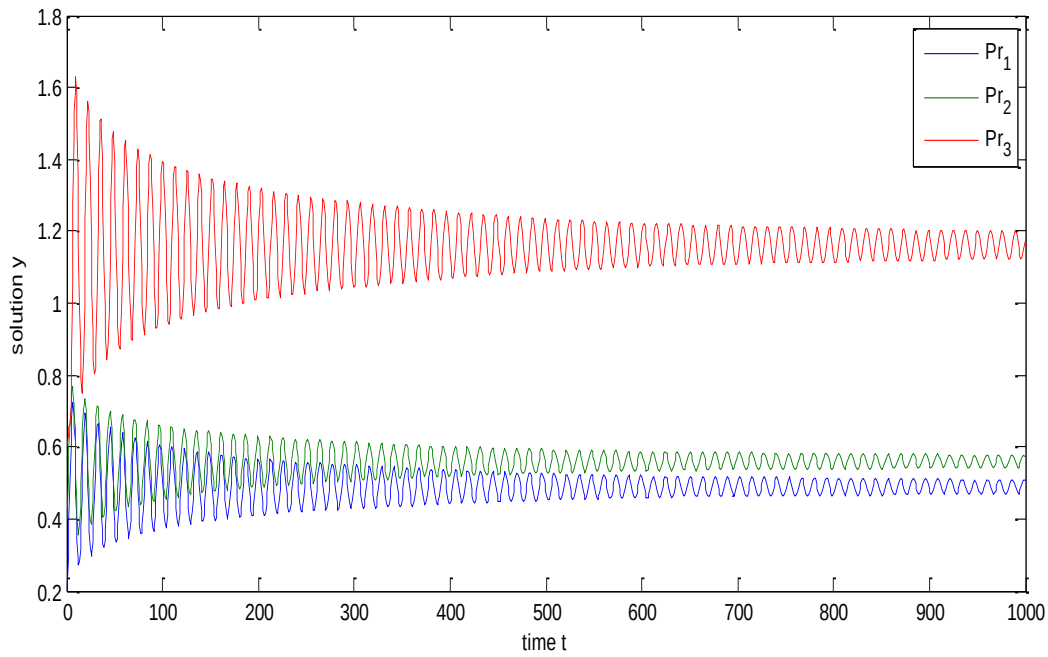

Figure 6. Hopf Bifurcation when $\tau = 2.5 > \tau_0 = 1.7387$

DOI:https//doi.org/10.22452/mjs.vol42no1.5
Malaysian Journal of Science 42(1): 42-61 (February 2023)

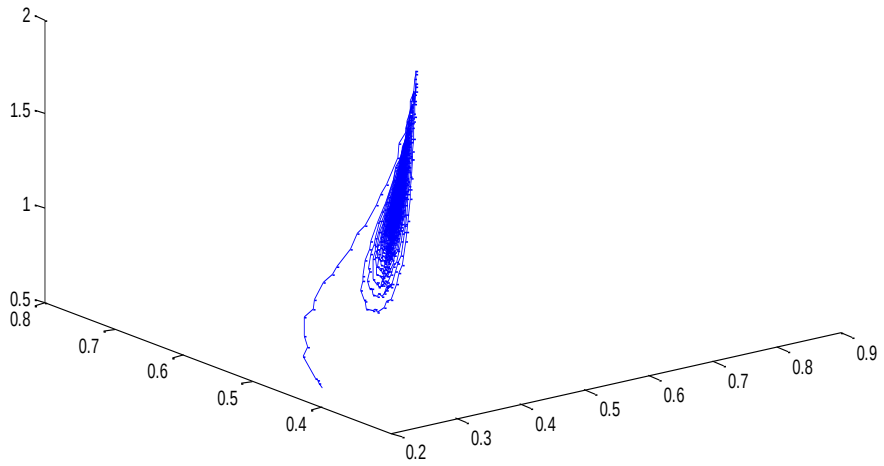

Figure 6.1 Phase plane graph for Hopf bifurcation when $\tau = 2.5 > \tau_0 = 1.7387$

5. Conclusion

Certain species, such as zebras and gazelles, form teams because it reduces the predation risk. Time delay caused by the age structure, maturation period, and feeding time is a major factor in real-time prey–predator dynamic that results in periodic solutions and the bifurcation phenomenon. This study investigated the impact of lag time on a multiteam prey–predator dynamic by examining two prey and one predator and considering that the two prey populations support each other when they are susceptible to predation. The insertion of a time delay destabilizes the system's stable equilibrium point. For set 1, the system is absolutely stable in the absence of delay (i.e, $\tau = 0$; Figure 1). The same finding is analytically supported by Ruth–Hurwitz's criteria. The system is asymptotically stable when the value of delay is less than the critical value (i.e., $\tau < 1.7387$; Figures 2 and 2.1). The Hopf bifurcation is observed when the delay parameter passes a critical value (i.e., $\tau \geq 1.7387$; Figures 3 and 3.1). For set 2, the system is absolutely stable in the absence of delay (i.e., $\tau = 0$; Figures 4, 4.1, and 4.2). The same finding is analytically supported by Ruth–Hurwitz's criteria. The system is asymptotically stable when the value of delay is less than the critical value (i.e., $\tau < 1.7387$; Figures 5 and 5.1). The Hopf bifurcation is observed when the delay parameter passes a critical value (i.e., $\tau \geq 1.7387$; Figures 6 and 6.1). These graphs have their basics covered in lemmas 1 and 2. Furthermore, the technique used to determine the direction and stability of a Hopf bifurcation solution is constructed using normal form theory and the centre manifold reduction hypothesis. Numerical results are substantiated using the dde23 code of MATLAB

6. References

Abrams, P., & Matsuda, H. (1993). Effects of adaptive predatory and anti-predator behaviour in a two-prey—one-predator system. Evolutionary Ecology, 7(3), 312-326. https://doi.org/10.2307/3544924

Alsakaji, H. J., Kundu, S., & Rihan, F. A. (2021). Delay differential model of one-predator two-prey system with Monod-Haldane and holling type II functional responses. Applied Mathematics and Computation, 397, 125919. https://doi.org/10.1016/j.amc.2020.125919

Aybar, I. K., Aybar, O. O., Dukarić, M., & Ferčec, B. (2018). Dynamical analysis of a two prey-one predator system with quadratic self-interaction. Applied Mathematics and Computation, 333, 118-132. DOI: 10.1016/j.amc.2018.03.123

Deka, B. D., Patra, A., Tushar, J., & Dubey, B. (2016). Stability and Hopf-bifurcation in a general Gauss type two-prey and one-predator system. Applied Mathematical Modelling, 40(11-12), 5793-5818. https://doi.org/10.1016/j.apm.2016.01.018

El-Gohary, A., & Al-Ruzaiza, A. S. (2007). Chaos and adaptive control in two prey, one predator system with nonlinear feedback. Chaos, Solitons & Fractals, 34(2), 443-453. https://doi.org/10.1016/j.chaos.2006.03.101

Elettreby, M. F. (2009). Two-prey one-predator model. Chaos, Solitons & Fractals, 39(5), 2018-2027. DOI: 10.1016/j.chaos.2007.06.058

Emery, S. E., & Mills, N. J. (2020). Effects of predation pressure and prey density on short-term indirect interactions between two prey species that share a common predator. Ecological Entomology, 45(4), 821-830.

Frahan, A. G. (2020). On the mathematical model of two-prey and two-predator species. Iraqi Journal of Science, 608-619. DOI:10.24996/ijs.2020.61.3.17

Grasman, J., Van Den Bosch, F., & Van Herwaarden, O. A. (2001). Mathematical conservation ecology: a one-predator–two-prey system as case study. Bulletin of

DOI:https//doi.org/10.22452/mjs.vol42no1.5
Malaysian Journal of Science 42(1): 42-61 (February 2023)

mathematical biology, 63(2), 259-269. DOI: 10.1006/bulm.2000.0218

Green, E. (2004). The Effect of a Smart 'Predator in a One Predator, Two Prey System. Rose-Hulman Undergraduate Mathematics Journal, 5(2), 5.

Kesh, D., Sarkar, A. K., & Roy, A. B. (2000). Persistence of two prey–one predator system with ratio-dependent predator influence. Mathematical methods in the applied sciences, 23(4), 347-356.

Klebanoff, A., & Hastings, A. (1994). Chaos in one-predator, two-prey models: general results from bifurcation theory. Mathematical biosciences, 122(2), 221-233. DOI: 10.1016/0025-5564(94)90059-0

Kumar, P., & Raj, S. (2021). Modelling and analysis of prey-predator model involving predation of mature prey using delay differential equations. Numerical Algebra, Control & Optimization. doi: 10.3934/naco.2021035

Kumar, P., & Raj, S. (2022, May). Modelling the Effect of Toxin Producing Prey on Predator Population using Delay Differential Equations. In Journal of Physics: Conference Series (Vol. 2267, No. 1, p. 012077). IOP Publishing. doi:10.1088/1742-6596/2267/1/012077

Kundu, S., & Maitra, S. (2018). Qualitative analysis of a three species predator–prey model with stochastic fluctuation. In Applications of Fluid Dynamics (pp. 643-659). Springer, Singapore. DOI:10.17654/MS102050865

Liu, M., & Wang, K. (2013). Dynamics of a two-prey one-predator system in random environments. Journal of Nonlinear Science, 23(5), 751-775. https://doi.org/10.1016/j.psra.2016.10.002

Manna, K., Volpert, V., & Banerjee, M. (2020). Dynamics of a diffusive two-prey-one-predator model with nonlocal intra-specific competition for both the prey species. Mathematics, 8(1), 101. https://doi.org/10.3390/math8010101

Mishra, P., & Raw, S. N. (2019). Dynamical complexities in a predator-prey system involving teams of two prey and one predator. Journal of Applied Mathematics and Computing, 61(1), 1-24. DOI:10.1007/s12190-018-01236-9

Pedersen, M., & Lin, Z. (2001). Stationary patterns in one-predator, two-prey models. Differential and Integral Equations, 14(5), 605-612.

Poole, R. W. (1974). A discrete time stochastic model of a two prey, one predator species interaction. Theoretical population biology, 5(2), 208-228. https://doi.org/10.1016/0040-5809(74)90042-2

Rihan, F. A., Alsakaji, H. J., & Rajivganthi, C. (2020). Stability and hopf bifurcation of three-species prey-predator System with time delays and Allee Effect. Complexity, 2020. https://doi.org/10.1155/2020/7306412

Rihan, F. A. (2021). Delay differential equations and applications to biology. Singapore: Springer. https://doi.org/10.1007/978-981-16-0626-7

Rihan, F. A., & Alsakaji, H. J. (2022). Stochastic delay differential equations of three-species prey-predator system with cooperation among prey species. Discrete & Continuous Dynamical Systems-S, 15(2), 245. doi:10.3934/dcdss.2020468

Sahoo, D., & Samanta, G. P. (2021). Impact of Fear Effect in a Two Prey-One Predator System with Switching Behaviour in Predation. Differential Equations and Dynamical Systems, 1-23. https://doi.org/10.1007/s12591-021-00575-7

Song, X., & Xiang, Z. (2006). The prey-dependent consumption two-prey one-predator models with stage structure for the predator and impulsive effects. Journal of Theoretical Biology, 242(3), 683-698. DOI: 10.1016/j.jtbi.2006.05.002

Tripathi, J. P., Abbas, S., & Thakur, M. (2014). Local and global stability analysis of a two prey one predator model with help. Communications in Nonlinear Science and Numerical Simulation, 19(9), 3284-3297. 10.1016/j.cnsns.2014.02.003

Vance, R. R. (1978). Predation and Resource Partitioning in One Predator Two Prey Model Communities. The American Naturalist, 112(987), 797-813. https://doi.org/10.1086/283324

Vayenas, D. V., Aggelis, G., Tsagou, V., & Pavlou, S. (2005). Dynamics of a two-prey–one-predator system with predator switching regulated by a catabolic repression control-like mode. Ecological modelling, 186(3), 345-357. DOI: 10.1016/j.ecolmodel.2005.01.032

Yamauchi, A., & Yamamura, N. (2005). Effects of defense evolution and diet choice on population dynamics in a one-predator–two-prey system. Ecology, 86(9), 2513-2524. https://doi.org/10.1890/04-1524

Zhang, J., & Yang, Y. (2020). Three-Prey One-Predator Continuous Time Nonlinear System Model. Complexity. https://doi.org/10.1155/2020/886998

DOI:https//doi.org/10.22452/mjs.vol42no1.5
Malaysian Journal of Science 42(1): 42-61 (February 2023)

MALAYSIAN JOURNAL OF SCIENCE
MJS
ISSN 1394-3065

Regular Issue

Malaysian Journal of Science 42 (1): 62-67 (February 2023) https://mjs.um.edu.my

AN INTEGRAL TRANSFORM TOGETHER WITH TAYLOR SERIES AND DECOMPOSITION METHOD FOR THE SOLUTION OF NONLINEAR BOUNDARY VALUE PROBLEMS OF HIGHER ORDER

Emmanuel Idowu Akinola[1a], Johnson Adekunle Owolabi[2a]*, Saheed Alao[3b], and Sunday Oloruntoyin Sangoniyi[4c]

Abstract: This work aims to determine the approximate solutions of nonlinear boundary value problems of higher order obtained through the Aboodh Transform Series Decomposition Method (ATSDM), a method designed to find the integral and the inverse transform of the problems, expand the exponential function, and simultaneously decompose the nonlinear terms. The results obtained demonstrate that ATSDM is an excellent and trusted approximate method that can be employed to obtain accurate results for any problem similar to the one presented in this work.

Keywords: *Aboodh transform, adomian decomposition, taylor series, twelfth, and thirteenth order.*

1. Introduction

Higher order boundary value problems have been a major concern due to their mathematical significance or prominence, as well as their great applicability in hydrodynamics and hydromagnetics (Agarwal, 1986; Wazwaz, 2000, 2000a; Chandrasekhar, 1961; Mahdy et al., 2020; Abdel-Halim Hassan et al., 2009; Othman et al., 2010).

The analytical solution of the afore-mentioned problems, especially the nonlinear ones, have been a problem that is challenging to solve. Consequently, researchers have devised an alternative approach for obtaining an approximate solution in the literature (Oderinu, 2014; Opanuga et al., 2015, 2017; Akinola et al., 2017; Noor & Mohyud-Din, 2008; Hymavathi & Kumar, 2014; Mohyud-din, 2009; Siddiqi et al., 2009; El-Gamel, 2015; Owolabi et al., 2019; Adeyefa & Kuboye, 2020; Farooq et al., 2020; Gbadamosi et al., 2010; Amer et al., 2018; Gepreel et al., 2020; Mahdy, 2019; Mahdy et al., 2021; Mandy and Youssef, 2021).

This research work derived its motivation from the work of Akinola et al. (2016), and extensively explained how the higher order problems considered are being transformed by the Aboodh Transformation and its inverse (Aboodh 2013, 2014; Abdelbagy & Mohand, 2016; Mahgoub & Sedeeg, 2017), how the Series Method is being employed to handle the exponential functions (Yalçinbaş, 2002), and how nonlinear terms are being decomposed by the means of Adomian Polynomials (Adomian, 1988; Abbaoui & Cherruault, 1994). The results obtained by the combination of the three mentioned methods have demonstrated the strength of the Aboodh Transform Series Decomposition Method (ATSDM) in terms of efficacy, accuracy and reliability over all other related methods available. This method is an alternative powerful mathematical tool that can be used in obtaining the solution of nonlinear differential equations of any order.

This paper is organized into five sections. Section One presents the introduction of the newly developed method, its formation, and its strength, and then reviews some of the related literature. Section Two presents the step by step approach of the said method. Section Three presents the application and implementation of the method on four different types of higher order nonlinear boundary value problems using Maple 18 software. Sections Four and Five present the conclusion and references of the literature cited, respectively.

Authors information:
[a]Bowen University, PMB 284, Iwo, Osun State, NIGERIA. E-mail: emmanuel.idowu@bowen.edu.ng[1]; johnson.owolabi@bowen.edu.ng[2]
[b]Department of Pure and Applied Mathematics, Ladoke Akintola University of Technology, PMB 4000, Ogbomoso, Oyo State, NIGERIA. E-mail: salao16@lautech.edu.ng[3]
[c]Mathematics Department, Emmanuel Alayande College of Education, Oyo, Oyo State, NIGERIA. E-mail: sangoniyisunday@gmail.com[4]
*Corresponding Author: johnson.owolabi@bowen.edu.ng

Received: November 17, 2021
Accepted: April 25, 2022
Published: February 28, 2022

DOI:https//doi.org/10.22452/mjs.vol42no1.6
Malaysian Journal of Science 42(1): 62-67 (February 2023)

2. Methodology

This section examines the general nonhomogeneous nonlinear differential equation.

$$Lu(x) + Ru(x) + Nu(x) = g(x)\,. \tag{1}$$

where $Lu(x)$, $Ru(x)$, $Nu(x)$ and $g(x)$ have their own usual meaning.

Eq. (2) was obtained by applying the Aboodh Transform on Eq. (1) (Aboodh, 2013, 2014; Abdelbagy & Mohand, 2016; Mahgoub & Sedeeg, 2017):

$$A\{Lu(x)\} = A\{g(x)\} - A\{Ru(x) + Nu(x)\}\,. \tag{2}$$

The Aboodh Transformation of the derivative Eq. (2) gives:

$$A\{u(x)\} = \sum_{k=0}^{n-1} \frac{1}{v^2-n+k} \frac{d^n f(0)}{dx^n} + \frac{1}{v^n} A\{g(x)\} - \frac{1}{v^n} A\{Ru(x) + Nu(x)\}. \tag{3}$$

The Aboodh inverse transform of Eq. (3) now becomes:

$$u(x) = A^{-1}\left[\sum_{k=0}^{n-1} \frac{1}{v^2-n+k} \frac{d^n f(0)}{dx^n}\right] + A^{-1}\left[\frac{1}{v^n} A\{g(x)\}\right] - A^{-1}\left[\frac{1}{v^n} A\{Ru(x) + Nu(x)\}\right]. \tag{4}$$

Let $u(x) = \sum_{n=0}^{\infty} U_n(x)$ be an infinite series. The decomposition of the nonlinear term is now:

$$Nu(x) = \sum_{n=0}^{\infty} A_n \tag{5}$$

where A_n can be calculated as:

$$A_n = \frac{1}{n!} \frac{\partial^n}{\partial \lambda^n} \left[N\left(\sum_{i=0}^{\infty} \lambda^i u_i\right)\right]_{\lambda=0}, \qquad n = 0, 1, 2 \ldots. \tag{6}$$

Substituting Eq. (6) into Eq. (4) gives:

$$\sum_{n=0}^{\infty} u_n(x) = f(x) - A^{-1}\left[\frac{1}{v^n} A\{R \sum_{n=0}^{\infty} u_n(x) + \sum_{n=0}^{\infty} A_n\}\right]. \tag{7}$$

where,

$$f(x) = A^{-1}\left[\sum_{k=0}^{n-1} \frac{1}{v^2-n+k} \frac{d^n f(0)}{dx^n}\right] + A^{-1}\left[\frac{1}{v^n} A\{g(x)\}\right]. \tag{8}$$

Suppose $u_0(x) = f(x)$. Then, the remaining terms $u_1(x)$, $u_2(x)$, … was obtained as:

$$u_{n+1} = A^{-1}\left[\frac{1}{v^n} A\{R \sum_{n=0}^{\infty} u_n(x) + \sum_{n=0}^{\infty} A_n\}\right], \quad n \geq 0. \tag{9}$$

The iteration was then obtained from Eq. (9), and the solution to Eq. (1) is now;

$$u(x) = u_0 + u_1 + u_2 + u_3 + \cdots \tag{10}$$

3. Application

Illustration I: Noor & Mohyud-Din (2008) and Othman et al. (2010):

$$y^{xii} - y''' = 2e^x y^2, \qquad 0 \leq x \leq 1. \tag{11}$$

subject to the initial-boundary conditions:

$$y(0) = y''(0) = y^{iv}(0) = y^{vi}(0) = y^{vii}(0) = y^x(0) = 1.$$

$$y(1) = y''(1) = y^{iv}(1) = y^{vi}(1) = y^{vii}(1) = y^x(1) = 1.$$

The analytical solution is: $y = e^{-x}$.

Then the exponential function e^x was expanded by Taylor series to have;

$$e^x = 1 + x + \frac{x^2}{2!} + \frac{x^3}{3!} + \frac{x^4}{4!} + \cdots. \tag{12}$$

Substituting the Taylor expansion Eq. (12) into Eq. (10) and following the process in Section 2, we have:

$$y = 1 - 0.9999999999999999x + \frac{1}{2}x^2 - 0.1666666666666667x^3 + \frac{1}{24}x^4 - 0.008333333333333342x^5 + \cdots.$$

DOI:https//doi.org/10.22452/mjs.vol42no1.6
Malaysian Journal of Science 42(1): 62-67 (February 2023)

Table 1. Comparative Analysis of the Absolute Errors for Illustration I

x	Exact	VIM Noor & Mohyud-Din (2008)	HMP Othman et al., (2010)	ATSDM
0	0	0	0	0
0.2	0.818730	3.07×10^{-7}	1.172×10^{-7}	4.19×10^{-17}
0.4	0.670320	4.97×10^{-7}	8.08×10^{-7}	2.34×10^{-18}
0.6	0.548811	4.97×10^{-7}	1.19×10^{-7}	1.23×10^{-16}
0.8	0.443289	3.07×10^{-7}	5.0×10^{-10}	7.50×10^{-17}
1.0	0.367879	2.00×10^{-10}	4.1×10^{-9}	1.07×10^{-17}

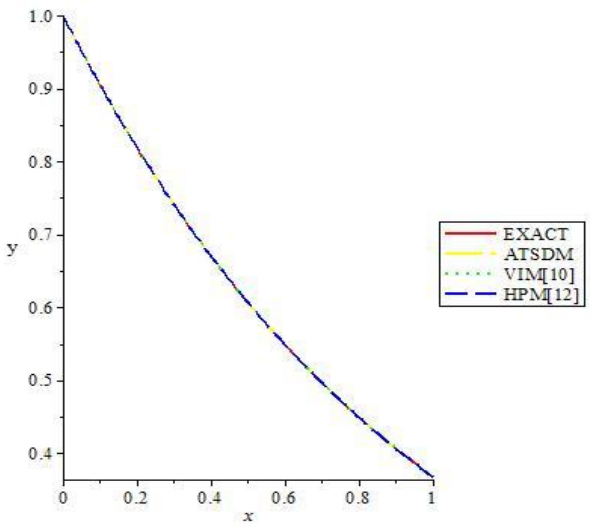

Figure 1. The Comparison between Exact, VIM, HPM, and ATSDM Solution of Illustration I

Illustration II: Considering Oderinu (2014) and Noor & Mohyud-Din (2008):

$$y^{xii} = \frac{1}{2}e^{-x}y^2, \qquad 0 \le x \le 1. \tag{13}$$

subject to

$$y(0) = y''(0) = y^{iv}(0) = y^{vi}(0) = y^{vii}(0) = y^{x}(0) = 2.$$

$$y(1) = y''(1) = y^{iv}(1) = y^{vi}(1) = y^{vii}(1) = y^{x}(1) = 2e.$$

The analytical solution was given as $y = 2e^x$.

Following the same method itemized in Illustration 1 gives:

$$y = 2 + 2.00000000000000x + x^2 + 0.3333333333333345x^3 + \frac{1}{24}x^4 + 0.01666666666666600x^5 + \cdots.$$

Table 2. Comparative Analysis of the Absolute Errors for Illustration II

x	Exact	WRM Oderinu (2014)	VIM Noor & Mohyud-Din (2008)	ATSDM
0	2.0	0	0	0
0.1	2.210341	0	2.07×10^{-4}	7.49×10^{-16}
0.2	2.442805	0	3.94×10^{-4}	3.23×10^{-16}
0.3	2.699717	1×10^{-14}	5.40×10^{-4}	2.38×10^{-16}
0.4	2.983649	0	6.32×10^{-4}	7.05×10^{-16}
0.5	3.297442	1×10^{-14}	6.61×10^{-4}	4.17×10^{-16}
0.6	3.644237	2×10^{-14}	6.26×10^{-4}	1.52×10^{-16}
0.7	4.027505	1×10^{-14}	5.31×10^{-4}	6.93×10^{-16}
0.8	4.451081	1×10^{-14}	3.84×10^{-4}	3.50×10^{-16}
0.9	4.919206	0	2.02×10^{-4}	1.01×10^{-16}
1.0	5.436564	0	2.02×10^{-4}	1.10×10^{-15}

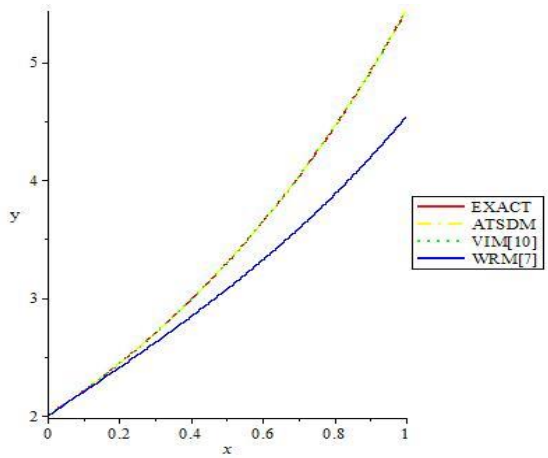

Figure 2: Comparison between Exact, VIM, WRM, and ATSDM Solution of Illustration II

Illustration III: Considering Siddiqi et al., (2009):

$$y^{xii} = (12 + x + x^2e^x)e^x - y^2, \qquad 0 \le x \le 1. \tag{14}$$

subject to the initial-boundary conditions

$$y(0) = 0, \quad y'(0) = 1, \quad y''(0) = 2, \quad y'''(0) = 3, \quad y^{iv}(0) = 4, \quad y^{v}(0) = 5.$$

$$y(1) = e, \quad y'(1) = 2e, \quad y''(1) = 3e, \quad y'''(1) = 4e, y^{iv}(1) = 5e, \quad y^{v}(1) = 6e.$$

DOI:https//doi.org/10.22452/mjs.vol42no1.6
Malaysian Journal of Science 42(1): 62-67 (February 2023)

Therefore, the analytical solution is given as $y = xe^x$.

Following the same method itemized in Illustration I gives:

$$y = \left(\frac{1}{2585016738884976640000}\right)\left(\begin{array}{c}647647525324800x^{12} + 53970627110400x^{13} \\ +4744670515200x^{14} + \cdots.\end{array}\right)$$

Table 3. Comparative Analysis of the Absolute Errors for Illustration III

X	Exact	VIM Siddiqi et al., (2009)	ATSDM
0	0	0	0
0.1	0.1105	5.14×10^{-16}	2.39×10^{-25}
0.2	0.2443	5.27×10^{-14}	4.08×10^{-21}
0.3	0.4050	7.63×10^{-13}	1.01×10^{-16}
0.4	0.5967	4.94×10^{-12}	2.28×10^{-16}
0.5	0.8244	2.08×10^{-11}	2.81×10^{-16}
0.6	1.0933	6.69×10^{-11}	9.76×10^{-16}
0.7	1.4096	1.81×10^{-10}	3.25×10^{-17}
0.8	1.7804	4.26×10^{-10}	8.28×10^{-17}
0.9	2.2136	9.12×10^{-10}	2.67×10^{-16}
1.0	2.7183	1.81×10^{-9}	2.33×10^{-16}

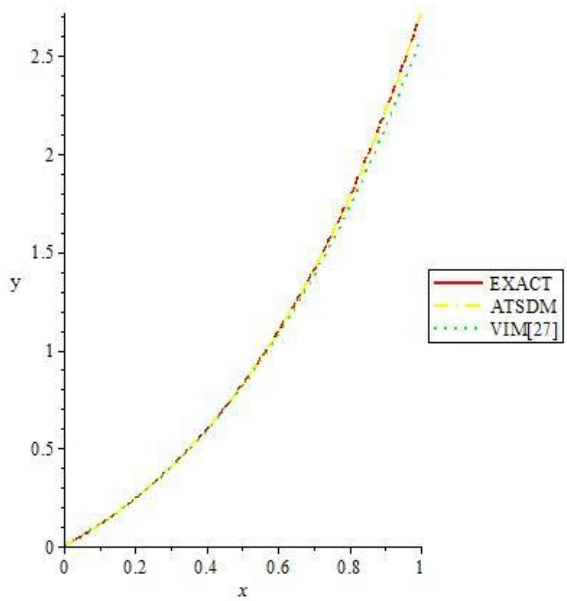

Figure 3. Comparison between Exact, VIM, and ATSDM Solution of Illustration III.

Illustration IV: Considering the work of Opanuga et al., (2017):

$$y^{xiii} = e^{-x}y^2, \qquad 0 \le x \le 1. \tag{15}$$

subject to

$$y(0) = y'(0) = y''(0) = y'''(0) = y^{iv}(0) = y^{v}(0) = y^{vi}(0) = 1.$$

$$y(1) = y'(1) = y''(1) = y'''(1) = y^{iv}(1) = y^{v}(1) = y^{vi}(1) = e.$$

The analytical solution was given as $y = xe^x$.

Following the same method itemized in Illustration I gives:

$$y = 1 + x + \frac{1}{2}x^2 + \frac{1}{6}x^3 + \frac{1}{24}x^4 + \frac{1}{120}x^5 + \frac{1}{720}x^6 + \cdots.$$

Table 4. Comparative Analysis of the Absolute Errors for Illustration IV

x	Exact	MADM Opanuga et al., (2017)	ATSDM
0	1	0	0
0.1	1.105170	5.107×10^{-15}	3.75×10^{-16}
0.2	1.221402	3.785×10^{-13}	1.66×10^{-16}
0.3	1.349858	3.986×10^{-12}	1.06×10^{-16}
0.4	1.491824	1.772×10^{-11}	3.29×10^{-16}
0.5	1.648721	4.829×10^{-11}	1.61×10^{-16}
0.6	1.822118	9.536×10^{-11}	1.35×10^{-18}
0.7	2.013752	1.506×10^{-10}	4.42×10^{-16}
0.8	2.225540	2.042×10^{-10}	3.72×10^{-16}
0.9	2.459603	2.517×10^{-10}	3.26×10^{-16}
1.0	2.718281	2.936×10^{-10}	2.63×10^{-16}

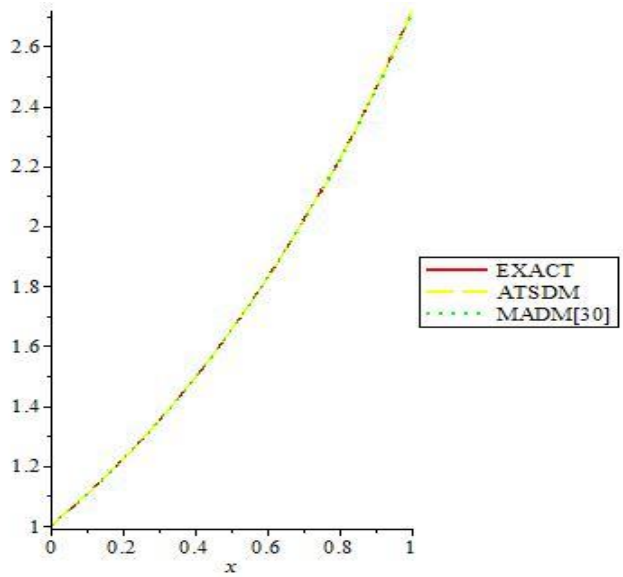

Figure 4. Comparison between Exact, MADM, and ATSDM Solution of Illustration IV.

DOI:https//doi.org/10.22452/mjs.vol42no1.6
Malaysian Journal of Science 42(1): 62-67 (February 2023)

4. Conclusion

The comparison of the approximate solutions through ATSDM with the analytical one and other approximate methods found in the literature was shown both in tables and figures above. It can be clearly seen from the tables that the magnitude of the errors of the new approximate method presented in this work was relatively insignificant or minute when placed side by side with the one already obtained in the reviewed literature. Similarly, the figures demonstrate the rapid convergence of the method to the exact.

Therefore, the results obtained indicate that the method studied in this research is comparatively better in terms of efficiency, accuracy, simplicity, and computational cost. Hence, the ATSDM or its modification is thus recommended to researchers interested in obtaining n exact or near exact approximate solution to any nonlinear differential equations, or of the form considered in this work, irrespective of the order.

5. References

Abbaoui, K., & Cherruault, Y. (1994). Convergence of Adomian's method applied to differential equations. Computers & Mathematics with Applications, 28(5), 103-109.

Abdelbagy, A., Alshikh., Mohand, M., Abdelrahim Mahgoub.(2016). Solving System of Ordinary Differential Equations by Aboodh Transform. World Applied Sciences Journal. 34(9):1144-1148.

Aboodh, K. S. (2013). The New Integral Transform'Aboodh Transform. Global Journal of Pure and Applied Mathematics, 9(1), 35-43.

Aboodh, K. S. (2014). Application of new transform “Aboodh Transform” to partial differential equations. Global Journal of Pure and Applied Mathematics, 10(2), 249-254.

Adeyefa, E. O., & Kuboye, J. O. (2020). Derivation of New Numerical Model Capable of Solving Second and Third Order Ordinary Differential Equations Directly. IAENG International Journal of Applied Mathematics, 50(2), 1-9.

Adomian, G. (1988). A review of the decomposition method in applied mathematics. Journal of mathematical analysis and applications, 135(2), 501-544.

Agarwal, R. P. (1986). Boundary value problems from higher order differential equations. World Scientific.

Akinola, E. I., Akinpelu, F. O., Areo, A. O., Akanni, J. O., & Oladejo, J. K. (2017). The Mathematical Formulation of Laplace Series Decomposition Method for Solving Nonlinear Higher-Order Boundary Value Problems in Finite Domain.

Akinola, E. I., Olopade, I. A., Akinpelu, F. O., Areo, A. O., & Oyewumi, A. A. (2016). Sumudu Transform Series Decomposition Method for Solving Nonlinear Volterra Integro-Differential Equations.

Amer, Y. A., Mahdy, A. M. S., Shwayaa, T. T., & Youssef, E. S. M. (2018). Laplace transform method for solving nonlinear biochemical reaction model and nonlinear Emden-Fowler system. Journal of Engineering and Applied Sciences, 13(17), 7388-7394.

Chandrasekhar, S. (1961). Hydromagnetic and Hydrodynamic Stability, Clarendon.

El-Gamel, M. (2015). Chebychev polynomial solutions of twelfth-order boundary-value problems. Journal of Advances in Mathematics and Computer Science, 13-23.

Farooq, M. A., Razia, S., & Mushtaq, A. (2020). Numerical comparison of constant and variable fluid properties for MHD flow over a nonlinearly stretching sheet.

Gbadamosi, B., Adebimpe, O., Akinola, E. I., & Olopade, I. A. (2012). Solving Riccati equation using Adomian decomposition method.

Gepreel, K. A., Higazy, M., & Mahdy, A. M. S. (2020). Optimal control, signal flow graph, and system electronic circuit realization for nonlinear Anopheles mosquito model. International Journal of Modern Physics C, 31(09), 2050130.

Hassan, I. A. H., Othman, M. I., & Mahdy, A. M. S. (2009). Variational iteration method for solving twelve order boundary value problems. International Journal of Mathematical Analysis, 3(13-16), 719-730.

Hymavathi, T., & Kumar, P. V. (2014). Numerical Solution of Twelfth Order Boundary Value Problems Using Homotopy Analysis Method. Journal of Engineering, Computers & Applied Sciences (JEC & AS) Volume, 3.

Mahdy, A. M. S., & Higazy, M. (2019). Numerical different methods for solving the nonlinear biochemical reaction model. International Journal of Applied and Computational Mathematics, 5(6), 1-17.

Mahdy, A. M. S., & Youssef, E. S. M. (2021). Numerical solution technique for solving isoperimetric variational problems. International Journal of Modern Physics C, 32(01), 2150002.

DOI:https//doi.org/10.22452/mjs.vol42no1.6
Malaysian Journal of Science 42(1): 62-67 (February 2023)

Mahdy, A. M. S., Mohamed, M. S., Lotfy, K., Alhazmi, M., El-Bary, A. A., & Raddadi, M. H. (2021). Numerical solution and dynamical behaviors for solving fractional nonlinear Rubella ailment disease model. Results in Physics, 24, 104091.

Mahdy, A. M., Amer, Y. A. E., Mohamed, M. S., & Sobhy, E. (2020). General fractional financial models of awareness with Caputo–Fabrizio derivative. Advances in Mechanical Engineering, 12(11), 1687814020975525.

Mahgoub, M. M. A., & Sedeeg, A. K. H. (2017). An efficient method for solving linear and nonlinear system of partial differential equations. Journal of Advances in Mathematics and Computer Science, 1-10.

Mohyud-din, S.T. (2009). Exp-function method for solving higher order boundary value problems. Bulletin of the Institute of Mathematics, Academia Sinica, 4(2):219-234

Noor, M. A., & Mohyud-Din, S. T. (2008). Solution of twelfth-order boundary value problems by variational iteration technique. Journal of Applied Mathematics and Computing, 28(1), 123-131.

Oderinu, R. A. (2014). On the numerical solution of tenth and twelfth order boundary value problems using weighted residual method (WRM). Gen. Math. Notes, 24(1), 17-24.

Opanuga, A. A., Okagbue, H. I., & Agboola, O. O. (2017). Application of Semi-Analytical Technique for Solving Thirteenth Order Boundary Value Problem.

Opanuga, A. A., Okagbue, H. I., Edeki, S. O., & Agboola, O. O. (2015). Differential transform technique for higher order boundary value problems. Modern Applied Science, 9(13), 224-230.

Othman, M. I., Mahdy, A. M. S., & Farouk, R. M. (2010). Numerical solution of 12th order boundary value problems by using homotopy perturbation method. Journal of Mathematics and Computer Science, 1(1), 14-27.

Owolabi, J. A., Ige, O. E., & Akinola, E. I. (2019). Application of Kamal Decomposition Transform Method in Solving Two-Dimensional Unsteady Flow. International Journal of Difference Equations (IJDE), 14(2), 207-214.

Siddiqi, S. S., Akram, G., & Zulfiqar, I. (2009). Solution of twelfth order boundary value problems using variational iteration technique. Eur. J. Sci. Res, 33(1), 96-114.

Wazwaz, A. M. (2000). Approximate solutions to boundary value problems of higher order by the modified decomposition method. Computers & Mathematics with Applications, 40(6-7), 679-691.

Wazwaz, A. M. (2000a). The modified Adomian decomposition method for solving linear and nonlinear boundary value problems of tenth-order and twelfth-order. International Journal of Nonlinear Sciences and Numerical Simulation, 1(1), 17-24.

Yalçinbaş, S. (2002). Taylor polynomial solutions of nonlinear Volterra–Fredholm integral equations. Applied Mathematics and Computation, 127(2-3), 195-206.

DOI:https//doi.org/10.22452/mjs.vol42no1.6
Malaysian Journal of Science 42(1): 62-67 (February 2023)

MALAYSIAN JOURNAL OF SCIENCE
MJS
ISSN 1394-3065

Regular Issue

Malaysian Journal of Science 42 (1): 68-77 (February 2023) https://mjs.um.edu.my

SMART FARMING USING A SOLAR-POWERED AQUAPONICS SYSTEM FOR SUSTAINABLE FOOD PRODUCTION

Muhd Nazrul Hisham Zainal Alam[a], Mohd Johari Kamaruddin[2a], Sani Amril Samsudin[3a], Raudhah Othman[4b]*, Nur Hanis Mohammad Radzi[5c], Abioye Abiodun Emmanuel[6d], Mohamad Shukri Zainal Abidin[7d]

Abstract: This paper discusses the prospect of using solar energy for aquaponics operations. Aquaponic is a platform for farmers to grow fish and plants in the same unit simultaneously. The system is considered a sustainable and green technology. Aquaponics operation may be hampered by the necessity for pumps for continuous water recirculation and air supply within the system, especially if the unit is located far from any power outlet. Given that Malaysia is positioned at the equator and receives an average of 9 hours of sunlight per day throughout the year, with solar intensity as high as 1800–1900 kWh/m2, it is unquestionably a practical solution. This paper examines utilities of aquaponics platforms that can be supported by solar energy and describes equipment for setting up a suitable solar PV system for aquaponics operation. Possible integration of the Internet-of-Things (IoT) for remote monitoring of such solar-operated aquaponics units is also discussed. Analysis revealed that the production and growth rates of the crop and fish grown in the system were unchanged even when fully supplied with energy for 12 hours. The finding indicates the potential for using solar energy as alternative energy for the operation of the aquaponics unit. Aquaponic system particularly benefits farming activities in rural locations without electricity. Despite the high installation costs (a 100 W PV system might cost nearly RM 600), the technology offers long-term savings on electricity expenses and national grid installation fees. In conclusion, the project provided the idea of smart farming using aquaponics for the sustainable production of crops and fish utilizing clean, renewable solar energy.

Keywords: *Aquaponics; Smart farming; sustainability; solar powered system; IoT*

1. Aquaponics as a Sustainable Platform for Food Production

Nowadays, vegetables and essential herbs are conventionally cultivated using soil as growing media. However, this conventional cultivation technique is labor-intensive and has long been associated with high operating costs and inconsistent yield caused by adverse and unpredictable weather conditions. Conventional cultivation also requires massive resources such as water, fertilizers, and labor during crop harvesting and post-harvesting periods. The situation is experienced in most developing countries where high-technology agriculture systems are uncommon.

Authors information:
[a]Faculty of Chemical & Energy Engineering, Universiti Teknologi Malaysia, 81310 Johor Bahru, Johor, MALAYSIA. E-mail: nazrulhisham@utm.my[1]; mjohari@utm.my[2]; saniamril@utm.my[3]
[b]Department of Manufacturing Engineering, Faculty of Mechanical & Manufacturing Engineering, Universiti Tun Hussein Onn Malaysia, 86400, Parit Raja, Johor, MALAYSIA. E-mail: raudha@uthm.edu.my[4]
[c]Green & Renewable Energy Focus Group, Universiti Tun Hussein Onn Malaysia, 86400, Parit Raja, Johor, MALAYSIA. E-mail: nurhanis@uthm.edu.my[5]
[d]Faculty of Electrical Engineering, Universiti Teknologi Malaysia, 81310 Johor Bahru, Johor, MALAYSIA. E-mail: abioyeabiodun1@gmail.com[6]; shukri@utm.my[7]
*Corresponding Author: raudha@uthm.edu.my

Aquaponics involves growing aquatic life and plants in a closed system under controlled environments (Maucieri et al., 2018). An example of an aquaponics setup is shown in Figure 1. The Aquaponics technique will give a new perspective on plant cultivation that differs from conventional farming in many ways. Aquaponics cultivation systems rely on the symbiotic balance of ecosystems between the aquatic species and hydroponics products, including vegetables and essential herbs (Hu et al., 2015; Tyson et al., 2011). Due to the absence of synthetic fertilizers used in the cultivation process, the products are considered organics. This technique significantly reduces operating costs, aquatic life waste products (e.g., feces, etc.), and chemical fertilizers usage. In an aquaponics system, waste products from aquatic life are transformed into nutrients that plants need, and plants return clean water to aquatic life. Because the system is recirculating the nutrient-rich water, there is minimal water consumption (Moriarty, 1997). In greenhouses or net houses, cultivation is possible throughout the year to protect plants from insects and the negative impacts of climate change. Aquaponic systems could also boost production yield per square area as the growing space could be constructed vertically or in a stacked layout. The system uses fewer human resources because it often operates automatically with minimal supervision.

Received: November 17, 2021
Accepted: April 25, 2022
Published: February 28, 2023

DOI:https//doi.org/10.22452/mjs.vol42no1.7
Malaysian Journal of Science 42(1): 68-77 (February 2023)

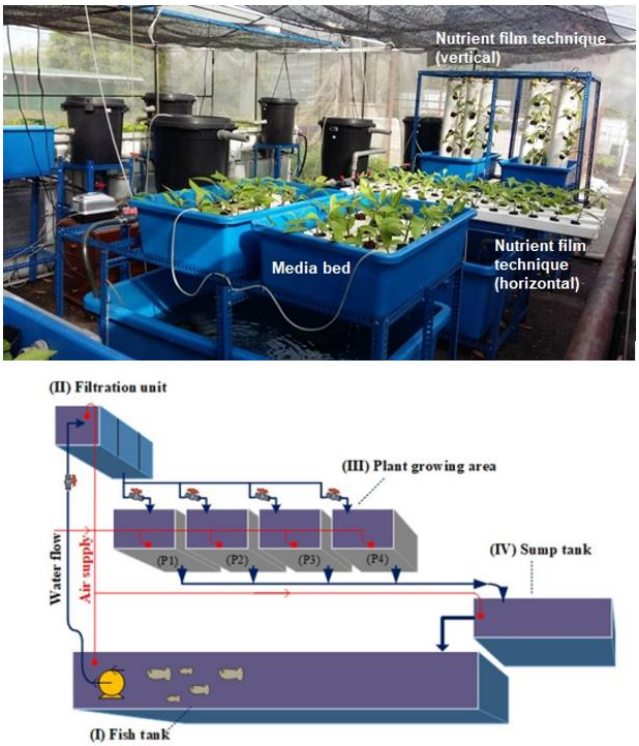

Figure 1. Our various backyard-scale aquaponics unit utilizes different types of hydroponic growers (top). Typical schematics of aquaponics operation as established by Zainal Alam et al. (2020) (bottom).

1.1 Main components of an aquaponics system

There are four main components of aquaponics: the aquaculture tank, hydroponics grower, water filtration unit, and water flow system. Materials such as fiber-reinforced polymer, polyethylene, concrete, and canvas can be used to construct aquaculture ponds/tanks. Rounded and sloped bottom tanks are preferable for ease of sludge removal and maintenance. Commercial aquaponic systems typically use aquatic life with rapid growth rates, such as tilapia, to maximize profits. The most popular hydroponic growers for aquaponics operations include media-filled (grow bed) growers, floating raft or deep water cultures (DWC), nutrient film techniques (NFT), and vertical growers. Each grower is distinctive and has their benefits and preferred plants to grow. The media-filled grower system is considered the simplest hydroponics system. One only needs to fill in an empty compartment or tank designated for culturing the plants with adequate substrates for plant growth to use the system without a water filtration unit. Light-expanded clay aggregate (LECA) and gravel larva rock are the typically used substrates for this grower. Both materials are porous and have a large surface area, so they could act as a nitrification and mineralization filter system and allow plant roots to develop within. Alternatively, one could opt for cheap waste substrates such as carbonized rice husk, cocopeat, and a mixture of cocopeat and carbonized rice husk. These alternative media are abundant and easy to purchase locally (Asian countries), ~80% cheaper than common media such as LECA. However, these alternative media require specific installation due to their low surface area and poor biofiltration capacity. The facility typically includes pierced polybags to prevent clogging and a water filtration unit supporting microbial activities in media with low specific surface area (area/volume). The study by Zainal Alam et al. (2020) reported detailed information on these alternative media. In addition, the grow bed system uses components such as a bell siphon that can drain nutrient-rich water effectively, thus compatible with flood and drain mechanisms (reciprocating flow). Consequently, waterlogging at the plant roots is prevented. Therefore, this type of grower is suitable for cultivating many plants, including leafy veggies, herbs, and woody plants such as chilies, eggplants, tomatoes, etc.

The NFT and vertical grower are hydroponics techniques that use horizontal and vertical pipes, respectively, with a thin stream of water from an aquaponics system rich in nutrients. In the NFT system, plants are positioned in holes (with net pots) at the top of the pipes or at the sides of the pipes in the vertical grower, where they can use a thin film of nutrient-rich water. These techniques have very low evaporation because the water is completely shielded from the sun. In addition, the vertical arrangement of the planting area optimizes space usage. However, both growers should have a dedicated water filtration system. Therefore, a mechanical filter must be specifically built to capture suspended materials, followed by a biological filter to facilitate nitrification.

Research has shown that the DWC grower is preferable for large-scale cultivation of a single crop, particularly leafy vegetables, including lettuce, salad leaves, and basil. The DWC technique involves suspending plants on polystyrene sheets, with their roots dipped into the water. However, this technique is unsuitable for growing tall, woody plants such as tomatoes and chilies (Valdez, 2017). In the DWC system, high water flow rates and turbulence would promote plant growth by distributing more necessary ions evenly throughout the roots of the plants. On the contrary, if slower water conditions were applied, it would create stagnant water conditions, which would only negatively impact plant growth due to the low mixing of ions and minerals. Aeration is important in the DWC system, especially in a densely planted canal. Thus, the oxygen demand for plants can cause dissolved oxygen levels to plummet below the minimum level (3 mg/L) (Maucieri et al., 2018). Several small air stones must be placed in the canals to overcome the problem. Similar to NFT and vertical growers, this technique required a dedicated water filtration unit to be installed between the aquatic tank and grower. A few researchers have reviewed comparison studies of these hydroponics systems. For instance, high yield has been reportedly obtained from growing leafy vegetables, such as lettuce (Latuca sativa), in

DOI:https//doi.org/10.22452/mjs.vol42no1.7
Malaysian Journal of Science 42(1): 68-77 (February 2023)

bed aquaponics system (Lennard and Leonard, 2006; Shete et al., 2016). According to a specific study on the cultivation of herbs like Gynura procumbens, the DWC approach with adequate aeration (dissolved oxygen) gave the maximum yield and growth rate for the Gynura because it allowed efficient nutrient absorption. (Zainal Alam et al., 2019).

1.2 Water filtration unit

Although the choice of hydroponic grower affects the plant growth rate and harvesting yield, the water filtration unit plays a crucial part in the aquaponics system performance as it serves as the heart of the system. The filters complete the nitrogen cycle by providing nutrients rich water to the plants in the hydroponics grower and clean water to the aquatic life in the aquaculture tank. Commonly used water filtration units combine mechanical filters and biofilters arranged in sequence, with the former coming first, followed by the latter. Solid fish wastes like feces and uneaten fish food are removed from fish tanks using mechanical filters, including sedimentation tanks, radial and axial flow clarifiers, sand/bead filters, and baffle filters (Bandi et al., 2016). However, because most fish waste is dissolved in the water as ammonia, it cannot generally be removed using the mechanical filter as the particle size is too small (Somerville et al., 2014). Therefore, the biofilter is required to process this microscopic waste. The bio-filter is designed to have a large surface area supplied with oxygenated water to house most nitrifying bacteria and installed between the mechanical filter and the hydroponic grower. The ammonia-oxidizing bacteria (AOB), such as Nitrosomonas sp., and nitrite-oxidizing bacteria (NOB), such as Nitrobacter sp., convert the ammonia into nitrites and nitrite into nitrates, respectively (Blidariu & Grozea, 2011). Since ammonia and nitrite are toxic to aquatic life, even at low concentrations, the installation of biofiltration is essential. Biofiltration also offers the capacity to boost the conversion of these toxic compounds into nitrates which is needed for plant growth (Bandi et al., 2016). Colonies of nitrifying bacteria can be extensively developed using commercial biofiltration materials with a high specific surface area (SSA). Bio-balls and bio-rings are the commonly used biofiltration media, which are specially shaped plastic or ceramics with huge SSA in the range of 500-700 m2/m3. Natural media such as volcanic tuff and LECA with an SSA of ~300 m2/m3 enables the growth of bacteria. The size (volume) of a biofilter is greater than that of commercial media since it has a lower SSA. Our recent study (Kamarudin et al., 2019) found that axial flow and bio-filter (using bio-balls and bio-rings) combined in a small vessel (single compartment) were sufficient and comparable with using both filters separately in sequence. The systems provide high-quality and nutrient water for healthily growing the red Nile tilapia and herbs, respectively. This compact filtration unit is an innovation by the authors that can reduce the area required to place the filter.

1.3 Water flow of aquaponics system

A pump and piping system is necessary for the aquaponics system, and there are important parts of the water flow system. The time for minerals or ions residing in each compartment of the aquaponics platform is closely related to the water flow within the aquaponics system. This factor directly affects the cultivation of the fish and the yield of the plants (Rakocy, 2007). Additionally, the water flow system affects energy consumption and running costs, particularly the pump. Submersible, airlifts, and momentum pumps, such as axial flow and centrifugal pumps, are three commonly used methods of transporting water through an aquaponics system. Submersible pumps are typically employed in various-sized aquaponics setups. Instead of using a water pump, airlift-based aquaponics operations employ air pumps such as air compressors and blowers. Bubbles for oxygenation and mixing are created by pumping air to the bottom of a pipe within the fish tank. The bubbles carry and/or push the water upwards through the column as it heads toward the surface of the water. Airlifts work best at water depths larger than 1 m and generate power in deeper tanks. Airlifts do not clog compared to submersible pumps, and water oxygenation is established through the vertical movement operated by the air bubbles. Air pumps generally have a longer life span than submersible pumps. Moreover, airlifts are more economical as a single air pump, which can be purchased for water circulation and aeration, reducing the capital investment in a second pump. According to Wayua (2015), momentum pumps such as axial flow pumps are used on larger scale systems because they have better pumping efficiencies than air pumps under low lift conditions, which are lesser than 3 m. These pumps are robust and highly resistant to clogging. Since the propeller is submerged in a recirculating aquaponics setup, pumping can start without priming, although axial pumps are more expensive than air pumps.

2. Main Utilities for Aquaponics Operation

Water heaters, air blowers, box fans, a pump, and lights for seedling germination in four-season nations are the main electrical components that must be powered by electricity in aquaponics systems (Love et al., 2015). On the contrary, less electrical equipment would be required if the aquaponics systems were set up in tropical regions like Malaysia. Electricity is mainly used for air supply and water circulation. Table 1 compares the electrical equipment and energy use in aquaponics systems built in four-season and tropical countries. In a typical aquaponics system, the water is continuously circulated for 24 hours a day, prompting the need for efficient power consumption. Due to friction, the pumping power is decreased along the pipelines (major losses) and possibly to a smaller extent at each pipe fitting. Additionally, as the water is pushed through the pipe connections, the total water flow rate is projected to decrease by up to 5% (Somerville et al., 2014). Therefore, it

DOI:https//doi.org/10.22452/mjs.vol42no1.7
Malaysian Journal of Science 42(1): 68-77 (February 2023)

is recommended to install pipelines with the optimal diameter and use fewer connectors to link the pump, fish tanks, and hydroponic plants to reduce energy consumption. Moreover, alternative power sources such as solar energy or a hybrid of photovoltaic and online grid electrical energy combined with a reciprocating water flow system (alternating on-off mode pump operation) may be a sustainable approach to meeting energy demand in a modern aquaponics system.

Table 1. Comparison of common mechanical equipment and energy use in aquaponics systems for four-season and tropical countries

Equipment	Energy source	Use	Region
Water pump	Electricity	Continuous	Four-season & tropical
Air blower	Electricity	Continuous	Four-season & tropical
Inflation blower	Electricity	Continuous	Four-season & tropical
Box fan	Electricity	Continuous	Four-season & tropical
Fluorescent light	Electricity	On-demand	Four-season only
Electrical water heaters	Electricity	On-demand	Four-season only
Greenhouse fan	Electricity	On-demand	Four-season only
Wall-mounted heater	Propane	On-demand	Four-season only
Generator	Propane	On-demand	Four-season & tropical

3. Solar Energy: What and How?

Nowadays, solar power is the most eco-friendly and reliable form of renewable energy available for consumers. Solar photovoltaic is one of the most used solar technologies because it converts sunlight directly to electricity. Solar panels are made up of a smaller unit of a solar cell. Photovoltaic cells absorb solar energy during the day. It is composed of n-type and p-type silicon with a depletion layer in the middle. When the sunlight reaches the semiconductor surface, the photons of the light rays absorbed by the semiconductor excite the electrons from atoms, generating electricity. These advantages make solar PV a suitable energy source for the aquaponics system.

3.1 Types of solar PV systems

The solar cell matrix is a crucial component in any solar PV system, which functions mainly to convert energy from light into electricity. Depending on the types of raw materials used, solar PV can be classified into three different types. These include single-crystal silicon solar cells, polycrystalline silicon solar cells, and amorphous silicon solar cells.

3.1.1 Monocrystalline silicon (single silicon)

The amount of silicon in the materials used for building solar panels directly influences system efficiency. Efficiency in energy generation improved with an increasing amount of silicon. A single silicon solar panel is currently widely used in numerous settings. Figure 2 briefly shows the construction of solar panels from the combination of monocrystalline solar cells. A single silicon-based solar panel can receive the same quantity of sunlight and thus, absorbs more energy than other solar panels and produce more electricity (i.e., current and/or DC voltage energy). Despite the benefits, silicon-based solar panels have a high per-panel cost, which becomes its major drawback (Eldin et al., 2015).

Figure 2. Combination of the monocrystalline cells to form a single silicon solar panel (Eldin et al., 2015).

3.1.2 Polycrystalline silicon (multi-silicon)

A polycrystalline solar panel is typically made of polycrystalline silicon solar cells. Energy demands for different applications can be met based on the arrangement of the PV modules. Depending on the intended application, PV modules are also available at different power wattages that can generate electricity at varying levels, i.e., from 40W up to 1kW. The two most popular options on the market are thin film solar cells and crystalline silicon solar cell films, each of which has advantages and disadvantages. Manufacturing costs for the crystalline silicon solar cell film may be comparably low, but silicon consumption is high, leading to high photoelectric conversion efficiency. When it comes to thin-film solar cells, the majority of them are used to provide electricity for outdoor power generation. However, the cost of the equipment is high for the system to generate high power efficiently (Sagar et al., 2018). Figure 3 depicts a solar panel that combines polycrystalline units into a multi-silicon panel.

DOI:https//doi.org/10.22452/mjs.vol42no1.7
Malaysian Journal of Science 42(1): 68-77 (February 2023)

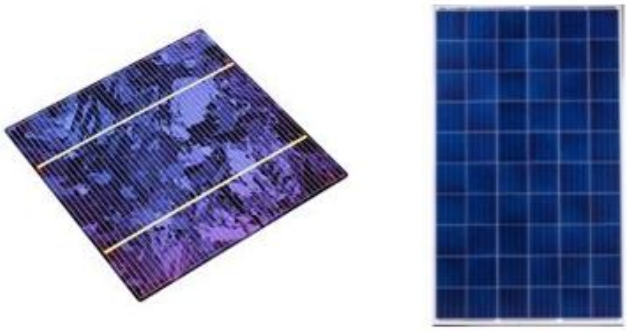

Figure 3. Combination of polycrystalline into a multi-silicon solar panel (Eldin et al., 2015).

3.1.3 Amorphous silicon solar panel

As shown in Figure 4, amorphous silicon solar cells are the new generation of thin-film solar cells. The production method is slightly different from monocrystalline and polycrystalline silicon solar cells and has been greatly simplified. This panel requires less silicon, hence the low electricity generated. The primary advantages of the panel include its ability to generate electricity under low light conditions. However, the conversion efficiency is poor due to the amorphous silicon solar cell and declines with time (Chandel et al., 2015).

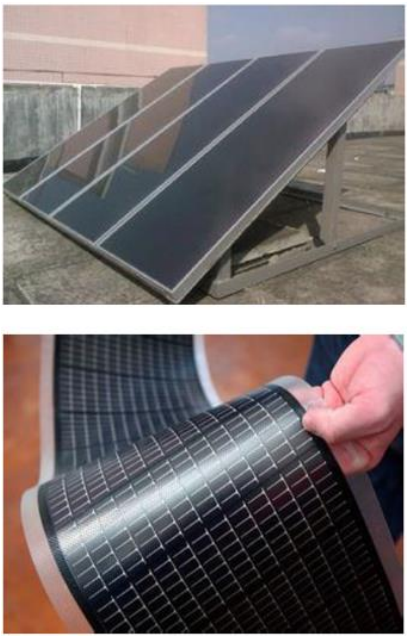

Figure 4. Amorphous silicon and flexible solar cells (Chandel et al., 2015).

3.2 Type of energy from solar cells

The two forms of electric current are alternating current (AC) and direct current (DC). Solar panels typically produce direct current (DC). The electrons generated from the sunlight flow in the same direction, generating a direct current. The mechanism is similar to batteries with positive and negative terminus and the current flowing in the same direction between the two points. On the contrary, the electrical grid and power supplied to most residential households are in the form of AC. Similarly, most plug-in submersible water pumps used in aquaponics systems are powered by AC. Inverters are required to convert DC into AC to support the functioning of water pumps. DC-coupled batteries are usually used to store the power received directly from the solar panels. A multi-purpose controller is often used to manage energy from solar panels efficiently. The primary function of the controller is to channel the energy received from the solar PV panel to batteries for energy storage and to the electrical appliances in the form of DC or AC. Notably, converting solar PV energy from DC to AC may result in a voltage drop in the system, lowering system efficiency. For this reason, a DC-powered water pump may be opted for if the aquaponic system were to be powered by solar energy.

4. Feasibility of Solar-Operated Aquaponic Platform

The prospect of electricity generation from solar energy in Malaysia is up-and-coming. Malaysia is strategically located near the equator, and its climate is hot and humid all year round (Ahmad et al., 2013). Malaysia receives an average of six hours of sunshine per day, with up to nine hours on some days in January, and local temperatures between 26 °C to 32 °C annually, despite the occasional heavy rainfall (Shafie et al., 2011). Solar energy is abundant in Malaysia, with records showing a yearly average solar intensity between 1500 kWh/m2 and 1900 kWh/m2, which is among the highest in the world (Ahmad et al., 2013; Shafie et al., 2011; Mohamad et al., 2013). The solar intensity distributions across the Peninsula and the Borneo Islands of Malaysia are shown in Figure 5. Based on the data from Ahmad et al. (2013), the Northern states of Malaysia and the northwest coast of Sabah have recorded the highest solar intensity, higher than 1750 kWh/m2. The central region and part of the southern region of Malaysia could also be potential sites for solar energy generation, with a solar intensity in the range of 1600-1700 kWh/m2.

DOI:https//doi.org/10.22452/mjs.vol42no1.7
Malaysian Journal of Science 42(1): 68-77 (February 2023)

Figure 5. Solar intensity distribution in Malaysia, redrawn based on solar intensity contour map retrieved from Ahmad et al. (2013).

Given its reputation as a clean, renewable energy source, the Malaysian government has started to provide attractive incentives to companies producing solar energy. The Feed-in-Tariff (FIT) program is part of a new policy that pays everyone for the renewable energy they create whether they connect it to the national grid or use it for personal use (Shukla et al., 2017). This program has inspired many stakeholders, including locals, business owners, and farmers, to install solar PV systems on their premises. Attractive new policies and/or incentives by the government and the long-term benefits of solar energy should become the driving force for incorporating solar energy into aquaponics systems.

However, integrating solar power into the aquaponics platform is not straightforward. Various design factors must be considered. The factors include the number of PV arrays and capacity (i.e., power generation in watts per square meter, W/m2) of each PV module. The PV must be carefully selected to meet the power required for aquaponic operation, where energy is mainly used for water aeration and circulation in numerous tanks. It is generally recommended to oversize the power wattage of a solar panel by approximately 30% higher than the wattage rating of the pump to account for the less ideal weather conditions (Kyi et al., 2016). The battery capacity must also be considered for a prolonged pump operation. Solar panels with a size larger than the battery bank are typically employed for voltage generation to address concerns with voltage drop and power fluctuation or to make up for any energy loss due to wear and tear (Kyi et al., 2016; Pradhan et al., 2012). Another crucial element is how the solar panels are installed and positioned. Since Malaysia is located within tropical latitudes, mounting the panels onto a rigid structure is more economical than an adjustable panel with sun-tracking features. This is because the sun does not change its angle much at this latitude, and installing a panel that tracks the sun as it moves across the sky is expensive. (Ahmad et al., 2013). A more logical choice would be to add more solar panels. Positioning the panels can be challenging but for a start, the panels can be placed to face a full sun without any shade. Each design element is interconnected with the others and significantly impacts energy generation.

Figure 6 shows the comparison of the power output from two different solar panels on a sunny day (Ahmad et al., 2013; Mohamad et al., 2013). The figure shows that the maximum average power output is achievable during the high noon period, i.e., between 12.00 p.m. and 3.00 p.m. Moreover, battery banks linked to the solar panels are expected to be fully charged during these hours. Beyond this time, it is assumed that less energy was generated and that pumps will likely operate less efficiently. The data highlights that a solar-powered system/pump is weather-dependent. Although solar energy can still be generated during cloudy and rainy days, the efficiency of the solar panels will decline, making the pump less efficient. Similarly, the pump operation is expected to last only a few hours after sunset.

DOI:https//doi.org/10.22452/mjs.vol42no1.7
Malaysian Journal of Science 42(1): 68-77 (February 2023)

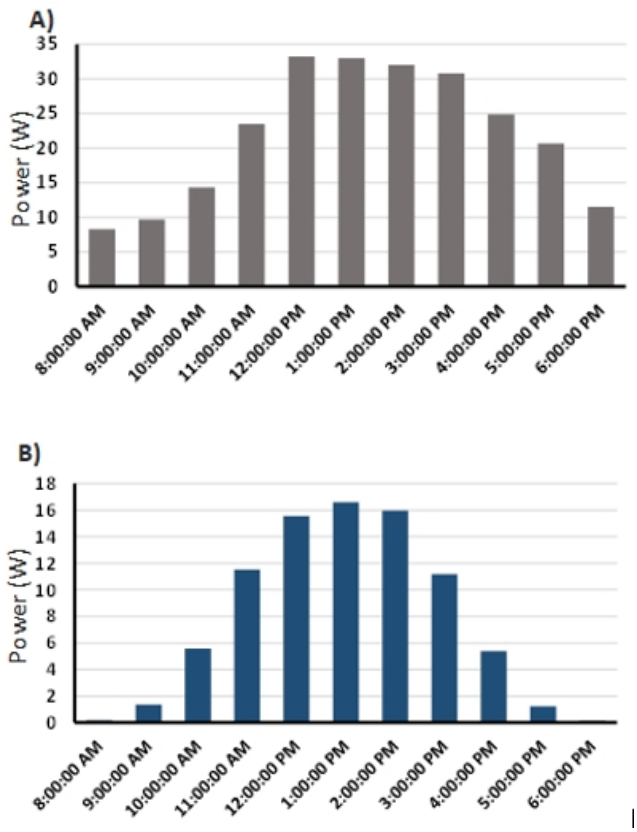

Figure 6. Average output power (W) of the solar module on a sunny day based on data from (a) Mohamad et al. (2013) and (b) Ahmad et al. (2013).

A brief investigation was carried out to evaluate the conditions of the crops and the water quality in an aquaponics setup equipped with water pumps that only operated during the day for 12 hours and were turned off throughout the night. The study was performed to simulate a scenario that resembles the operation of a solar-powered aquaponics system where a whole-day pump operation may not be sustainable. Plants were grown utilizing a floating raft grower for the trial duration, which lasted 12 weeks. Our findings reveal that the ammonia level in the fish tank remained reasonably low, i.e., about 0.22 mg/L, below the critical level of 1 mg/L for the survival of aquatic life. The dissolved oxygen level was also maintained within the range of 6 to 7.2 mg/L, with the mean water pH measured at approximately 6.68 ± 0.05. Notably, no fish death was recorded, and the growth of both plants and fish was reportedly steady. The plants were growing steadily despite the slight nutritional deficit, probably due to the lack of water circulation.

The research showed that the aquaponics system could continue to run properly even if the pump was turned off for 24 hours. This finding suggests that a solar-powered aquaponics platform is feasible and that crop yield would be comparable to crops grown with constant pumping. A vertical nutrition film technique (NFT) grower is deemed an inappropriate choice considering the absence of water flowing in the system when the pump is turned off, creating osmotic stress in the plants. As a result, plant growth is halted, and plant leaves begin to collapse because of a lack of nutrients and a significant reduction in respiration and photosynthesis activities (Delaide et al., 2017; Bittsanszky et al., 2016). While solar energy may have seemed like a viable alternative, a high installation cost compared to a monthly electricity bill may hamper its usefulness and could negatively impact the sustainability of the entire aquaponics operation. The cost of installing a PV system that comprises the pump, solar panel, 100 Ah battery, AC-DC converter, solar charge controller, and the associated electronics wiring and components might reach RM 1450 for a 40-W AC pump operation that runs continuously throughout the year. Suppose one decided to use the solar-operated pump, i.e., installation of a PV system for domestic use. In that case, the payback period is about eight years (i.e., based on electricity bill rates of about RM 0.50 per kWh). Alternatively, suppose one decided to sell the electricity generated back to the main grid. In that case, a shorter payback period can be achieved, i.e., around five years of revenues based on a Feed-in Tariff of RM 1.13 per kWh (rates designated for electricity generation by solar introduced by the government of Malaysia). A comparison of both scenarios is presented in Figure 7. Ideally, a solar PV system is considered a cost-effective option that reduces monthly electricity bills. Installing a solar-powered aquaponic system may be feasible in a rural area with no electricity. With the advantage of a simpler setup, solar energy generation performs comparably with a biological approach using bacteria for generating electricity (Makhtar and Tajarudin, 2020).

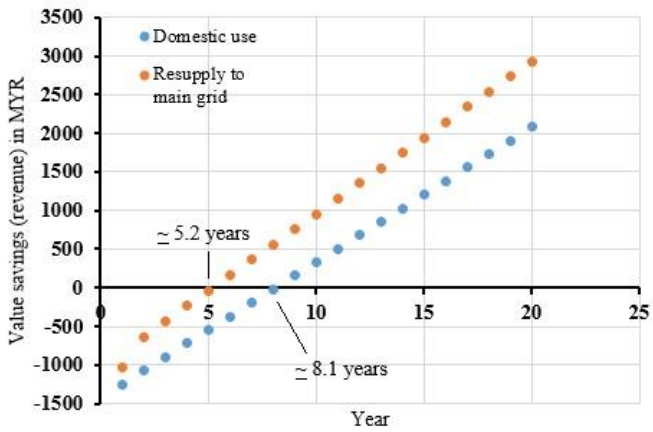

Figure 7. The estimated payback period based on the production of solar energy for domestic use and the resupply of power to the main grid for the daily operation of a 40-W pump.

DOI:https//doi.org/10.22452/mjs.vol42no1.7
Malaysian Journal of Science 42(1): 68-77 (February 2023)

5. Management of Solar Energy Via Internet-of-Things (IoT)

Real-time monitoring of the various parameters and functions of the photovoltaic system component using the IoT is crucial for managing solar-powered aquaponics systems. IoT can be employed to improve energy use efficiency, increase the share of renewable energy, and reduce the associated environmental impacts (Motlagh et al., 2020).

The Aquaponics platform setup requires a constant and clean electric energy supply to power the various pumps for water circulation, aeration for oxygen distribution, sensors, and other devices needed for the survival of aquatic life. IoT involves the interconnection and communication of devices through the internet using wireless standards, such as Wi-Fi, Lora, and Sigfox, for efficient data transmission (Elihaj et al., 2018; Emmanuel et al., 2020). This technology could be adapted to monitor solar-related parameters and devices to ensure optimal system performance. Figure 9 illustrates the framework of interconnected devices for monitoring photovoltaic energy systems via IoT. The framework consists of the photo voltaic energy system, the wireless gateway, and the visualization (Kumar et al., 2018).

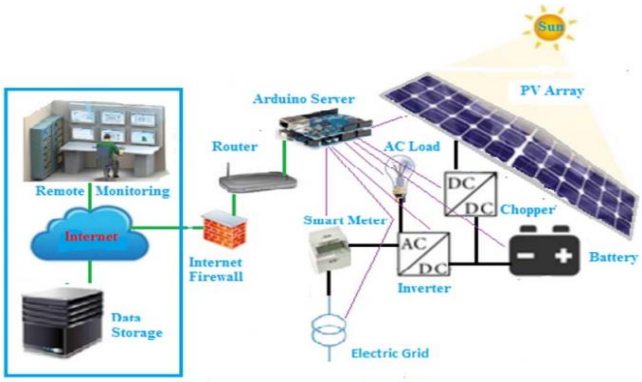

Figure 8. IoT-based architecture for the management of photovoltaic energy systems (Kumar et al., 2018)

Sensors are vital components of IoT used in a solar-powered aquaponics system, allowing real-time weather monitoring that affects solar radiation and the light incident on photovoltaic cells. IoT-based sensors may measure the variables such as air temperature, rainfall, air humidity, wind, UV index, and value. One of its most important components is the light-dependent resistor (LDR), whose resistance changes depending on the amount of light that hits it. The value and intensity of these variables help maintain the solar panel, such as the direction of placement, tilt angle, etc. The collection of dust on the solar panel can also be detected using an LDR, camera, and any IoT-based processing board with a suitable inbuilt algorithm and calibration (Babu et al., 2018; Lee and Park, 2019). This approach can help optimize the energy efficiency of solar panels for effective storage of battery charges in the system.

To monitor power consumption, solar energy devices, including photovoltaic cells, deep-cycle batteries, DC-to-DC converters (choppers), and AC-to-DC inverters can be wirelessly interfaced with Arduino or Raspberry Pi prototyping boards and coupled with current and voltage monitoring sensors (Sathiya et al., 2018; Phung et al., 2017). Monitoring parameters will let users know the performance and status of the system. Additionally, the gateway acts as a conduit for information transfer via the network between energy devices and the internet-based visualization for real-time monitoring. When using an IoT dashboard like ThingSpeak or another website platform or mobile app, the data collected may be utilized to assess the system's effectiveness based on factors like energy usage, weather, and other factors (Rahman et al., 2019). IoT makes sharing information between the farm operator and the management possible.

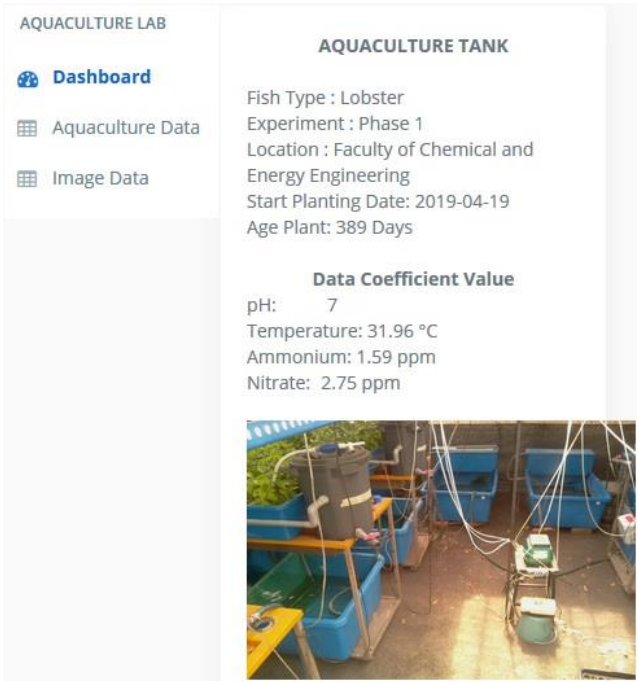

Figure 9. One of our IoT-based monitoring systems for measuring water quality in aquaponics systems (www.agritech.com).

Integrating IoT into the management of solar energy for aquaponics system can help reduce the number of visits to aquaponics farms since all the monitored parameters can be remotely viewed via phone or computer, as shown in Figure 8. Users will also be able to recognize uncommon faults on each parameter related to photovoltaic equipment, allowing them to control them remotely or go to the location for repair. Therefore, IoT-based solar energy management can help enhance the monitoring and tracking control of the system to ensure an efficient aquaponics system.

DOI:https//doi.org/10.22452/mjs.vol42no1.7
Malaysian Journal of Science 42(1): 68-77 (February 2023)

6. Concluding Remarks

Aquaponics has emerged as an increasingly popular food production method worldwide. It brings forth the smart farming concept, combining aquaculture with hydroponic farming. In aquaponics, nutrient-rich water houses aquatic life, such as fish, and provides fertilizers for plants. The plants return the clean water to the system by taking up the nutrient. The technology consumes less water than the conventional soil-based plant-growing system since the water is circulated through the plant growers. Aquaponics also generate relatively little waste and are soil-less. The system can also be installed at various scales, from as small as ~1 m2 indoor or backyard growing to a large-scale pond system. Most importantly, the system can generate two agricultural products (fish and vegetables) from a single nitrogen cycle source and is considered sustainable. However, the need for electricity to run pumps (for water recirculation and aeration) can be a problem if the aquaponics is set up far away from any power outlets. Analysis revealed that it is possible to run an aquaponics system powered by a solar PV system, in which the pumps function by harnessing the energy from the solar panels. Solar energy has been proven a viable alternative for long-term benefits despite the high installation cost. The power can be generated continuously for at least nine hours daily with a solar intensity of around 1800–1900 kWh/m2. IoT integration uses little energy, is helpful for remote process monitoring, and reduces the labor required for the operation.

7. Acknowledgement

This research was financially supported by the Universiti Tun Hussein Onn Malaysia (UTHM) Grant scheme through Tier 1 (vote Q109) and Universiti Teknologi Malaysia Fundamental Research Grant Scheme (vote No. Q.J130000.2551.2IH27).

8. References

Ahmad, S., Shafie, S., Ab Kadir, M. Z. A., Ahmad, N. S. (2013). On the effectiveness of time and date-based sun positioning solar collector in tropical climate: A case study in Northern Peninsular Malaysia. *Renewable and Sustainable Energy Reviews*. 28: 635-642.

Babu, R. L., Rambabu, D., Rajesh Naidu, A., Prasad, R.D., Gopi Krishna, P. (2018). IoT enabled solar power monitoring system. *Int. J. Eng. Technol.* 7(12): 526–530.

Bandi, A. C., Cristea, V., Dediu, L., Petrea, S. M., Cretu, M., Rahoveanu, A. T., Zugravu, A, Dorina, M., Soare., I. (2016). The review of existing and in-progress technologies of the different subsystems required for the structural and functional elements of the model of multi-purpose aquaponic production system. *Romanian Biotechnological Letters*, 21 (4), 11621-11631.

Bittsanszky, A., Uzinger, N., Gyulai, G., Mathis, A., Junge, R., Villarroel, M., Kotzen, B., Komives, T. (2016). Nutrient supply of plants in aquaponic systems. *Ecocycles* 2 (2): 17–20.

Blidariu, F., Grozea, A. (2011). Increasing the Economical Efficiency and Sustainability of Indoor Fish Farming by Means of Aquaponics. *Animal Science and Biotechnologies* , 44(2), 1-8.

Chandel, S., Naik, M.N., Chandel, R. (2015). Review of solar photovoltaic water pumping system technology for irrigation and community drinking water supplies. *Renew. Sustain. Energy Rev.*49: 1084–1099.

Delaide, B., Delhaye, G., Dermience, M., Gott, J., Soyeurt, H., Jijakli, M.H. (2017). Plant and fish production performance, nutrient mass balances, energy and water use of the PAFF Box, a small-scale aquaponic system. *Aquaculture Engineering*, 78: 130–139.

Emmanuel, A., Zainal Abidin, M.S., Azimi, S., Buyamin, S., Izran Ishak, M.H., Abdul Rahman, M.K.I., Otuoze, A., Onotu, P., Ramli, M.S.A. (2020). A review on monitoring and advanced control strategies for precision irrigation. *Comput. Electron. Agric.*173: p. 105441.

Eldin, A.H., Refaey, M., Farghly, A. (2015) A Review on Photovoltaic Solar Energy Technology and its Efficiency. 1–8. *Access online on 9 May 2020*.

Elijah, O., Rahman, T.A., Orikumhi, I., Leow, C.Y., M. N. Hindia. (2018) An Overview of Internet of Things (IoT) and Data Analytics in Agriculture: Benefits and Challenges. *IEEE Internet Things J.*, 4662: 1–17.

Hu, Z., Woo Lee, J., Chandran, K., Kim, S., Brotto, A. C., Khanal, S.K. (2015). Effect of plant species on nitrogen recovery in aquaponics, *Bio-resource Technology,* 188, 92 -98.

Kamaruddin, M.J., Izzati N.S., Othman, A., Abu Bakar, M.H., Johari, A., Hassim, M.H., (2019). Performance of Water Treatment Techniques on Cocopeat Media Filled Grow Bed Aquaponics System. E3S Web Conference. 90 02001.

Kumar, N.M., Atluri, K., Palaparthi, S. (2018). Internet of Things (IoT) in Photovoltaic Systems. *2018 National Power Engineering Conference, NPEC 2018*. 1–4.

Kyi, M.S., Maw L., Tun, H.M. (2016). Study of water pumping system for irrigation of Asparagus. *International Journal of Scientific & Technology Research*. 5(6): 71-75.

Lee, Y., Park, M. (2019). Energy management for solar-powered IoT devices with performance adjustment. *Int. J. Smart Grid Clean Energy*. 8(1): 22–30.

Lennard, W. A., Leonard, B. V. (2006). A comparison of three different hydroponic sub-systems (gravel bed, floating and nutrient film technique) in an Aquaponics test system. *Aquaculture. Int.,* 14, 539 - 550.

DOI:https//doi.org/10.22452/mjs.vol42no1.7
Malaysian Journal of Science 42(1): 68-77 (February 2023)

Love, D.C., Uhl, M.S., Genello, L. (2015). Energy and water use of a small-scale raft aquaponics system in Baltimore, Maryland, United States. *Aquacultural Engineering*, 68 19–27

Makhtar, M.M.Z. and Tajarudin, H.A. (2020). Electricity generation using membrane-less microbial fuel cell powered by sludge supplemented with lignocellulosic waste. International Journal of Energy Research. 44(4): 3260-3265.

Maucieri, C., Nicoletto, C., Junge, R., Schmautz, Z., Sambo, P., Borin, M. (2018). Hydroponic systems and water management in aquaponics: A review. *Ita. J. Agro*. 13:1012.

Mohamad, N.R., Soh, S.A.M., Salleh, A., Hashim, N.M.Z., Abd Aziz, M.Z.A., Sarimin, N., Othman, A., Ghani, Z.A. (2013). Development of aquaponic system using solar powered control pump'. *Journal of Electrical and Electronics Engineering*. 8(6): 1-6.

Moriarty, D. J. W. (1997). The role of microorganisms in aquaculture ponds. *Aquaculture,* 151, 333- 349.

Motlagh, N.H., Mohammad rezaei, M., Hunt, J., B. Zakeri, B. (2020). Internet of things (IoT) and the energy sector. *Energies*. 13(2): 1–27.

Phung, M.D., De La Villefromoy, M., Ha, Q. (2017) Management of solar energy in microgrids using IoT-based dependable control. *20th Int. Conf. Electr. Mach. Syst. ICEMS 2017*.

Pradhan, A., Ali, S.M., Behera, P. (2012). Utilisation of battery bank in case of solar PV system and classification of various storage batteries. *International Journal of Scientific & Technology Research*. 2(12): 1-5.

Rahman, M. K. I. A., Abidin, M. S. Z., Azimi, M. S., Mahmud, S. B., Ishak, M. H., Emmanuel, A. A. (2019). Advancement of a smart fibrous capillary irrigation management system with an internet of things intgration. *Bull. Electr. Eng. Informatics*, 8(4): 1402–1410.

Rakocy, J. (2007). Ten Guidelines for Aquaponic Systems. *Aquaponics Journal, 3rd Quarte*(46), 14-17.

Sagar, B., Madhav, K., Kishor, S., Rameshwar, B., Tushar, P. (2018). Solar water pumping system, *Int. Res. J. Eng. Technol.*, 1324–1326.

Sathiya, R., Pavithra, R.R.S., Harini, C. (2018). IoT Based Hybrid Power Generation and Management using Solar and Peltier plate. *Int. J. Pure Appl. Math.* 119(15) 1017–1022.

Shafie, S.M., Mahlia, T.M.I, Masjuki, H.H., Andriyana, A. (2011). Current energy usage and sustainable energy in Malaysia: a review. *Renewable and Sustainable Energy Reviews*. 15(9):4370–7.

Shukla, A.K., Sudhakar, K., Baredar, P. (2017). Renewable energy resources in South Asian countries: challenges, policy and recommendations. *Resource-Efficient Technologies*. 3(3): 342-346.

Shete, A. P., Verma, A. K., Chadha, N. K., Prakash, C., Peter, R. M., Ahmad, I. (2016). Optimization of hydraulic loading rate in aquaponic system with Common carp and Mint, *Aquacultural Engineering*,72, 53-57.

Somerville, C., Cohen, M., Pantanella, E., Stankus, A., Lovatelli, A. (2014). Small-scale aquaponic Food Production: Integrated Fish and Plant Farming. U. FAO (Ed.), *FAO Fisheries and Aquaculture Technical Paper*, 1-262.

Tyson, R. V., Treadwell, D. D., Simonne, E. H. (2011). Opportunities and challenges to sustainability in aquaponics, *Hort Technol.* 21 (1), 6-13.

Valdez, J., (2017). The Best Crops for Raft System (DWC). *Access online on 9 May 2020*.

Wayua, W. L. (2015). Design of an Aquaponic System (Vol. F21/173/2).

Zainal Alam, M.N.H., Ali Othman, N.S.I., Samsudin, S.A., Johari, A., Hassim, M.H., Kamaruddin, M.J. (2020). Carbonized Rice Husk and Cocopeat as Alternative Media Bed for Aquaponic System. *Sains Malaysiana*, 49(3), 482-492.

Zainal Alam, M.N.H., Samsudin, S.A., Xiu Han, C., Hassim, M.H., Johari, A., Kamaruddin, M.J. (2019). Performance of Hydroponic Growers for Organic Cultivation of Gynura procumbens. *2nd International Conference on Sustainable Development Goals*, Olive Tree Hotel, Penang.

DOI:https//doi.org/10.22452/mjs.vol42no1.7
Malaysian Journal of Science 42(1): 68-77 (February 2023)

MALAYSIAN JOURNAL OF SCIENCE
MJS
ISSN 1394-3065

Regular Issue

Malaysian Journal of Science 42 (1): 78-91 (February 2023) https://mjs.um.edu.my

THE HEALTH BENEFITS OF FERMENTED FOOD: A NARRATIVE REVIEW

Mohd. Kamalul Abrar Nabil Husaini[1a] and Md. Jaffri, Juliana[2a]*

Abstract: Fermented foods form a significant proportion of human diets from across the world. Increasing evidence promotes the health benefits of fermented foods on human health. The microorganisms present in these foods improve many health conditions. They include various fungi and probiotic bacterial species that are intentionally added as starter cultures or are naturally present in certain foods. Through fermentation, microbes metabolise food components including carbohydrates and proteins, to produce molecules that benefit the human host within and beyond the intestines. Among these are molecules that suppress the overgrowth of commensal and pathogenic microbes. Chronic dysbiosis is linked to inflammatory bowel diseases and has been reported in subjects with major depression and metabolic risk factors. Regular intake of fermented foods can improve these conditions and alleviate various risk factors of certain chronic diseases. Incorporating fermented foods as part of a healthy diet for chronic disease prevention offers a promising prospect. This study reviews the different types of fermented foods and the underlying microbes in modifying disease and health conditions. An overview of the disease-modulating effects is also summarised, which covers health conditions related to intestinal health, metabolic syndrome (MetS), cardiovascular health and neurological health.

Keywords: *Fermented food, gastrointestinal, probiotics, health, lactic acid bacteria (LAB)*

1. Introduction

Fermentation is one of the oldest chemical processes performed by humankind. Traces of fermented alcohol and grains can be found in ancient archaeological sites. Men utilised fermentation to prolong the edible life of food during times when refrigeration had not yet been invented, and freezing was only applicable to those living in frigid areas. Most commonly consumed foods are the products of fermentation, for example, cheese, yoghurt, tempeh and tapai. In many regions of the world then, fermentation started with the artisanal expertise of food makers and indigenous ways of food preservation. Today, fermentation has become the focus of many large-scale food industries, though the commercialised selection of food types remains limited, with cultured drinks and dairy products being the most popular (Intelligence, 2021). It follows that fermented foods and beverages make up a big part of human life.

In an anaerobic environment, fermentation involves the action of selected microbes, including yeasts and bacteria, on several substrates found in food, such as carbohydrates and proteins. A starter culture may initiate fermentation, spontaneously or otherwise, as when making tempoyak. In the case of alcoholic beverages, sugars in foods such as grapes, barley, wheat, and rice are fermented by yeast using zymase to form carbon dioxide and ethanol. Apart from this classic fermentation reaction, many other foods, such as fish, meat, fruits, and vegetables, can be fermented by various bacterial species, including lactic acid bacteria (LAB) and non-LAB.

Excluding alcoholic beverages, regular consumption of fermented foods has many benefits for human health (Parvez et al., 2006). Most fermented foods contain beneficial microbes called probiotics, live microbes that offer health benefits to the human host when consumed in adequate amounts (Hill et al., 2014). The reported health benefits of fermented foods include promoting gastrointestinal (GI) health, alleviating cardiovascular and metabolic disorders, and promoting brain functions (Dimidi et al., 2019; Galland, 2014; Gille et al., 2018).

The intake of fermented foods as part of a healthy diet is gaining interest in Malaysia. This study aims to explain the health benefits of fermented foods and relate them to the respective microbial and bioactive metabolite content. The common health conditions included in this review are GI health, metabolic syndrome (MetS), cardiovascular health, and neurological health. Fundamental knowledge of fermented foods and the interaction between the food components and the probiotic content with the human host becomes a prerequisite.

Authors information:
[a]Kulliyyah of Pharmacy, International Islamic University Malaysia, Bandar Indera Mahkota, 25200 Kuantan, Pahang, MALAYSIA.Email: nabilabrar.1115@gmail.com[1]; juliana@iium.edu.my[2]
*Corresponding Author: juliana@iium.edu.my

Received: January 11, 2022
Accepted: April 5, 2022
Published: February 28, 2022

DOI:https//doi.org/10.22452/mjs.vol42no1.8
Malaysian Journal of Science 42(1): 78-91 (February 2023)

2. Beneficial Microbes in Fermented Foods

The physicochemical and organoleptic properties of fermented foods are distinctive to the metabolic products of the microbes found in them. LAB are the most abundant microbes in fermented foods (Table 1) and has become the go-to starter culture in foods such as yoghurt and cultured drinks. These LAB-populated foods have a distinguished acidic taste from the lactic acid produced during fermentation. The genera that fall under this category of microbes are *Lactobacillus*, *Leuconostoc*, *Lactococcus*, *Weissella*, and *Streptococcus thermophilus*.

The non-LAB in fermented foods include other bacteria and fungi (Table 2). These microbes provide various characteristics to fermented foods, such as changes in flavour, a lower pH, and additive nutritional values. Among the non-LAB in fermented foods are acetic acid bacteria such as *Acetobacter* spp., lipolytic bacteria that include several species of the genus *Bacillus*, and fungi like *Saccharomyces* spp.

Table 1. LAB Genera Found in Different Fermented Foods

Genus	Fermented food	References
Bifidobacterium	Kefir *Lait caillé* *Yucha*	(Demir, 2020) (Parker et al., 2018) (Zhang et al., 2016)
Enterococcus	*Chicha* *Fu yu* *Koozh* *Lait caillé*	(Puerari et al., 2015) (J. K. H. Chen & Lim, 2018) (Veerapagu & Jeya, 2017) (Parker et al., 2018)
Lactobacillus	Cereal, dairy, cassava, alcoholic and locust bean fermentations *Chhurpi, churkam, gheu/mar, dahi* *Chicha* Fermented vegetables Kefir *Kisra, hulumur* *Kaeng-som* *Lait caillé* Palm wine Shanxi aged vinegar *Yucha*	(Diaz et al., 2019) (Shangpliang et al., 2018) (Puerari et al., 2015) (Peng et al., 2018) (Demir, 2020; Korsak et al., 2015; Walsh et al., 2016; X. Wang et al., 2018) (Eltayeb et al., 2020) (Sanchart et al., 2017) (Parker et al., 2018) (Djeni et al., 2020) (Zhu et al., 2018) (Zhang et al., 2016)
Lactococcus	*Chhurpi, churkam, gheu/mar, dahi* Kefir *Lait caillé* Shanxi aged vinegar *Yucha*	(Shangpliang et al., 2018) (Demir, 2020; Korsak et al., 2015) (Parker et al., 2018) (Zhu et al., 2018) (Zhang et al., 2016)
Leuconostoc	Cassava and alcoholic fermentations *Chhurpi, churkam, gheu/mar, dahi* *Chicha* Kefir Lait caillé Palm wine	(Diaz et al., 2019) (Shangpliang et al., 2018) (Puerari et al., 2015) (Korsak et al., 2015; Walsh et al., 2016) (Parker et al., 2018) (Djeni et al., 2020)
Pediococcus	Fermented vegetables *Fu yu* *Kalarei* *Kisra, hulumur* *Lait caillé* Shanxi aged vinegar *Yucha*	(Peng et al., 2018) (J. K. H. Chen & Lim, 2018) (Bhagat et al., 2020) (Eltayeb et al., 2020) (Parker et al., 2018) (Zhu et al., 2018) (Zhang et al., 2016)
Streptococcus	Cereal, dairy and alcoholic fermentations Kefir *Lait caille*	(Diaz et al., 2019) (Demir, 2020) (Parker et al., 2018)
Weissella	Cereal, dairy and cassava fermentations Fermented vegetables *Lait caillé* *Yucha*	(Diaz et al., 2019) (Peng et al., 2018) (Parker et al., 2018) (Zhang et al., 2016)

Table 2. Non-LAB and Fungi Genera Found in Fermented Food

Genus	Fermented food	Source
Bacteria		
Acetobacter	Cereal and dairy fermentations *Chhurpi, churkam, gheu/mar, dahi* *Hulumur* *Kefir* *Lait caillé* *Palm wine* Shanxi aged vinegar	(Diaz et al., 2019) (Shangpliang et al., 2018) (Eltayeb et al., 2020) (Korsak et al., 2015; Walsh et al., 2016) (Parker et al., 2018)

DOI:https//doi.org/10.22452/mjs.vol42no1.8
Malaysian Journal of Science 42(1): 78-91 (February 2023)

		(Djeni et al., 2020) (Zhu et al., 2018)
Acinetobacter	*Chicha* Fermented vegetables *Lait caillé* *Yucha*	(Puerari et al., 2015) (Peng et al., 2018) (Parker et al., 2018) (J. Zhang et al., 2016)
Bacillus	Cassava, alcoholic and locust bean fermentations *Chicha* *Lait caillé* *Nham, pla-ra, kaeng-chom, sai-krog-prieo*	(Diaz et al., 2019) (Puerari et al., 2015) (Parker et al., 2018) (Phoottosavako et al., 2015)
Gluconobacter	*Chhurpi, churkam, gheu/mar, dahi* *Hulumur* *Kefir* Palm wine	(Shangpliang et al., 2018) (Eltayeb et al., 2020) (Korsak et al., 2015; Walsh et al., 2016) (Djeni et al., 2020)
Gluconacetobacter	Kefir Palm wine	(Walsh et al., 2016) (Djeni et al., 2020)
Paenibacillus	*Nham*	(Phoottosavako et al., 2015)
Rhizobium	Fermented vegetables Shanxi aged vinegar	(Peng et al., 2018) (Zhu et al., 2018)
Streptomyces	*Chicha*	(Puerari et al., 2015)
Zymomonas	Cereal, dairy, alcoholic and locust bean fermentations Palm wine	(Diaz et al., 2019) (Djeni et al., 2020)
Fungi		
Alternaria	*Hulumur*	(Eltayeb et al., 2020)
Aspergillus	*Kisra*	(Eltayeb et al., 2020)
Penicillium	*Hulumur*	(Eltayeb et al., 2020)
Rhizopus	*Kisra*	(Eltayeb et al., 2020)
Saccharomyces	Kefir Palm wine	(Demir, 2020; Walsh et al., 2016; X. Wang et al., 2018) (Djeni et al., 2020)
Kazachstania	Kefir	(Korsak et al., 2015; Walsh et al., 2016)

3. Improvement of Gastrointestinal Microbiota and Health

One of the essential health benefits of fermented foods is the improvement of GI health due to the significant content of the probiotic population. Probiotic-rich fermented foods contribute to intestinal health by modulating intestinal microbiota diversity, protecting the intestinal mucosal lining and modulating the humoral immune system.

Microbes with good probiotic potential can withstand the digestive conditions of the gut, including highly acidic pH, digestive enzymes and bile salts. These characteristics enable them to inhabit and multiply in the intestines, as demonstrated by the LAB derived from fermented foods, including the *Pediococcus acidilactici, Pediococcus pentosaceus* and *Enterococcus* strains (Bhagat et al., 2020; Gupta & Sharma, 2017; Veerapagu & Jeya, 2017). Similarly, the *Lactobacillus* strains can survive through high gastric acidity, resist GI digestion, adhere to the intestinal mucosal cells and lack antibiotic resistance (Bautista-Gallego et al., 2019; Khalil et al., 2018). Selecting probiotic strains that do not develop antibiotic resistance is essential, as pathogenic microbes can transfer to antibiotic resistance genes (Khalil et al., 2018).

To confer health benefits to the host, the probiotics in fermented foods must suppress the growth of commensal and pathogenic microbes, including bacteria, fungi, and viruses (Hernández-González et al., 2021). This competitive survival ability ensures that the probiotics can further multiply and increase in population. The *Lactococcus lactis* strain isolated from kaeng-som (a fermented shrimp product from Thailand) produces bacteriocin that inhibits the growth of *Staphylococcus aureus*, a dominant food pathogen and opportunistic bacterium (Saelao et al., 2017). Several LAB strains from various Chinese fermented foods demonstrate antimicrobial properties against many opportunistic pathogens, including *Staphylococcus aureus*, *Helicobacter pylori* and *Escherichia coli*, by producing biosurfactants that inhibit the formation of biofilm by pathogens (Kaur et al., 2015; Ren et al., 2018; Sun et al., 2018). This may explain why kefir (a Russian fermented dairy product) significantly inhibits the growth of *Enterobacter cloacae*, *Escherichia coli* and *Enterococcus faecalis*, as it is rich in several LAB genera such as *Lactobacillus*, *Lactococcus*, *Streptococcus*, and *Bifidobacterium* (Demir, 2020).

Probiotics also produce organic acids that create an unfavourable environment for the growth of pathogenic microbes in the intestines. Kefir, when inoculated with *Escherichia coli* and *Staphylococcus aureus*, inhibits the growth of both pathogens due to the development of acidic conditions from the lactic and acetic acid produced by the probiotics (Kivanc & Yapici, 2019). Hor et al. (2019) demonstrate the ability of aqueous extracts of khambir (fermented sourdough bread from India) to inhibit the growth of several enteropathogens such as *Salmonella typhi*, *Shigella dysenteriae* and *Streptococcus faecalis*.

Positive changes in the gut microbiota of individuals who regularly consume fermented foods have also been observed. First, the gut microbiota of these individuals show higher proportions of LAB, such as *Lactobacillus acidophilus*, *Lactococcus lactis*, *Leuconostoc mesenteroides,* and several other

DOI:https//doi.org/10.22452/mjs.vol42no1.8
Malaysian Journal of Science 42(1): 78-91 (February 2023)

Lactobacillus strains (Taylor et al., 2020). Second, their intestines have significantly suppressed levels of harmful pathogenic bacteria such as *Clostridium* spp. and *Bilophila wadsworthia* (Messaoudi et al., 2011; Veiga et al., 2014). The evidence suggests that probiotic-rich fermented foods restore the gut microbiota to its healthy characteristic, which is crucial in maintaining GI health.

Probiotics and beneficial commensal bacteria also produce fatty acids like conjugated linoleic acid (CLA) and short-chain fatty acids (SCFA) that contribute to intestinal health. *Eubacterium* and *Bifidobacterium* spp. produce CLA, which has anti-inflammatory properties (Taylor et al., 2020). As the probiotics populate the gut and promote the growth of beneficial commensal bacteria, they also assist in maintaining the CLA at a high level to sustain the anti-inflammatory properties of the intestines. SCFA consist of acetate, propionate and butyrate, with a chain length of up to six carbon atoms. These fatty acids, particularly butyrate, are utilised by the colonocytes as an essential energy source (Venegas et al., 2019). Cow's milk, fermented with *Lactobacillus paracasei*, promotes the population of butyrate producers *Roseburia* and *Blautia* in a host (Berni Canani et al., 2017). This subsequently enhances the production of butyrate, supporting the intestinal physiological function (H. Liu et al., 2018).

Fermented foods also protect the integrity of the intestinal mucosal barrier. Chronic inflammation can disrupt the integrity and decrease the intestinal barrier function if triggered by an overgrowth of pathogenic bacteria such as *Clostridium* spp. and *Bilophila wadsworthia* (Messaoudi et al., 2011; Veiga et al., 2014). Regular intake of fermented dairy products like yoghurt may restore inflammation-disrupted intestinal integrity by improving the epithelial tight junction barrier (Putt et al., 2017). *Bifidobacterium bifidum,* a typical starter culture for fermented dairy products, has been shown to bind with Toll-like receptor-2 on the enterocytes, activating the p38 kinase pathway without causing NF-κB activation (Al-Sadi et al., 2021). This probiotic/enterocyte interaction prevents the proliferation and colonisation of pathogens and reduces inflammation (Ohland & MacNaughton, 2010). Probiotics in fermented foods also strengthen the intestinal mucous layer by increasing mucin secretion by goblet cells. The mucin creates a shield that restricts potentially harmful molecules and bacterial movement across the mucous layer (Ohland & MacNaughton, 2010).

Besides being a barrier, the intestinal mucosal surface produces immunoglobulin A (IgA), forming part of the intestinal immunological barrier. Probiotics interact with the enterocytes, stimulating the production of IgA to promote the clearance of antigens and pathogenic microbes from the intestinal lumen. Mice fed with dahi (Indian curd), containing *Lactobacillus acidophilus* and *Bifidobacterium bifidum*, show increased intestinal IgA levels with suppressed serum IgE, suggesting immunoprotection without causing hypersensitivity (Shandilya et al., 2016).

Other than the probiotic/enterocyte interaction, specific bioactive bacterial metabolites isolated from fermented foods can contribute to intestinal immunomodulation. D-phenyllactic acid (D-PLA), a LAB metabolite found in sauerkraut (German cabbage pickle), is a potent agonist of human hydroxycarboxylic acid receptor 3 (HCA3). HCA3 is highly expressed in immune cells, suggesting D-PLA's positive role in regulating the immune system and helping to maintain gut health (Peters et al., 2019). Consuming Bulgarian yoghurt, which has a starter culture of *Streptococcus thermophilus* and *Lactobacillus bulgaricus*, can result in elevated major faecal SCFA (Khuropakhonphong et al., 2021). Acetate, in particular, can promote the production of IgA and help strengthen the immunological barrier of a host (Wu et al., 2017). Certain intestinal inflammatory conditions, including irritable bowel syndrome and ulcerative colitis, have been associated with dysbiosis and gut microbiota imbalance, resulting in an immunocompromised intestinal mucosal barrier (L. Wang et al., 2020; Zakerska-Banaszak et al., 2021). Restoring the healthy balance of the gut microbiota is pivotal in reducing the immune dysregulation induced by pathogenic microbes. Consuming fermented foods containing probiotics may help restore that healthy balance, alleviating inflammation. Colitis-induced mice, administered with two *Lactobacillus* strains derived from Funazushi (fermented sushi), show significantly reduced inflammation in the colonic mucosa (Okada et al., 2018). It follows that the inflammation is reduced substantially with the expression of β8 integrin on dendritic cells, thereby inducing the proliferation and differentiation of regulatory T cells in the inflamed colonic mucosa (Okada et al., 2018). In another instance, one-year-old infants with gastroenteritis are fed yoghurt and subsequently display significantly attenuated inflammation (Nakamura et al., 2019).

Apart from the protective effect of probiotics on the intestinal lining, bioactive molecules derived from probiotics in fermented foods have also been reported to exhibit functional effects on the GI system. The pylorus in the stomach has a high expression of human trace amine-associated receptor 1 (hTAAR1). It is hypothesised that certain amino acids in fermented foods can interact with these receptors. Tyramine and phenylalanine, found in cheese and tofu-misozuke (Japanese fermented tofu), interact with hTAAR1r to stimulate gastric acid secretion and motility, and gastric epithelium proliferation by Stomach G cells (Ohta et al., 2017). The overall outcome is an improvement in protein digestion.

DOI:https//doi.org/10.22452/mjs.vol42no1.8
Malaysian Journal of Science 42(1): 78-91 (February 2023)

4. Improvement of Metabolic Syndrome

MetS is a group of health risk factors that increases the risk of heart disease, stroke and diabetes. The underlying causes include insulin resistance, abdominal obesity and physical inactivity. Significant studies have been conducted to evaluate the effect of fermented foods from different regions of the world on various parameters of MetS. It follows that the intake of these foods relates to the improvement of blood pressure, insulin resistance, fasting blood glucose and blood lipid profile.

In the Mediterranean region, elderly subjects who routinely consumed full-fat yoghurt had a lower incidence of developing MetS risk factors (Babio et al., 2015). However, elevated risks of MetS were observed in individuals consuming cheese, partly because of its higher sodium, phosphorus and fat content than other dairy products (Babio et al., 2015). Prediabetic individuals consuming Korean had reduced body weight, increased insulin sensitivity, enhanced glucose tolerance, and improved systolic and diastolic blood pressure (An et al., 2013). These positive effects can be associated with a decrease in the Firmicutes/Bacteroidetes ratio, which becomes relatively greater in obese individuals (Crovesy et al., 2020; Han et al., 2015). In Indonesia, a trial conducted on obese women showed that tempeh gembus (fermented soybean pulp) reduced triglyceride and high-sensitivity C-reactive protein levels and improved insulin resistance and HDL cholesterol levels (Nadia et al., 2020; Wati et al., 2020). *Rhizopus oligosporus*, utilised in fermenting soybean pulp, increases fibre and decreases the carbohydrate content of tempeh gembus, which may partly explain the improvement in blood lipid levels and glucose tolerance (Olanipekun & Adelakun, 2015). A cohort study involving Japanese adults reported that an intake of 20 g of natto (fermented soy food) per day lowered the total cholesterol, LDL cholesterol, and triglyceride levels in obese and overweight subjects (Wilunda et al., 2020). However, these effects were not significantly evident in the subjects of the lower BMI categories. *Bacillus subtilis natto*, as the starter culture for the production of natto, contributes to the beneficial effect by regulating the gut microbiota. However, the direct impact on serum lipid levels has not been clearly defined (P. Wang et al., 2020). Lacto-fermented annurca apple increases serum HDL cholesterol levels and reduces trimethylamine-N-oxide, an essential marker of oxidative stress (Tenore et al., 2019). An increase in oxidative stress contributes to MetS (Roberts & Sindhu, 2009).

One possible mechanism to improve MetS with fermented foods is to modulate gene expressions in the normal metabolic pathways. A study has found that traditional kefir preparations can reduce the expression of the fatty acid synthase and the peroxisome proliferator-activated receptor (PPAR) γ, translated as a reduction in triglyceride deposition in the livers of mice (Bourrie et al., 2018). Another study demonstrates the improvement of insulin resistance in mice after the supplementation of a LAB-enriched fermented food paste (FFP) through the upregulation of glucose transporter proteins and insulin receptors in the adipose tissues (Zulkawi et al., 2018). The FFP-supplemented mice also showed an increase in the expression of genes encoding glycolytic enzymes such as glucose-6-phosphate dehydrogenase, glucokinase, phosphofructokinase, and 6-phosphogluconate dehydrogenase, also activated by insulin in normal conditions (Zulkawi et al., 2018).

Evidence also suggests that fermented foods directly attenuate the development of MetS. The supplementation of *Bifidobacterium* spp., isolated from an ethnic rice beverage, on diet-induced obese mice causes reduced weight gain, improved lipid parameters, lowered high blood glucose levels, and sustained liver function. These are outcomes from the elevated expression of the lipolysis-regulating enzymes PPARα and PPARδ. The downregulation of lipogenic factors and enzymes, including PPARγ, sterol regulatory element-binding protein 1s, acetyl-CoA carboxylase, fatty acid synthase, and tumour necrosis factor α, was also observed (Ray et al., 2018). *Lactobacillus paracasei* L3C21M6, isolated from an artisanal cheese, was reported to reduce cholesterol and histamine levels. *Lactobacillus* strains, isolated from fermented foods like tapai (fermented tapioca), display cholesterol-lowering abilities, increasing the catabolism of cholesterol to bile acid and reducing enterohepatic recycling of bile acid (Lim et al., 2020; Qu et al., 2020). All these properties potentially decrease the risk of heart disease and histamine intolerance (Domingos-Lopes et al., 2020).

SCFA from probiotics in fermented foods also contribute to preventing MetS. The SCFA supplementation in mice suppresses the accumulation of hepatic triglycerides and downregulates the genes related to fatty acid synthesis. These effects are mediated physiologically by the endogenous receptor free fatty acid receptor 3 (Shimizu et al., 2019). Fermented foods increase the population of SCFA-producing bacteria in the gut, indirectly reducing fatty acid synthesis.

Evidence indicates MetS risk factor improvement from animal studies, as trials on human subjects are still lacking.

5. Improvement of Cardiovascular Health

Many risk factors of cardiovascular diseases (CVD) overlap with those related to MetS. Studies selected for this research focus mainly on the cardiovascular risk factors without obesity and insulin resistance as part of the study design. In the absence of obesity, hypertension is the most significant CVD risk factor. Fermented dairy and cheese attenuate arterial stiffness in ageing individuals with isolated systolic hypertension (Ribeiro et al., 2018). Bioactive peptides, from milk proteins produced during fermentation, inhibit the Angiotensin-converting enzyme, reducing Angiotensin II (Rai et al., 2017). The outcome is a lowering of blood pressure and a decrease in the risk of arterial stiffness.

DOI:https//doi.org/10.22452/mjs.vol42no1.8
Malaysian Journal of Science 42(1): 78-91 (February 2023)

A study in Japan reports that natto consumption has a significant inverse association with total CVD-related mortality (Katagiri et al., 2020). Nattokinase, a serine protease isolated from natto, exhibits fibrinolytic properties (Weng et al., 2017). Similarly, a fibrinolytic enzyme obtained from the *Stenotrophomonas* spp. and isolated from oncom (a soybean-based fermented food) can dissolve blood clots in rats injected with kappa-carrageenan (Nailufar et al., 2016). The formation of an obstructive thrombus is closely related to extensive vascular disease. Fibrinolysis is cardioprotective as it reduces pathological abnormalities in the fibrinolytic system and eliminates atherothrombotic risk.

Several other fermented foods also contain microbes that produce compounds with anticoagulant properties. Pickled opossum shrimp, a Korean delicacy, produces two novel fibrinolytic enzymes (Kim et al., 2020). Fermented garlic also exhibits cardiovascular protective properties due to *S*-allylcysteine (SAC) and *S*-allylmercaptocysteine (SAM), which prevents platelet aggregation and thrombus formation (Rahman & Billington, 2000). The LAB population in garlic increases during fermentation and is likely responsible for the formation of SAC and SAM. Other cardiovascular protective properties of SAC and SAM include reducing triglyceride levels to prevent hepatic steatosis, promoting angiogenesis, and protecting endothelial cells from oxidative injury (Irfan et al., 2019; X. Zhang et al., 2019).

6. Improvement of Neurological Health

Increasing evidence indicates the relationship between GI health and the brain, known as the gut-brain axis. Recent findings report that gut microbiota synthesises substances that act as signalling molecules, facilitating interaction between the gut and the brain. Such interactions represent normal brain functions such as memory, cognition, sleep patterns, stress reactivity and mood (Galland, 2014). Disturbances in the gut-brain axis increase the prevalence of chronic non-communicable diseases like irritable bowel syndrome (IBS), obesity, type 2 diabetes mellitus, chronic fatigue syndrome, and psychologic disorders such as depression (Slyepchenko et al., 2017). A matched cohort study reveals that patients diagnosed with IBS are more likely to experience depression and anxiety, along with several other physical problems such as asthma and diverticulosis (Jones et al., 2006). It follows that significant changes to the gut microbiome resulting from dietary habits are likely to affect one's psychological conditions.

Literature relating food consumption to mental health and brain function has been expanding, though studies with conclusive evidence remain sparse. However, promising findings demonstrate fermented foods and probiotics as dietary interventions. A cross-sectional survey of young adults indicated a significant effect of fermented food consumption on social anxiety, especially in subjects with high traits of neuroticism (Hilimire et al., 2015). In these subjects, a more frequent intake of fermented foods decreased the symptoms of social anxiety. Stress reduction is also another effect associated with the intake of fermented foods. The intake of fermented milk, which has *Lactobacillus* strains, decreases anxiety and stress and physical symptoms such as fever, headache, and abdominal pains, in medical students undergoing academic examination (Kato-Kataoka et al., 2016; Takada et al., 2016). Other positive effects of fermented foods related to mental health include reduced fatigue and eased depression, resulting in a better quality of life (Jiang et al., 2017).

However, some studies show a lack of relationship between fermented food intake and mental health. One study involved pregnant volunteers in their second and third trimesters (Takahashi et al., 2016). The lack of a positive effect was because the enrolled subjects were health-conscious pregnant women in the peak of good health; they displayed no signs of physiological stress. Another study found no physical or psychological improvements in patients with IBS after consuming yoghurt (Simrén et al., 2009). The above represents a limitation of this study.

Increasing evidence suggests microbiota dysbiosis is present at the onset of depressive disorders (Y. Liu et al., 2021). In patients with major depressive disorder, the gut microbial population is biased towards the phyla of *Bacteroidetes* and *Firmicutes* instead of the beneficial strains from the *Actinobacteria* phylum (Zheng et al., 2016). Therefore, diversifying the gut microbiota through a diet of fermented foods can promote mental and neurological health due to the content of beneficial probiotics and the associated bioactive molecules. Furthermore, probiotics can suppress the stress reactivity of the hypothalamus-pituitary-adrenal axis by reducing plasma corticosterone levels, the corticotropin-releasing factor neurons reducing the c-Fos expression (Takada et al., 2016). Fermented foods are rich in γ-aminobutyric acid (GABA), a well-known neurotransmitter. LAB, yeasts and moulds are among the microbes that can synthesise GABA; hence, fermented dairy products, tapai and tempeh are likely to contain a significant amount of GABA (Y.-C. Chen et al., 2021; Sahab et al., 2020; Yu et al., 2020). GABA in fermented foods induces a sedative effect, beneficial in managing insomnia and depression (Daglia et al., 2017; Embark & Abdalla, 2019; Mabunga et al., 2015). The mechanics behind the sedative effect have not been elucidated; whether it involves local regulation or changes to blood and/or CNS. Increased intestinal SCFA are likely related to the sedative effect, suggesting that modulating the gut microbiota induces more SCFA-producing bacteria such as *Actinobacteria* (including *Bifidobacterium* spp.) (Y.-C. Chen et al., 2021; Yu et al., 2020). In rats with anxiety-like behaviour induced by antibiotics, a cocktail of probiotics isolated from various fermented foods implies a neuroprotective reaction. The rats displayed reduced symptoms of neuron damage with better locomotor function, improved memory and reduced anxiety, alongside an enhanced intestinal microbial population (Luang-In et al., 2020). A link exists between the improvement of gut

DOI:https//doi.org/10.22452/mjs.vol42no1.8
Malaysian Journal of Science 42(1): 78-91 (February 2023)

microbiota and mental health; however, it requires further investigation.

Evidence suggests that dietary intervention with fermented foods can improve cognition and enhance memory and learning. Fermented soybeans contain *Lactobacillus plantarum* and have been reported to improve mild cognitive impairment in subjects aged 55 to 85. It associates with increased serum brain-derived neurotrophic factor (BDNF) and improved cognition, including attention, working memory and verbal memory (Hwang et al., 2019). Camembert cheese, fermented with *Penicillium candidum,* has been found to suppress brain inflammation in mice with Alzheimer's. A novel bioactive metabolite, Oleamide, isolated from the cheese, is observed to possess *microglial anti-inflammatory properties (Ano et al., 2015).* An increase in BDNF and the *glial cell line-derived neurotrophic factor follows*, slowing the progress of the disease and preventing reduced cognition and further deterioration of the neurons (Ano et al., 2015). Other bioactive molecules, isolated from various fermented dairy and cereal products, are found to prevent cognitive decline, including tryptophan-tyrosine and tryptophan-methionine peptides, fermented rice peptides, β-lactolin and poly-γ-glutamic acid (Ano et al., 2019; Corpuz et al., 2019; Jeong et al., 2021; Kita et al., 2019). These molecules possess anti-inflammatory properties, producing increased BDNF levels, suppressing brain insulin resistance and promoting neuroprotection (Ano et al., 2019; Jeong et al., 2021).

7. Fermented Food Safety and Quality Consideration

An essential aspect of fermented food safety in mass production is eliminating the risk of contamination by harmful microbes. To minimise this risk, it is crucial that the raw material is clean and has the lowest possible microbial load, ensuring fermentation is solely due to the starter culture. Microbial contaminants are metabolites produced by contaminating fungi or bacteria. Mycotoxins, such as *Aspergillus, Penicillium* and *Cladosporium,* are harmful secondary metabolites of fungi (Anal et al., 2020). Certain LAB produce biogenic amines in cheese, fermented fish and soybean products. However, contaminating bacteria like *Enterobacteriaceae* and *Enterococci* can produce toxic levels of biogenic amines that are harmful if consumed (Anal et al., 2020). Reducing these contaminations is possible with the practice of hygiene throughout food production. Aseptic processes and a clean environment make for good manufacturing practice for large-scale productions.

Fermented foods are enjoyed in many regions due to the unique flavour developed during fermentation. Microbial metabolites, particularly the more volatile compounds, impart a distinctive smell and taste, characteristic of the type of fermented food. Temperature variations during fermentation can result in different flavours due to the various biochemical processes of the microbes and the varying amounts of microbial metabolites (Hong et al., 2016). It follows that fermented foods may have different flavours if prepared in other regions of the world due to variations in climate and temperature. To maintain consistent flavours, the fermentation environment, particularly the temperature, is controlled using bioreactors, with congruous monitoring of the metabolites. It represents another important quality aspect that requires attention especially when the fermented food is mass produced.

8. The Future of Fermented Foods in Malaysia

The regulated use of fermented foods as a dietary intervention for disease prevention in Japan has been well-established for over 30 years. Japan's Ministry of Health, Labour and Welfare initiated the Food for Specific Health Use (FOSHU) in 1991 to target people who were still healthy or in the preliminary stage of chronic disease (Iwatani & Yamamoto, 2019). The initiative involved highly regulated functional foods labelled with health claims that included those related to improving GI health. In 2017, 55% of the total sales of FOSHU products were from the GI health improvement category, related to prebiotics and fermented foods with the *Lactobacillus* spp.(Iwatani & Yamamoto, 2019). This evidence implies a healthy Japanese population with a high life expectancy.

Currently, awareness is lacking in Malaysia on the health benefits of traditional fermented foods because consumers need access to adequate information. Although strong evidence is available, awareness on the benefits of fermented foods is still far behind that of Japan. The prospect of widespread consumption of various fermented foods is promising. However, it can only be successful in maintaining the population's health and well-being if the use is regulated to ensure safety and all health claims are supported by solid evidence (Koirala & Anal, 2021).

Malaysians have a natural affinity for food and are receptive to different tastes and flavours across the country. The future holds new possibilities for industry-based research focusing on production processes, quality assurance and prolonged shelf-life of fermented foods to meet local and global demands. Efforts should identify and standardise the microbes utilised for commercially-available fermented foods, especially those from the cottage industry. Over time, these foods can establish a more robust commercial presence and be available for consumers locally and globally.

9. Conclusion

Can fermented foods be classified as functional foods? The answer is yes since these foods demonstrate a potentially positive effect on health beyond basic nutrition. Consuming fermented foods modulate the gut microbiota to a healthy characteristic, indirectly promoting the host's health. Although optimal health can be achieved without the routine intake of fermented foods, evidence suggests that fermented foods

DOI:https//doi.org/10.22452/mjs.vol42no1.8
Malaysian Journal of Science 42(1): 78-91 (February 2023)

containing live probiotics improve health conditions, including intestinal and metabolic health. With the prevalence of chronic diseases, especially those relating to the lower GI tract depicting an upward trend, food-based intervention can be promoted as an adjunct to pharmacotherapy to manage selected health conditions. It is without side effects and is a more pleasant and delectable approach that can be part of an individual's healthy dietary habits. The prospect of these foods for health and wellness is promising. The market for fermented foods is growing, and consumers have begun to accept various food types from all cultural backgrounds. With strong, accessible evidence, consumers can make informed choices about their health. Fermented foods can then have an indicative place in the functional food market.

10. References

Al-Sadi, R., Dharmaprakash, V., Nighot, P., Guo, S., Nighot, M., Do, T., & Ma, T. Y. (2021). Bifidobacterium bifidum Enhances the Intestinal Epithelial Tight Junction Barrier and Protects against Intestinal Inflammation by Targeting the Toll-like Receptor-2 Pathway in an NF-κB-Independent Manner. International Journal of Molecular Sciences, 22(15), 8070.

An, S.-Y., Lee, M. S., Jeon, J. Y., Ha, E. S., Kim, T. H., Yoon, J. Y., Ok, C.-O., Lee, H.-K., Hwang, W.-S., Choe, S. J., Han, S. J., Kim, H. J., Kim, D. J., & Lee, K.-W. (2013). Beneficial effects of fresh and fermented kimchi in prediabetic individuals. Annals of Nutrition and Metabolism, 63, 111–119.

Anal, A. K., Perpetuini, G., Petchkongkaew, A., Tan, R., Avallone, S., Tofalo, R., Nguyen, H. Van, Chu-Ky, S., Ho, P. H., Phan, T. T., & Waché, Y. (2020). Food safety risks in traditional fermented food from South-East Asia. Food Control, 109, 106922.

Ano, Y., Ozawa, M., Kutsukake, T., Sugiyama, S., Uchida, K., Yoshida, A., & Nakayama, H. (2015). Preventive Effects of a Fermented Dairy Product against Alzheimer's Disease and Identification of a Novel Oleamide with Enhanced Microglial Phagocytosis and Anti-Inflammatory Activity. PLOS ONE, 10(3), e0118512.

Ano, Y., Yoshino, Y., Uchida, K., & Nakayama, H. (2019). Preventive Effects of Tryptophan–Methionine Dipeptide on Neural Inflammation and Alzheimer's Pathology. International Journal of Molecular Sciences, 20(13), 3206.

Babio, N., Becerra-Tomás, N., Martínez-González, M. Á., Corella, D., Estruch, R., Ros, E., Sayón-Orea, C., Fitó, M., Serra-Majem, L., Arós, F., Lamuela-Raventós, R. M., Lapetra, J., Gómez-Gracia, E., Fiol, M., Díaz-López, A., Sorlí, J. V, Martínez, J. A., & Salas-Salvadó, J. (2015). Consumption of yogurt, low-fat milk, and other low-fat dairy products is associated with lower risk of metabolic syndrome incidence in an elderly Mediterranean population. The Journal of Nutrition, 145(10), 2308–2316.

Bautista-Gallego, J., Ferrocino, I., Botta, C., Ercolini, D., Cocolin, L., & Rantsiou, K. (2019). Probiotic potential of a Lactobacillus rhamnosus cheese isolate and its effect on the fecal microbiota of healthy volunteers. Food Research International, 119, 305–314.

Berni Canani, R., De Filippis, F., Nocerino, R., Laiola, M., Paparo, L., Calignano, A., De Caro, C., Coretti, L., Chiariotti, L., Gilbert, J. A., & Ercolini, D. (2017). Specific signatures of the gut microbiota and increased levels of butyrate in children treated with fermented cow's milk containing heat-killed Lactobacillus paracasei CBA L74. Applied and Environmental Microbiology, 83(19), e01206-17.

Bhagat, D., Raina, N., Kumar, A., Katoch, M., Khajuria, Y., Slathia, P. S., & Sharma, P. (2020). Probiotic properties of a phytase producing Pediococcus acidilactici strain SMVDUDB2 isolated from traditional fermented cheese product, Kalarei. Scientific Reports, 10, 1926.

Bourrie, B. C. T., Cotter, P. D., & Willing, B. P. (2018). Traditional kefir reduces weight gain and improves plasma and liver lipid profiles more successfully than a commercial equivalent in a mouse model of obesity. Journal of Functional Foods, 46, 29–37.

Chen, J. K. H., & Lim, Y. S. (2018). Isolation, identification and characterization of enzyme-producing lactic acid bacteria from traditional fermented foods. Bioscience Horizons: The International Journal of Student Research, 11, hzy004.

Chen, Y.-C., Tao, N.-L., Hu, S.-Y., Tsai, H.-Y., Liao, S.-C., Tsai, W.-L., & Hu, C.-Y. (2021). Effect of Tempeh on Gut Microbiota and Anti-Stress Activity in Zebrafish. International Journal of Molecular Sciences, 22, 12660.

Corpuz, H. M., Fujii, H., Nakamura, S., & Katayama, S. (2019). Fermented rice peptides attenuate scopolamine-induced memory impairment in mice by regulating neurotrophic signaling pathways in the hippocampus. Brain Research, 1720, 146322.

Crovesy, L., Masterson, D., & Rosado, E. L. (2020). Profile of the gut microbiota of adults with obesity: a systematic review. European Journal of Clinical Nutrition, 74(9), 1251–1262.

DOI:https//doi.org/10.22452/mjs.vol42no1.8
Malaysian Journal of Science 42(1): 78-91 (February 2023)

Daglia, M., Di Lorenzo, A., Nabavi, S. F., Sureda, A., Khanjani, S., Moghaddam, A. H., Braidy, N., & Nabavi, S. M. (2017). Improvement of Antioxidant Defences and Mood Status by Oral GABA Tea Administration in a Mouse Model of Post-Stroke Depression. Nutrients, 9(5), 446.

Demir, H. (2020). Comparison of traditional and commercial kefir microorganism compositions and inhibitory effects on certain pathogens. International Journal of Food Properties, 23(1), 375–386.

Diaz, M., Kellingray, L., Akinyemi, N., Adefiranye, O. O., Olaonipekun, A. B., Bayili, G. R., Ibezim, J., du Plessis, A. S., Houngbédji, M., Kamya, D., Mukisa, I. M., Mulaw, G., Josiah, S. M., Chienjo, W. O., Atter, A., Agbemafle, E., Annan, T., Ackah, N. B., Buys, E. M., … Narbad, A. (2019). Comparison of the microbial composition of African fermented foods using amplicon sequencing. Scientific Reports, 9, 13863.

Dimidi, E., Cox, S. R., Rossi, M., & Whelan, K. (2019). Fermented foods: Definitions and characteristics, impact on the gut microbiota and effects on gastrointestinal health and disease. Nutrients, 11(8), 1806.

Djeni, T. N., Kouame, K. H., Ake, F. D. M., Amoikon, L. S. T., Dje, M. K., & Jeyaram, K. (2020). Microbial diversity and metabolite profiles of palm wine produced From three different palm tree species in Côte d'Ivoire. Scientific Reports, 10, 1715.

Domingos-Lopes, M. F. P., Stanton, C., Ross, P. R., & Silva, C. C. G. (2020). Histamine and cholesterol lowering abilities of lactic acid bacteria isolated from artisanal Pico cheese. Journal of Applied Microbiology, 129(6), 1428–1440.

Eltayeb, M. M., Eltigani, S. A., & Taniguchi, T. (2020). Pyrosequencing scrutiny of bacterial and fungal communities in two Sudanese sorghum-based fermented foods. Annals of Microbiology, 70, 53.

Embark, H. M., & Abdalla, A. K. (2019). Evaluation of sedative effects of daily consumption of yoghurt in rats. Assiut Veterinary Medical Journal, 65(163), 38–46.

Galland, L. (2014). The Gut Microbiome and the Brain. Journal of Medicinal Food, 17(12), 1261–1272.

Gille, D., Schmid, A., Walther, B., & Vergères, G. (2018). Fermented food and non-communicable chronic diseases: A review. Nutrients, 10(4), 448.

Gupta, A., & Sharma, N. (2017). In vitro characterization of lactic acid bacteria isolated from lasoda bari - A rare fermented food of Himachal Pradesh-India for potential probiotic attributes. Journal of Microbiology, Biotechnology and Food Sciences, 6(6), 1323–1328.

Han, K., Bose, S., Wang, J., Kim, B.-S., Kim, M. J., Kim, E.-J., & Kim, H. (2015). Contrasting effects of fresh and fermented kimchi consumption on gut microbiota composition and gene expression related to metabolic syndrome in obese Korean women. Molecular Nutrition & Food Research, 59(5), 1004–1008.

Hernández-González, J. C., Martínez-Tapia, A., Lazcano-Hernández, G., García-Pérez, B. E., & Castrejón-Jiménez, N. S. (2021). Bacteriocins from Lactic Acid Bacteria. A Powerful Alternative as Antimicrobials, Probiotics, and Immunomodulators in Veterinary Medicine. Animals, 11(4), 979.

Hilimire, M. R., DeVylder, J. E., & Forestell, C. A. (2015). Fermented foods, neuroticism, and social anxiety: An interaction model. Psychiatry Research, 228(2), 203–208.

Hill, C., Guarner, F., Reid, G., Gibson, G. R., Merenstein, D. J., Pot, B., Morelli, L., Berni Canani, R., Flint, H. J., Salminen, S., Calder, P. C., & Sanders, M. E. (2014). The International Scientific Association for Probiotics and Prebiotics consensus statement on the scope and appropriate use of the term probiotic. Nature Reviews Gastroenterology & Hepatology, 11(8), 506–514.

Hong, S. P., Lee, E. J., Kim, Y. H., & Ahn, D. U. (2016). Effect of Fermentation Temperature on the Volatile Composition of Kimchi. Journal of Food Science, 81(11), C2623–C2629.

Hor, P. K., Ray, M., Pal, S., Ghosh, K., Soren, J. P., Maiti, S., Bera, D., Singh, S., Dwivedi, S., Takó, M., DasMohapatra, P. K., & Mondal, K. C. (2019). Some functional properties of khambir, an ethnic fermented cereal-based food of Western Himalayas. Frontiers in Microbiology, 10, 730.

Hwang, Y.-H., Park, S., Paik, J.-W., Chae, S.-W., Kim, D.-H., Jeong, D.-G., Ha, E., Kim, M., Hong, G., Park, S.-H., Jung, S.-J., Lee, S.-M., Na, K.-H., Kim, J., & Chung, Y.-C. (2019). Efficacy and Safety of Lactobacillus Plantarum C29-Fermented Soybean (DW2009) in Individuals with Mild Cognitive Impairment: A 12-Week, Multi-Center, Randomized, Double-Blind, Placebo-Controlled Clinical Trial. Nutrients, 11, 305.

Intelligence, M. (2021). Global fermented foods and beverages market (2022 - 2027). Mordor Intelligence. https://www.mordorintelligence.com/industry-reports/fermented-foods-beverages-market

Irfan, M., Kim, M., Kim, K.-S., Kim, T.-H., Kim, S.-D., Hong, S.-B., Kim, H. K., & Rhee, M. H. (2019). Fermented Garlic

DOI:https//doi.org/10.22452/mjs.vol42no1.8
Malaysian Journal of Science 42(1): 78-91 (February 2023)

Ameliorates Hypercholesterolemia and Inhibits Platelet Activation. Evidence-Based Complementary and Alternative Medicine, Article ID 3030967.

Iwatani, S., & Yamamoto, N. (2019). Functional food products in Japan: A review. Food Science and Human Wellness, 8, 96–101.

Jeong, D.-Y., Ryu, M. S., Yang, H.-J., & Park, S. (2021). γ-PGA-Rich Chungkookjang, Short-Term Fermented Soybeans: Prevents Memory Impairment by Modulating Brain Insulin Sensitivity, Neuro-Inflammation, and the Gut–Microbiome–Brain Axis. Foods, 10(2), 221.

Jiang, S., Liu, H., Liu, Z., Liu, N., Liu, R., Kang, Y.-R., Ji, J.-G., Zhang, C., Hua, B., & Kang, S.-J. (2017). Adjuvant effects of fermented red ginseng extract on advanced non-small cell lung cancer patients treated with chemotherapy. Chinese Journal of Integrative Medicine, 23(5), 331–337.

Jones, R., Latinovic, R., Charlton, J., & Gulliford, M. (2006). Physical and psychological co-morbidity in irritable bowel syndrome: a matched cohort study using the General Practice Research Database. Alimentary Pharmacology and Therapeutics, 24(5), 879–886.

Katagiri, R., Sawada, N., Goto, A., Yamaji, T., Iwasaki, M., Noda, M., Iso, H., & Tsugane, S. (2020). Association of soy and fermented soy product intake with total and cause specific mortality: prospective cohort study. BMJ, 368, m34–m34.

Kato-Kataoka, A., Nishida, K., Takada, M., Suda, K., Kawai, M., Shimizu, K., Kushiro, A., Hoshi, R., Watanabe, O., Igarashi, T., Miyazaki, K., Kuwano, Y., & Rokutan, K. (2016). Fermented milk containing Lactobacillus casei strain Shirota prevents the onset of physical symptoms in medical students under academic examination stress. Beneficial Microbes, 7(2), 153–156.

Kaur, S., Amrita, Kaur, P., & Nagpal, R. (2015). In vitro biosurfactant production and biofilm inhibition by lactic acid bacteria isolated from fermented food products. International Journal of Probiotics and Prebiotics, 10(1), 17–22.

Khalil, E. S., Manap, M. Y., Mustafa, S., Amid, M., Alhelli, A. M., & Aljoubori, A. (2018). Probiotic characteristics of exopolysaccharides-producing lactobacillus isolated from some traditional Malaysian fermented foods. CyTA - Journal of Food, 16(1), 287–298.

Khuropakhonphong, R., Whanmek, K., Purttiponthanee, S., Chathiran, W., Srichamnong, W., Santivarangkna, C., & Trachootham, D. (2021). Bulgarian yogurt relieved symptoms and distress and increased fecal short-chain fatty acids in healthy constipated women: A randomized, blinded crossover controlled trial. NFS Journal, 22, 20–31.

Kim, C., Ri, K., & Choe, S. (2020). A novel fibrinolytic enzymes from the Korean traditional fermented food—Jotgal: Purification and characterization. Journal of Food Biochemistry, 44(7), e13255.

Kita, M., Kobayashi, K., Obara, K., Koikeda, T., Umeda, S., & Ano, Y. (2019). Supplementation With Whey Peptide Rich in β-Lactolin Improves Cognitive Performance in Healthy Older Adults: A Randomized, Double-Blind, Placebo-Controlled Study. Frontiers in Neuroscience, 13, 399.

Kivanc, M., & Yapici, E. (2019). Survival of Escherichia coli O157:H7 and Staphylococcus aureus during the fermentation and storage of kefir. Food Science and Technology, 39(Suppl. 1), 225–230.

Koirala, S., & Anal, A. K. (2021). Probiotics-based foods and beverages as future foods and their overall safety and regulatory claims. Future Foods, 3, 100013.

Korsak, N., Taminiau, B., Leclercq, M., Nezer, C., Crevecoeur, S., Ferauche, C., Detry, E., Delcenserie, V., & Daube, G. (2015). Short communication: Evaluation of the microbiota of kefir samples using metagenetic analysis targeting the 16S and 26S ribosomal DNA fragments. Journal of Dairy Science, 98(6), 3684–3689.

Lim, P. S., Loke, C. F., Ho, Y. W., & Tan, H. Y. (2020). Cholesterol homeostasis associated with probiotic supplementation in vivo. Journal of Applied Microbiology, 129(5), 1374–1388.

Liu, H., Wang, J., He, T., Becker, S., Zhang, G., Li, D., & Ma, X. (2018). Butyrate: A Double-Edged Sword for Health? Advances in Nutrition, 9(1), 21–29.

Liu, Y., Wang, H., Gui, S., Zeng, B., Pu, J., Zheng, P., Zeng, L., Luo, Y., Wu, Y., Zhou, C., Song, J., Ji, P., Wei, H., & Xie, P. (2021). Proteomics analysis of the gut–brain axis in a gut microbiota-dysbiosis model of depression. Translational Psychiatry, 11(568).

Luang-In, V., Katisart, T., Konsue, A., Nudmamud-Thanoi, S., Narbad, A., Saengha, W., Wangkahart, E., Pumriw, S., Samappito, W., & Ma, N. L. (2020). Psychobiotic Effects of Multi-Strain Probiotics Originated from Thai Fermented Foods in a Rat Model. Food Science of Animal Resources, 40(6), 1014–1032.

Mabunga, D. F. N., Gonzales, E. L. T., Kim, H. J., & Choung, S. Y. (2015). Treatment of GABA from Fermented Rice Germ

DOI:https//doi.org/10.22452/mjs.vol42no1.8
Malaysian Journal of Science 42(1): 78-91 (February 2023)

Ameliorates Caffeine-Induced Sleep Disturbance in Mice. Biomolecules & Therapeutics, 23(3), 268–274.

Messaoudi, M., Lalonde, R., Violle, N., Javelot, H., Desor, D., Nejdi, A., Bisson, J.-F., Rougeot, C., Pichelin, M., Cazaubiel, M., & Cazaubiel, J.-M. (2011). Assessment of psychotropic-like properties of a probiotic formulation (Lactobacillus helveticus R0052 and Bifidobacterium longum R0175) in rats and human subjects. British Journal of Nutrition, 105(5), 755–764.

Nadia, F. S., Wati, D. A., Isnawati, M., Sulchan, M., & Afifah, D. N. (2020). The effect of processed Tempeh Gembus to triglycerides levels and insulin resistance status in women with obesity. Food Research, 4(4), 1000–1010.

Nailufar, F., Tjandrawinata, R. R., & Suhartono, M. T. (2016). Thrombus degradation by fibrinolytic enzyme of Stenotrophomonas sp. originated from Indonesian soybean-based fermented food on Wistar rats. Advances in Pharmacological Sciences.

Nakamura, M., Hamazaki, K., Matsumura, K., Kasamatsu, H., Tsuchida, A., & Inadera, H. (2019). Infant dietary intake of yogurt and cheese and gastroenteritis at 1 year of age: The Japan Environment and Children's Study. PLoS ONE, 14(10).

Ohland, C. L., & MacNaughton, W. K. (2010). Probiotic bacteria and intestinal epithelial barrier function. American Journal of Physiology-Gastrointestinal and Liver Physiology, 298(6), G807–G819.

Ohta, H., Takebe, Y., Murakami, Y., Takahama, Y., & Morimura, S. (2017). Tyramine and β-phenylethylamine, from fermented food products, as agonists for the human trace amine-associated receptor 1 (hTAAR1) in the stomach. Bioscience, Biotechnology and Biochemistry, 81(5), 1002–1006.

Okada, Y., Tsuzuki, Y., Takeshi, T., Furuhashi, H., Higashiyama, M., Watanabe, C., Shirakabe, K., Kurihara, C., Komoto, S., Tomita, K., Nagao, S., Miura, S., & Hokari, R. (2018). Novel probiotics isolated from a Japanese traditional fermented food, Funazushi, attenuates DSS-induced colitis by increasing the induction of high integrin αv/β8-expressing dendritic cells. Journal of Gastroenterology, 53, 407–418.

Olanipekun, B., & Adelakun, O. (2015). Nutritional and microbiological attributes of soybean (Glycine max) during fermentation with Rhizopus oligosporus. Food Science and Quality Management, 39, 111–119.

Parker, M., Zobrist, S., Donahue, C., Edick, C., Mansen, K., Nadjari, M. H. Z., Heerikhuisen, M., Sybesma, W., Molenaar, D., Diallo, A. M., Milani, P., & Kort, R. (2018). Naturally fermented milk from Northern Senegal: Bacterial community composition and probiotic enrichment with Lactobacillus rhamnosus. Frontiers in Microbiology, 9, 2218.

Parvez, S., Malik, K. A., Ah Kang, S., & Kim, H.-Y. (2006). Probiotics and their fermented food products are beneficial for health. Journal of Applied Microbiology, 100(6), 1171–1185.

Peng, Q., Jiang, S., Chen, J., Ma, C., Huo, D., Shao, Y., & Zhang, J. (2018). Unique microbial diversity and metabolic pathway features of fermented vegetables from Hainan, China. Frontiers in Microbiology, 9, 399.

Peters, A., Krumbholz, P., Jäger, E., Heintz-Buschart, A., Çakir, M. V., Rothemund, S., Gaudl, A., Ceglarek, U., Schöneberg, T., & Stäubert, C. (2019). Metabolites of lactic acid bacteria present in fermented foods are highly potent agonists of human hydroxycarboxylic acid receptor 3. PLoS Genetics, 15(7), e1008283.

Phoottosavako, M., Keeratipibul, S., Techo, S., & Tanasupawat, S. (2015). Identification and characterization of lipolytic bacteria from Thai fermented foods. Malaysian Journal of Microbiology, 11(3), 231–239.

Puerari, C., Magalhães-Guedes, K. T., & Schwan, R. F. (2015). Physicochemical and microbiological characterization of chicha, a rice-based fermented beverage produced by Umutina Brazilian Amerindians. Food Microbiology, 46, 210–217.

Putt, K. K., Pei, R., White, H. M., & Bolling, B. W. (2017). Yogurt inhibits intestinal barrier dysfunction in Caco-2 cells by increasing tight junctions. Food & Function, 8(1), 406–414.

Qu, T., Yang, L., Wang, Y., Jiang, B., Shen, M., & Ren, D. (2020). Reduction of serum cholesterol and its mechanism by Lactobacillus plantarum H6 screened from local fermented food products. Food & Function, 11(2), 1397–1409.

Rahman, K., & Billington, D. (2000). Dietary Supplementation with Aged Garlic Extract Inhibits ADP-Induced Platelet Aggregation in Humans. The Journal of Nutrition, 130(11), 2662–2665.

DOI:https//doi.org/10.22452/mjs.vol42no1.8
Malaysian Journal of Science 42(1): 78-91 (February 2023)

Rai, A. K., Sanjukta, S., & Jeyaram, K. (2017). Production of angiotensin I converting enzyme inhibitory (ACE-I) peptides during milk fermentation and their role in reducing hypertension. Critical Reviews in Food Science and Nutrition, 57(13), 2789–2800.

Ray, M., Hor, P. K., Ojha, D., Soren, J. P., Singh, S. N., & Mondal, K. C. (2018). Bifidobacteria and its rice fermented products on diet induced obese mice: Analysis of physical status, serum profile and gene expressions. Beneficial Microbes, 9(3), 441–452.

Ren, D., Zhu, J., Gong, S., Liu, H., & Yu, H. (2018). Antimicrobial characteristics of lactic acid bacteria isolated from homemade fermented foods. BioMed Research International, Article ID 5416725.

Ribeiro, A. G., Mill, J. G., Cade, N. V., Velasquez-Melendez, G., Matos, S. M. A., & Molina, M. del C. B. (2018). Associations of Dairy Intake with Arterial Stiffness in Brazilian Adults: The Brazilian Longitudinal Study of Adult Health (ELSA-Brasil). Nutrients, 10(6), 701. Oxidative stress and metabolic syndrome. Life Sciences, 84(21–22), 705–712.

Saelao, S., Maneerat, S., Kaewsuwan, S., Rabesona, H., Choiset, Y., Haertlé, T., & Chobert, J.-M. (2017). Inhibition of Staphylococcus aureus in vitro by bacteriocinogenic Lactococcus lactis KTH0-1S isolated from Thai fermented shrimp (Kung-som) and safety evaluation. Archives of Microbiology, 199, 551–562.

Sahab, N. R. M., Subroto, E., Balia, R. L., & Utama, G. L. (2020). γ-Aminobutyric acid found in fermented foods and beverages: current trends. Heliyon, 6(11), e05526.

Sanchart, C., Rattanaporn, O., Haltrich, D., Phukpattaranont, P., & Maneerat, S. (2017). Lactobacillus futsaii CS3, a new GABA-producing strain isolated from Thai fermented shrimp (Kung-Som). Indian Journal of Microbiology, 57(2), 211–217.

Shandilya, U. K., Sharma, A., Kapila, R., & Kansal, V. K. (2016). Probiotic Dahi containing Lactobacillus acidophilus and Bifidobacterium bifidum modulates immunoglobulin levels and cytokines expression in whey proteins sensitised mice. Journal of the Science of Food and Agriculture, 96(9), 3180–3187.

Shangpliang, H. N. J., Rai, R., Keisam, S., Jeyaram, K., & Tamang, J. P. (2018). Bacterial community in naturally fermented milk products of Arunachal Pradesh and Sikkim of India analysed by high-throughput amplicon sequencing. Scientific Reports, 8, 1532.

Shimizu, H., Masujima, Y., Ushiroda, C., Mizushima, R., Taira, S., Ohue-Kitano, R., & Kimura, I. (2019). Dietary short-chain fatty acid intake improves the hepatic metabolic condition via FFAR3. Scientific Reports, 9, 16574.

Simrén, M., Öhman, L., Olsson, J., Svensson, U., Ohlson, K., Posserud, I., & Strid, H. (2009). Clinical trial: the effects of a fermented milk containing three probiotic bacteria in patients with irritable bowel syndrome - a randomized, double-blind, controlled study. Alimentary Pharmacology & Therapeutics, 31(2), 218–227.

Slyepchenko, A., Maes, M., Jacka, F. N., Köhler, C. A., Barichello, T., McIntyre, R. S., Berk, M., Grande, I., Foster, J. A., Vieta, E., & Carvalho, A. F. (2017). Gut Microbiota, Bacterial Translocation, and Interactions with Diet: Pathophysiological Links between Major Depressive Disorder and Non-Communicable Medical Comorbidities. Psychotherapy and Psychosomatics, 86(1), 31–46.

Sun, L., Zhao, H., Liu, L., Wu, X., Gao, Q., & Zhao, Y. (2018). Effects of Lactobacillus on the inhibition of Helicobacter pylori growth. Biotechnology and Biotechnological Equipment, 32(6), 1533–1540.

Takada, M., Nishida, K., Kataoka-Kato, A., Gondo, Y., Ishikawa, H., Suda, K., Kawai, M., Hoshi, R., Watanabe, O., Igarashi, T., Kuwano, Y., Miyazaki, K., & Rokutan, K. (2016). Probiotic Lactobacillus casei strain Shirota relieves stress-associated symptoms by modulating the gut–brain interaction in human and animal models. Neurogastroenterology & Motility, 28(7), 1027–1036.

Takahashi, F., Nishigori, H., Nishigori, T., Mizuno, S., Obara, T., Metoki, H., Sakurai, K., Ishikuro, M., Iwama, N., Tatsuta, N., Nishijima, I., Fujiwara, I., Arima, T., Nakai, K., Sugiyama, T., Kuriyama, S., & Yaegashi, N. (2016). Fermented Food Consumption and Psychological Distress in Pregnant Women: A Nationwide Birth Cohort Study of the Japan Environment and Children's Study. The Tohoku Journal of Experimental Medicine, 240(4), 309–321.

Taylor, B. C., Lejzerowicz, F., Poirel, M., Shaffer, J. P., Jiang, L., Aksenov, A., Litwin, N., Humphrey, G., Martino, C., Miller-Montgomery, S., Dorrestein, P. C., Veiga, P., Song, S. J., McDonald, D., Derrien, M., & Knight, R. (2020). Consumption of fermented foods is associated with systematic differences in the gut microbiome and metabolome. MSystems, 5(2), e00901-19.

DOI:https//doi.org/10.22452/mjs.vol42no1.8
Malaysian Journal of Science 42(1): 78-91 (February 2023)

Tenore, G. C., Caruso, D., Buonomo, G., D'Avino, M., Ciampaglia, R., Maisto, M., Schisano, C., Bocchino, B., & Novellino, E. (2019). Lactofermented Annurca Apple Puree as a Functional Food Indicated for the Control of Plasma Lipid and Oxidative Amine Levels: Results from a Randomised Clinical Trial. Nutrients, 11, 122.

Veerapagu, M., & Jeya, K. R. (2017). Evaluation of probiotic characteristics of bacteria isolated from fermented foods. The Pharma Innovation Journal, 6(7), 322–325.

Veiga, P., Pons, N., Agrawal, A., Oozeer, R., Guyonnet, D., Brazeilles, R., Faurie, J.-M., van Hylckama Vlieg, J. E. T., Houghton, L. A., Whorwell, P. J., Ehrlich, S. D., & Kennedy, S. P. (2014). Changes of the human gut microbiome induced by a fermented milk product. Scientific Reports, 4, 6328.

Venegas, D. P., De La Fuente, M. K., Landskron, G., González, M. J., Quera, R., Dijkstra, G., Harmsen, H. J. M., Faber, K. N., & Hermoso, M. A. (2019). Short chain fatty acids (SCFAs)mediated gut epithelial and immune regulation and its relevance for inflammatory bowel diseases. Frontiers in Immunology, 10(MAR).

Walsh, A. M., Crispie, F., Kilcawley, K., O'Sullivan, O., O'Sullivan, M. G., Claesson, M. J., & Cotter, P. D. (2016). Microbial succession and flavor production in the fermented dairy beverage kefir. MSystems, 1(5), e00052-16.

Wang, L., Alammar, N., Singh, R., Nanavati, J., Song, Y., Chaudhary, R., & Mullin, G. E. (2020). Gut Microbial Dysbiosis in the Irritable Bowel Syndrome: A Systematic Review and Meta-Analysis of Case-Control Studies. Journal of the Academy of Nutrition and Dietetics, 120(4), 565–586.

Wang, P., Gao, X., Li, Y., Wang, S., Yu, J., & Wei, Y. (2020). Bacillus natto regulates gut microbiota and adipose tissue accumulation in a high-fat diet mouse model of obesity. Journal of Functional Foods, 68, 103923.

Wang, X., Xiao, J., Jia, Y., Pan, Y., & Wang, Y. (2018). Lactobacillus kefiranofaciens, the sole dominant and stable bacterial species, exhibits distinct morphotypes upon colonization in Tibetan kefir grains. Heliyon, 4(6).

Wati, D. A., Nadia, F. S., Isnawati, M., Sulchan, M., & Afifah, D. N. (2020). The effect of processed Tempeh gembus to high sensitivity C-reactive protein (hsCRP) and high-density lipoprotein (HDL) levels in women with obesity. Potravinarstvo Slovak Journal of Food Sciences, 14, 8–16.

Weng, Y., Yao, J., Sparks, S., & Wang, K. (2017). Nattokinase: An Oral Antithrombotic Agent for the Prevention of Cardiovascular Disease. International Journal of Molecular Sciences, 18(3), 523.

Wilunda, C., Sawada, N., Goto, A., Yamaji, T., Iwasaki, M., Tsugane, S., & Noda, M. (2020). Soy food and isoflavones are not associated with changes in serum lipids and glycohemoglobin concentrations among Japanese adults: a cohort study. European Journal of Nutrition, 59(5), 2075–2087.

Wu, W., Sun, M., Chen, F., Cao, A. T., Liu, H., Zhao, Y., Huang, X., Xiao, Y., Yao, S., Zhao, Q., Liu, Z., & Cong, Y. (2017). Microbiota metabolite short-chain fatty acid acetate promotes intestinal IgA response to microbiota which is mediated by GPR43. Mucosal Immunology, 10(4), 946–956.

Yu, L., Han, X., Cen, S., Duan, H., Feng, S., Xue, Y., Tian, F., Zhao, J., Zhang, H., Zhai, Q., & Chen, W. (2020). Beneficial effect of GABA-rich fermented milk on insomnia involving regulation of gut microbiota. Microbiological Research, 233, 126409.

Zakerska-Banaszak, O., Tomczak, H., Gabryel, M., Baturo, A., Wolko, L., Michalak, M., Malinska, N., Mankowska-Wierzbicka, D., Eder, P., Dobrowolska, A., Slomski, R., & Skrzypczak-Zielinska, M. (2021). Dysbiosis of gut microbiota in Polish patients with ulcerative colitis: a pilot study. Scientific Reports, 11, 2166.

Zhang, J., Wang, X., Huo, D., Li, W., Hu, Q., Xu, C., Liu, S., & Li, C. (2016). Metagenomic approach reveals microbial diversity and predictive microbial metabolic pathways in Yucha, a traditional Li fermented food. Scientific Reports, 6, 32524.

Zhang, X., Shi, Y., Wang, L., Li, X., Zhang, S., Wang, X., Jin, M., Hsiao, C.-D., Lin, H.-W., Han, L., & Liu, K. (2019). Metabolomics for Biomarker Discovery in Fermented Black Garlic and Potential Bioprotective Responses against Cardiovascular Diseases. Journal of Agricultural and Food Chemistry, 67(44), 12191–12198.

DOI:https//doi.org/10.22452/mjs.vol42no1.8
Malaysian Journal of Science 42(1): 78-91 (February 2023)

Zheng, P., Zeng, B., Zhou, C., Liu, M., Fang, Z., Xu, X., Zeng, L., Chen, J., Fan, S., Du, X., Zhang, X., Yang, D., Yang, Y., Meng, H., Li, W., Melgiri, N. D., Licinio, J., Wei, H., & Xie, P. (2016). Gut microbiome remodeling induces depressive-like behaviors through a pathway mediated by the host's metabolism. Molecular Psychiatry, 21(6), 786–796.

Zhu, Y., Zhang, F., Zhang, C., Yang, L., Fan, G., Xu, Y., Sun, B., & Li, X. (2018). Dynamic microbial succession of Shanxi aged vinegar and its correlation with flavor metabolites during different stages of acetic acid fermentation. Scientific Reports, 8, 8612.

Zulkawi, N., Ng, K. H., Zamberi, N. R., Yeap, S. K., Satharasinghe, D. A., Tan, S. W., Ho, W. Y., Abd. Rashid, N. Y., Md. Lazim, M. I., Jamaluddin, A., Alitheen, N. B., & Long, K. (2018). Antihyperglycemic and anti-inflammatory effects of fermented food paste in high-fat diet and streptozotocin-challenged mice. Drug Design, Development and Therapy, 12, 1373–1383.

DOI:https//doi.org/10.22452/mjs.vol42no1.8
Malaysian Journal of Science 42(1): 78-91 (February 2023)

MALAYSIAN JOURNAL OF SCIENCE
MJS
ISSN 1394-3065

Regular Issue

Malaysian Journal of Science 42 (1): 92-105 (February 2023) https://mjs.um.edu.my

STUDY OF FECAL GLUCOCORTICOID METABOLITE IN BEARS: A REVIEW

Elden bin Zoumin[1a], Siti Sarayati Abdul Mawah[2a]*, Lo Chor Wai [3a], Farnidah Jasnie[4a]

Abstract: Fecal glucocorticoid metabolite (FGM) analysis is a non-invasive method to monitor animals' welfare in captivity and wild environments. Glucocorticoid also known as cortisol is a hormone that indicates the level of stress in animals and humans. This paper reviews the use of FGM analysis on bears and the methodologies used to study this hormone in every species of bear. The review method used was descriptive review. The bears that were included in this review are the brown bear (*Ursus arctos*), Polar bear (*Ursus maritimus*), Asiatic black bear (*Ursus thibetanus*), American black bear (*Ursus americanus*), Malayan sun bear (*Helarctos malayanus*), sloth bear (*Melursus ursinus*), Andean spectacled bear (*Tremactos ornatus*), and giant panda (*Ailuropodia melanoleuca*). Studies of FGM on polar bears showed that zoo-to-zoo transportation could cause an increase in FGM level during transportation and FGM is not suitable to be used to differentiate between pseudo-pregnancy and true pregnancy. In Malayan sun bear, FGM level is high in female bears that show agonistic behavior and is associated with low progesterone levels. In addition, studies on Malayan sun bear show that not only FGM can be analyzed from fecal samples, but also the reproductive hormones of estrogen and progesterone. In Asiatic black bears, FGM is higher in bears that live in a bile farm than forage outside the forest reserve. High parasite load in giant pandas is associated with a high level of FGM since parasite infection is considered a stressor that can elicit a stress response. Also both male and female panda have high FGM during the breeding season to increase metabolism to generate energy required for reproductive activities. The Alopecia syndrome in Andean spectacled bear has no significant relation to FGM level. Brown bears with several types of food in their diet have lower FGM than those with only one type of food. There is no specific study of FGM that focused on sloth bear and American black bear, but there were several studies on glucocorticoid in black bears that are not extracted from fecal samples. FGM can be analyzed using both enzyme-immunoassay (EIA) and radioimmunoassay (RIA) but, EIA is preferable due to safety reasons.

Keywords: *Fecal glucocorticoid metabolite, bears, stress, reproduction*

1. Introduction

The fecal glucocorticoid metabolite (FGM) is commonly used in studying animal stress as it is a non-invasive way of investigating adrenal activities of animals either in captivity or free-ranging (Keay et al., 2006; Sheriff, et al., 2011). The advantages of using FGM in monitoring animals' adrenal activities are that samples can be collected easily as FGM comes from the fecal sample (Sheriff et al., 2011). Next, FGM represents the total fraction of the whole free (unbound) glucocorticoid in an organism. FGM is also not affected by researcher-induced biases of handling events or short-term fluctuations in glucocorticoid due to normal pulsatile changes in glucocorticoid secretion (Sheriff et al., 2011). Besides, FGM is not heavily influenced by the time of the day due to the circadian pattern of an organism unlike the plasma glucocorticoid (Sheriff et al., 2011).

Around the world, there are only 8 bear species namely the brown bear (*Ursus arctos*), Polar bear (*Ursus maritimus*), Asiatic black bear (*Ursus thibetanus*), American black bear (*Ursus americanus*), Malayan sun bear (*Helarctos malayanus*), sloth bear (*Melursus ursinus*), Andean spectacled bear (*Tremactos ornatus*), and giant panda (*Ailuropodia melanoleuca*).

The population of bears worldwide is under threat due to climate changes, loss of habitats because of urban development, agricultural activities, logging, and poaching. Humans are also hunting bears for their furs and meats (James & Serge Lariviere, 2019). Since bears are commonly being held captive as part of conservation efforts by placing them at zoos, rehabilitation centers or wildlife parks, it is important to monitor their well-being by assessing their adrenal activities to determine their stress level. As the continuous release of glucocorticoid as part of feedback mechanism controlled by the hypothalamus-pituitary-adrenal (HPA) axis can be detrimental to an organism, it is important to inspect the level of glucocorticoid of an animal in captivity (Sheriff et al., 2011). The level of glucocorticoid can be obtained by taking samples of blood, hair, saliva, urine, and fecal sample of the studied animal. However, among all of the mentioned samples, fecal samples are the easiest mean of assessing the level of glucocorticoid of an animal (Keay et al., 2006; Sheriff et al., 2011; Young et al., 2004).

Authors information:
[a]Faculty of Applied Sciences, Universiti Teknologi MARA Sabah Branch, Kota Kinabalu Campus, 88997, Kota Kinabalu, Sabah, MALAYSIA. Email: elden96zoumin68@gmail.com[1]; sarayati@uitm.edu.my[2]; lochor068@uitm.edu.my[3]; farni224@uitm.edu.my[4]
*Corresponding Author: sarayati@uitm.edu.my

Received: February 15, 2022
Accepted: April 15, 2022
Published: February 28, 2022

DOI:https//doi.org/10.22452/mjs.vol42no1.9
Malaysian Journal of Science 42(1): 92-105 (February 2023)

Hence, this review was made to describe the study of FGM that has been done to the 8 species of bears from around the world in the past 10 years or further. This review will discuss the purpose of studying FGM in bears, the methodologies used in those studies, and the outcomes of each study. Besides discussing the use of FGM in assessing the level of stress and correlates it with other variables such as parasites infection, pregnancy and behaviour, this review will also discuss the factors that affect the level of FGM in fecal samples such as how the fecal sample is being handled and the preservation method used. The articles that were reviewed are listed in Table 1.

DOI:https//doi.org/10.22452/mjs.vol42no1.9
Malaysian Journal of Science 42(1): 92-105 (February 2023)

Table 1. Studies of fecal glucocorticoid metabolites that was done on 8 species of bears.

Bear	*Species*	Title of study	Findings	Author
Polar bear	*Ursus martimus*	Fecal glucocorticoid metabolites as a measure of adrenocortical activity in polar bears (Ursus maritimus).	Five polar bears in captivity that have undergo five zoo-to-zoo transports show increased level of fecal glucocorticoid after been validate through enzyme-immunoassay (EIA).	Hein et. al., (2020)
		Annual fecal glucocorticoid metabolite concentrations in pregnant and pseudopregnant polar bears (*Ursus maritimus*) in North American zoos.	Study to determine whether FGM level analysis via EIA can be used to differentiate true-pregnancy and pseudopregnancy in polar bear, shows that FGM level between polar bear that undergo true pregnancy and polar bear that undergo pseudopregnancy are not significantly different.	Bryant & Roth, (2018)
		Individual and environmental factors associated with stereotypic behavior and fecal glucocorticoid metabolite levels in zoo housed polar bears.	Polar bears that live in captivity in zoos, that shows stereotypic pacing behaviour, is associated with an increased level in FGM. The study used radioimmunoassay (RIA) to analyze the level of FGM in studied polar bear.	Shepherdson et. al. (2013)
Brown bears	*Ursus arctos*	Methodological Considerations for Using Fecal Glucocorticoid Metabolite Concentrations as an Indicator of Physiological Stress in the Brown Bear (*Ursus arctos*).	Their study on to validate the use cortisol-assay in EIA to determine FGM level of brown bears living in a rehabilitation centre in Spain and Wilhelma Zoo, Germany shows that cortisol assay in EIA is the best assay to study FGM level in brown bears.	Dalerum et. al., (2020)
		Effects of Exposure, Diet, and Thermoregulation on Fecal Glucocorticoid Measures in Wild Bears.	This study was done on free-ranging wild bears (brown bears and black bears) that inhabits the Montana National Park in United States of America. Their study shows that FGM levels in collected fecal samples of wild bears are affected by seasonal changes and diet quality. The FGM level was analyze through RIA.	Stetz et. al. (2013)
		Factors Associated with Fecal Glucocorticoids in Alaskan Brown Bears (*Ursus arctos horribilis*).	Their study aims to validate the use of RIA to analyse the FGM level of wild brown bears in Alaska and to identify the factors affecting the level of FGM in their study subject. Their study shows that RIA can be used to study FGM level from fecal sample of wild brown bears and the factors affecting the FGM level in wild Alaskan brown bears (*Ursus arctos horriblis*) are type of diet and date of seasonal changes.	von der Ohe et. al., (2004)
American black bear	*Ursus americanus*	Effects of Exposure, Diet, and Thermoregulation on Fecal	This study was done on free-ranging wild bears (brown bears and black bears) that inhabit the Montana National Park in United States of America (USA). Their study shows that FGM levels in a	Stetz et. al. (2013)

DOI:https//doi.org/10.22452/mjs.vol42no1.9
Malaysian Journal of Science 42(1): 92-105 (February 2023)

		Glucocorticoid Measures in Wild Bears.	collected fecal sample of wild bears are affected by the seasonal changes and the quality of diet. The FGM level was analyze through RIA.	
Asiatic black bear	*Ursus thibetanus*	Increased stress in Asiatic black bears relates to food limitation, crop raiding, and foraging beyond nature reserve boundaries in China.	This study was made to determine the stress level of wild Asiatic black bears that live inside and outside of nature reserve in China, by using FGM analysis through RIA. Their finding shows that bear that live outside of nature reserve have higher FGM level compared to those living inside the nature reserve.	Malcolm et. al., (2014)
		Analyses of fecal and hair glucocorticoids to evaluate short- and long-term stress and recovery of Asiatic black bears (*Ursus thibetanus*) removed from bile farms in China.	This study aims to evaluate the stress level of the Asiatic black bears that were relocated from bile farms to a rehabilitation centre in China. The stress level was analyse by using the hair and fecal sample of the studied bears. The study shows that FGM level of the bear (analyze through RIA) living in bile farms are high and decreasing after been move to the rehabilitation centre after a period time.	Malcolm et. al., (2013)
		Noninvasive monitoring of adrenocortical activity in carnivores by fecal glucocorticoid analyses.	In this study, the Asiatic black bears that lives in one of North America zoos (Le Zoo de Granby and Little Rock Zoo) were studied along with other 5 animals from Order Carnivora. The study aims to determine whether RIA and EIA can both be used to analyse FGM to assess animals' stress in captivity. Their study shows that both RIA and EIA are useful to analyse the FGM levels of any captive animals.	Young et. al., (2004).
Andean spectacled bear	*Tremarctos ornatus*	Spectacled bear (*Tremarctos ornatus*) alopecia syndrome: An update.	This study was conducted on captive spectacled bear. The location was not mentioned specifically in the preceding paper presented by the author. However, their study stated that the alopecia syndrome in spectacled bear does not correlate with the FGM level in the studied bear.	Leclerc et. al., (2015)
Sloth bear	*Melursus ursinus*	Noninvasive monitoring of adrenocortical activity in carnivores by fecal glucocorticoid analyses.	The studied sloth bear that lives in one of North America zoos (Little Rock Zoo), were studied along with other 5 animals from Order Carnivora. The study aims to determine whether RIA and EIA can both be used to analyse FGM to assess animals' stress in captivity. Their study shows that both RIA and EIA are useful to analyse the FGM levels of any captive animals.	Young et. al., (2004)
Giant panda	*Ailuropoda melanoleuca*	Seasonal dynamics of parasitism and stress physiology in wild giant pandas.	The study aims to study the effect of sex, age, reproductive season and seasonal food availability on the parasitism and the level of stress of wild giant pandas. FGM analysis through RIA shows that parasite prevalence increased during bamboo shoot	Zhou et. al., (2020)

DOI:https//doi.org/10.22452/mjs.vol42no1.9
Malaysian Journal of Science 42(1): 92-105 (February 2023)

			season and caused increased level of FGM and most infected age class are juvenile and sub-adult pandas.	
		Rising fecal glucocorticoid concentrations track reproductive activity in the female giant panda (*Ailuropoda melanoleuca*).	The study was conducted to monitor the FGM level between parturient and non-parturient female panda that lives in Smithsonian National Zoological Park and Zoo Atlanta through EIA. The study shows that FGM level was highest during the periestrus stage in both parturient and non-parturient female panda. In contrast, FGM level was lower during the late luteal phase in the non-parturient female giant panda.	Kersey et. al., (2011)
		Non-invasive determination of fecal steroid hormones relating to conservation practice of giant panda (*Ailuropoda melanoleuca*).	The author aims to validate that sex steroid level can be used to distinguish the sexes of giant panda and to observe the fecal cortisol level to monitor stress level. The study subjects are nine giant pandas which captivity in Center of Breeding and Conservation of the Rare and Endangered Wildlife, Shaanxi Province, China. The analysis of fecal sample through ELISA shows that fecal sample can be used to monitor~~s~~ both sex steroids and cortisol level which indicates stress level.	Yu et. al., 2011
		Parallel and seasonal changes in gonadal and adrenal hormones in male giant pandas (*Ailuropoda melanoleuca*).	The author aims to analyze the level of stress and androgen hormones by using fecal sample of male pandas in Smithsonian National Zoological Park and Atlanta Zoo. Their study shows that using fecal sample to analyze androgen is more convenient than using urine sample. Also, FGM level in male panda increased during the reproductive season. FGM and androgen analysis was done via EIA.	Kersey et. al., (2010)
Malayan sun bear	*Helarctos malayanus*	Social Influences on the Estrous Cycle of the Captive Sun Bear (*Helarctos Malayanus*).	The author studies on the effect of social influences on the FGM level and reproductive cycling of female Malayan sun bear in several zoos in USA. The study shows that female sun bear under high social influence possesses agonistic behaviour with high FGM level which could suppress the mating behaviour.	Frederick et. al, (2013).
		Reproductive timing and aseasonality in the sun bear (*Helarctos malayanus*).	The study aims to determine whether Malayan sun bear is a seasonal breeder or non-seasonal breeder. Analysis was done on the level of progesterone and estrogen of the female Malayan sun bear via fecal sample through RIA proves that sun bear is non-seasonal breeder. The studied bears were living in captive at 8 government zoos in USA.	Frederick et. al., (2012)
		Fecal steroid analysis for monitoring reproduction in the sun bear (*Helarctos malayanus*).	The study aims to establish a non-invasive technique to evaluate the reproductive cycle of female Malayan sun bear, to study the effect of porcine zona pellucida (PZP) protein on the reproductive	Schwarzenberger et. al., (2004)

DOI:https//doi.org/10.22452/mjs.vol42no1.9
Malaysian Journal of Science 42(1): 92-105 (February 2023)

		system of sun bear and to determine whether Malayan sun bear is a seasonal breeder or non-seasonal breeder. Their study shows that fecal sample can be used to observe the reproductive cycle of Malayan sun bear through hormone analysis via EIA, female Malayan sun bear is a non-seasonal breeder, and female sun bear treated with PZP have missing ovarian activity.	
	Annual Changes in Fecal Estradiol-17β Concentrations of the Sun Bear (*Helarctos malayanus*) in Sarawak, Malaysia.	This study was done to investigate the reproductive cycle of female Malayan sun bear through analysis of estradiol hormone from fecal sample via EIA. Their results show that female Malayan sun bear is a seasonal breeder.	Onuma et. al., (2001)
	Reproductive Pattern of the Sun Bear (*Helarctos malayanus*) in Sarawak, Malaysia	This study was done to investigate the reproductive cycle of female Malayan sun bear through analysis of progesterone hormone from fecal sample via EIA. Their results show that female Malayan sun bear is a seasonal breeder.	Onuma et. al., (2000)

DOI:https//doi.org/10.22452/mjs.vol42no1.9
Malaysian Journal of Science 42(1): 92-105 (February 2023)

2. Fecal Glucocorticoid Metabolite Studies in All Bears

2.1 Study on fecal glucocorticoid metabolite (FGM) in captive polar bear (*Ursus maritimus*)

Hein et. al. (2020), study the practicality of enzyme-linked immunoassay to analyse the FGM level in polar bears. They aim to prove that the measuring of polar bears' FGM can be used as diagnostic tool for the long-term assessment of the polar bears' welfare either in captivity or wild. According to the authors, animals' transportation from one place to another can cause stress. This transport-related stress can be validated by conducting EIA to detect FGM levels from fecal samples of polar bears. Fecal sampling was done before transportation, during transportation, and after transportation. Their study confirmed that the FGM level in polar bears (*Ursus martimus*) undergone a significant increase after 5 zoo-to-zoo transport, especially during transportation. After transportation, the FGM level of the studied polar bears drop, but below the baseline level.

Bryant and Roth (2018) investigated if FGM can be used to distinguish between a pregnant bear and a pseudo-pregnant bear. Their objective was to compare the FGM profile between the female polar bear with true pregnancy and the female bear that undergoes pseudo-pregnancy. They hypothesized that the FGM level between a pregnant female bear and a pseudo-pregnant female bear will be different. They also predict that pregnant female bear has a higher FGM level than the pseudo-pregnant female bear or vice versa. However, after doing FGM level analysis through EIA, they found out that there was no significant difference in FGM level between the pregnant female polar bear and pseudo-pregnant female polar bear. Hence, the result of their study shows that FGM cannot be used as a mean to differentiate pregnant polar bears from the pseudo-pregnant polar bears.

Studies on the level of FGM and its relationship with the stereotypic behavior of polar bears (*Ursus martimus*) that were being held captive in several zoos in North America shows that polar bears that exhibit stereotypic pacing behavior are associated with an increased level of FGM (Shepherdson et al., 2013). Thus, living in captivity and surrounded by concrete walls has caused the polar bears to have little view outside their immediate surroundings (Shepherdson et al., 2013). Enrichment of the surrounding area where the polar bears were held, increasing the number of social engagements among individuals, and allowing the bears to view of their outer surroundings are known to reduce the pacing behavior. This will in turn lower the FGM level (Shepherdson et al., 2013).

2.2 Study on FGM level in captive Malayan sun bear (*Helarctos malayanus*)

A study on the FGM level on captive Malayan sun bears was done by Frederick et. al. (2013). Their study aims to observe the effect of agonistic interactions on the level of FGM and fecal estrogen and fecal progesterone of the female Malayan sun bear. Their study shows that agonistic interaction between female sun bears in captivity is associated with a high level of FGM. A high level of FGM will lower the level of fecal progesterone. In contrast, low agonistic behavior is associated with a high level of estrogen (Frederick et al., 2013).

Study by Frederick et. al. (2013) showed that not only glucocorticoid can be analyzed from the fecal sample, but also female reproductive hormones such as estrogen and progesterone. In 2012, they investigate whether sun bear is a seasonal breeder or a non-seasonal breeder. This was done by analyzing the level of progesterone or estrogen from the fecal sample of 13 adult female sun bears that was collected every month for a year. Their study showed that the female Malayan sun bear is not a seasonal breeder and does not exhibit pseudo-pregnancy behavior, which is common in bears that live in 4 seasons countries (Frederick et al., 2012).

Same study has also been done in the past by Schwarzenberger et. al. (2004) and Onuma et. al. (2001, 2002). Both researchers used the same method to analyze the reproductive hormone of the female Malayan sun bear by extracting the hormones from fecal samples (Onuma et al., 2001, 2002; Schwarzenberger et al., 2004). However, their results contradict each other whereby Onuma et. al. (2001, 2002) found that sun bear is a seasonal breeder, which is not the same as the result reported by Schwarzenberger et. al. (2004). In 2012, Frederick and colleagues confirmed the Malayan sun bear as a non-seasonal breeder.

These studies not only show that sun bear is a non-seasonal breeder and agonistic behavior, or interactions can suppress the reproduction hormone of the female bears, but they also proved that not only stress hormone (glucocorticoid or cortisol) can be assessed from fecal sample but can also be used to monitor reproductive hormones such as estrogen and progesterone.

2.3 Study of FGM level in Asiatic black bears (*Ursus thibetanus*) and sloth bear (*Melursus ursinus*)

In Asiatic black bear (*Ursus thibetanus*), FGM was used to study the short-term and long-term stress and recovery of the Asiatic black bears that were removed from bile farms in China

(Malcolm et. al., 2013). In the study, bears that live in the bile farm have elevated levels of FGM compared to those that live at a rehabilitation center. The Asiatic black bear that lives in bile farms has a permanent hole or fistula that was made in their abdomen and gall bladder to allow the bile to drip out freely through a collection tube. Bile collection was done when the bears were distracted by food or sometimes were restrained in a holding cage. These are the factors that cause the elevation of the FGM level of the Asiatic black bear at the bile farm. The bears that were saved from the bile farm, upon arrival at the rehabilitation center, have a high FGM level. However, the FGM level decreases over time as the bear in the rehabilitation center are being treated well, feed well, and have social interaction with other Asiatic black bears (Malcolm et. al., 2013).

FGM can also be used to assess the well-being of animals that live in the free-ranging area and this study was done by Malcolm *et. al.* (2014). Their study shows that reducing habitat can be a factor of stress in free-ranging Asiatic black bears in China. Due to habitat reduction, the bears were forced to forage for food in the area where they are prone to be poached such as raiding a farm or stealing livestock. By analyzing the FGM level from the collected fecal sample using EIA, they found out bears that live outside of the nature reserve have a higher level of FGM than those that live in the nature reserve. Limited fall food and perceived risk of mortality due to crop raiding at human areas are factors of the stress of the free-ranging Asiatic black bear that lives outside of the nature reserve (Malcolm et. al., 2014).

The use of fecal sample to investigate FGM in sloth bear (*Melursus ursinus*) also been done by Young et. al. (2004). They investigated the ability for FGM analysis to detect adrenocortical responses to stressful stimuli. Their study was done on sloth bears and other animals from 5 families within order Carnivora which are the Himalayan black bear (*Ursus thibetanus laniger*), domestic cat (*Felis catus*), cheetah (*Acinonyx jubatus*), clouded leopard (*Neofelis nebulosa*), black-footed ferret (*Mustela nigripes*), slender-tailed meerkat (*Suricata suricatta*), and red wolf (*Canis rufus*). Their study shows that FGM levels from fecal samples can be detected by using both EIA and RIA. So far, this is the only study of FGM that was done on sloth bears.

2.4 Study of FGM level in giant panda (*Ailuropoda melanoleuca*) and spectacled bear (*Tremarctos ornatus*)

FGM has also been used in studying the effect of sex, age, reproductive season, and seasonal food availability on the parasitism and stress physiology in wild giant pandas by Zhou et al. (2020). In their study, FGM was used to measure physiological stress in pandas. Their study shows that reproductive season and seasonal food availability significantly affect the FGM level of wild panda. This is because during high food availability and mating season, the giant pandas expand their home range, and this increases their encounter with the environmental transmission stages of parasites. Age class also affected the parasite load and stress level. It was shown in this study that, juvenile and sub-adult pandas have higher parasite burden associated with high level of FGM compared to the adult and old pandas. This study confirms that higher parasite loads in the giant pandas increase their FGM level. Meanwhile, sex and reproductive season have no significant correlation with cortisol level of the studied giant pandas (Zhou et al., 2020).

A study on giant pandas in China used fecal androgen and FGM levels to determine the reproductive seasonality of the male giant panda (Kersey et al., 2010). The study states that the use of fecal samples to study the relationship of androgen level with FGM level is easier to be done than using urine samples as feces are more readily available than urine samples as giant panda defecates more than 20 times per day. Their study shows that male giant panda has elevated levels of excreted androgens during the 5-month-long breeding season together with the elevated level of FGM. High FGM level in male giant pandas during breeding season is due to the fact that they have increased metabolism that help them to sustain energy, move longer distances, and express aggressive behaviors that are important for winning breeding competitions (Kersey et al., 2010).

Another study using FGM to track reproductive activity in the female giant panda was done by Kersey et al. (2011). Their study proposes that even though FGM was used to monitor stress levels, the main function of glucocorticoid (GC) is to modulate metabolism which include the response to calorie intake, lactation and/or environmental seasonality. The study also shows that among all reproductive states, FGM level was highest during the periestrus stage in both parturient and non-parturient female panda, whereas FGM level was lower during the late luteal phase in the non-parturient female giant panda. This shows that the pattern of excreted FGM clearly reflected the adrenal responses to reproductive stimuli.

Yu et. al. (2011), study on the use of fecal sex steroids to distinguish sexes and to monitor the FGM level to measure the stress response to artificial semen collection, artificial insemination, and parturition, in nine giant pandas which live in captive at Center of Breeding and Conservation of the Rare and Endangered Wildlife, Shaanxi Province, China. Their study hypothesizes that the use of fecal sample to monitors hormone levels in giant panda can remove direct handling on the animal to draw blood to get the information of their physiological well-being. Their study shows that male pandas have higher level of fecal testosterone compared to female across three seasons (Spring, Autumn and Winter), while the level of fecal estradiol between males and females are not significantly different across the three seasons. Artificial semen collection, artificial insemination, and parturition cause increased level of FGM. In their study, Yu et al. (2011) use EIA to analyze the level of fecal testosterone, fecal estradiol and FGM. The study shows that fecal

sample not only can be used as a mean to assess the level of stress in giant panda, but also to assess the reproductive hormone of male and female giant panda.

In Andean spectacled bear, the relationship between FGM and alopecia syndrome was studied by Leclerc et al. (2015). They hypothesize that alopecia syndrome in Andean spectacled bears can be associated with a high level of FGM. However, their study shows that there is no significant difference in the level of FGM between the affected and non-affected panda. Later in 2019, Horn et al. (2019) shows that most female spectacled bears in captivity have alopecia syndrome compared to the male spectacled bear. According to the study, stereotypical behaviors were common among both males and females whether they were affected by alopecia or not, but the syndrome was seen only in females who had been socially housed. They suggest that female Andean bears be housed with adult conspecifics only when the females choose to cohabitate. However, this study does not involve FGM analysis to examine whether these stereotypic behaviors are related to the FGM level.

2.5 Using FGM to study thermoregulatory demands in free-ranging brown bears (*Ursus arctos*) and American black bear (*Ursus americanus*)

The FGM can also be used to study the thermoregulatory demands in free-ranging bears. A study conducted by Stetz et al. (2013) shows that bear's FGM level increased linearly with the biological effects of temperature (early September – end of October) during fall seasons as the temperature drops (temperature between 27°C to 35°C). Meanwhile, in summer, the FGM level in the bear's fecal sample is low for bears that are presumed to spend more time in the hottest area. Their study shows that FGM concentration also corresponds to the diet quality of the free-ranging wild bears. For fecal samples of bears with less nutritious diet, where their feces consist of coarse vegetation, FGM concentration is higher than the FGM level in the feces of bears that have a nutritious diet consisted of berries and meats. However, their study was conducted generally on free-ranging wild bears that inhabit the area of Glacier National Park, Montana, USA. In their reports, it was mentioned that the area of their study is an area where both wild brown bears (*Ursus arctos*) and black bears (*Ursus americanus*) can be found. Thus, the fecal sample that was collected may belong to brown bears or black bears.

In 2004, Ohe et. al. studied the factors affecting the FGM level in fecal samples of Alaskan brown bears. Their study shows that FGM levels in the fecal sample of Alaskan brown bear can be affected by the types of diet and date of seasonal changes. In their study, bears that their diet consists of several types of foods has a decreasing level of FGM over time compared to the bear that their diet consists of one type of food only. To explain their finding, they stated that brown bears in the wild rely on a wide range of food sources from plant matter to terrestrial and marine meat, and the selection of specific foods changes seasonally (Ohe et al., 2004).

In 2020, Dalerum et al. investigate the quantification of FGM in brown bears using the enzyme immunoassay (EIA) method. Studies of FGM were conducted by Stetz et al. (2013) and Ohe et al. (2004) using radio-immunoassay (RIA) to quantify the level of FGM contained in fecal samples. In this investigation, they found that EIA using cortisol assay is the best to be used as an assay to quantify FGM from fecal samples. However, fecal samples that will be analyzed using EIA must be frozen immediately after defecation to prevent the loss of bioreactivity of the FGM in the sample. This will be challenging if the study of FGM was conducted on-field situation.

For the study of FGM in black bears (*Ursus americanus*), there is no study of FGM that focused specifically on the species. The feces of American black bear might be collected by Stetz et al. (2013) in their study, but as mentioned in the first paragraph of this subtopic, the samples might belongs to either brown bears or American black bear. Even so, that does not mean that there is no study on the glucocorticoid metabolite (GM) level of black bears was done. There are several studies of the GM level of black bears that were conducted but the GM was not extracted from fecal samples. The following Table 2 lists the studies of GM level on black bears.

Table 2. Study of glucocorticoid metabolite on the black bear (*Ursus americanus*).

Bear	Title of study	Source of glucocorticoid metabolite	Findings	Author
American black bear (*Ursus americanus*)	Sex, Diet, and the Social Environment: Factors Influencing Hair Cortisol Concentration in Free-Ranging Black Bears (*Ursus americanus*).	Hair	The study aims to investigate the effect of diet, sex and the social environment on American black bear past hypothalamic-pituitary-adrenal (HPA) activity via hair cortisol concentration (HCC) through EIA. The study shows that the HCC of American black bear are varied by sex which results from variability in the nutritional needs of larger-bodied males relative to smaller-bodied females. The studied bears are wild American black bears at Parsnip Plateau and Hart Ranges of the Rocky Mountains.	Lafferty et. al., (2015)
	Seasonal serum glucose, progesterone, and cortisol levels of black bears (*Ursus americanus*).	Blood	The study was done to investigate the relationship between the utilization of body fat and protein during a period of food deprivation, with the level of serum cortisol in 62 wild black bears. RIA analysis on serum cortisol of studied bear shows that elevated level of serum cortisol during winter not as a stimulus for protein-derived glucose, but for the catabolism of fat as an energy source.	Harlow et al. (1990)
	Insulin and Glucagon Responses in the Hibernating Black Bear.	Blood	This study aims to observe the hormonal changes in two hibernating black bears that were held captive in ills farm Institute and Research Center (Mayo Clinic) in Rochester, Minnesota. The study shows that the corticosteroids level is lower during active phase but higher during hibernating phase. It was not mentioned in detail in the article of what method was used to analyze the plasma corticosteroid level.	Palumbo et al., (1983)

DOI:https//doi.org/10.22452/mjs.vol42no1.9
Malaysian Journal of Science 42(1): 92-105 (February 2023)

3. Methods Used to Analyze Fecal Glucocorticoid Metabolite (FGM) in Bears

3.1 Extraction of FGM from fecal sample

To quantify the FGM levels of an organism, the FGM must be extracted from the fecal samples that were collected as described by Keay et al. (2006) in which 90% methanol is commonly used as the extraction agent. The common methods of FGM extraction are dry extraction and wet extraction methods. In the dry extraction method, the moisture on fecal samples was removed either by drying or using a lyophilizer. The purpose of using a lyophilizer is to freeze-dry the fecal sample. The dried fecal sample will then be pulverized into powder using mortar and pestle. These fecal powders will be vortexed by mixing them with ethanol or methanol and centrifuged to form an aliquot. In the wet extraction method, the frozen fecal sample will be thawed before mixing it into a centrifuge tube containing methanol. The sample will be vortexed, centrifuged followed by serial dilution using phosphate buffer solution (PBS) (Keay et al., 2006; Vimalraj & Jayanthagaraj, 2012).

Studies by Malcolm et al. (2014) and Malcolm et al. (2013) on the stress level of Asiatic black bears by the use of FGM from fecal samples of Asiatic black bears used the dry extraction method. The fecal samples were dried using an oven at 100℃ for 12 hours (Malcolm et al., 2013). After drying, the fecal samples were pulverized into powder and those fecal powders were inserted into a tube and mixed with 90% ethanol. The mixture in the tube was vortexed before being boiled at 85℃ for 15 minutes and then centrifuged. After centrifuge, the pellet formed was mixed with ethanol, vortexed, boiled, and centrifuged again. The combined ethanol supernatant was then dried under open air before being stored in a freezer before analysis.

Most of the studies that were being reviewed in this review have their fecal sample lyophilized (freeze-dried) as a method to preserve the fecal sample before the FGM was extracted from the sample. Bryant & Roth (2018) in their study on polar bears used the freeze-dried fecal sample that was pulverized into powder. However, to extract FGM from the fecal sample, they used 90% methanol solution, and they did not boil the mixture of the methanol and fecal powder. The mixture was vortexed and then centrifuged followed by serial dilution using PBS. Studies by Kersey et al. (2010) and Deng et. al. (2014) on giant pandas used the dry extraction method on the lyophilized (freeze-dried) fecal sample using ethanol as the extraction agent. Studies by Stetz et al. (2013) on wild bears and Ohe et al. (2004) on Alaskan brown bears extracted FGM from the lyophilized fecal sample by dry extraction method using methanol solution as the extraction agent.

Shepherdson et al. (2013) used the wet extraction method on polar bears where the fecal sample was shaken overnight in a solution containing PBS, 50% methanol, and bovine serum albumin (BSA) before being centrifuged. A method by Shepherdson et al. (2013) does not involve vortexing the fecal sample as the fecal sample was shaken overnight. Frederick et al. (2013) and Schwarzenberger et al. (2004) studies were on fecal steroid analysis in Malayan sun bear but Schwarzenberger et al. (2004) study does not include FGM, but only involves fecal estrogen and progesterone. Both studies have almost the same fecal hormone extraction method, which is wet extraction. Prior to extraction, the frozen fecal samples were thawed to room temperature before being lyophilized. Their samples were freeze-dried as removal of moisture from the fecal sample will increase the concentration of the hormone in the fecal samples by four to five-fold (Schwarzenberger et al., 2004). After lyophilization, the samples were then mixed with 90% methanol solution, vortexed, centrifuged followed by serial dilution using PBS (Frederick et al., 2013; Schwarzenberger et al., 2004).

3.2 Quantification of FGM using immuno-assay

After the extraction method, the FGM will then be quantified using RIA or EIA commonly known as enzyme-linked immunoassay (ELISA). The selection of antibodies to be used in the immunoassay method is important because the type of glucocorticoid metabolite excreted varies among species (Keay et al., 2006). Different antibodies have different cross-reactivity for other steroids or steroid metabolites in the fecal samples (Keay et al., 2006). Antibodies that are specific for a steroid hormone may have little cross-reactivity with other hormones (Keay et al., 2006).

For studies that use RIA to quantify the FGM levels in bear, the researchers are known to use the double-antibody ^{125}I Corticosterone RIA kit as the antibodies in the kit are cross-reactive with the cortisol in the fecal sample for the RIA method (Frederick et al., 2013; Ohe et al., 2004; Shepherdson et al., 2013; Stetz et al., 2013). For studies that use EIA or ELISA, researchers use the single-antibody cortisol EIA kit in order to determine the FGM level in the fecal samples (Bryant & Roth, 2018; Deng et al., 2014; Malcolm et al., 2013; Malcolm et al., 2014). According to Sheriff et al. (2011), the use of EIA is known to be advantageous compared to RIA as it is possible to develop group-specific antibodies for FGM and it does not involve the use of radioactive substances.

3.3 Method of preserving fecal sample for studying FGM level in bear

Another factor that needs to be taken into consideration in quantifying the FGM from fecal samples is the way the sample is preserved. Since FGM levels in fecal samples can be affected by environmental temperature and degradation by microbial activities, it is then needed to preserve the fecal sample (Sheriff et al., 2011). Collecting fecal samples of free-ranging animals in the field has been proven to be a challenge for wildlife researchers if the collection was done in an area where the distance from the laboratory or any facilities that have a freezer is far (Sheriff et al., 2011). The way the fecal sample is being preserved could affect the FGM level in the sample. For example,

fecal sample of a brown bear that was preserved in ethanol and then stored at -20℃ will completely eliminate the FGM level in the fecal sample (Hunt & Wasser, 2003). A study done by Hunt & Wasser (2003) shows that for bear fecal samples, it is best for the sample to be frozen without the use of any solution (methanol, ethanol, and others) or the fecal sample is being lyophilized (freeze-dry).

Studies done by Kersey et al. (2010), Ohe et al. (2004), Shepherdson et al. (2013), and Stetz et al. (2013) are known to use lyophilizer in their study as a way to preserve their fecal sample before being extracted and assayed. Malcolm et al. (2014), Malcolm et al. (2013), and Frederick et al. (2013) have their fecal sample frozen at -20℃. However, during processing (extraction of FGM), Frederick et al. (2013) lyophilized their fecal sample to increase the concentration of FGM by four to five folds. The advantage that can be seen for preserving fecal samples using a lyophilizer is that it could increase the detection of FGM by increasing the concentration of FGM through the removal of moisture. The time and the condition where the fecal sample was collected must also be taken into consideration. Malcolm et. al. (2014) studied the free-ranging Asiatic black bear in China's nature reserve, collected their samples, stored them in a zip-lock plastic bag before placing the samples into the freezer within 12 hours. For Asiatic black bear that lives in captivity, the fecal samples are collected and immediately frozen at -20℃ before being processed for extraction (Malcolm et al., 2013). Fecal samples can be combined with preservatives such as sodium azide, ethanol or methanol as an effort to prevent bacterial growth since it has been demonstrated that naturally occurring bacteria and their enzymes will degrade steroid metabolites within a few hours (Hunt & Wasser, 2003; Keay et al., 2006). However, the types of preservatives used must be chosen carefully as they also can affect the FGM level reading when stored for a long-term (Hunt & Wasser, 2003).

4. Conclusion

In this review, FGM is known to be used to study the adrenocortical activities in several species of bear, which are the brown bears, polar bears, sun bears, Asiatic black bears, giant pandas, and spectacled bears. It is known that FGM cannot be a reliable indicator to differentiate the pregnant polar bear from the pseudo-pregnant polar bear. However, FGM can be used to measure the level of stress by observing the presence of agonistic behavior in female sun bears and correlating the level of FGM (cortisol) with the level of reproductive hormone (estrogen and progesterone) in female sun bears. The level of FGM in bears are also known to be influenced by a variety of food and environmental temperature in different seasons. Bears with high parasite load and possess stereotypic behavior has elevated level of FGM.

For quantification of FGM via RIA, double antibodies ^{125}I Corticosterone RIA kit is commonly used. While for quantification of FGM by EIA or ELISA, the use of single-antibody cortisol EIA kit is common.

For storage of fecal samples before processing, it is recommended that the sample is immediately lyophilized or frozen at -20℃. If the sample was collected in a very secluded area, the addition of a preservative is necessary to prevent microbial degradation in the fecal sample. As for the extraction method, fecal samples can be extracted by the dry extraction method or the wet extraction method. In the wet extraction method, lyophilizing the sample can increase the concentration of FGM by four to five folds.

The fecal glucocorticoid metabolite (FGM) is commonly used in studying animal stress as it is a non-invasive way of investigating adrenal activities of animals either in captivity or free-ranging (Keay et al., 2006; Sheriff, et al., 2011). The advantages of using FGM in monitoring animals' adrenal activities are that samples can be collected easily as FGM comes from the fecal sample (Sheriff et al., 2011). Next, FGM represents the total fraction of the whole free (unbound) glucocorticoid in an organism. FGM is also not affected by researcher-induced biases of handling events or short-term fluctuations in glucocorticoid due to normal pulsatile changes in glucocorticoid secretion (Sheriff et al., 2011). Besides, FGM is not heavily influenced by the time of the day due to the circadian pattern of an organism unlike the plasma glucocorticoid (Sheriff et al., 2011).

5. References

Bryant, J. L., & Roth, T. L. (2018). *Annual faecal glucocorticoid metabolite concentrations in pregnant and pseudopregnant polar bears (Ursus maritimus) in North American zoos*. *6*(1), 6–11.

Dalerum, F., Dehnhard, M., Freire, S., González, R. G., Marcos, J., Miranda, M., & Vázquez, V. M. (2020). Methodological Considerations for Using Fecal Glucocorticoid Metabolite Concentrations as an Indicator of Physiological Stress in the Brown Bear (Ursus arctos). *Physiological and Biochemical Zoology*, *93*(3), 227–234. https://doi.org/10.1086/708630

Deng, H., Liu, S., Jin, X., & Ge, X. (2014). Research on methods of preserving fecal steroid hormones in giant panda (Ailuropoda melanoleuca). *North-West Journal of Zoology*, *10*(1), 210–216.

Frederick, C., Hunt E., K., Kyes, R., Collins, D., & K. Wasser, S. (2012). Reproductive timing and aseasonality in the sun bear (Helarctos malayanus). *Journal of Mammalogy*, *93*(2), 522–531. https://doi.org/10.1644/11-MAMM-A-108.1

Frederick, C., Hunt, K., Kyes, R., Collins, D., Durrant, B., Ha, J., & Wasser, S. K. (2013). Social influences on the estrous cycle of the captive sun bear (Helarctos Malayanus). *Zoo Biology*, *32*(6), 581–591. https://doi.org/10.1002/zoo.21092

Harlow, J., Beck, D. I., & Walters, L. M. (1990). Seasonal serum glucose , progesterone, and cortisol levels of black bears (Ursus americanus). *Canadian Journal Fof Zoology*, *68*, 183–187. https://doi.org/10.1139/z90-025

Horn, R. C. Van, Thomas, G., Smith, M. S., Shanks, J. A., & Owen, M. A. (2019). The Andean bear alopecia syndrome may be caused by social housing. *Zoo Biology*, *38*(5), 434–441. https://doi.org/10.1002/zoo.21512

Hunt, K. E., & Wasser, S. K. (2003). Effect of Long-Term Preservation Methods on Fecal Glucocorticoid Concentrations of Grizzly Bear and African Elephant Effect of Long-Term Preservation Methods on Fecal Glucocorticoid Concentrations of Grizzly Bear and African Elephant. *Physiological and Biochemical Zoology*, *76*(6), 918–928. https://doi.org/10.1086/380209

James, H., & Serge Lariviere, S. (2019). *Bear*. Encyclopaedia Brittanica. https://www.britannica.com/animal/bear

Keay, J. M., Singh, J., Gaunt, M. C., & Kaur, T. (2006). Fecal glucocorticoids and their metabolites as indicators of stress in various mammalian species: A literature review. *Journal of Zoo and Wildlife Medicine*, *37*(3), 234–244. https://doi.org/10.1638/05-050.1

Kersey, D. C., Wildt, D. E., Brown, J. L., Huang, Y., Snyder, R. J., & Monfort, S. L. (2010). Parallel and seasonal changes in gonadal and adrenal hormones in male giant pandas (Ailuropoda melanoleuca). *Journal of Mammalogy*, *91*(6), 1496–1507. https://doi.org/10.1644/09-MAMM-A-404.1

Kersey, D. C., Wildt, D. E., Brown, J. L., Snyder, R. J., Huang, Y., & Monfort, S. L. (2011). Rising fecal glucocorticoid concentrations track reproductive activity in the female giant panda (Ailuropoda melanoleuca). *General and Comparative Endocrinology*, *173*(2), 364–370. https://doi.org/10.1016/j.ygcen.2011.06.013

Lafferty, D. J. R., Laudenslager, M. L., Mowat, G., & Heard, D. (2015). Sex , Diet, and the Social Environment: Factors Influencing Hair Cortisol Concentration in Free-Ranging Black Bears (Ursus americanus). *PLoS ONE*, *10*(11), 1–14. https://doi.org/10.1371/journal.pone.0141489

Leclerc, A., Bechstein, N., Lemberger, K., Drake, G. J., Magnone, W., Pin, D., Einspanier, A., Nevado, E. M., Barbon, A., & Nicolau, A. (2015). SPECTACLED BEAR (Tremarctos ornatus) ALOPECIA SYNDROME : AN UPDATE. *2015 Proceedings Annual Conference AAZV*, *October*, 8–10.

Malcolm, K. D., Mcshea, W. J., Deelen, T. R. Van, Bacon, H. J., Liu, F., Putman, S., Zhu, X., & Brown, J. L. (2013). Analyses of fecal and hair glucocorticoids to evaluate short- and long-term stress and recovery of Asiatic black bears (Ursus thibetanus) removed from bile farms in China General and Comparative Endocrinology Analyses of fecal and hair glucocorticoids t. *GENERAL AND COMPARATIVE ENDOCRINOLOGY*, *185*(2013), 97–106. https://doi.org/10.1016/j.ygcen.2013.01.014

Malcolm, K. D., Mcshea, W. J., Garshelis, D. L., Luo, S., Deelen, T. R. Van, Liu, F., Li, S., Miao, L., & Wang, D. (2014). Increased stress in Asiatic black bears relates to food limitation , crop raiding , and foraging beyond nature reserve boundaries in China. *Global Ecology and Conservation*, *2*, 267–276. https://doi.org/10.1016/j.gecco.2014.09.010

Malcolm, K. D., McShea, W. J., Van Deelen, T. R., Bacon, H. J., Liu, F., Putman, S., Zhu, X., & Brown, J. L. (2013). Analyses of fecal and hair glucocorticoids to evaluate short- and long-term stress and recovery of Asiatic black bears (Ursus thibetanus) removed from bile farms in China. *General and Comparative Endocrinology*, *185*(February 2013), 97–106. https://doi.org/10.1016/j.ygcen.2013.01.014

Ohe, C. G. Von Der, Wasser, S. K., Hunt, K. E., & Servheen, C. (2004). Factors Associated with Fecal Glucocorticoids in Alaskan Brown Bears (Ursus arctos horribilis) Factors Associated with Fecal Glucocorticoids in Alaskan Brown Bears (Ursus arctos horribilis). *Physiological and Biochemical Zoology*, 313–320. https://doi.org/10.1086/378139

Onuma, M., Suzuki, M., & Ohtaishi, N. (2001). Reproductive Pattern of the Sun Bear (Helarctos malayanus) in Sarawak, Malaysia. *Journal of Veterinary Medical Science*, *63*(3), 293–297.

Onuma, M., Suzuki, M., Uchida, E., Niiyama, M., & Ohtaishi, N. (2002). Annual Changes in Fecal Estradiol-17 β Concentrations of the Sun Bear (Helarctos. *Journal of Veterinary Medical Science*, *64*(4), 309–313.

Palumbo, P. J., Wellik, D. L., Bagley, N. A., & Nelson, R. A. (1983). Insulin and Glucagon Responses in the Hibernating Black Bear. *Bears: Their Biology and Management*, *5*, 291–296.

Schwarzenberger, F., Fredriksson, G., Schaller, K., & Kolter, L. (2004). Fecal steroid analysis for monitoring reproduction in the sun bear (Helarctos malayanus). *Theriogenology*, *62*, 1677–1692. https://doi.org/10.1016/j.theriogenology.2004.03.007

Shepherdson, D., Lewis, K. D., Carlstead, K., Bauman, J., & Perrin, N. (2013). Individual and environmental factors associated with stereotypic behavior and fecal glucocorticoid metabolite levels in zoo housed polar bears. *Applied Animal Behaviour Science*, *147*, 268–277. https://doi.org/http://dx.doi.org/10.1016/j.applanim.2013.01.001

Sheriff, M. J., Dantzer, B., & Delehanty, B. (2011). Measuring stress in wildlife : Techniques for quantifying glucocorticoids Measuring stress in wildlife : techniques for quantifying glucocorticoids. *Oecologia*, *166*, 869–887. https://doi.org/10.1007/s00442-011-1943-y

Stetz, J., Hunt, K., Kendall, K. C., & Wasser, S. K. (2013). Effects of Exposure , Diet , and Thermoregulation on Fecal Glucocorticoid Measures in Wild Bears. *PLoS ONE*, *8*(2), 1–6. https://doi.org/10.1371/journal.pone.0055967

Vimalraj, P. G., & Jayanthagaraj, M. G. (2012). Non-Invasive Monitoring of Fecal Cortisol Metabolites Level in Free-Ranging Asiatic Elephants In Response To Stress Due To Environmental Factors. *Australian Journal of Basic and Applied Science*, *6*(13), 154–158. https://www.mdpi.com/2076-2615/9/8/553/pdf

Young, K. M., Walker, S. L., Lanthier, C., Waddell, W. T., Monfort, S. L., & Brown, J. L. (2004). Noninvasive monitoring of adrenocortical activity in carnivores by fecal glucocorticoid analyses. *General and Comparative Endocrinology*, *137*(2), 148–165. https://doi.org/10.1016/j.ygcen.2004.02.016

Yu, X. J., Hu, D. F., Jin, X. L., Ge, X. F., Yang, L. L., Zhao, P. P., & Zhang, Q. (2011). Non-invasive determination of fecal steroid hormones relating to conservation practice in giant panda (Ailuropoda melanoleuca). *Animal Biology*, *61*(3), 335–347. https://doi.org/10.1163/157075511X584263

Zhou, W., Gao, K., Ma, Y., Wang, L., Wang, M., Wei, F., & Nie, Y. (2020). Seasonal dynamics of parasitism and stress physiology in wild giant pandas. *Conservation Physiology*, *8*(1), 1–12. https://doi.org/10.1093/conphys/coaa085

DOI:https//doi.org/10.22452/mjs.vol42no1.9
Malaysian Journal of Science 42(1): 92-105 (February 2023)

MALAYSIAN JOURNAL OF SCIENCE
MJS
ISSN 1394-3065

Regular Issue

Malaysian Journal of Science 42 (1): 106-125 (February 2023) https://mjs.um.edu.my

ANTHOCYANINS: A HUE FOR HISTOLOGY - SYSTEMATIC REVIEW

Shiny Jasphin[1a], Archana Parampalli Raghavendra[2a]*, Monica Charlotte Solomon[3b], Arul Amuthan[4c,d], Brij Mohan Kumar Singh[5e], Nikitha Valerina Kairanna[6e]

Abstract: Background: Many histological stains cause health hazards to technicians, pathologists, and researchers. The hazard-free and eco-friendly natural anthocyanins have the potential to be a new source for histological stains. This study aims to systematically review the use of plant products containing anthocyanin for histopathological diagnosis. Methods: A comprehensive literature search was done using suitable keywords on Wiley, PubMed, Scopus, Google Scholar, and Web of Science databases. A total of 30 articles were selected for systematic review, where data obtained from the studies were tabulated. Results: About 90% of the reviewed studies have proven that anthocyanin-containing plant products may be used as natural stains. Out of the 30 studies, 49% involved the use of Hibiscus extract, 11% utilised mulberry extract, 9% utilised pomegranate, another 9% involved rose, and the remaining ones utilised black plum, black rice, butterfly pea, the flame of woods, onion skin, and red poppy extracts. Almost 40% of the studies concluded that aqueous extracts are superior to alcohol ones, and 46% used either iron or alum as mordant. Conclusion: Natural stains containing anthocyanin could be a better alternative to synthetic histological stains. Further extensive studies should be conducted to observe the use of these stains in pathological diagnosis.

Keywords: *Anthocyanin, histology, natural dyes, natural stains*

1. Introduction

Histopathology is the study of biological tissues to detect diseased cells using a microscope – a major diagnostic tool in preclinical and clinical conditions research. Various processes like fixation, dehydration, clearing, embedding, sectioning, and staining are involved in converting tissue into stained sections (Ramamoorthy et al., 2016). Because of the transparent nature of the tissue samples, the cellular and intercellular structures are not visible microscopically. Therefore, they are coloured using dyes during the staining process. Usually, the histopathological diagnosis of any disease involves the examination of slides stained with the following three stains: Haematoxylin & Eosin (H&E) (the routine stain used in laboratories), special stains (stains specific cells, tissues, structures, microorganisms, etc.), and immunohistochemistry (stains specific proteins. The staining process involves various chemicals that may cause health hazards to pathologists, technicians, researchers, and the environment. Hence, there is a necessity to discover and develop new natural stains for histopathological diagnoses.

Authors information:
[a]Dept of Physiology, Melaka Manipal Medical College (Manipal Campus), Manipal Academy of Higher Education, Manipal, Karnataka, INDIA-576104. Email: shiny.jasphin@learner.manipal.edu[1]; archana.h@manipal.edu[2]
[b]Dept of Oral Pathology, Manipal College of Dental Sciences, Manipal, Manipal Academy of Higher Education, Manipal, Karnataka, INDIA-576104. Email: monica.charlotte@manipal.edu[3]
[c]Dept of Pharmacology, Melaka Manipal Medical College, (Manipal Campus), Manipal Academy of Higher Education, Manipal, Karnataka, INDIA-576104. Email: dramuthanmd@gmail.com[4]
[d]Division of Siddha, Center for Integrative Medicine and Research, Manipal Academy of Higher Education, Manipal, Karnataka, INDIA-576104. E-mail: dramuthanmd@gmail.com[4]
[e]Dept. of Pathology, Kasturba Medical College, Manipal, Manipal Academy of Higher Education, Manipal, Karnataka, INDIA-576104. Email: brij.singh@manipal.edu[5]; nikita.kairanna@manipal.edu[6]
*Corresponding Author: archana.h@manipal.edu

1.1 Stains used for histopathological diagnoses

1.1.1 Haematoxylin & Eosin

H&E is the most commonly used stain for identifying the nucleus and cytoplasm in cells. Haematoxylin is a natural dye obtained from the Mexican logwood tree, Haematoxylum campechianum (Ajileye et al., 2015). Haematoxylin has a good affinity to the myelin sheath, nuclei, collagen, and elastic fibres. Easy differentiation, durability, and comparative permanency are haematoxylin's advantages, making it a popular stain for the nucleus. There is a worldwide shortage of haematoxylin, so its cost has steadily increased (Dapson et al., 2010; Mohandas et al., 2019).

On the other hand, Eosin is a synthetic acidic xanthene dye formed through the reaction between fluorescein and bromine (Mohandas et al., 2019). It is used as a counterstain that colours the essential components of tissues in shades of red and pink (Lahiani et al., 2018). The International Agency

Received: November 2, 2021
Accepted: September 5, 2022
Published: February 28, 2023

DOI:https//doi.org/10.22452/mjs.vol42no1.10
Malaysian Journal of Science 42(1): 106-125 (February 2023)

of Research in Cancer has considered Eosin as a group 3 carcinogen (Anonymous, 2020). Even though this synthetic dye works well as a staining agent, it is hazardous to humans and animals (Mohandas et al., 2019).

1.1.2 Special stains

Special stains are an alternative staining technique to H&E used when the latter does not highlight adequate information required by pathologists and researchers. The use of special stains utilises various techniques and dyes that stain specific structures, tissues, or pathogens that help pathologists with their diagnosis (Bordoloi et al., 2017). The stains used for colouring sperm structures and their viabilities are Eosin & Nigrosin, Giemsa, Diff Quick, and silver nitrate. These are non-biodegradable synthetic substances hazardous to water sources and the environment (Ebrahimi & Parham, 2020). Besides that, Giemsa and Diff-Quick stains are used for staining cytological smears (Suebkhampet & Sotthibandhu, 2012). On the other hand, peripheral blood smears are stained with Romanowsky stains like Giemsa and Leishman's. The composition of these stains includes Eosin B or Eosin Y – which are acidic – and methylene blue – which is basic (Cruz et al., 2018). Giemsa stains are also used for staining parasites like Plasmodium, Microflaria, Leishmania donovani, Entamoeba histolytica, and others (Kamal, 2018). Common microbial stains used in laboratories are Acid Fast and Gram stains for bacteria and Lactophenol and Gomori's methamine silver stains for fungi (Ma'aruf et al., 2020). The crystal violet in Gram staining is a possible carcinogen and is harmful to aquatic animals (Bordoloi et al., 2017). Most synthetic dyes are allergenic, carcinogenic, mutagenic, immunogenic, challenging to prepare, and expensive. They can damage the environment and reduce soil fertility (Bondoc, 2018). Frequent and constant Exposure to these chemicals has led to health hazards for laboratory technicians, pathologists, and researchers (Sudhakaran et al., 2018).

1.2 Natural dyes

The increasing awareness of the hazards of synthetic dyes has led to the use of eco-friendly, non-allergic, non-toxic dyes in textiles (Verma & Gupta, 2017). Natural dyes derived from natural resources like plants, microbes, animals, and minerals are called natural dyes. The most common source of natural dye are plants (Singh, 2017; Siva, 2007). Natural dyes have no allergenic or carcinogenic effects on human beings. They are biodegradable, renewable, and readily available. Natural dyes are used widely in industries like cosmetics, leather, textiles, food products, paint, etc. (Verma & Gupta, 2017).

Plants produce many colourful phytochemicals in stems, roots, leaves, fruits, and flowers which can be used as dyes (Akinloye & Olagoke, 2010; Siva, 2007). These dyes consist of compounds like anthraquinones, flavones, dihydropyrans, anthocyanins, carotenoids, and others (Vankar, 2000). Nowadays, natural dyes are also used to stain histological tissue specimens. Most natural dyes require chemicals called mordants that help to fix and intensify the stains to tissues and cells during the staining preparations. Together with the dyes, mordants form a coordination complex called 'lake', which is then attached to the tissues. Because of this property, mordants are regularly used in staining protocols (Suebkhampet & Sotthibandhu, 2012). The complex formed is mostly positively charged and acts as a cationic dye at low pH values. The most common mordants used in staining protocols are salts of iron, chromium, aluminium, and others (Veuthey et al., 2014).

Natural dyes are classified based on their source, chemical structure, colour, etc. The most important classification is based on their chemical structures, where they are categorized into indigoid dyes, anthraquinone dyes, carotenoids, anthocyanins, etc. (Siva, 2007; Vankar, 2000).

1.2.1 Anthocyanins

The term 'Anthocyanins' is derived from two Greek words – Anthos (flower) and kianos (blue) (Castañeda et al., 2009). Anthocyanin accounts for a large group of plant pigments that give attractive colours to fruits, flowers, and grains (Hou et al., 2013). Anthocyanins are water-soluble coloured pigments that belong to the phenol group (Khoo et al., 2017). These pigments are presented in the form of heterosides. Anthocyanins contain a flavonoid molecule that is synthesised by the phenylpropanoid pathway (Shaik et al., 2018).

The basic structure of anthocyanin is anthocyanidin. The structure of anthocyanidin consists of an aromatic ring that is bonded to a heterocyclic ring. The heterocyclic ring consists of an oxygen atom which is bonded by a carbon-carbon bond to another aromatic ring (Fig 1).

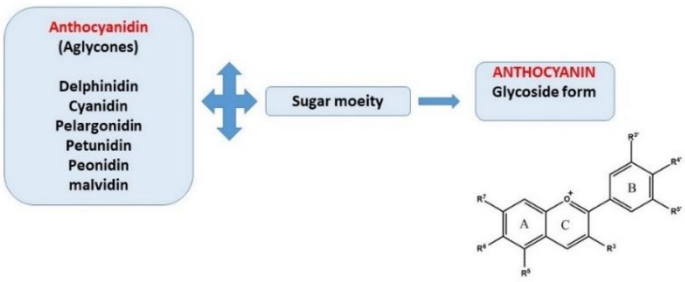

Figure 1. The basic structure of anthocyanin

DOI:https//doi.org/10.22452/mjs.vol42no1.10
Malaysian Journal of Science 42(1): 106-125 (February 2023)

The common types of anthocyanidins are delphinidin, cyanidin, pelargonidin, petunidin, peonidin, and malvidin. Anthocyanidins (aglycone) are called anthocyanin when they are attached to a sugar moiety (glycoside form) (Castañeda et al., 2009; Khoo et al., 2017; Zulfajri & Muttakin, 2018). The 7-hydroxy flavylium ion is the basic chromophore of anthocyanins. The colours of anthocyanins range from yellow to purple and depend on many factors like pH, substituents in the B-ring, aggregations of anthocyanin, complexation by organic molecules and metal ions, and others (Quina et al., 2009).

Besides that, most anthocyanins act as pH indicators (Zulfajri & Muttakin, 2018). They are soluble in many polar solvents like ethanol, acidified methanol, and water due to their polar nature. The extraction of anthocyanins is usually done with methanol. An acid is added to lower the pH, which prevents the degradation of non-acylated anthocyanin colourants. The extraction of anthocyanin from plant products is influenced by many factors including solvent used, temperature, and time is taken for the extraction (Mat Nor & Arof, 2016). In plants, the anthocyanin level is less during high-temperature conditions, which might be due to reduced synthesis or increased degradation (Charurungsipong et al., 2020; Dela et al., 2003). Anthocyanins' stability is very low and may be destroyed due to many factors like light, pH, enzymes, oxygen, thermal treatment, ascorbic acid, co-pigments, and metal ions (Castañeda et al., 2009; Hou et al., 2013). Furthermore, Anthocyanin pigments are more stable in acidic conditions with red colour. It produces a pH-dependent colour that changes from red to yellow, purple, violet and blue in alkaline conditions. At low pH, the molecule is pronated (cation or positive ion). It becomes deprotonated (anion, negative ion) as its pH is gradually increased. Therefore, the ideal working pH to retain the original anthocyanins' colour is below 4 (Khoo et al., 2017; Wahyuningsih et al., 2017).

Many nuclear stains used in histology contain phenolic compounds. The cationic nature of anthocyanins and their planar structure allow them to interact with nuclear DNAs by intercalation. As there are cations in the chemical structure of anthocyanins, they easily interact with the polynucleotides of the nucleus (Suebkhampet & Sotthibandhu, 2012).

Numerous studies have explored the staining effects of natural dyes on histopathological diagnoses. Different plant products containing anthocyanins are also used to stain histological tissues, cytological smears, and micro-organisms. Leveraging the vast literature on this topic, this study aims to systematically review the use of anthocyanin-based natural stains from plant products like Morus nigra (black mulberry), Oryza sativa (black rice), Clitoria ternatea L. (butterfly pea), Allium cepa (onion skin), Syzygium cumini (black plum), Punica granulatum (pomegranate), Ixora coccinea L. (santan flower), Hibiscus sabdariffa (rosella), Rosa damascene (damask rose), and Papaver rhoeas (common poppy) for histopathology. This review is more concerned with exploring the methodology involved in processing the stains, including elements like the extraction methods, the use of mordants, the pH value maintained, and staining time.

2. Methodology

2.1. Systematic review

The researchers carried out a comprehensive literature search from Wiley, PubMed, Scopus, Google Scholar, and the Web of Science databases. Keywords like anthocyanin, organic stains, natural dyes, dye extract, and individual plants containing anthocyanins like hibiscus, berry, and others (with their botanical names) were used in combination with words like histology and staining. Studies that have used anthocyanin-based plant parts for staining animal and human tissues, blood smears, sperm, bacteria, fungus, and parasites are selected for the review. Studies involving the staining of plant tissues were excluded from this review. The researchers have also selected 30 articles from different databases showing the staining properties of ten different plant products containing anthocyanin in animal and human tissues, blood smears, sperm, bacteria, fungus, and parasites (Flowchart 1). The basic structure of anthocyanin is anthocyanidin. The structure of anthocyanidin consists of an aromatic ring that is bonded to a heterocyclic ring. The heterocyclic ring consists of an oxygen atom which is bonded by a carbon-carbon bond to another aromatic ring (Fig 1).

DOI:https//doi.org/10.22452/mjs.vol42no1.10
Malaysian Journal of Science 42(1): 106-125 (February 2023)

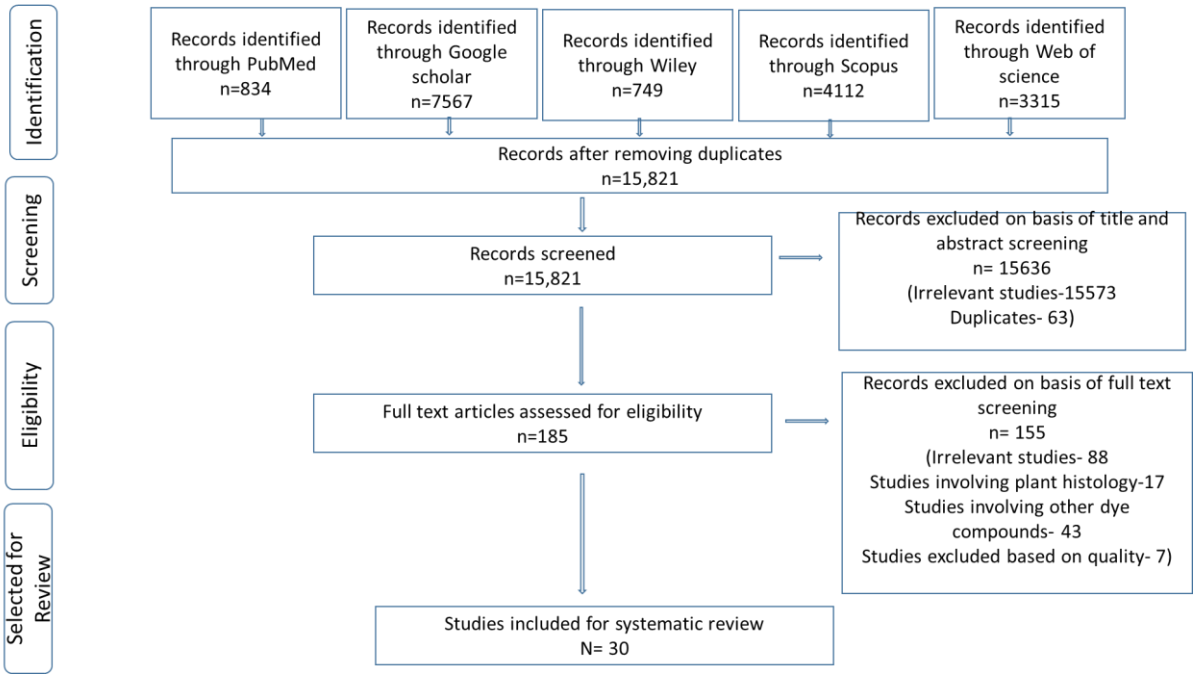

Flowchart 1. Prisma flowchart of this review

3. Results and Discussions

Upon obtaining the final set of studies, a systematic review was carried out, and data obtained from the review was tabulated. A meta-analysis could not be performed due to the heterogeneity of the reviewed studies.

3 RESULTS

3.1 Systematic review

The researchers reviewed 30 studies that utilized ten plant products producing anthocyanin. Out of the 30 articles, three reported comparative staining properties of more than one plant product, while the remaining reported staining properties of single plant products. In 49% of the studies, staining was done with Hibiscus sabdariffa and Hibiscus rosa-sinensis; 11% of them used Morus nigra and Morus alba, 9% used Punica granulatum, another 9% used Rosa damascene, while the remaining ones involve other plants. About 45% of the study was carried out on histological tissues, while the remaining were on cell smears, sperm, parasites, and fungi. Nearly 91% of the studies proved that anthocyanin-containing plant products could be used for staining. Data obtained from the studies are outlined in Table 1.

Table 1. Total fecal samples collected and parasites identified

No.	Dye source, extract, staining solution (SS), staining time (ST), tissues	Observation/Result	Inference, Reference
1	Morus nigra Extract - aqueous (50 g/200 ml) ST - 30-60 min Tissue - rat brain	Neurons: Cortex-dark brown Hippocampus-dark brown Thalamus-light brown Hypothalamus-light brown Astrocytes: Cortex-strong staining Hippocampus-strong staining Thalamus-faint staining Hypothalamus-faint staining	Identification of different parts of the brain is possible. Comparison between astrocytes and neurons is possible (E. M. Tousson & Al-Behbehani, 2010).

DOI:https//doi.org/10.22452/mjs.vol42no1.10
Malaysian Journal of Science 42(1): 106-125 (February 2023)

No.	Dye source, extract, staining solution (SS), staining time (ST), tissues	Observation/Result	Inference, Reference
2	Morus nigra Extract-aqueous (50 g/200 ml) ST - 5-10 min, Tissue - adult liver flukes (Fasciola sp)	All parts of a liver fluke like the oral and ventral sucker, pharynx, and intestine, are stained. Reproductive organs are more easily identified by blackberry dyes compared with carmine staining.	Black mulberry has many advantages over conventional staining. (E. Tousson & Al-Behbehani, 2011).
3	Morus nigra Extract- aqueous (50 g/100 ml) SS -1 g of extract + 2 ml of distilled water (DW) Tissue - bull semen	Black mulberry stained red in colour with pale pink background	Control slides stained with eosin/nigrosine could differentiate between live and dead sperm cells, but blackberry could not differentiate (Ebrahimi & Parham, 2020).
4	Oryza Sativa, Clitoria ternatea, Hibiscus sabdariffa, Morus alba Extract - aqueous SS- 100 g extract + 100 ml of solvent A, B, C. A=5 ml ethanol+10 ml alum+4 ml acetic acid+100 ml DW. B=5 ml ethanol+ 4 ml acetic acid+ 100 ml DW. C=5 ml ethanol+10 ml alum+ 100 ml DW. ST-15 min. Tissue - sperm	Slides stained with black rice and mulberry extracted with Solvent C showed clear morphology of acrosome, middle piece and tail.	Potash alum is an essential component of black rice dye staining. Black rice extract can be a cheap alternative to standard PAP stain for spermatozoa assessment. (Chomean et al., 2019).
5	Oryza sativa Extract - aqueous SS- Sperm in clothing (100 g in 10 g of potassium alum in 100 ml distilled water), Vaginal swab-100 g in 10 g of potassium alum +100 ml distilled water+4, ml of ethanol+5 ml of acetic acid). ST-1,3,5, and 7 mins Tissue- spermatozoa in vaginal swab and clothing sample	The staining time of 5, 7, and 9 mins stained well with sperm morphology comparable to reference stain (Dip quick stain)	Oryza sativa extract can be used as an alternative to haematoxylin for detecting spermatozoa on vaginal swabs and clothing (Saenguthai et al., 2018).
6	Clitoria ternatea L. Extract - aqueous (1:10) SS- extract +1% aluminium chloride +1.2% Iron III chloride, Ph-0.2. ST-30 mins Tissue- blood smear of chicken, pigeon, dog, and horse	The cytoplasm of RBC of all species - is greyish pink. Nuclei of RBC of pigeons and chickens were stained more intensely than WBC. Different types of WBC showed different nuclei shapes and specific cytoplasmic granules.	Aqueous extract of Clitoria ternatea L. could be used to differentiate blood cells of animal smears compared with a Diff-quick stain. (Suebkhampet & Sotthibandhu, 2012).
7	Allium cepa Extract-Aqueous (20 g in 100 ml) SS- extract without mordant, extract + alum, extract + FeSO4, extract + CuSO4 ST-1 hr at 25°, 50°, and 80°Tissue- buccal epithelial cells	The best cytoplasm staining condition was seen when stained for 1 hr at 50o and 80o without mordant. Best nucleus staining was seen with mordants FeSO4 and CuSO4 at 25°, 50°, and 80°	Onion skin can be used for replacing histological staining. (Kusculuo et al., 2017).
8	Syzygium cumini Extract- aqueous- fresh material (1:2) and dried material (1:5)	All prepared stains stained the nucleus and cytoplasm in violet colour. The intensity of staining	Black plum can be used as an alternative for histological staining. (Suabjakyong et al., 2011).

DOI:https//doi.org/10.22452/mjs.vol42no1.10
Malaysian Journal of Science 42(1): 106-125 (February 2023)

No.	Dye source, extract, staining solution (SS), staining time (ST), tissues	Observation/Result	Inference, Reference
	SS - fresh- 45% glacial acetic acid (1:5) and dried- 45% glacial acetic acid (1:10). Both were with and without 1% ferric alum. ST-10, 15, and 20 min. Tissue - rat liver	done for 15 to 20 mins was more than 10 mins.	
9	Punica granulatum Extract-aqueous (20 g in 100 ml) SS- no alum and 2 g alum ST-1 hr at 100° in oven Tissue - human blood cells	Blood cells like neutrophils and basophils showed orange-brown colour with the nuclei deep orange to the brown colour in all groups.	Pomegranate is an environment-friendly, natural stain for human blood cells. (Kuskuluo & Benli, 2017).
10	Punica granulatum Extract-aqueous (20 g in 100 ml) ST-1 hr at 60° in the oven. Tissue - rat lung, liver, heart, kidney	Weak staining of both cytoplasm and nuclei was seen in all tissues, with more intensity staining in heart tissue.	Darker stain can be obtained by changing temperature and pH, increasing staining time, and adding mordant. (Kusculu & Aslan, 2019).
11	Punica granulatum Extract- ethanol (20 g in 100 ml) SS- different pH 1-2, 4-5 ST- Room temperature for 1 hr, 100° for 1 hr. Tissue - rat ovary, testis	At pH 1-2: Tissues stained purple. At pH 4-5: Tissues stained green-yellow. At 100° - brown. At room temperature- light green	Pomegranate stain can be used for staining testicular tissue for histopathological diagnosis. (Kusculuo, 2018).
12	Ixora coccinea L Extract - ethanol 25% (33.85 g/ 101.5 ml) and 36%-(33.85/ 60.18 ml) Tissue - blood smear	The smears were poorly stained.	25% stain is more potent for staining WBC than 36% concentration. However, Ixora coccinea is not effective staining for WBC due to poor quality, poor and unclear demonstration of cell morphologies (Cruz et al., 2018).
13	Hibiscus sabdariffa, Rosa damascene Extract- aqueous (10 g /100 ml), 96% ethanol (50 g/100 ml) Rosa-96% ethanol (50 g/100 ml) ST-30 mins Tissue- Leishmania donovani	Hibiscus Water-Pinkish colour Alcohol- Bluish pink colour Rosa Alcohol-Pink red	Water extract and alcoholic extract of Hibiscus sabdariffa followed by Rosa damascene have the potential to replace the standard stain used for staining Leishmania parasite. (Kamal, 2018)
14	Hibiscuss sabdariffa, Rosa hybrida Extract-aqueous (50 g/100 ml), 96% ethanol (50 g/100 ml) ST-1-2 days Tissue - Fasciola gigantica, Gastrothylax crumenifer, Platyhelminthes, Taenia solium, and Moniezia expansa	Water and alcoholic extracts of Rosa hybrida stained all parts, including the internal organs of the parasites, compared with the hibiscus. Aqueous extracts of both flowers gave good contrasts compared with alcoholic extracts.	Rosa hybrida, followed by Hibiscus sabdariffa, has the potential to replace standard stains used to stain helminth parasites. (Kumar et al., 2015).
15	Rosa damascene- 95% ethanol (maceration-15 g/500 ml, Soxhlet- 500 g/500 ml) SS- no mordant and with 10 g of potassium alum, pH-6.2 ST-20 mins Tissue-normal oral mucosa and pathological oral tissues	Soxhlet apparatus extraction is better than maceration. The staining with mordant showed better staining than extract without mordant. Rose extract showed comparable results with H & E.	Rosa damascene extracted with advanced technique and appropriate mordant can give staining comparable with H & E. (Surendra et al., 2018).

DOI:https//doi.org/10.22452/mjs.vol42no1.10
Malaysian Journal of Science 42(1): 106-125 (February 2023)

No.	Dye source, extract, staining solution (SS), staining time (ST), tissues	Observation/Result	Inference, Reference
16	Papaver rhoeas Extract- aqueous (40 g/100 ml), ethanol (30 g/100 ml) SS- extract + acetified ethylene glycol+ NaIO3 + $AlCl_3$ + beta cyclo dextrin. ST-5 min. Tissue - rat lung and intestine	The nucleus was prominent and well-defined dark purple in all cells.	Papaver rhoeas can be an alternative to haematoxylin, which is cheap, convenient, and renewable. (Budak & Budak, 2015).
17	Hibiscus sabdariffa Extract- aqueous (25 g/125 ml), alcohol (25 g/125 ml) SS- extract +3 g potassium alum. Tissue- fungi like Aspergillus nidulans, Rhizoctonia, Rhizopus stolonifera, P. citrinum, and Cladosporium species	Both extracts have a good affinity towards fungal sporangia, mycelia, and all external features. The aqueous extract was a little superior to the alcoholic extract.	The staining obtained was similar to the standard dyes. A cheaper and eco-friendly dye from Hibiscus sabdariffa calyx can be used for fungal staining (Abubakar et al., 2012).
18	Hibiscus sabdariffa Extract- aqueous (10 g/200 ml) SS- extract + NaCl 5 g + 10% FeCl3 + Glacial acetic acid-3 ml. Tissue- cerebellum, cerebrum, pons	The nucleus of the brain tissues stained dark violet, comparable with the H&E control	Hibiscus sabdariffa can be used as a nuclear substitute for staining brain tissues (Benard et al., 2015)
19	Hibiscus sabdariffa Extract- aqueous (10 g/200 ml) SS- extract + NaCl 5 g + 10% FeCl3 + glacial acetic acid-3 ml ST-5 min. Tissue – skin	Nucleus staining was seen in blue-black colour.	Hibiscus sabdariffa can be used as a progressive nuclear stain to demonstrate connective tissue of the skin (S. Benard, Afolabi, et al., 2017).
20	Hibiscus sabdariffa Extract- aqueous (10 g/200 ml) SS- extract + NaCl 5 g + 10% FeCl3 + glacial acetic acid-3 ml ST-20 min. Tissue - lymph node and appendix tissue	Nuclei stained dark violet-blue.	Hibiscus sabdariffa can be used as an alternative to haematoxylin (Solomon A. Benard, 2008).
21	Hibiscus sabdariffa Extract- aqueous (10 g /200 ml) SS- extract + NaCl 5 gm + 10% FeCl3 + Glacial acetic acid-3 ml SS-5 min Tissue - human skin	Hibiscus gave good staining of skin morphology and collagen fibres.	Histomorphological features of the skin, collagen, and nucleus can be well demonstrated with the hibiscus Van Gieson method. (Benard, Muhammed, et al., 2017).
22	Hibiscus sabdariffa Extract- aqueous (10 g /100 ml) SS-100 ml of hibiscus solution + 10 ml of saturated picric acid ST-30 min Tissue - biopsy from patients of muscular dystrophy, cardiac myo infarction, skeletal muscle specimen from MDX mice	Normal muscle and red blood cells stained yellow, and degenerated muscle fibres stained dull pink.	Picro-hibiscus staining helps to differentiate viable muscle fibres from necrotic muscle fibres and normal from degenerated muscle fibres. (Gowali, 1995).
23	Hibiscus sabdariffa Extract- aqueous (10 g /200 ml) SS- extract + NaCl 5 g + 10% FeCl3 + Glacial acetic acid-3 ml ST-5 min. Tissue- human skin	The nucleus stained bluish purple colour, which was comparable to the H&E control.	Hibiscus sabdariffa extract will be an alternative to haematoxylin with eosin as a counterstain. (Agbede et al., 2017).
24	Hibiscus sabdariffa	Hibiscus stained reddish brown.	Hibiscus sabdariffa can be considered a histological stain for staining sperm

DOI:https//doi.org/10.22452/mjs.vol42no1.10
Malaysian Journal of Science 42(1): 106-125 (February 2023)

No.	Dye source, extract, staining solution (SS), staining time (ST), tissues	Observation/Result	Inference, Reference
	Extract- ethanol. SS-1 g extract+ 10 ml of 70% ethanol. ST-20 min. Tissue - rat sperm		(Rosemary B. Bassey et al., 2012).
25	Hibiscus sabdariffa Extract- ethanol SS- extract+ 1% acetic acid + 70% ethanol ST-5,10,15,30, 45, and 60 min Tissue – testis	Hibiscus stained the basophilic parts like spermatogenic cells and the lumen of seminiferous tubules. Best staining was seen in 0.2 concentration, and staining was seen within five min	Hibiscus sabdariffa can be considered a basic dye (Bassey et al., 2012).
26	Hibiscus sabdariffa Extract - aqueous SS- extract without mordant, extract + Potassium alum, extract + Iron ST-30 min Tissue - testis	Alum mordant-nuclear cytoplasmic differentiation is not good Alum mordant + acetic acid-nuclear cytoplasmic differentiation good, reduced affinity to eosin Alum mordant + ammonia-nuclear cytoplasmic differentiation is poor, with more uptake of eosin Iron mordant + ammonia-nuclear cytoplasmic differentiation is good.	Hibiscus sabdariffa can be a substitute for nuclear staining when mordanted with alum or iron. Enhanced staining is seen when acidified with acetic acid. (Egbujo et al., 2008).
27	Hibiscus sabdariffa Extract – aqueous (20 g /100 ml) Tissue -mice kidney and artery	The cytoplasm of glomeruli and tubules, the cytoplasm of smooth muscle fibres, and RBC stained faint brown colour.	Acidic components, which are separated by chemical purification, can be a better substitute for eosin and can specifically work in cellular components. (Hashim, 2006).
28	Hibiscus sabdariffa Extract – methanol. SS- extract+ potassium alum + glacial acetic acid. Tissue - A. niger, P. notatum and R. stolonifera	The hibiscus extract staining showed better staining than standard lactophenol.	Hibiscus sabdariffa can be a good staining agent for the fungus, which is comparable to lactophenol. (Ihuma J O et al., 2012).
29	Hibiscus sabdariffa Extract- aqueous (50 g /600 ml), 95% alcohol (40 g/500 ml) SS- extract + NH_4OH, extract + glacial acetic acid, extract alone ST-30 sec and 60 min Tissue - bacteria positive lungs and appendix tissue	The extract stained inflammatory cells better than bacteria.	Any solutions did not demonstrate bacteria well. The change in pH did not affect the staining. (Ma'aruf et al., 2020).
30	Hibiscus rosa-sinensis Extract- aqueous (40 g /500 ml) 80% alcohol (5 g/100 ml) SS- PH at 3.7, 5.7, and 12.7 Tissue- human skin and oral mucosa tissues	The alcoholic extract showed better staining than the aqueous. pH 5.7 showed better staining intensity and contrast.	Hibiscus rosa-sinensis which is easily available and economical and can be used as an alternative to eosin (Sridhara et al., 2016).

DOI:https//doi.org/10.22452/mjs.vol42no1.10
Malaysian Journal of Science 42(1): 106-125 (February 2023)

Nearly 60% of the studies used aqueous extracts, 20% used alcoholic extracts and 20% used both aqueous and alcohol extracts of the corresponding plants for staining. A few studies on hibiscus have compared the use of aqueous and alcoholic extracts, where 40% of them concluded that aqueous extracts are superior to alcohol, 20% concluded alcoholic extracts are superior to aqueous, and 40% concluded that there is no significant difference between aqueous and alcoholic extracts. About 46% of the study added mordants to the staining solution, of which an equal percentage used alum or iron. Meanwhile, four studies have used both iron and alum as mordants. In studies that have compared staining with and without mordants, 40% of them mentioned that there are no significant effects of adding alum to the stain. In a comparative study between iron and alum mordants, the former is found to be better than the latter. Almost all studies conducted staining in acidic pH values.

4. Discussion

Anthocyanins are red, purple, or blue pigments that are commonly found in plant parts like fruits, flowers, and tubers (Khoo et al., 2017). Flowers (like hibiscus and rose), fruits (like berries, plum, purple grapes, figs, and black currant), and vegetables (like eggplant, cabbage, etc.) are rich in anthocyanins (Lakshmi, 2014). The common types of anthocyanidins include delphinidin, pelargonidin, cyanidin, petunidin, peonidin, and malvidin (Khoo et al., 2017). The reviewed studies have used ten plants producing anthocyanins, including Morus nigra, Oryza sativa, Clitoria ternatea L, Syzygium cumini, Punica granulatum, Allium cepa, Ixora coccinea L, Rosa damascene and Rosa hybrida, Papaver rhoeas, Hibiscus Sabdariffa and Hibiscus rosa sinensis. The types of anthocyanins commonly present in these plants are presented in Table 2.

Table 2. Common anthocyanins present in plants featured in the reviewed studies

No.	Plant name, family	Anthocyanin	Reference
1	Morus nigra, Moraceae	Cyanidin-3-glucoside 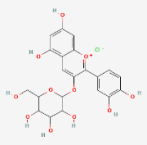 Cyanidin-3-glucosyl rhamnoside 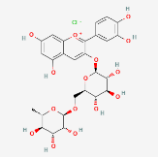	(Hassimotto et al., 2007)
2	Oryza sativa, Oryzeae	Cyanide-3-glucoside 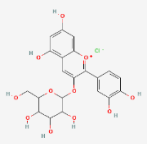	(Pedro et al., 2016)
3	Clitoria ternatea L, Fabaceae	Malonylated delphinidin 3,3'5'-triglucosides 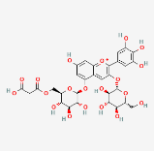 Delphinidin 3-O-(2"-O-α-rhamnosyl-6'-O- β -malonyl-glucoside Delphinidin 3-O-(2"-O-rhamnosyl-6'-O-β-malonyl-glucoside	(Abdullah et al., 2010; Lee & Abdullah, 2011)
4	Syzygium cumini, Myrtaceae	Delphinidin 3,5-diglucoside	(Carmo Brito et al., 2017)

DOI:https//doi.org/10.22452/mjs.vol42no1.10
Malaysian Journal of Science 42(1): 106-125 (February 2023)

No.	Plant name, family	Anthocyanin	Reference
		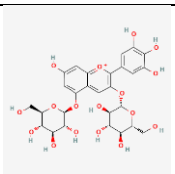 Petunidin 3,5-diglucoside	
		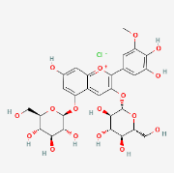 Malvidin 3,5-diglucoside	
		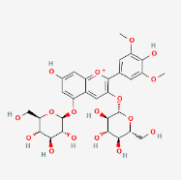	
5	Punica granulatum, Punicaceae	Cyanidin-3,5-diglucoside 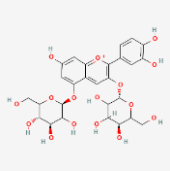 Cyanidin-3-glucoside	(Pirzadeh et al., 2020)
		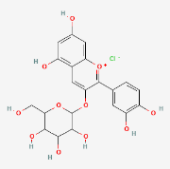 Delphinidin-3-glucoside	
		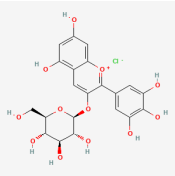	
6	Allium cepa, Alliaceae	Cyanidin 3-glucoside 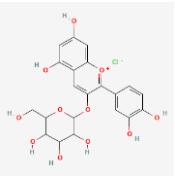 Cyanidin 3-diglucoside	(Fuleki, 1971; Moosazad et al., 2019)
7	Ixora coccinea, Rubiaceae	Cyanidin -3-rutinoside 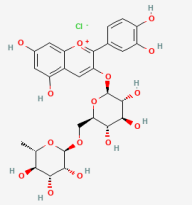	(Patil & Datar, 2015)

DOI:https//doi.org/10.22452/mjs.vol42no1.10
Malaysian Journal of Science 42(1): 106-125 (February 2023)

No.	Plant name, family	Anthocyanin	Reference
8	Rosa damascene and Rosa hybrid, Rosaceae	Cyanidin 3,5-O-diglucoside 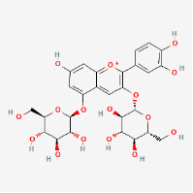 Pelargonidin 3,5-di-O-glucoside 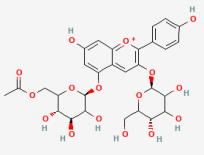	(Wan et al., 2019)
9	Papaver rhoeas, Papaveraceae	Delphinidin-3-O-glucoside 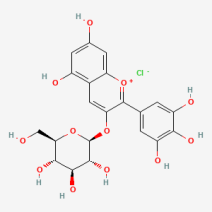 Cyanidin-3-O-glucoside 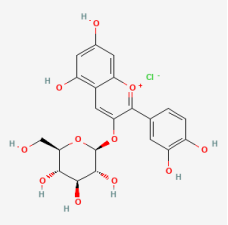 Cyanidin-3-O-rutinoside 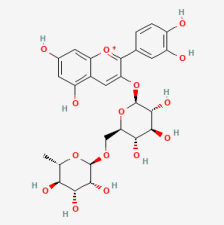	(Velickovic et al., 2019)
10	Hibiscus Sabdariffa and Hibiscus rosa-sinensis, Malvaceae	Delphinidin-3-sambubioside 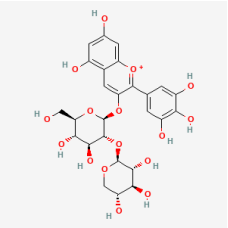 Cyanidine-3-sambubioside 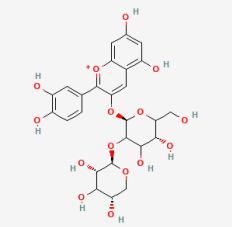	(Hinojosa-Gómez et al., 2020)

DOI:https//doi.org/10.22452/mjs.vol42no1.10
Malaysian Journal of Science 42(1): 106-125 (February 2023)

4.1 *Morus nigra*

The various species of mulberry include *Morus alba* (white mulberry), *Morus rubra* (red mulberry), and *Morus nigra* (black mulberry), which produce colours ranging from white to red and black (Hassimotto et al., 2007). Morus is a juicy fruit with an acidic character. Glucose and fructose and cintric and malic acids are the main sugars and the main organic acids found in Morus, respectively (Ozgen et al., 2009). Upon maturity, it becomes dark red to black and has a good staining ability (E. Tousson & Al-Behbehani, 2011). Aqueous extracts of *Morus nigra* have been used to stain nervous tissues, parasites, and sperm (Ebrahimi & Parham, 2020; E. Tousson & Al-Behbehani, 2011; E. M. Tousson & Al-Behbehani, 2010).

Tousson et al. (2010) concluded that *Morus nigra* can be used to stain brain tissues. The stain features various strengths of colours in different areas and cells, like neurons and astrocytes in the brain (Tousson & Al-Behbehani, 2010). Another study by the same authors on liver fluke concluded that *Morus nigra* staining poses more advantages than conventional carmine staining (Tousson & Al-Behbehani, 2011). In both studies, concentrated juices of *Morus nigra* obtained by aqueous extraction (50 g/200 ml) were used. The staining time for brain tissue and liver fluke was 30-60 minutes and 5-10 minutes, respectively. In a similar study, Ebrahimi et al. (2020) stained bull semen with a *Morus nigra* aqueous extract and found that it exhibited red stains with sharp colour contrast. However, the stain could not differentiate between live and dead sperm cells compared with the control stain (Ebrahimi & Parham, 2020). Besides that, a comparative study by Chomean et al. (2019) used *Morus alba* to stain sperm. They concluded that *Morus alba* could visualise sperm's acrosome, middle piece, and tail (Chomean et al., 2019).

Morus nigra – among the most deeply coloured stain – has the highest total monomeric anthocyanins, while *Morus alba* has the lowest (Jiang & Nie, 2015). For this reason, the water extract of *Morus nigra* can be used as an alternative to stain sperm, histological tissues, and parasites.

4.2 *Oryza sativa*

There are wide varieties of red and black rice that produce coloured pigments. The dark purple colour of black rice is contributed by the presence of anthocyanin in its pericarp layers (Hiemori et al., 2009). Black rice contains anthocyanins in free forms, which account for 99% of its total anthocyanin (Shao et al., 2014). To stain sperms, aqueous extracts of *Oryza sativa* are added with alum as a mordant (Chomean et al., 2019; Saenguthai et al., 2018). In a study by Saenguthai et al. (2018), a black rice extract was used to highlight spermatozoa in cotton and vaginal swabs. In this study, potassium alum was added to the black rice extract, acting as a mordant. In addition, ethanol and acetic acid were added, as the vaginal swab contains cellular debris and epithelial cells. This same study has also concluded that sex determination may also be done using DNA extracted from the black rice-stained semen slide for forensic purposes (Saenguthai et al., 2018).

Furthermore, in a study by Chomean et al. (2019) on *Oryza sativa*, *Clitoria ternatea*, *Hibiscus sabdariffa*, and *Morus nigra* for spermatozoa assessment, *Oryza sativa* extracted with ethanol, potash alum, and distilled water was found to be best used for assessing the morphology of spermatozoa. Here, the authors have mentioned that potash alum is a mordant that is necessary for better staining. The positive charge of alum helps to bind the stain molecules with anionic regions like nuclear chromatin. It also helps to improve the intensity of cell and tissue staining. The authors have also mentioned that the purple colour comes from the purple anthocyanin pigment extracted by ethanol (Chomean et al., 2019).

Both studies have given promising results that the water extract of *Oryza sativa* with alum as a mordant can be used for staining sperm.

4.3 *Clitoria ternatea L*

Clitoria ternatea L – commonly called butterfly pea – comes in different colours like white, mauve, light blue, and dark blue (Lee & Abdullah, 2011). Seubhkampet and Sotthibandhu (2012) stained blood smears of birds and animals with a *Clitoria ternatea L* extract, with aluminium chloride and ferric chloride as mordants. As anthocyanins are stable in acidic pH, the staining solution used was prepared at pH 0.2. Different types of staining were seen for different cells of the blood smear and are comparable to reference stains. The authors have mentioned that as anthocyanin has a cationic chemical structure, there might have been an interaction between the polynucleotide nucleus and anthocyanin (Suebkhampet & Sotthibandhu, 2012). Nonetheless, a comparative study by Chomean et al. (2019) has produced poor staining of sperm with *Clitoria* extracts.

Anthocyanins in *Clitorea ternatae* produce a range of colours from orange-red, blue, green, and brownish yellow, with pH values ranging from 0.04 to 12 (Abdullah et al., 2010). Besides that, adding co-pigments like catechin has been found to increase the stability of anthocyanins in *Clitoria* (Charurungsipong et al., 2020). In a conclusion, research involving *Clitoria ternatea* with different pH, with the addition of suitable co pigments, suggests that this plant may be an efficient natural dye for staining tissues, smears, etc.

4.4 *Syzygium cumini*

Syzygium cumini is an elongated, round, purple-fleshed fruit with a single seed. Anthocyanins are present in the red and purple peels of the fruit, while the green peel does not contain any (Zulfajri & Muttakin, 2018). Suabjakyong et al. (2011) studied the staining efficiency of *Syzygium cumini* when used on rat hepatic tissues. The researchers have created different scenarios by utilising different combinations of dry and fresh fruits, different

DOI:https//doi.org/10.22452/mjs.vol42no1.10
Malaysian Journal of Science 42(1): 106-125 (February 2023)

solvents like distilled water and 45% glacial acetic acid, with or without ferric alum, and by staining for different durations: 10, 15, and 20 mins. They found that there was no significant staining difference between the groups except for the staining time. Moreover, there was no significant difference in the staining intensity of stained slides and staining solution kept for 14 days. Furthermore, the researchers have also mentioned that the stain has stained both the cytoplasm and nucleus of hepatic tissues with a violet colour. The authors also mentioned that the chemical components of the dye might be non-polar or neutral (Suabjakyong et al., 2011).

Brito et al. (2017) concluded that the best solvent to extract anthocyanins from plum fruits is 95% ethanol with 1% HCl. Additionally, maximum flavylium cation with red colour is observed when the extract has a pH value between 1 to 2 (Brito et al., 2017).

4.5 *Punica granulatum*

Punica granulatum is a round and hexagonal berry fruit, about 5-12 cm in diameter, with reddish and thick skin. In a single *Punica granulatum* fruit, there are nearly 600 seeds surrounded by water-laden pulps, with colours varying from white to deep red to purple (Rahimi et al., 2012). Kuskulu and Benli (2017) stained human blood cells using the fruit and obtained orange-brown staining. In another study involving the staining of rat's lung, liver, and heart tissues with *Punica granulatum* extract, Kuskulu and Aslan (2019) observed weaker staining compared to H&E staining. Kuskulu et al. stained rat ovary and testis with *Punica granulatum* extract of different pH values and temperatures. They found that different colours of staining are observed at the ovary and testis tissues when different temperatures and pH values are used. The researchers concluded that *Punica granulatum* extract could be used for staining testis tissues better than ovary tissues for histopathological diagnoses purposes (Kusculuo, 2018).

4.6 *Allium cepa*

In a study by Kuskulu et al. (2017), an aqueous extract of *Allium cepa* was mixed with different mordants like alum, $CuSO_4$ and $FeSO_4$ at different temperatures to stain buccal epithelial cells. The researchers found that the cytoplasm was well-stained when no mordant was used, and the nucleus was well-stained when $CuSO_4$ and $FeSO_4$ were used as mordants (Kusculuo et al., 2017).

According to Hashem et al., anthocyanins from *Allium cepa's* skin extracted by both acidified methanol and ethanol at 40°C to 80°C were found to be more stable than other anthocyanins (Ali et al., 2016).

4.7 *Ixora coccinea*

The flowers of *Ixora coccinea* are corymbiform, dense, actinomorphic, pedunculated, or sessile cymes (Gopalkrishnan & Chiranjeev, 2018). Cruz et al. (2018) stained blood smears with an extract from *Ixora coccinea's* flowers. In this study, an ethanol extract was used in 25% and 36% concentrations. Even though the 25% ethanol extract was better than the 36% one, the authors found that *Ixora coccinea* is not an effective stain for staining blood smears. They have recommended a few suggestions to improve the results, including using soxhlet extractions, mechanical compression of flowers, monitoring the pH, maintaining standard staining time, and increasing the concentration of extracts (Cruz et al., 2018).

Additionally, in a study by Patil and Datar (2015), it was found that the *Ixora coccinea* extract was stable at low pH values, where the stability was affected by light and temperature (Patil & Datar, 2015).

4.8 *Rosa damascene and Rosa hybrid*

There are more than 100 species of plants within the *Rosa* genus that belong to the *Rosaceae* family (Kumar et al., 2015). *Rosa damascene* is grown in gardens as decorative plant. They produce flowers of different colours ranging from white, pink, yellow, purple, and red (Kamal, 2018). An alcoholic extract of *Rosa damascene* has been used by Kamal et al. (2018) to stain a Leishmania parasite sample that became red in colour. Another study by Kumar et al. (2015) involved the use of an aqueous and alcoholic extract of *Rosa hybrida* and *Hibiscus sabdariffa* to stain helminth parasite samples. This study found that *Rosa hybrida* stains were better than *Hibiscus sabdariffa* (Kumar et al., 2015). On the other hand, Surendra et al. (2018) stained normal and pathological oral tissues with rose stains extracted using maceration and soxhlet methods with or without adding potassium alum. The researchers concluded that soxhlet extract with the addition of potassium alum as mordants exhibited better staining properties compared to other groups (Surendra et al., 2018).

4.9 *Papaver rhoeas*

Papaver rhoeas is a deep red-coloured flower with large and thin petals. The petal base is a black-coloured area that is bordered by white lines (van der Kooi & Stavenga, 2019). Budak and Budak (2015) stained lung and liver tissues with a *Papaver* stain prepared by adding mordants and a solvent with a weak acid, oxidant, and antioxidant. The slides demonstrated good staining of the nucleus, which was depicted as clear and well-defined. The stain was dark purple in colour and was depicted in the images seen in the article. From this observation, the researchers concluded that *Papaver rhoeas* might be used as an alternative for haematoxylin stains. The *Papaver rhoeas* stain was red when added to the slide. Upon bluing with tap water, it turned blue. A similar principle was also observed in haematoxylin staining. Because of these properties, *Papaver rhoeas* stain may be a better alternative to haematoxylin stains (Budak & Budak, 2015).

Meanwhile, Ekici (2014) demonstrated that the maximum concentration of anthocyanin in *Papaver rhoeas* was obtained by concentrating the extract using a vacuum evaporation method.

DOI:https//doi.org/10.22452/mjs.vol42no1.10
Malaysian Journal of Science 42(1): 106-125 (February 2023)

The degradation of anthocyanin was found to be higher when the conventional method of concentration was used compared to microwave and vacuum approaches. The researchers also mentioned that temperature increase had accelerated anthocyanin degradation in *Papaver rhoeas* flower extracts (Ekici, 2014).

4.10 *Hibiscus sabdariffa and Hibiscus rosa-sinensis*

The phytochemical constituents of hibiscus include phenolic compounds, flavonoids, anthocyanin, and protocatechuic acid. The most abundant phytochemical of the above is anthocyanin (Ademiluyi et al., 2013). A hibiscus extract with more than 20% concentration solidifies when boiled due to the presence of pectin (Hashim, 2006). Many studies have been done to examine the staining effects of hibiscus on parasites, fungi, bacteria, animal and human tissues.

4.10.1 Parasites

Kamal (2018), in their study stained Leishmania with water and alcoholic hibiscus extracts, which produced pink and bluish-pink stains, respectively (Kamal, 2018).

4.10.2 Fungi

Abubakar et al. (2012) stained a few fungal species with both aqueous and alcoholic extracts and found that the staining was similar to the standard lactophenol and methylene blue stains, except for the red colour. The authors also mentioned that aqueous extracts are superior in staining compared to alcoholic ones (Abubakar et al., 2012). Ihuma et al. (2012) stained a few fungal species with a methanolic extract of hibiscus. They found that the staining was better than lactophenol. The authors also mentioned that since methanolic extract (Ph-2.7) and lactophenol (Ph-3.6) are acidic, the staining is similar (Ihuma et al., 2012).

4.10.3 Bacteria

Ma'aruf et al. (2020) made an attempt at staining bacteria found in lung and appendix tissues with different extracts but did not achieve their objectives. They concluded that inflammatory cells are stained better than bacteria (Ma'aruf et al., 2020). Furthermore, hibiscus was found to be more soluble in alcohol than in water. In this study, the use of aqueous extracts and staining for a shorter duration demonstrated better staining potentials (Ma'aruf et al., 2020).

4.10.4 Tissue histology

Hibiscus has been used in histological staining as a nuclear (substitute for haematoxylin) and cytoplasmic stain (substitute for eosin).

4.10.5 Tissue histology (Nuclear stain)

Bernard et al. (2017) and Agbede et al. (2017) used an aqueous hibiscus extract to stain nuclei as a substitute for haematoxylin in H&E staining. In this context, the solvent is prepared by adding NaCl, 10% $FeCl_3$, and glacial acetic acid into the extract. The nuclear staining results turned out to be similar to haematoxylin. The authors concluded that hibiscus is a good nuclear stain for brain tissues, skin, lymph nodes, and appendix tissues (Agbede et al., 2017; Benard et al., 2017; Benard et al., 2015; Benard, 2008). Meanwhile, Egbujo et al. (2008) stained testicular tissues with an aqueous extract of hibiscus with different mordants like alum and iron. The researchers also added acetic acid or ammonia to alter the extract's pH values. They found good nuclear-cytoplasmic differentiation with iron mordant. At the same time, acetic acid was also found to enhance the staining. Iron mordant was better than alum, as the former was able to also highlight the connective tissues. This might be due to the fact that the dye lake bond formed by iron alum is stronger than potassium alum (Egbujo et al., 2008). On top of that, Bassey et al. (2012) stained testicular tissues and sperms with an alcoholic extract of hibiscus mixed with 70% ethanol. They concluded that hibiscus might act as a basic dye (Bassey et al., 2012).

4.10.6 Tissue histology (Cytoplasmic stain)

Hashim (2006) stained kidney and artery tissues with aqueous extract as a substitute for eosin. As a result, faint brown staining was obtained in the cytoplasm of renal glomeruli and tubules (Hashim, 2006). Besides that, Gowali (1995) stained biopsies from muscular dystrophy and cardiac myo infarction patients with a combination of picric acid and hibiscus stain. This extract could differentiate between intact and necrotic muscle fibres using different colours. In this study, staining was done according to the principle and method of Masson trichrome staining. Steps like treating with 1% iron alum and mordanting with 5% phosphotungstic acid were also included in the procedure. This study shows that hibiscus may also be used as a differential stain (Gowali, 1995). Furthermore, Sridhara et al. (2016) used both alcoholic and aqueous hibiscus extracts with different pH values to stain oral mucosa and skin tissue blocks. The researchers found that there was no statistical significance in staining parameters between hibiscus and H&E staining. The study has also concluded that alcoholic extracts (5.7 pH) demonstrated better staining than aqueous ones (Sridhara et al., 2016).

Studies that used hibiscus as a substitute for haematoxylin have mostly used acetic acid as one of the constituents. Moreover, both ethanolic and aqueous extracts have been used as nuclear and cytoplasmic stains. Hibiscus may also be used as a nuclear and cytoplasmic stain, depending on the stain it replaces in the procedure.

4.11 *Factors influencing histology staining*

The ability of dyes to stain tissues is influenced by the affinities between the two. The dye-tissue affinity depends on many factors like coulombic attractions, Van der Waal's forces, hydrogen bonding, and covalent bonding between the tissue and the reagent (dye) (Suvarna et al., 2013; Veuthey et al., 2014).

Stains containing anthocyanin can be used as substitutes for synthetic stains to stain histological tissues, microorganisms,

DOI:https//doi.org/10.22452/mjs.vol42no1.10
Malaysian Journal of Science 42(1): 106-125 (February 2023)

smears, etc. The staining effect depends on the plant products, type of extract, the concentration of anthocyanin, pH value of the staining solutions, temperature, use of mordants, etc.

Even though most of the reviewed studies have been done using aqueous extracts, there is essentially not much significant difference between aqueous and alcoholic ones. This is because, since anthocyanins are polar molecules, the common solvents used for extraction purposes are aqueous mixtures of ethanol, methanol, and acetone. These methods will also extract other non-phenolic substances like organic acids, sugar, and proteins which require a further purification process. Besides that, acidified methanol or ethanol is also commonly used for extraction (Awika et al., 2005; Cacace & Mazza, 2003; Fossen & Andersen, 2003). This might also be the reason why many studies have added a small percentage of glacial acetic acid to their solvents. The addition of strong acid should be avoided, as it might degrade the acylated anthocyanin and destroy the glycoside bond in anthocyanins (Castañeda et al., 2009).

4.11.1 The Effect of pH on Histology Staining

Almost all studies involve staining under acidic pH. Flavylium ions are more predominant at pH one and produce a red or purple colour. At pH 2 to 4, quinoidal bases are more predominant, producing a blue colour. Meanwhile, at pH 5 and 6, two colourless specie like chalcone and carbinol pseudo base are produced. When the pH exceeds 7, the anthocyanins are degraded. At pH 4 to 6, the four structural forms – anhydrous quinoidal base, yellow chalcone, colourless carbinol, and flavylium cation – exist together. For this reason, anthocyanin's colour changes are more prominent in alkaline solutions (Cabrita et al., 2000; Castañeda et al., 2009). According to Budak and Budak (2015), the addition of a weak acid to the solvent will help to adjust the pH between 2 and 3.7, and provide a more stable and effective composition. The other uses of acids include acting as a buffer and prolonging the shelf life of the solution. It also increases the selectivity of nuclei and prevents over-oxidation (Budak & Budak, 2015).

Additionally, specific staining of tissue structures by the dye also depends on the pH of the extract. Acidic and basic stains are used for staining basic and acidic structures, respectively. The charge distribution in the dyes determines their repulsive and attractive nature. Anions with negative charges are attracted to positively-charged molecules, while cations with positive charges are attracted to negatively-charged molecules. Therefore, charges are greatly determined by the pH of the dye. Low pH solutions increase the number of charged groups within the tissues and vice versa. Hence, the pH of the extract is an imperative factor that determines the dye's staining effect (Kumar et al., 2015; Avwioro, 2002; Avwioro, 2010).

4.11.2 Effect of Mordants on Histology Staining

Iron or alum mordants are used in many studies to improve the staining effects. One main characteristic of anthocyanins that have *O*-di-hydroxyl groups in their ring is their capacity to form metal-anthocyanin complexes (Boulton, 2001). A few studies on the colour stability of anthocyanins have suggested that the blue colour is attributed to the complexation observed between anthocyanins and metals like Al, Fe, Cu, etc. The complexation formed by Al (III)-anthocyanin interaction stabilizes the blue quinoidal base, a process that prevents its oxidation (Moncada et al., 2003). Recent studies have also shown that the complexation process between Fe (III) and *O*-di-hydroxyl groups at pH 5 is necessary for the formation of the blue colour (Castañeda et al., 2009; Yoshida et al., 2006).

Anthocyanin-based natural stains have good potential to replace synthetic stains used in histopathological diagnosis. None of the studies talk about the stability of natural staining solutions as well as its fading tendency in slides. For this reason, there is a gap in the literature for researchers to fill by exploring the natural anthocyanin chemistry, isolation from plants, and optimizing appropriate staining medium with mordants at suitable pH, solubility, and stability.

5. Conclusion

Oryza sativa aqueous extracts with potassium alum as mordant can be used for staining semen to allow researchers to observe the morphology of sperms. Aqueous extract of *Papaver rhoeas* with added chemicals like acetified ethylene glycol, sodium iodide, aluminium chloride, beta-cyclodextrin, and potassium alum can act as a good alternative stain to haematoxylin, as they both share the same staining principle. Besides that, *Hibiscus sabdariffa* and *Rosa hybrida* aqueous extracts with the presence of iron or alum as mordant can also be used for histopathological staining. Further studies are needed to investigate the effectiveness of *Morus nigra*, *Clitoria ternatea*, *Allium cepa*, *Syzygium cumini*, and *Punica granulatum* by using different solvents to increase their staining potentials when used on various histological tissues. There is a lack of studies that analyze the stability of slides stained with natural stains, which is a very important requirement for histopathology. These lacunae presents a space for the discovery and invention of new natural stains.

6. References

Abdullah, R., Lee, P. M., & Lee, K. H. (2010). Multiple colours and pH stability of floral anthocyanin extract: Clitoria ternatea. 2010 International Conference on Science and Social Research 254–258.

Abubakar, S., Usman, A. B., Etim, V., Nnadi, O., & Alaku, C. (2012). Application of Organic Dyes from Roselle calyx (Hibiscus sabdariffa linn) for Mycological Staining. Indian Journal of Innovations and Developments 1(9): 687–690.

Ademiluyi, A. O., Oboh, G., & Oluwaseun, A. J. (2013). Anthocyanin – Rich Red Dye of Hibiscus sabdariffa calyx Modulates Cisplatin-induced Nephrotoxicity and

DOI:https//doi.org/10.22452/mjs.vol42no1.10
Malaysian Journal of Science 42(1): 106-125 (February 2023)

Oxidative Stress in Rats. International Journal of Biomedical Science 9(4) 243–248.

Agbede, M. B., Benard, S. A., Afolabi, O. O., Okoye, J. O., Bankole, J. K., Fowotade, A. A., Olutunde, O. A., & Muhammed, O. A. (2017). The Use of Hibiscus sabdariffa Extract as Nuclear Stain for Skin Morphology and Connective Tissue with Eosin Counterstain. Sokoto Journal of Medical Laboratory Science 2(4), 28–32.

Ajileye, A. B., Iteire, A. K., & Arigi, Q. B. (2015). Zingiber officinale (ginger) extract as a histological dye for muscle fibers and cytoplasm. International Journal of Medical Science and Public Health 4(10): 1445–1448.

Akinloye, A. J., & Olagoke, A. (2010). Screening of some indigenous herbal dyes for use in plant histological staining. Journal of Forestry Research 21(1): 81–84.

Ali, O.-H., Al-sayed, H., Yasin, N., & Afifi, E. (2016). Effect of Different Extraction Methods on Stablity of Anthocyanins Extracted from Red Onion peels (Allium cepa) and Its Uses as Food Colorants. Bulletin of the National Nutrition Institute 47(2): 196–219. https://doi.org/10.21608/bnni.2016.4218

Anonymous. (2020). IARC Monographs on the Identification of Carcinogenic Hazards to Humans – International Agency for research on cancer. WHO. https://monographs.iarc.fr/

Avwioro, G. O. (2002). Histochemistry and Tissue Pathology, pp.134-213, Abraka, Nigeria: University press.

Avwioro, G. O. (2010). Histochemistry and tissue pathology, principles and techniques, pp.561-568 Abraka, Nigeria: University press.

Awika, J. M., Rooney, L. W., & Waniska, R. D. (2005). Anthocyanins from black sorghum and their antioxidant properties. Food Chemistry 90(1–2): 293–301.

Bassey, R. B., Bakare, A. A., Peter, A. I., Oremosu, A. A., & Osinubi, A. A. (2012). Factors influencing extract of Hibiscus sabdariffa staining of rat testes. Biotechnic and Histochemistry 87(6): 403–407. https://doi.org/10.3109/10520295.2012.679365

Bassey, Rosemary B., Osinubi, A. A., & Oremosu, A. A. (2012). Staining effect of Hibiscus sabdariffa extract on sperm cell morphology of Sprague-Dawley rats. Journal of Histotechnology 35(3): 110–113. https://doi.org/10.1179/2046023612Y.0000000010

Benard, S., Afolabi, O., Fowotade, A., Okoye, J., Olutunde, O., & Bankole, J. (2017). Hibiscus-Van Gieson Stain for collagen fibers. African Journal of Cellular Pathology 9: 1–4.

Benard, S., Muhammed, A., Fowotade, A., Afolabi, O., & Olutunde, O. (2017). Iron-Roselle: A Progressive Nuclear Stain for Connective Tissue of Skin. International Journal of Health Research and Innovation 5(2): 25–31.

Benard, S A, Muhammaed, A., Fowotade A A, Afolabi O O, & Olutunde, O. A. (2015). Hibiscus sabdariffa extract as haematoxylin substitute in the histological demonstration of brain tissues. African Journal of Cellular Pathology 5: 32–35.

Benard, Solomon A. (2008). Iron-roselle: A progressive nuclear stain substitute for haematoxylin. Journal of Histotechnology 31(2): 57–59. https://doi.org/10.1179/his.2008.31.2.57

Bondoc, C. C. (2018). Curcuma longa Linn rhizome extract as an alternative stain for histological studies. Journal of Pharmacognosy and Phytochemistry 7(5): 3010–3017.

Bordoloi, B., Jaiswal, R., Siddiqui, S., & Tandon, A. (2017). Health Hazards of Special Stains. Saudi Journal of Pathology and Microbiology 2(5): 175–178.

Boulton, R. (2001). The Copigmentation of Anthocyanins and Its Role in the Color of Red Wine: A Critical Review. American Journal of Enology and Viticulture 52(2): 67–87.

Budak, M., & Budak, G. G. (2015). A new biochemical dye molecule and nuclear stain formulation in histotechnology diagnostics as an alternative to haematoxylin. Journal of Histotechnology 38(4): 113–121. https://doi.org/10.1179/2046023615Y.0000000009

Cabrita, L., Fossen, T., & Andersen, Ø. M. (2000). Colour and stability of the six common anthocyanidin 3-glucosides in aqueous solutions. Food Chemistry 68(1): 101–107. https://doi.org/10.1016/S0308-8146(99)00170-3

Cacace, J. E., & Mazza, G. (2003). Mass transfer process during extraction of phenolic compounds from milled berries. Journal of Food Engineering 59(4): 379–389. https://doi.org/10.1016/S0260-8774(02)00497-1

Castañeda, A., Hernández, L. P., Elena, P., Rodríguez, J. A., & Galán-Vidal, C. A. (2009). Chemical studies of anthocyanins: A review. Food Chemistry 113(4): 859–871. https://doi.org/10.1016/j.foodchem.2008.09.001

DOI:https//doi.org/10.22452/mjs.vol42no1.10
Malaysian Journal of Science 42(1): 106-125 (February 2023)

Charurungsipong, P., Tangduangdee, C., Amornraksa, S., Asavasanti, S., & Lin, J. (2020). Improvement of Anthocyanin Stability in Butterfly Pea Flower Extract by Co-pigmentation with Catechin. E3S Web of Conferences, 141(9). https://doi.org/10.1051/E3SCONF/202014103008

Chomean, S., Nantabut, M., Kongtia, W., Saenguthai, K., & Kaset, C. (2019). Evaluation of natural dyes for human spermatozoa morphology assessment. Acta Histochemica 121(2): 227–233. https://doi.org/10.1016/j.acthis.2018.12.010

Cruz, P. E., De Vera, A. P., & Villa, A. D. (2018). The efficiancy of Santan flower (Ixora occinea Linn.) as an alternative stain to eosinY in Wright-Giemsa stain. LPU-Laguna Journal of Allied Medicine 3(1): 11–21.

Dapson, R., Horobin, R. W., & Kiernan, J. A. (2010). Hematoxylin shortages: Their causes and duration, and other dyes that can replace hemalum in routine haematoxylin and eosin staining. Biotechnic and Histochemistry 85(1): 55–63. https://doi.org/10.3109/10520290903048400

Dela, G., Or, E., Ovadia, R., Nissim-Levi, A., Weiss, D., & Oren-Shamir, M. (2003). Changes in anthocyanin concentration and composition in "Jaguar" rose flowers due to transient high-temperature conditions. Plant Science 164(3): 333–340. https://doi.org/10.1016/S0168-9452(02)00417-X

do Carmo Brito, B. de N., da Silva Pena, R., Santos Lopes, A., & Campos Chiste, R. (2017). Anthocyanins of Jambolao (Syzygium cumini): Extraction and pH-Dependent Colour Changes. Journal of Food Science 82(10): 2286–2290. https://doi.org/10.1111/1750-3841.13847

Ebrahimi, M., & Parham, A. (2020). Using Herbal dyes as an alternative staining method for sperm evaluation. Veterinary Medicine and Science 6: 441-446. https://doi.org/10.1002/vms3.268

Egbujo, E. C., Adisa, O. J., & Yahaya, A. B. (2008). A Study of the Staining Effect of Roselle (Hibiscus sabdariffa) on the Histologic Section of the Testis. International Journal of Morphology 26(4): 927–930. https://doi.org/10.4067/S0717-95022008000400022

Ekici, L. (2014). Effects of concentration methods on bioactivity and colour properties of poppy (Papaver rhoeas L.) sorbet, a traditional Turkish beverage. LWT - Food Science and Technology 56(1): 40–48. https://doi.org/10.1016/j.lwt.2013.11.015

Fossen, T., & Andersen, Ø. M. (2003). Anthocyanins from red onion, Allium cepa, with novel aglycone. Phytochemistry 62(8): 1217–1220.

Fuleki, T. (1971). Anthocyanins in red onion, Allium cepa. Journal of Food Science 36(1): 101–104.

Gopalkrishnan, B., & Chiranjeev, R. (2018). Pharmacognostical study of Ixora coccinea flower. Pharmacognosy Journal 10(5): 1042–1046. https://doi.org/10.5530/pj.2018.5.176

Gowali, F. M. (1995). Picro-Hibiscin Stain for Degenerated Muscle Fibers. Laboratory Medicine 26(7): 470–473. https://doi.org/10.1093/LABMED/26.7.470

Hashim, E. A. (2006). The use of watery extract of kujarat flowers Hibiscus sabdariffa as a natural histological stain. Iraqi Journal of Medical Science 5(1): 29–33.

Hassimotto, N. M. A., Genovese, M. I., & Lajolo, F. M. (2007). Identification and characterisation of anthocyanins from wild mulberry (Morus nigra L.) growing in Brazil. Food Science and Technology International 13(1): 17–25. https://doi.org/10.1177/1082013207075602

Hiemori, M., Koh, E., & Mitchell, A. E. (2009). Influence of cooking on anthocyanins in black rice (Oryza sativa L. japonica var. SBR). Journal of Agricultural and Food Chemistry 57(5): 1908–1914. https://doi.org/10.1021/jf803153z

Hinojosa-Gómez, J., San Martín-Hernández, C., Heredia, J. B., León-Félix, J., Osuna-Enciso, T., & Muy-Rangel, M. D. (2020). Anthocyanin Induction by Drought Stress in the Calyx of Roselle Cultivars. Molecules 25(7): 1555. https://doi.org/10.3390/molecules25071555

Hou, Z., Qin, P., Zhang, Y., Cui, S., & Ren, G. (2013). Identification of anthocyanins isolated from black rice (Oryza sativa L.) and their degradation kinetics. Food Research International 50(2): 691–697. https://doi.org/10.1016/j.foodres.2011.07.037

Ihuma J O, Asenge, G. H., Abioye, J. O. K., & Dick, S. K. (2012). Application of methonolic extracts from Hibiscus sabdariffa linn as a biological staining agent for some fungal species. International Journal of Plant Animal and Environmental Sciences 2(2): 254–259.

Jiang, Y., & Nie, W. J. (2015). Chemical properties in fruits of mulberry species from the Xinjiang province of China. Food Chemistry 174: 460–466. https://doi.org/10.1016/j.foodchem.2014.11.083

DOI:https//doi.org/10.22452/mjs.vol42no1.10
Malaysian Journal of Science 42(1): 106-125 (February 2023)

Kamal, S. B. (2018). Staining of Leishmania donavani Promastigotes by natural flower dyes. Pakistan Journal of Biotechnology 15(2): 299–302.

Khoo, H. E., Azlan, A., Tang, S. T., & Lim, S. M. (2017). Anthocyanidins and anthocyanins: Coloured pigments as food, pharmaceutical ingredients, and the potential health benefits. Food and Nutrition Research 61(1). https://doi.org/10.1080/16546628.2017.1361779

Kumar, N., Mehul, J., Das, B., & Solanki, J. B. (2015). Staining of Platyhelminthes by herbal dyes: An eco-friendly technique for the taxonomist. Veterinary World 8(11): 1321–1325. https://doi.org/10.14202/vetworld.2015.1321-1325

Kusculu, N. G., & Aslan, H. G. (2019). Evaluation of an extract of the Punica granatum flower as a biological stain of rat tissues: A preliminary study. Molecular Biology Reports 46(1): 581–585. https://doi.org/10.1007/S11033-018-4510-3

Kusculuo, N. G. (2018). Evaluation and comparison of staining effect of Punica granatum flower extract on testis and ovary of Wistar rats: First results. African Journal of Biotechnology 17(32): 989–993. https://doi.org/10.5897/ajb2018.16535

Kusculuo, N. G., Cucer, N., & Onal, A. (2017). Staining of Onion and Buccal Epithelial Cells with Onion Skin Extract | Open Access Journals. Research & Reviews: Research Journal of Biology 5(2): 1–6.

Kuskuluo, N. G., & Benli, H. (2017). Staining Effect of Pomegranate Flower Extract on Human Blood Cells: First Results. Journal of Environmental Science and Engineering 6:249–251.

Lahiani, A., Klaiman, E., & Grimm, O. (2018). Enabling Histopathological Annotations on Immunofluorescent Images through Virtualization of Haematoxylin and Eosin. Journal of Pathology Informatics, 9: 1. https://www.ncbi.nlm.nih.gov/pmc/articles/PMC5841016/

Lakshmi, C. (2014). Food Colouring: The Natural Way. Research Journal of Chemical Sciences, 4(2): 87–96. www.isca.me

Lee, P. M., & Abdullah, R. (2011). Thermal Degradation of Blue Anthocyanin Extract of Clitoria ternatea Flower. 2nd International Conference on Biotechnology and Food Science 49–53.

Ma'aruf, S. Y., Mohammed, M. O., Muhammad, A. T., Okechi, O. O., Tsamiya, R. I., Abubakar, U., Mohammed, I., Umar, A., Sani, S. M., Kabir, H., Bello, B. A., Garba, S., & Abubakar, S. D. (2020). Staining Property of Alcoholic and Aqueous Hibiscus sabdariffa Extract in Demonstration of Selected Bacteria in Tissue Sections of Wistar Rats. Microbiology Research Journal International 30(2), 26–33.

Mat Nor, N. A., & Arof, A. K. (2016). On statistical analysis of factors affecting anthocyanin extraction from Ixora siamensis. Optical Materials 60: 462–466. https://doi.org/10.1016/j.optmat.2016.08.034

Mohandas, R., Ramani, P., Sherlin j, H., Gheena, S., Ramasubramanian, A., Don, K. R., Jayaraj, G., & Santhanam, A. (2019). Organic stains used in histopathology-A systematic review. Drug Invention Today 11: 426–432.

Moncada, M. C., Moura, S., Melo, M. J., Roque, A., Lodeiro, C., & Pina, F. (2003). Complexation of aluminum (III) by anthocyanins and synthetic flavylium salts: A source for blue and purple colour. Inorganica Chimica Acta 356: 51–61. https://doi.org/10.1016/S0020-1693(03)00394-3

Moosazad, S., Ghajarbeigi, P., Mahmoudi, R., Shahsavari, S., Vahidi, R., & Soltani, A. (2019). Antibacterial and Antioxidant Properties of Colorant Extracted from Red Onion Skin. Journal of Chemical Health Risks, 9(3): 235–243. https://www.magiran.com/paper/2038588

Ozgen, M., Serce, S., & Kaya, C. (2009). Phytochemical and antioxidant properties of anthocyanin-rich Morus nigra and Morus rubra fruits. Scientia Horticulturae, 119(3): 275–279. https://doi.org/10.1016/j.scienta.2008.08.007

Patil, N., & Datar, A. G. (2015). Extraction, stability and separation of anthocyanins of Ixora coccinea linn. International Journal of Pharmacy and Pharmaceutical Sciences 7(3): 198–202.

Pedro, A. C., Granato, D., & Rosso, N. D. (2016). Extraction of anthocyanins and polyphenols from black rice (Oryza sativa L.) by modeling and assessing their reversibility and stability. Food Chemistry 191: 12–20. https://doi.org/10.1016/j.foodchem.2015.02.045

Pirzadeh, M., Caporaso, N., Rauf, A., Shariati, M. A., Yessimbekov, Z., Khan, M. U., Imran, M., & Mubarak, M. S. (2021). Pomegranate as a source of bioactive constituents: A review on their characterization, properties and applications. Critical Reviews in Food Science and Nutrition 61(6):982-999. https://doi.org/10.1080/10408398.2020.1749825

DOI:https//doi.org/10.22452/mjs.vol42no1.10
Malaysian Journal of Science 42(1): 106-125 (February 2023)

Quina, F. H., Moreira, P. F., Vautier-Giongo, C., Rettori, D., Rodrigues, R. F., Freitas, A. A., Silva, P. F., & Maçanita, A. L. (2009). Photochemistry of anthocyanins and their biological role in plant tissues. Pure and Applied Chemistry 81(9): 1687–1694. https://doi.org/10.1351/PAC-CON-08-09-28

Rahimi, H. R., Arastoo, M., & Ostad, S. N. (2012). A comprehensive review of Punica granatum (Pomegranate) properties in toxicological, pharmacological, cellular and molecular biology researches. Iranian Journal of Pharmaceutical Research 11(2): 385–400. https://doi.org/10.22037/ijpr.2012.1148

Ramamoorthy, A., Ravi, S., Jeddy, N., Thangavelu, R., & Janardhanan, S. (2016). Natural alternatives for chemicals used in histopathology lab- A literature review. In Journal of Clinical and Diagnostic Research 10(11): EE01-EE04. https://doi.org/10.7860/JCDR/2016/23420.8860

Saenguthai, K., Chomean, S., & Kaset, C. (2018). The evaluation of Oryza sativa L. (Black rice) extracts for detection of spermatozoa on the clothing and vaginal swab samples. Legal Medicine 35: 91–97. https://doi.org/10.1016/j.legalmed.2018.09.020

Shaik, A., Naidu, K. K., & Panda, J. (2018). A review on anthocyanins: A promising role on phytochemistry and pharmacology. International Research Journal of Pharmacy 9(1): 1–9.

Shao, Y., Xu, F., Sun, X., Bao, J., & Beta, T. (2014). Phenolic acids, anthocyanins, and antioxidant capacity in rice (Oryza sativa L.) grains at four stages of development after flowering. Food Chemistry 143: 90–96. https://doi.org/10.1016/j.foodchem.2013.07.042

Singh, R. (2017). Sources of natural dye-A critical review. International Journal of Engineering, Science and Mathematics 6(5): 180–186.

Siva, R. (2007). Status of natural dyes and dye-yielding plants in India. Current Science 92(7): 916–925.

Sridhara, S. U., Raju, S., Gopalkrishna, A. H., Haragannavar, V. C., Latha, D., & Mirshad, R. (2016). Hibiscus: A different hue in histopathology. Journal of Medicine Radiology Pathology and Surgery 2: 9–11.

Suabjakyong, P., Romratanapun, S., & Thitipramote, N. (2011). Extraction of Natural Histological Dye from Black Plum Fruit (Syzygium cumini). Journal of the Microscopy Society of Thailand 4(1): 13–15.

Sudhakaran, A., Hallikeri, K., & Babu, B. (2018). Natural stains Zingiber officinale Roscoe (ginger) and Curcuma longa L. (turmeric) – A substitute to eosin. AYU 39(4): 220–225. https://doi.org/10.4103/ayu.ayu_232_17

Suebkhampet, A., & Sotthibandhu, P. (2012). Effect of using aqueous crude extract from butterfly pea flowers (Clitoria ternatae L.) as a dye on animal blood smear staining. Suranaree Journal of Science and Technology 19(1): 15–19.

Surendra, L., Nambiar, K. S., Haragannavar, V. C., Augustine, D., Sowmya, S. V., Babu, A., & Rao, R. S. (2018). Staining efficacy of rose extract in comparison with eosin stain: A histological study on oral tissues. World Journal of Dentistry 9(6): 500–504. https://doi.org/10.5005/jp-journals-10015-1587

Suvarna, K., Layton, C., & Bancroft, J. (2013). Bancroft's Theory and Practice of Histological Techniques (7th ed.). Churchill Livingston Elsiever.

Tousson, E., & Al-Behbehani, B. (2011). Black mulberries (Morus nigra) as a natural dye for animal tissues staining. Animal Biology 61(1): 49–56.

Tousson, E. M., & Al-Behbehani, B. (2010). Black Mulberries (Morus nigra) as a natural dye for nervous tissues staining. The Egyptian Journal of Experimental Biology (Zoology) 6(1): 159–164.

van der Kooi, C. J., & Stavenga, D. G. (2019). Vividly coloured poppy flowers due to dense pigmentation and strong scattering in thin petals. Journal of Comparative Physiology A: Neuroethology, Sensory, Neural, and Behavioral Physiology 205(3): 363–372. https://doi.org/10.1007/s00359-018-01313-1

Vankar, P. S. (2000). Chemistry of Natural Dyes. Resonance 5(10): 73–80.

Velickovic, J. M., Mitic, M. N., Arsic, B. B., Paunovic, D. Đ., Stojanovic, T., Veljkovic, J. N., Dimitrijevic, D. S., Stevanovic, S. D., & Kostic, D. A. (2019). HPLC Analysis of extracts of fresh petals of Papaver rhoeas L. Studia Universitatis Babes-Bolyai, Chemia 3: 239–247. https://doi.org/10.24193/subbchem.2019.3.20

Verma, S., & Gupta, G. (2017). Natural dyes and its applications: A brief review. International Journal of Research and Analytical Reviews 4(4): 57–60.

Veuthey, T. V., Herrera, G. M., & Dodero, V. I. (2014). Dyes and stains: From molecular structure to histological application. Frontiers in Bioscience 19(1): 91–112. https://doi.org/10.2741/4197

DOI:https//doi.org/10.22452/mjs.vol42no1.10
Malaysian Journal of Science 42(1): 106-125 (February 2023)

Wahyuningsih, S., Wulandari, L., Wartono, M. W., Munawaroh, H., & Ramelan, A. H. (2017). The Effect of pH and Color Stability of Anthocyanin on Food Colorant. IOP Conference Series: Materials Science and Engineering 193(1). https://doi.org/10.1088/1757-899X/193/1/012047

Wan, H., Yu, C., Han, Y., Guo, X., Luo, L., Pan, H., Zheng, T., Wang, J., Cheng, T., & Zhang, Q. (2019). Determination of flavonoids and carotenoids and their contributions to various colours of rose cultivars (Rosa spp.). Frontiers in Plant Science 10: 123. https://doi.org/10.3389/fpls.2019.00123

Yoshida, K., Kitahara, S., Ito, D., & Kondo, T. (2006). Ferric ions involved in the flower colour development of the Himalayan blue poppy, Meconopsis grandis. Phytochemistry 67(10): 992–998. https://doi.org/10.1016/J.PHYTOCHEM.2006.03.013

Zulfajri, M., & Muttakin. (2018). Activity analysis of anthocyanin from Syzygium cumini (L.) skeels as a natural indicator in acid-base titration. Rasayan J. Chem 11(1): 135–141. https://doi.org/10.7324/RJC.2018.1111983

DOI:https//doi.org/10.22452/mjs.vol42no1.10
Malaysian Journal of Science 42(1): 106-125 (February 2023)